

CRYSTAL NUCLEATION AND GROWTH  
IN BARIA-SILICA GLASSES

A Thesis presented by  
ANTHONY HUGH RAMSDEN

For the degree of  
Doctor of Philosophy  
of  
The University of Sheffield

Department of Ceramics, Glasses and Polymers,  
The University of Sheffield

September, 1977

**BEST COPY**

**AVAILABLE**

Variable print quality

### ACKNOWLEDGEMENTS

I am immensely indebted to my supervisor, Dr P.F. James, and would like to thank him for his guidance and encouragement throughout the course of this work.

I am also grateful to Dr J.O. Isard for many discussions and advice on the electric field phenomenon.

Many thanks are due to the technical staff of the department, particularly Mr R. Bacon, for their co-operation and assistance.

I also wish to acknowledge Mrs M. Hodgins for her patience and skill in typing this thesis.

Finally, I gratefully acknowledge the Science Research Council for financial support.

## CONTENTS

	<u>Page</u>
Acknowledgements	
Table of Contents	
Summary	
List of General Symbols	
CHAPTER ONE - General Introduction	1
CHAPTER TWO - Liquid-liquid immiscibility in glass-forming systems	6
CHAPTER THREE - Kinetics of phase transformations in glass-forming systems	15
CHAPTER FOUR - The relation between liquid-liquid immiscibility and crystallization	43
CHAPTER FIVE - Experimental methods	52
CHAPTER SIX - Crystal nucleation and liquid-liquid immiscibility. Results and Discussion	75
CHAPTER SEVEN - Crystal growth in baria-silica glasses	119
CHAPTER EIGHT - The effect of electric fields on crystal nucleation and growth in glasses	146
CHAPTER NINE - Summary, conclusions and suggestions for further work	164
Appendix	
References	

## SUMMARY

The kinetics of crystal nucleation and growth of barium disilicate were studied in baria-silica glasses containing 25 to 35 mole% baria. In this composition range, liquid-liquid immiscibility exerted a pronounced influence on crystal nucleation kinetics. The progressive shift in composition of the baria-rich matrix phase with time caused changes in both the thermodynamic driving force and in the kinetic barrier to nucleation which in turn caused a marked increase of nucleation rate. Study of the nucleation kinetics in relation to quantitative data of the morphology of the two liquid phases showed no evidence of heterogeneous nucleation at the liquid-liquid interfaces.

Crystal growth measurements at lower temperatures showed appreciable induction times which were caused by a change in growth morphology from spheres to rapidly growing needles nucleated at the sphere-glass interfaces. The induction time decreased with rise in temperature.

Comparison of crystal growth rates in phase separating and non-phase separating glasses showed that phase separation increased the growth rates due to the accompanying shift in composition of the baria-rich phase during heat treatment. This composition shift also caused an apparent reduction in the measured activation enthalpies for growth in the phase separated glasses. The morphology of the two liquid phases had no influence on crystal growth rates.

All the glasses gave constant growth rates, except at high temperatures where growth rates increased with time. Reasons for this behaviour are discussed.

No effects on the kinetics of nucleation and growth in a baria-silica

based glass were observed on application of electric fields of  $4 \text{ kV cm}^{-1}$ . A theoretical calculation showed that the field necessary to observe an effect would be much larger than is possible to achieve in practice, due to joule heating and electrical breakdown.

## SYMBOLS

### Operator Signs

d	Ordinary differential
$\partial$	Partial differential
$\Delta$	Excess of final over initial value
$\Sigma$	Summation
ln	Natural logarithm
log <sub>10</sub>	Logarithm to base 10

### Capital Roman Characters

A	Area of cross-section of glass (p. 155)
A and A <sub>D</sub>	Pre-exponential constant (p. 28 and
A <sub>1</sub> and A <sub>2</sub>	Refers to adjustable parameters in equations for $\Delta mH$ using sub-regular solution model (p. 12).
A*	Surface area of critically sized embryo (p. 18-19).
A <sub><math>\alpha\beta</math></sub> , A <sub><math>\beta\gamma</math></sub> , A <sub><math>\alpha\gamma</math></sub>	Area of $\alpha$ - $\beta$ , $\beta$ - $\gamma$ , $\alpha$ - $\gamma$ interface.
ABS <sub>2</sub>	Glass mol% 1Al <sub>2</sub> O <sub>3</sub> , 66SiO <sub>2</sub> , 33BaO.
A <sub>n</sub>	Surface area of embryo Q <sub>n</sub> (p. 18).
ASTM	American Society for Testing Materials.
B	Constant governing the relation between alumina content and its influence on nucleation kinetics of a BaO <sub>2</sub> SiO <sub>2</sub> glass (p. 91).
	Constant in electric field equations ( $= \frac{16\pi\sigma^3}{3kT}$ p.148)
	Bottom disc in electric field experiment.
	Constant in surface nucleation model of crystal growth (p. 35).
	Half width of spot on SAD (p. 127).

BS <sub>2</sub>	BaO <sub>2</sub> SiO <sub>2</sub>
B <sub>3</sub> S <sub>5</sub>	3BaO <sub>5</sub> SiO <sub>2</sub>
B <sub>5</sub> S <sub>8</sub>	5BaO <sub>8</sub> SiO <sub>2</sub>
B <sub>2</sub> S <sub>3</sub>	2BaO <sub>3</sub> SiO <sub>2</sub>
BS	BaOSiO <sub>2</sub>
B <sub>2</sub> S	2BaOSiO <sub>2</sub>
C	Constant defining particle shape in equation (5.1) used to evaluate $N_v$ (For sphere $C = 2/\pi$ ; p. 71).
°C	°Centigrade
C <sub>0</sub>	Equilibrium solubility of a particle of infinite radius (p. 39).
C <sub>r</sub>	Solubility of a particle radius r (p. 39).
D	Diffusion coefficient
$\bar{D}_v$	Mean perpendicular distance between tangent planes to particles whose numbers are under investigation (p.70-71).
$\bar{D}_{v_i}$	Mean value of $D_v$ for particles in size interval i (p. 71).
DTA	Differential thermal analysis
E	Electric field strength
E <sub>C</sub>	Critical field strength required to increase or decrease the nucleation rate by e times.
E <sub>AB</sub> , E <sub>BC</sub> , E <sub>AC</sub>	Energy of bonds between atoms AB, BC, AC respectively. (p. 9).
EHT	Extra high tension
G	Gibbs free energy.
G <sup>α</sup>	Gibbs free energy of phase α (p. 6).
G <sub>crystal</sub> and G <sub>liquid</sub>	Free energy (per mole* <sup>1</sup> ) of crystal and liquid respectively (p. 15).
ΔG	Thermodynamic driving force for crystal nucleation and growth (defined as the change in Gibbs free energy per mole* <sup>1</sup> of solid phase when a solid phase is formed in a liquid, neglecting any interfacial free energy contributions)

$\Delta G_D$	The kinetic barrier to crystal nucleation, (defined as the diffusion activation free energy per mole or molecule for motion across the matrix-embryo or matrix-nucleus interface).
$\Delta G_D'$	Kinetic barrier to crystal growth (defined as the diffusion activation free energy per mole or molecule for crystal growth).
$\Delta mG$	Free energy of mixing of a solution (defined as the difference between the free energies of a solution and the unmixed components).
$\Delta G_V$	Volume free energy change during crystal nucleation and growth (i.e. $\Delta G/V_M$ ).
H	Enthalpy
$\Delta H$	Enthalpy of fusion per mole or molecule of a solid phase.
$\Delta H_D'$	Activation enthalpy of crystal growth (p. 33).
$\Delta mH$	Enthalpy of mixing of a solution (defined similar to $\Delta mG$ ).
$\Delta H_\tau$	Induction time activation enthalpy
Hz	Hertz (measures frequency)
I	Nucleation rate
$I_h$	Heterogeneous nucleation rate (p. 32).
$I_o$	Steady state nucleation rate. Nucleation rate in the absence of an electric field (p. 148).
t	Nucleation rate at time t.
$K'$	Constant (p. 27)
$^\circ K$	$^\circ$ Kelvin
L	Length from objective lens to SAD pattern (p. 96).
M	Middle disc in electric field experiment
N	Avogadro's Number Number of molecules or atoms in the system (p. 18).

$N^*$	Number of critically sized embryos in Volmer-Weber embryo distribution (p. 18-19).
$N_A$	Number of particles intersected per unit area.
$N_{A_i}$	Number of particles in size class $i$ .
$N_L$	Number of intersections of a test line with interfaces between phases (used to calculate $S_v$ , p. 73-74).
$N_n$	Number of $Q_n$ embryo in the Volmer-Weber embryo distribution (p. 18).
$N_s$	Number of contacting molecules of matrix at the surface of a heterogeneity.
$N_v$	Number of crystalline nuclei in a glass
$P$	Total number of counts needed to attain a defined degree of accuracy (p. 73).
$Q$	Embryo
$Q_c$	Critically sized embryo
$Q_n$	Embryo of size $n$
$R$	Universal gas constant Resistance General symbol for alkali metal
$R'$	Rate of change of $Q_n$ the number of $Q_n$ embryos to $Q_{n+1}$ embryos (p. 18).
$R_g$	Resistance of glass (p. 155).
$S$	Entropy, also dimension of a crystal (p. 36).
$\Delta S_D'$	Activation entropy of crystal growth (p. 33).
$\Delta mS$	Entropy of mixing of a solution (defined similar to $\Delta mG$ ).
SAD	Selected area diffraction
SE	Standard error (used to calculate statistical error, see Appendix 5.2).

$S_v$	Surface area between phases in a phase separated glass.
$T$	Top disc in electric field experiment Temperature
$\Delta T$	$T_L - T$ or undercooling (defined as the supercooling below the melting point or liquidus temperature).
$T_c$	Consolute temperature.
$T_g$	Glass transformation temperature (referred to as 'DTA $T_g$ ' when determined by DTA).
$T_H$	Phase separation temperature, prior to nucleation heat treatment.
$T_L$	Liquidus temperature
$T_M$	Immiscibility temperature (also known as the miscibility or binodal temperature).
$T_M'$	Equilibrium melting temperature of a phase.
$T_{max}$	Temperature corresponding to maximum crystal nucleation temperature.
$T_N$	Nucleation temperature
$T_S$	Spinodal temperature
TBS <sub>2</sub>	A glass, mol% 1TiO <sub>2</sub> , 66SiO <sub>2</sub> , 33BaO
$U_R$	Reduced growth rate (p. 37).
$V$	Voltage or volts or potential difference (p.d.).
$V_\rho$	Volume of phase $\beta$
$V_f$	Volume fraction of a phase in a phase separated glass
$V_K$	Potential difference across Keithley (p. 154-155).
$V_L$	Molar volume of parent glass (p. 22).
$V_M$	Molar volume of a phase (p. 22).
$V_T$	Potential difference across Keithley and glass (p.155).

$W$ or $W_0$	Total free energy change for the formation of a cluster or embryo (including interfacial free energy contributions).
$W^*$	Total free energy change for the formation of a critical nucleus.
$W_{het}^*$	Thermodynamic barrier of heterogeneous nucleation.
$W_E$	Contribution of an electric field to the free energy of formation of a cluster or embryo ( $-\frac{\epsilon m f(\lambda) E^2 r^3}{2}$ ) p. 146).
$W_n$	Free energy change (including surface energy contributions) involved in forming a $Q_n$ embryo (p. 18).
$\chi, x$	Mole fraction
$\chi_i, x_i$	Mole fraction of the 'i'th component.
$y_A$	Mole fraction of $Al_2O_3$ (p. 91).
$Z$	Number of nearest neighbours surrounding each atom. Also defined to be the reciprocal of the intersection diameter of particles on a plane section under consideration (used to calculate $N_v$ , p. 71). Also refers to number of embryos in Becker-Doring embryo distribution.
$Z^*$	Number of $Q_c$ embryos in Becker-Doring embryo distribution.

### Small Roman Characters

$a_A$	Activity of A in solution with respect to the pure component.
a.c.	Alternating current.
$a_\lambda$	Growth coefficient (p. 36).
b	Constant
c	Number of components

d	Interplanar distance of the planes responsible for a spot on a SAD pattern or a peak on a X-ray diffractogram.
d.c.	Direct current.
e	Universal constant (= 2.71828)
f	Active site fraction factor in screw dislocation crystal growth model.
f( $\lambda$ )	Function of $\lambda$ ( $\frac{1-\lambda}{2+\lambda}$ , p.146)
f( $\theta$ )	Function of $\theta$
$\Delta g$	Thermodynamic driving force for liquid-liquid immiscibility (defined similar to $\Delta G$ ).
h	Planck's Constant Constant in electric field equations (= $\frac{-3\epsilon m f(\lambda)}{8\pi}$ p. 147)
i	Current flowing through glass and Keithley (p. 155).
k	Boltzmann's Constant.
$k_s$	Crystal shape factor (p. 28).
kv	Kilovolt
l	Length of glass (p. 157).
$n_v$	Number of liquid droplets in a phase separated glass.
r	Radius of cluster embryo or nucleus. Distance separating a diffracted spot from the central spot in a SAD pattern (p. 61).
$\bar{r}_0$	Mean radius of a particle at onset of coarsening (p. 39).
r	Radius of a critical nucleus.
r'	Average distance between interfacial boundaries.
s	Crystal dimension (radius of sphere or cylinder or half-width of plate) (p. 36).
t	Time

$\bar{t}$	Mean time to build radius of a cluster to the critical size.
$t'$	Crystal thickness, radii of spherulite.
$u$	Crystal growth rate
$u_R$	Reduced growth rate (p. 37).
$X_i, x_i$	Mole fraction of 'i'th component
$x$	Mole fraction of multimer (p. 11).
$\bar{x}$	Fractional concentration of a immiscible liquid (p. 11).
$x'$	Mole fraction of mixed oxide.
$y$	Mole fraction of multimer (p. 11).
$\bar{y}$	Fractional concentration of a immiscible liquid (p. 11).
$y'$	Mole fraction of mixed oxide.

#### Greek characters

$\alpha$	Shape factor (p. 27). Factor relating $\Delta mH$ and composition in regular solutions (p. 9).
$\mu$	Chemical potential.
$\mu_i$	Chemical potential of 'i'th component.
$\eta$	Viscosity
$\Lambda$	Correlation length (related to the average distance between boundaries $\bar{r}'$ ) (p. 40).
$\lambda$	$\epsilon_c/\epsilon_m$ (p. 146) Jump distance (p. 32-33). Wavelength of X-ray and electron beam
$\nu$	Jump or vibration frequency of atoms or molecules facing an interface (p. 32-33).
$\epsilon_c$	Dielectric permittivity of precipitating crystal.

$\epsilon_m$	Dielectric permittivity of parent glass
$\chi$	Electrical conductivity
$\rho$	Electrical resistivity
$\Omega$	Ohm (measure of resistance)
$M\Omega$	Megaohms
$\theta$	Contact angle in heterogeneous nucleation Also X-ray diffraction and electron diffraction angle equals $2\theta$ .
$\sigma$	Standard deviation of data (usually $V_f, S_v, N_v, n_v$ ). The standard deviation was used to estimate the statistical error (Appendix 5.2). Surface or interfacial energy
$\sigma_\infty$	Macroscopic surface energy
$\sigma_{\alpha\beta}, \sigma_{\beta\gamma}, \sigma_{\alpha\gamma}$	Surface energy of $\alpha$ - $\beta$ , $\beta$ - $\gamma$ , $\alpha$ - $\gamma$ interfaces.
$\bar{\sigma}$	Average surface energy
$\tau, \tau_1, \tau_2$	Intercept or induction time in nucleation.
$\tau_1$	Crystal growth induction time.

**CHAPTER ONE**

**GENERAL INTRODUCTION**

## CHAPTER ONE - GENERAL INTRODUCTION

	<u>Page</u>
1.1 Introduction	1
1.2 Aims of the project	3
1.3 The baria-silica glass forming system	4
1.4 Plan of the thesis	5

## 1.1 INTRODUCTION

In the 1950's S.D. Stookey at the Corning Glass Works crystallized glasses under controlled conditions and produced what are now known as glass ceramics<sup>(1)</sup>. The internal structure of these materials consisted of numerous small randomly orientated crystals and their properties, such as mechanical strength, chemical durability, electrical resistivity and thermal expansion were often greatly improved compared with the original glasses. As a consequence glass ceramics have increased in importance for industrial and domestic applications. Examples are cooking ware, telescope mirror blanks, printed circuit boards and reactor control rods<sup>(2-5)</sup>.

The controlled crystallization of glasses involves a two stage heat treatment: a) at a nucleation temperature that encourages the formation of many small crystals, and b) at a higher temperature, usually where nucleation is negligible, but where the crystals are grown until crystallization is complete. The most effective nucleation temperature is usually just above the glass transformation temperature  $T_g$ , the latter defining the minimum temperature limit where structural relaxation can still occur. As  $T_g$  is approached the relaxation and nucleation become exceedingly slow and the excessive nucleation time required will greatly add to the expense of crystallizing the glass. The growth temperature must satisfy a balance between the demands of rapid crystallization and the occurrence of article distortion at high temperatures.

Changes in the heat treatment process can alter the initial micro-structure and produce glass ceramics having different properties. The wide range of glass forming systems available for controlled crystallization enables the manufacture of a large number of different types of glass ceramics covering a wide diversity of properties. In fact it is possible to engineer a glass ceramic with a required property, such as thermal

expansion coefficient, by a careful control of the overall composition and an accurate monitoring of the heat treatment process.

The type of nucleation where crystals form at interfaces of particles or inclusions within the glass, is known as heterogeneous. When crystals form internally without such aid they are said to nucleate homogeneously. In glasses where homogeneous nucleation does not readily occur, catalysts have to be introduced to produce numerous internal sites within the glass where crystals can heterogeneously nucleate. Thus heterogeneous nucleation is often of great importance in the successful production of glass ceramics. The variety of nucleation catalysts is very large and includes, for example, metals (e.g. Pt, Cu, Ag, Au); oxides (e.g. TiO<sub>2</sub>, P<sub>2</sub>O<sub>5</sub>, ZrO<sub>2</sub>) and halides (e.g. NaF, Na<sub>3</sub>AlF<sub>6</sub>, CaF<sub>2</sub>)<sup>(2,3)</sup>.

The role of these nucleating catalysts has been studied extensively. In the case of metallic agents, metal particles of colloidal dimensions precipitate in the glass and grow sufficiently large to act as heterogeneous nucleation sites for the precipitation of major crystalline phases. This method was employed by Stookey in forming the first satisfactory glass ceramics.

The oxide catalysts are thought to have two main actions, either to a) cause the precipitation of very fine crystals of the particular oxide or a compound containing the oxide, which subsequently heterogeneously nucleate the major crystalline phases, or to b) cause a reduction in the crystal-liquid interfacial energy and thus increase the nucleation rate of the major phases. In some cases these oxides also promote liquid-liquid phase separation, either on cooling from the melt or during the early stages of heat treatment, and this phase separation may play a part in the crystal nucleation mechanism.

The role of liquid-liquid phase separation in influencing crystal nucleation is still open to question. It is thought by some workers<sup>(6,7)</sup>

that the creation of interfaces or compositional zones adjacent to the interfaces by liquid immiscibility could enhance nucleation. Others believe that the local changes in glass composition caused by liquid-liquid phase separation can increase or decrease the thermodynamic driving force for crystallization<sup>(8,9)</sup>. All of these mechanisms may contribute towards the increase of nucleation rates in glasses.

Recently a modest electric field was observed to enhance the nucleation of liquid droplets in a cordierite based glass composition<sup>(10)</sup>. This observation is of obvious significance for the glass ceramic process where rapid crystal nucleation is desirable. A theoretical analysis based on the free energy changes induced by electric fields has shown that under certain circumstances nucleation rates can be altered<sup>(11)</sup>.

## 1.2 AIMS OF THE PROJECT

In the first part of the work, experiments were designed to discover whether liquid immiscibility played an important role in influencing crystal nucleation and growth in the BaO-SiO<sub>2</sub> glass-forming system. In particular, attempts were made to understand how the kinetics of crystal nucleation and growth were influenced by liquid-liquid immiscibility. Also, the morphology and crystallography of early stage growth of BaO<sub>2</sub>SiO<sub>2</sub> crystals were studied and compared with recent theories of crystal growth mechanisms.

In the latter part of the work, the nucleation and growth characteristics of BaO-SiO<sub>2</sub> glasses subjected to electric fields were studied quantitatively. The modifications of Isard<sup>(12)</sup> to Kaschiev's theory of field induced nucleation were employed in a calculation of the theoretical critical field strength required to alter the crystal nucleation rate. These results allowed a prediction of the potential influence of electric fields on the controlled crystallization processes to be made.

### 1.3 THE BARIUM-SILICA GLASS FORMING SYSTEM

In this system various investigations have been made of the phase diagram, of liquid-liquid immiscibility and crystallization<sup>(13-17)</sup>. Recently a detailed study was made of the kinetics of nucleation and growth for the barium disilicate composition<sup>(18)</sup>.

The work in the thesis provides information on compositions in the BaO-SiO<sub>2</sub> system for which the nucleation and crystal growth kinetics have not been previously studied in detail.

The BaO-SiO<sub>2</sub> system was chosen for investigation for the following reasons:

a) The system exhibits internal crystal nucleation without the deliberate additions of nucleation catalysts, hence simplifying the interpretation of the results.

b) A large zone of metastable liquid immiscibility exists from approximately 70 to 100 mol% SiO<sub>2</sub> in this system (see Figure 1.1).

c) Glass formation extends from 0 to about 40 mol% BaO. Within this range several stable compounds occur, (see Figure 1.1). Compositions containing less than about 24 mol% BaO liquid phase separate very rapidly on quenching from the melt and too rapidly for convenient study. However, compositions between 24 and 40 mol% BaO can crystallize and/or phase separate under controlled conditions. Thus it was convenient to prepare glasses in this range for the experiments.

d) The electrical resistivity of these glasses is sufficiently high to support considerable electric fields without significant joule heating.

It is hoped that accumulation of information in the relatively simple systems, such as BaO-SiO<sub>2</sub>, may lead to a better understanding of the formation of glass ceramics in more complicated and commercially important systems and ultimately to improvements in the whole glass ceramic process.

Figure 1.1 The phase diagram of a section of the baria-silica system. The dashed line denotes the liquid-liquid immiscibility boundary.

Liquidus data, ref (13)

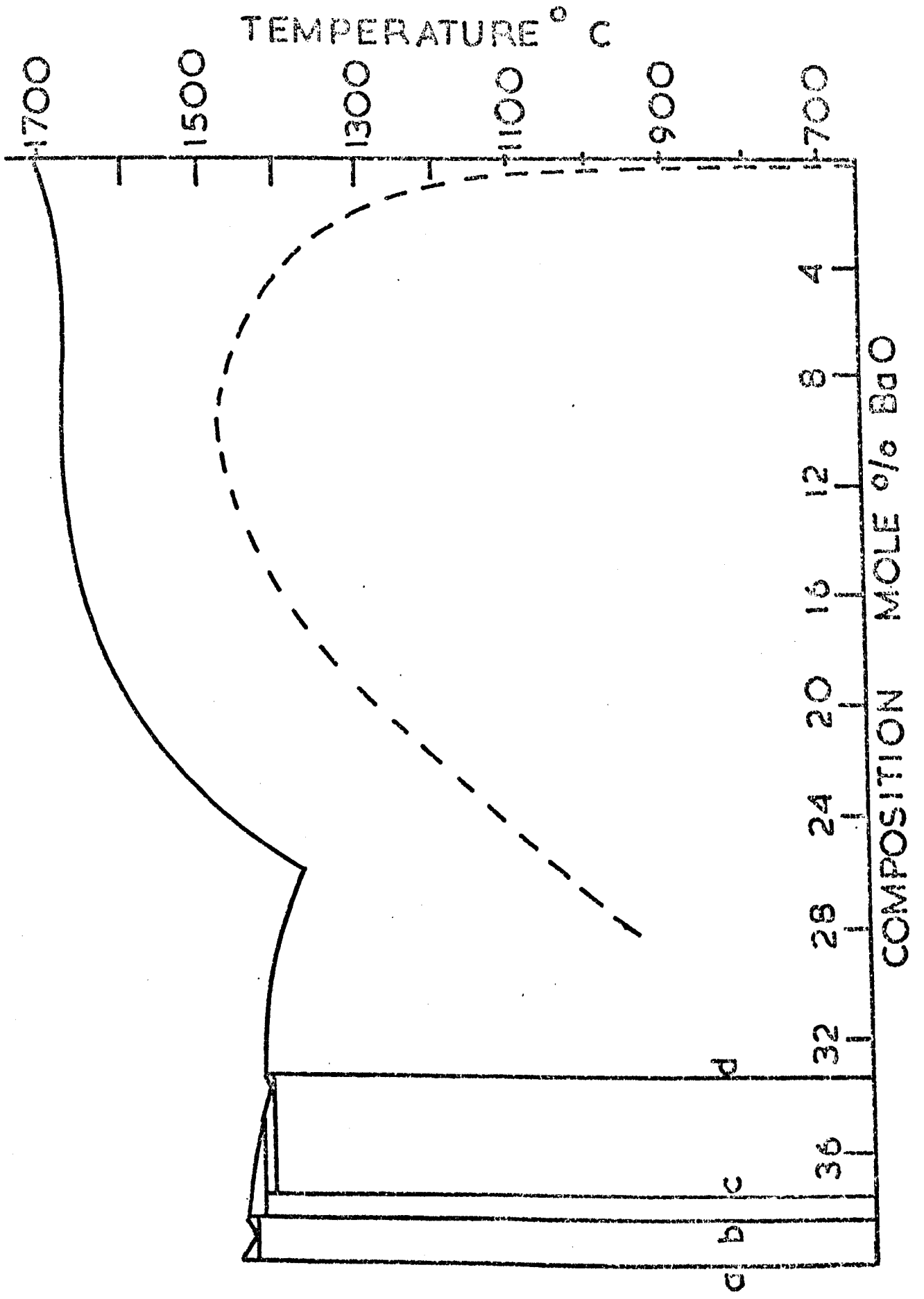
Immiscibility data, ref (14)

a,  $2\text{BaO}3\text{SiO}_2$

b,  $5\text{BaO}8\text{SiO}_2$

c,  $3\text{BaO}5\text{SiO}_2$

d,  $\text{BaO}2\text{SiO}_2$



#### 1.4 PLAN OF THE THESIS

In Chapter Two the derivation of phase diagrams from free energy functions is outlined. Some important solution models are considered and the origin of liquid immiscibility and its relation to free energy diagrams is discussed.

The theories of phase transformations in terms of nucleation, growth and coarsening are covered in Chapter Three. The results of experiments designed to test the applicability of the theories to glasses are described.

The effect of liquid-liquid immiscibility on crystal nucleation kinetics is briefly considered, theoretically in Chapter Four. A literature survey of the experimental results of previous work is presented.

The general experimental procedures are described in Chapter Five.

In Chapter Six results for the kinetics of crystal nucleation and the effects of liquid-liquid immiscibility are presented and discussed.

In Chapter Seven the crystal growth kinetics results are presented and the effects of liquid-liquid immiscibility assessed. Also, the electron microscopic study of the early stages of crystal growth is discussed. The mechanism of spherulitic growth in the glasses is considered.

In Chapter Eight experiments to study the effects of electric fields on crystal nucleation and growth are described. The results are discussed in relation to Kaschiev's theory of field induced nucleation and the modification of Isard to this theory.

The final chapter contains a summary of the main conclusions and suggestions for future work.

**CHAPTER TWO**

**LIQUID-LIQUID IMMISCIBILITY IN GLASS-  
FORMING SYSTEMS**

CHAPTER TWO - LIQUID-LIQUID IMMISCIBILITY IN GLASS-FORMING SYSTEMS

	<u>Page</u>
2.1 Thermodynamic derivation of phase diagrams	6
2.2 Simple solution models and liquid-liquid immiscibility	7
2.3 Other solution models	12
2.4 The phase diagram of baria-silica	13

## 2.1 THERMODYNAMIC DERIVATION OF PHASE DIAGRAMS

The conditions for phase equilibria are most conveniently described by the use of the Gibbs free energy function  $G$ . First, consider a system subject to no external forces except hydrostatic pressure, and in which the energy due to interfaces is negligible. From standard thermodynamic treatments<sup>(19)</sup> the Gibbs free energy of a phase  $\alpha$  is given by:

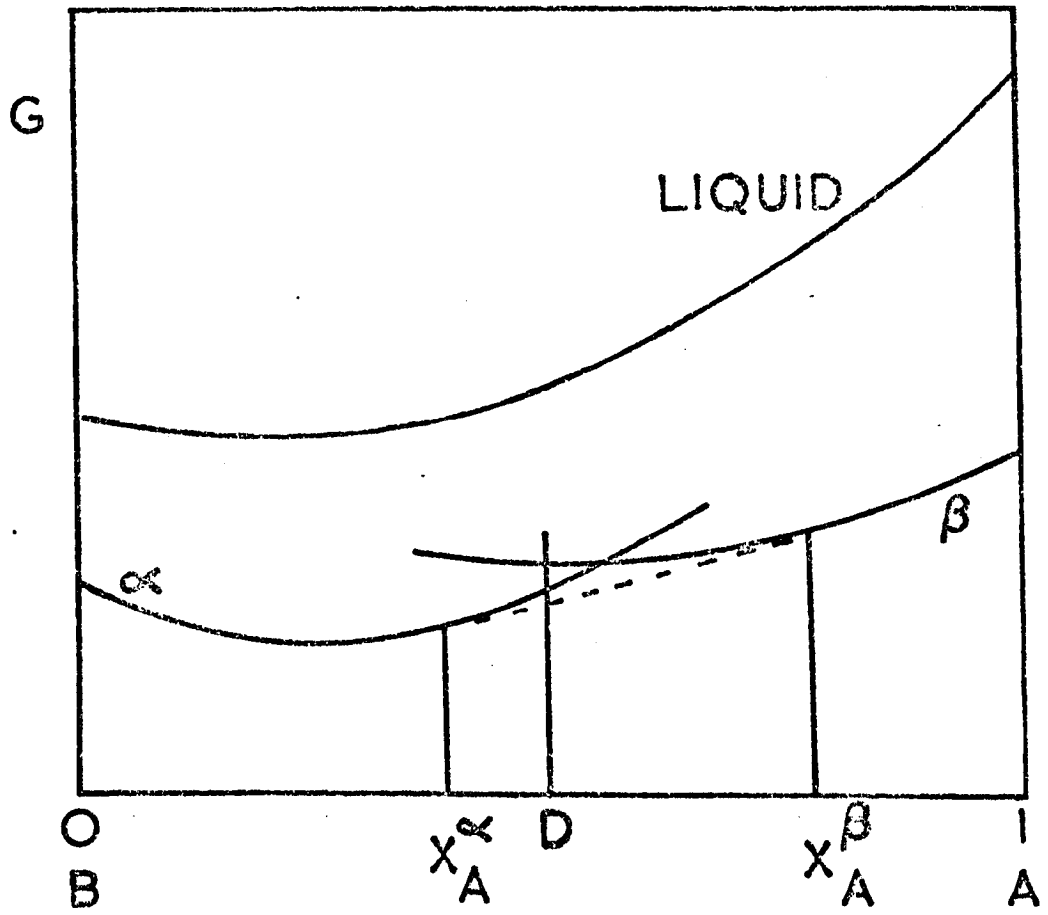
$$G^\alpha = \sum_{i=1}^C \mu_i^\alpha x_i^\alpha \quad (2.1)$$

where  $C$  is the number of components,  $\mu_i^\alpha$  is the chemical potential of the 'ith' component and  $x_i^\alpha$  is the mole fraction of the 'ith' component.

An important criterion for equilibrium is that the Gibbs free energy in equation (2.1) is a minimum at constant temperature, pressure and composition. At equilibrium (pressure and temperature being constant) all components are distributed among the different phases in such a way that the total free energy is a minimum.

If the pressure on the system is constant, the free energies of the phases are functions of  $T$  and  $x$  that can be expressed as surfaces in an isobaric  $T, G$  and  $x$  space. From these surfaces an equilibrium surface corresponding to minimum free energy may be determined. Figure (2.1) shows how such a surface can be constructed from a knowledge of the free energy functions for two solid solution phases  $\alpha$  and  $\beta$  and a liquid phase for a given temperature. At this temperature the liquid phase cannot exist at equilibrium. When  $0 < x < x_A^\alpha$  the phase  $\alpha$  exists solely at equilibrium because this phase provides the lowest free energy. Similarly, when  $x_A^\beta < x < 1$ ,  $\beta$  is the only phase present. However, at compositions  $x_A^\alpha < x < x_A^\beta$  the total free energy can be lowered to values indicated by the common tangent if  $\alpha$  and  $\beta$  coexist. The compositions of the phases in

Figure 2.1 Isothermal cut through a free energy surface (G) for a two-component system.  $\alpha$  and  $\beta$  denote two solid solution phases,  $X_A$  is the mole fraction of A.



equilibrium are given by the common tangent to the  $\alpha$  and  $\beta$  free energy curves i.e.  $x_A^\alpha, x_A^\beta$ . The proportion of each phase is calculated by the Lever Rule, i.e. for composition  $x = D$ , the molar ratio of phase  $\alpha$  to phase  $\beta$  is:

$$\frac{x_A^\beta - D}{D - x_A^\alpha}$$

The common tangent construction to the free energy curves of the various phases, as the temperature is altered, will outline the composition boundaries of the two phase coexistence area at constant pressure on the phase diagram. Figure (2.2) shows how this can be done for a hypothetical binary eutectic system.

The liquidus and solidus compositions are fixed by common tangent intersections between the liquid free energy curves and the stable solid composition curves. The variation of these intersections as a function of temperature traces the liquidus and solidus curves on the phase diagram.

## 2.2 SIMPLE SOLUTION MODELS AND LIQUID-LIQUID IMMISCIBILITY

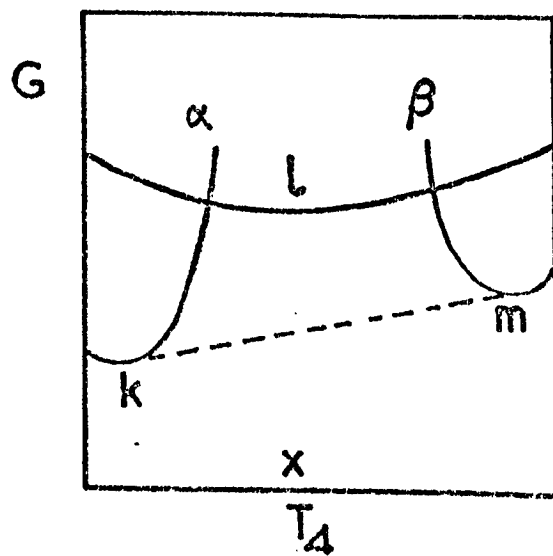
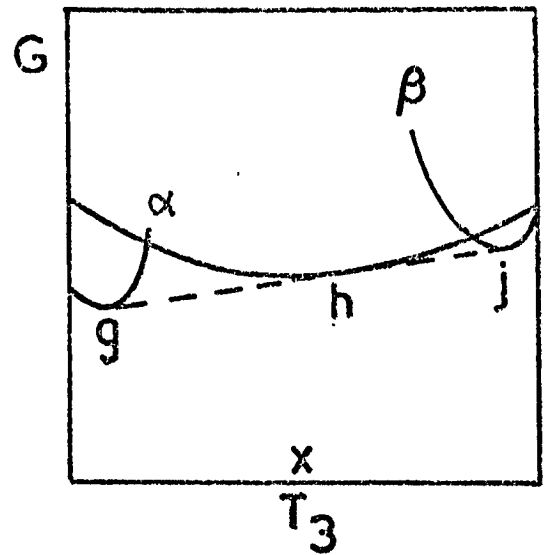
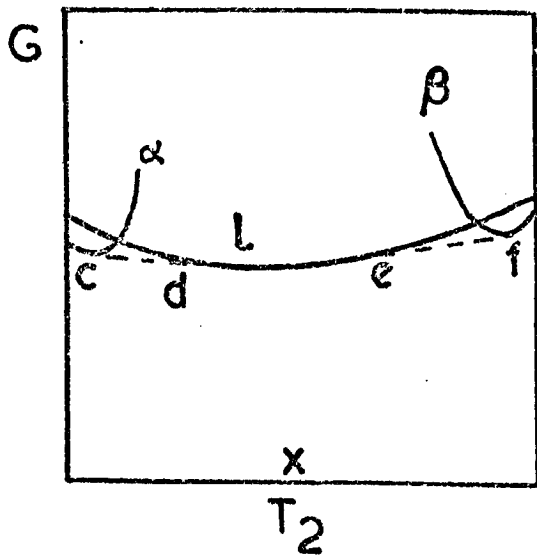
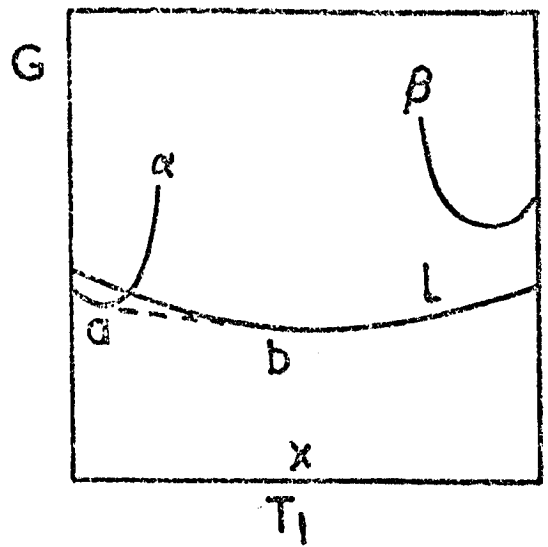
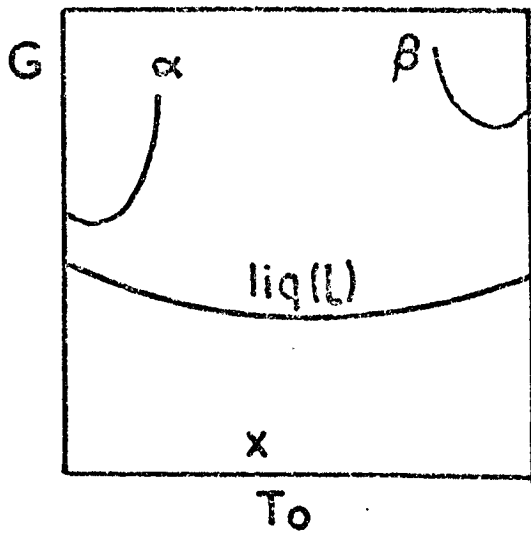
The free energy of mixing  $\Delta_m G$  of a homogeneous solution is defined as the difference between the free energies of the solution and unmixed components. Entropy  $\Delta_m S$  and enthalpy  $\Delta_m H$  of mixing are defined similarly.

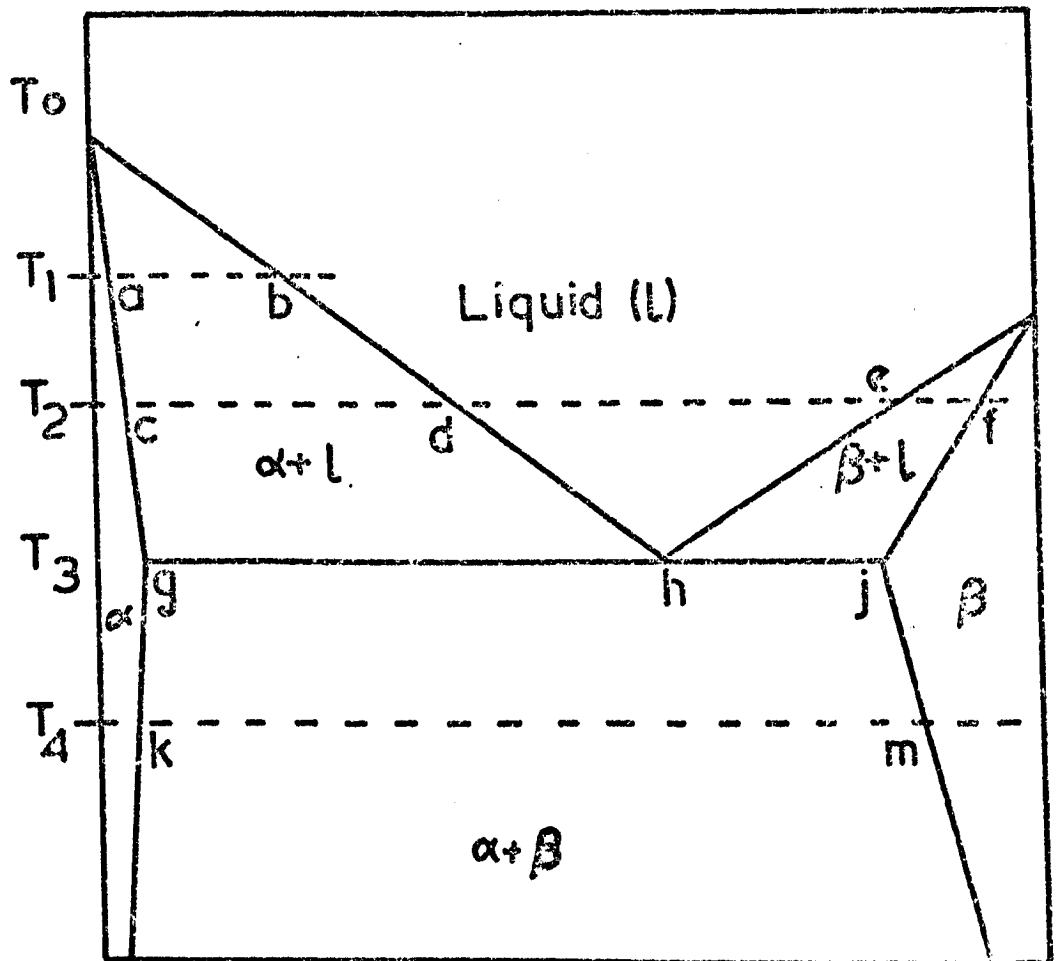
If the solution consists of atoms A and B randomly mixed on a regular lattice, from statistical considerations it can be shown<sup>(20)</sup> that:

$$\Delta_m S = -R[x_A \ln x_A + (1 - x_A) \ln(1 - x_A)]$$

In an ideal solution the enthalpy of mixing is:

**Figure 2.2** Schematic free energy (G) diagrams and  
(two pages) their relation to a hypothetical binary  
eutectic phase diagram.  $\alpha$  and  $\beta$  denote  
two solid solution phases.





$$\Delta_m H = 0$$

and 
$$\Delta_m G = RT[x_A \ln x_A + (1 - x_A) \ln(1 - x_A)] \quad (2.2)$$

where R is the gas constant and  $x_A$  is the mole fraction of A. From equation (2.2)  $\Delta_m G$  is always negative and is plotted in Figure (2.3).

More generally, for non ideal solutions<sup>(21)</sup>:

$$\Delta_m G = RT[x_A \ln a_A + x_B \ln a_B] \quad (2.3)$$

where  $a_A$  and  $a_B$  are the activities of A and B in solution with respect to the pure components. Raoult's Law is valid in an ideal solution:

$$a_A = x_A$$

So equation (2.3) reduces to (2.2).

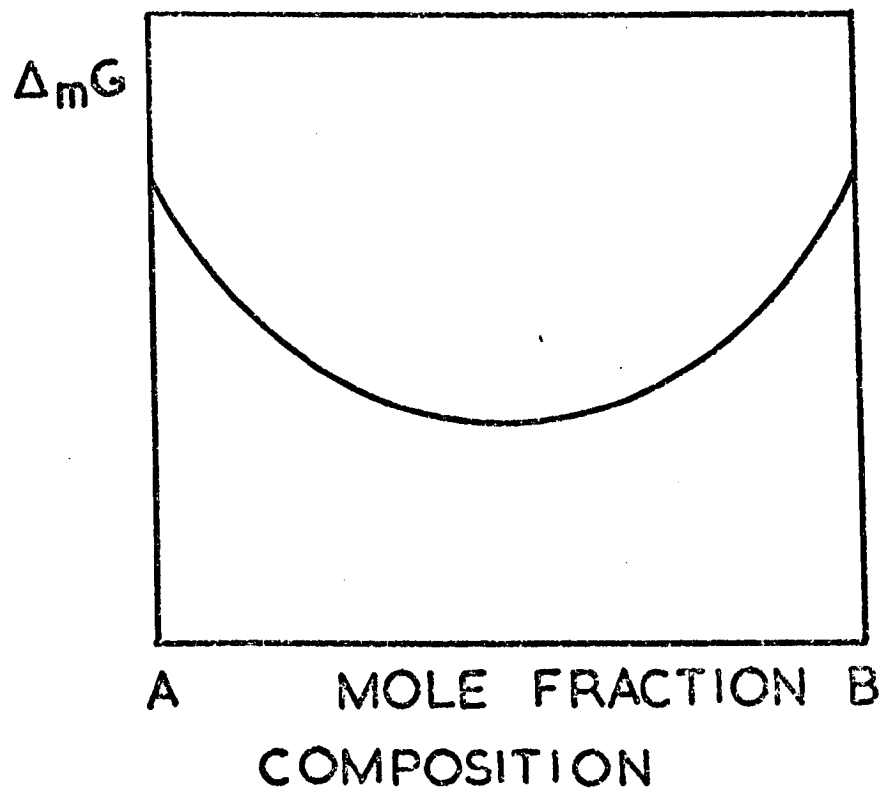
The ideal solution model predicts accurately the behaviour of some liquid solutions but cannot explain the ability of systems to undergo liquid immiscibility. The regular solution model, proposed by Hildebrand,<sup>(22)</sup> has had much greater success in this direction. This model assumes that:

$$\Delta_m S = \Delta_m S (\text{ideal})$$

From simple considerations the enthalpy of mixing is given as:

$$\Delta_m H = \alpha x_A (1 - x_A)$$

**Figure 2.3** Schematic plot of free energy of mixing ( $\Delta_m G$ ) versus composition for an ideal solution.



where  $\alpha = NZ[E_{AB} - \frac{1}{2}(E_{AA} + E_{BB})]$

where  $E_{AA}$ ,  $E_{BB}$  and  $E_{AB}$  are the energies of the various bonds between the atoms,  $Z$  is the number of nearest neighbours surrounding each atom and  $N$  is Avogadro's Number. Plots of  $-T\Delta_m S$ ,  $\Delta_m H$  and  $\Delta_m G$  against composition for regular solutions are shown in Figure (2.4).

Depending on the sign of  $\Delta_m H$ , the curve  $\Delta_m G$  versus composition may have one minimum or two minima and one maximum. A solution within the minimas will divide into two phases whose compositions are given by the common tangent construction. The locus of the two minimas as a function of temperature forms the binodal and similarly the locus of the inflexion points traces out the spinodal. The equation of the binodal and its dependence on temperature is calculated by differentiating the  $\Delta_m G$  equation with respect to composition, setting the resulting equation to zero and solving for  $T$ :

$$T_m = \frac{\alpha(2x_A - 1)}{R[\ln(x_A/1 - x_A)]}$$

The curve of  $T_m$ , the miscibility temperature, against composition is shown to be symmetrical in Figure (2.5). Similarly the curve of the spinodal can be estimated by equating the differential  $(-\frac{d^2\Delta_m G}{dx^2})$  to zero and solving for  $T$ :

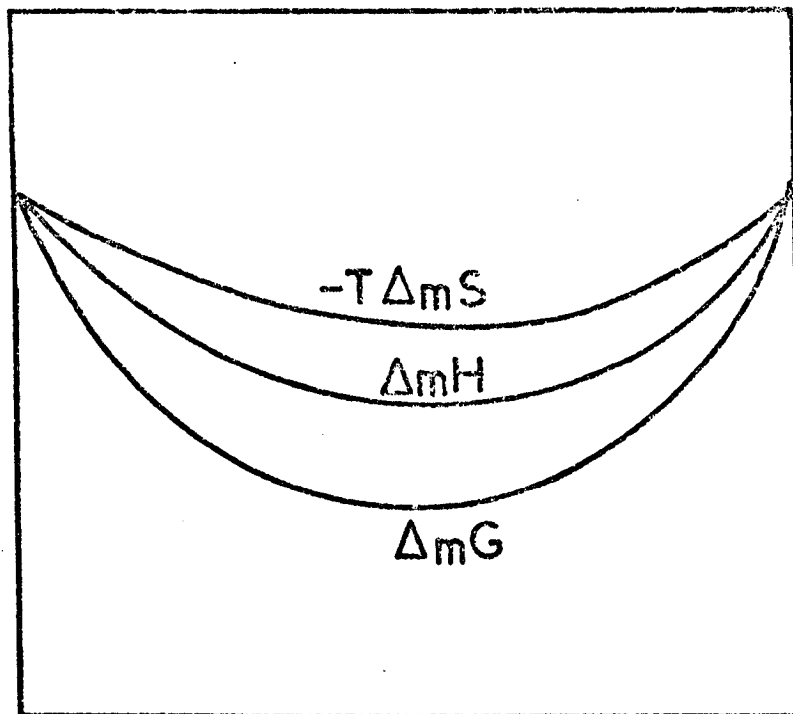
$$T_s = \frac{2\alpha x_A(1 - x_A)}{R}$$

The spinodal and binodal are symmetrical about  $x_A = 0.5$  and coincide with each other at the consolute temperature  $T_c$ . This leads to the simple relation between  $\alpha$  and  $T_c$ :

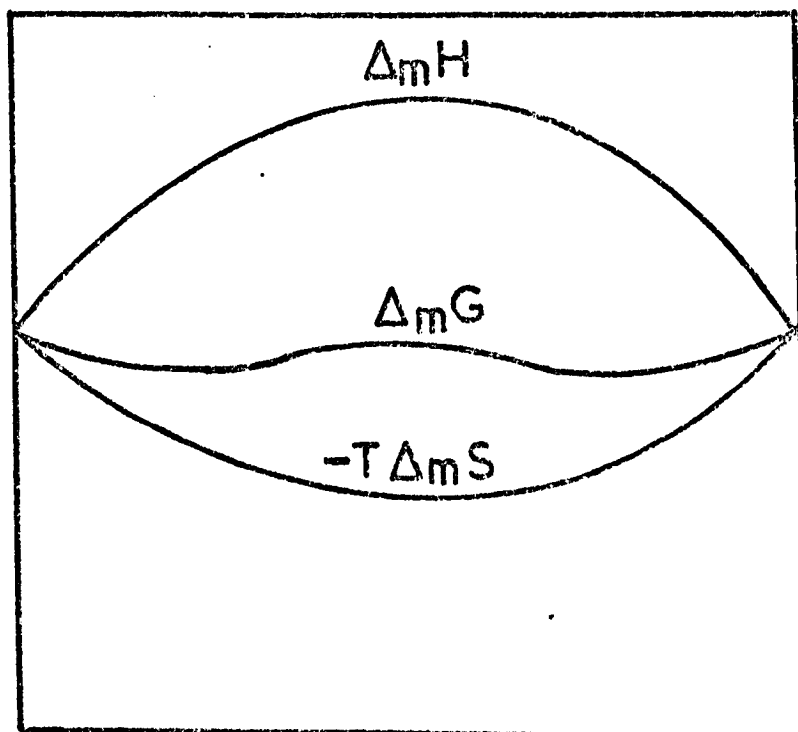
Figure 2.4 Schematic diagrams of  $-T \Delta mS$ ,  $\Delta mH$   
and  $\Delta mG$  versus composition:

top:  $E_{AB} < \frac{1}{2}(E_{AA} + E_{BB})$

bottom:  $E_{AB} > \frac{1}{2}(E_{AA} + E_{BB})$



MOLE FRACTION

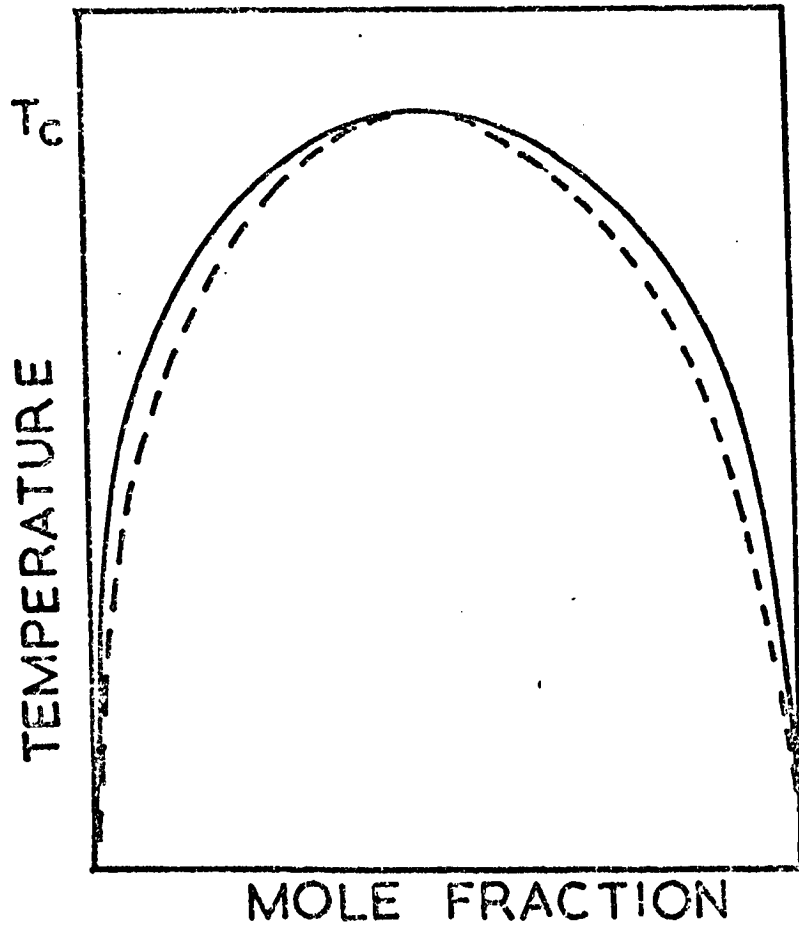


MOLE FRACTION

Figure 2.5 Schematic plot of binodal and spinodal temperature versus composition.

———— binodal temperature

----- spinodal temperature



$$\alpha = 2RT_c$$

When  $T_c$  occurs above the liquidus temperature in a given system, there is a region of stable immiscibility. Examples of glass-forming systems that exhibit stable immiscibility include silica with the following oxides<sup>(23)</sup>: MgO, FeO, NiO, ZnO, CaO, SrO, MnO and CoO.

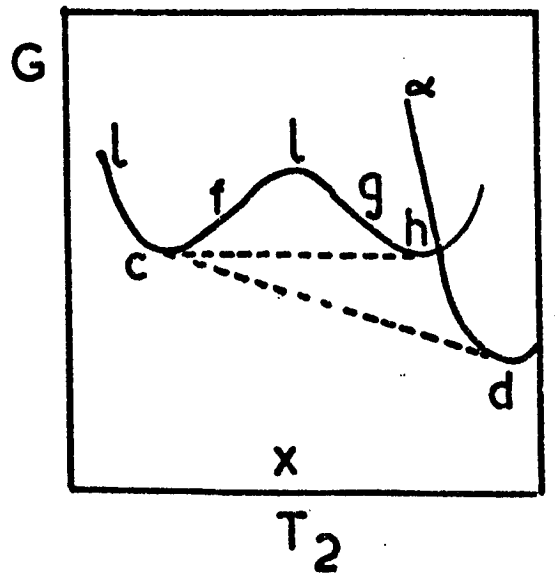
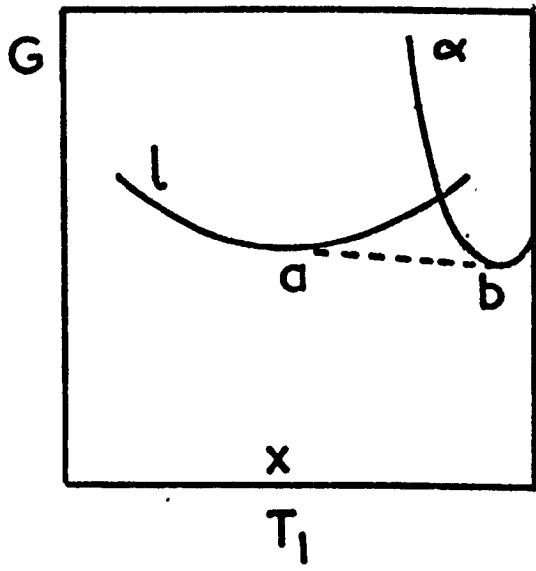
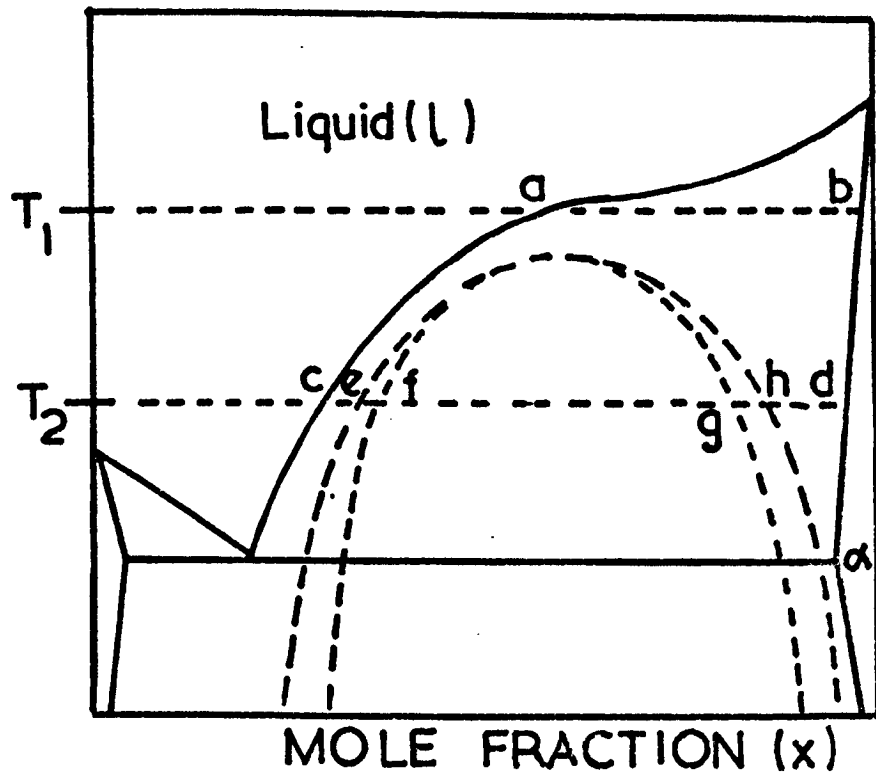
If  $T_c$  exists below the liquidus then metastable immiscibility can occur if the system fails to crystallize. The presence of the impending immiscibility dome imposes a significant inflexion on the liquidus curve. This is illustrated by the strongly sigmoidal liquidus curves in the  $\text{Li}_2\text{O-SiO}_2$  and  $\text{BaO-SiO}_2$  systems that both exhibit metastable immiscibility<sup>(24)</sup>.

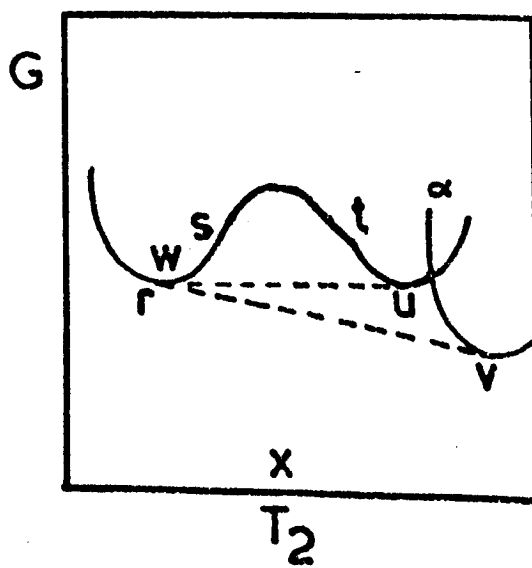
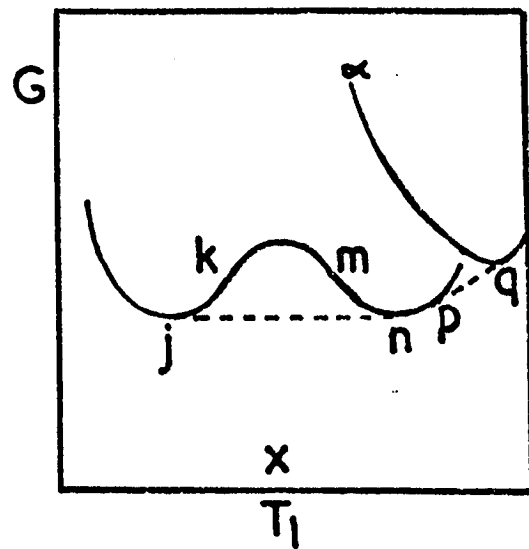
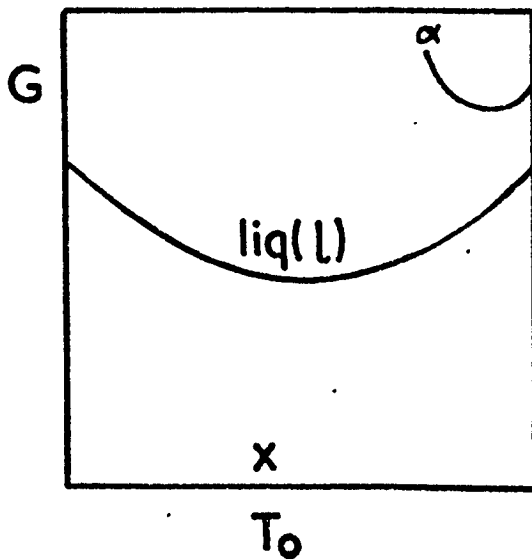
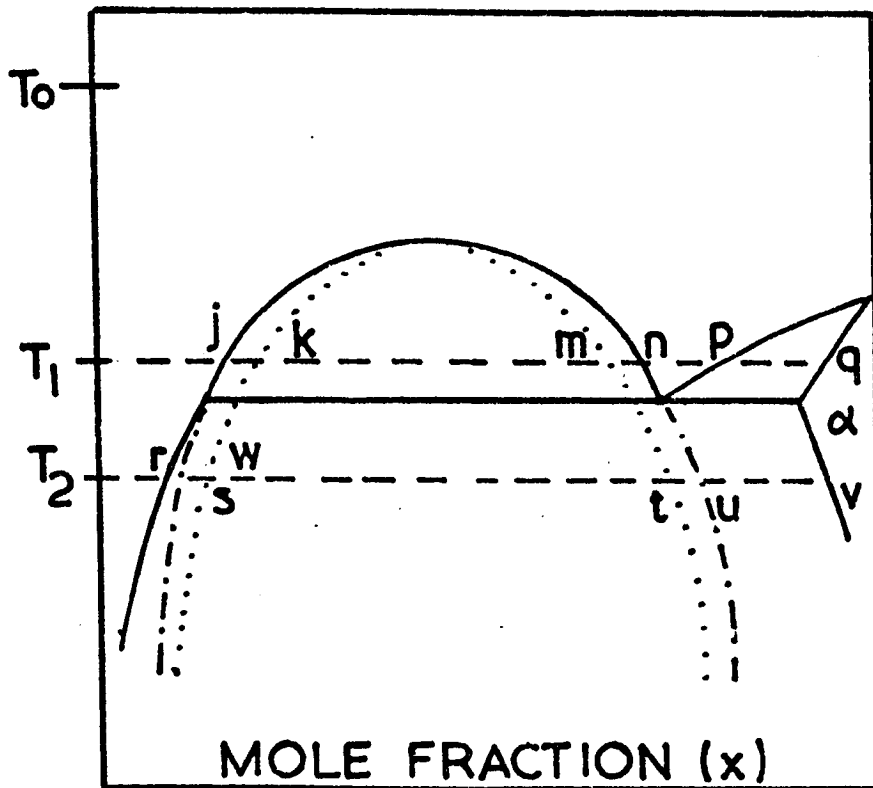
Schematic free energy curves for a glass-forming system exhibiting both metastable and stable phase separation are shown in Figure (2.6) taken from Cahn and Charles<sup>(25,24)</sup>.

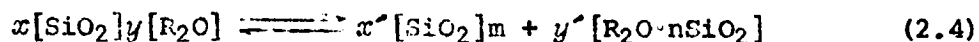
The regular solution model is useful in describing metal solutions where the assumption of random mixing of discrete atoms A and B implicit in this model is quite accurate, but for silicate solutions where a complicated three dimensional network of  $\text{SiO}_4$  tetrahedra exists, the liquid immiscibility and free energy data do not show the symmetrical features predicted. For example, in the binary-lithia and soda-silica systems the critical composition (corresponding to  $T_c$ ) occurs at a mole fraction of alkali oxide of about 0.1 rather than 0.5<sup>(26,27)</sup>.

Haller et al<sup>(28)</sup> have developed a model involving the regular mixing of polynomials or 'multimers' of  $(\text{SiO}_2)_m$  and  $\text{R}_2\text{O} \cdot n\text{SiO}_2$ . They selected appropriate values for  $m$ ,  $n$  and  $\Delta S$  (representing the additional entropy change due to changes in internal degrees of freedom of liquids on mixing) for  $\text{Li}_2\text{O-}$ ,  $\text{Na}_2\text{O-}$  and  $\text{BaO-SiO}_2$ . At the unmixing boundary the following process occurs in a homogeneous liquid:

**Figure 2.6**      **Schematic free energy (G) diagrams of**  
**(two pages)**      **two hypothetical binary systems**  
                         **exhibiting**  
                         **metastable liquid-liquid immiscibility**  
                         **(Facing page)**  
                         **stable liquid-liquid immiscibility**  
                         **(Following page)**







where  $x$  and  $y$  are the mole fractions of the mixed oxides and  $x'$ ,  $y'$  are the mole fractions of the multimers. From equation (2.4)

$$x = x'm + y'n$$

$$y = y'$$

The fractional concentrations of the immiscible liquids are denoted by  $\bar{x}$  and  $\bar{y}$  calculated according to:

$$\bar{y} = y' / (x' + y')$$

$$\bar{x} = x' / (x' + y')$$

Applying regular solution theory they obtained:

$$\frac{T_m}{T_c} = \left(2 + \frac{\Delta S}{R}\right) \left\{ \frac{1 - 2\bar{y}}{\ln[1 - \bar{y}]/\bar{y}] + (1 - 2\bar{y})\frac{\Delta S}{R}} \right\} \quad (2.5)$$

and

$$\frac{T_s}{T_c} = 2 \left(2 + \frac{\Delta S}{R}\right) \left\{ \frac{1}{1/[\bar{y}(1 - \bar{y})] + \frac{2\Delta S}{R}} \right\}$$

where  $T_m$  and  $T_s$  are the miscibility and spinodal temperatures respectively.

For  $\text{Li}_2\text{O-SiO}_2$  a good fit is obtained if  $m = 6$ ,  $n = 2$  and  $\Delta S = 1.2R$ . Similarly, the experimental data agrees well with the predicted data for  $\text{Na}_2\text{O-SiO}_2$  if  $m = 8$ ,  $n = 3$  and  $\Delta S = 0.3R$ .  $\text{BaO-SiO}_2$  results show reasonable correlation with the theory when  $m = 8$ ,  $n = 2$  and  $\Delta S = 0.3R$ . The lowest

common denominator of the silica multimer in the three systems is  $(\text{SiO}_2)_{24}$ , and it would be an interesting sequel to these calculations if the existence of such a multimer could be proved.

### 2.3 OTHER SOLUTION MODELS

A sub-regular solution model, proposed by Hardy<sup>(29)</sup>, defines the enthalpy and entropy of mixing as follows:

$$\Delta_m H = (A_1 + A_2 x_A) x_A (1 - x_A)$$

$$\Delta_m S = \Delta_m S (\text{ideal})$$

where  $A_1$  and  $A_2$  are adjustable parameters determined from the phase boundary data. In the sub-regular solution model the binodal curve is not symmetrical and must be defined by equating the chemical potentials of component A in both phases, and similarly for B.

Burnett<sup>(30)</sup> found that fairly good agreement was obtained with theory for  $\text{CaO-SiO}_2$  and  $\text{Li}_2\text{O-SiO}_2$  systems, and hence this model gives an approximate empirical description of the liquid immiscibility in these two chosen systems.

A variation of the sub-regular solution that takes into account the different atomic sizes of A and B was proposed by Lumsden<sup>(31)</sup> for metallic systems, and has been used by Hammel<sup>(32)</sup> to calculate the driving force for nucleation of phase separation in a  $\text{SiO}_2\text{-Na}_2\text{O-CaO}$  glass. Comparisons of the theoretical determinations of nucleation rates with experiment were good.

More complicated solution models have been developed but they do not always describe the immiscibility in glasses accurately. The Van der Toorn

and Tiedema model,<sup>(33)</sup> obtained by expanding the excess free energy of mixing as a series in  $x_A$ , has so far been of little practical use in silicate systems<sup>(34)</sup>. However, the associated solution model<sup>(35)</sup> in which complexes of silica are assumed to mix ideally with a metal oxide, can predict phase separation<sup>(30)</sup>. Clearly this model has a close relationship with the approach of Haller et al<sup>(28)</sup> mentioned earlier. It appears at present that association of silica units can allow conventional solution theories to predict accurately the characteristics of phase separation. Whether this is a reflection of a real situation or is simply fortuitous cannot be resolved without further experiment.

#### 2.4 THE PHASE DIAGRAM OF BARIA-SILICA

The phase diagram of this system was first derived experimentally by Eskola,<sup>(36)</sup> and later modified by Greig<sup>(37)</sup>. The following compounds were known to exist:  $BaOSiO_2$  (BS),  $BaO_2SiO_2$  ( $BS_2$ ),  $2BaOSiO_2$  ( $B_2S$ ),  $2BaO_3SiO_2$  ( $B_2S_3$ ) and a solid solution was believed to occur between  $BS_2$  and  $B_2S_3$ . Controversy arose over the existence of the solid solution, and this problem was finally resolved by Roth and Levin<sup>(13)</sup> who reported two further compounds:  $5BaO_8SiO_2$  ( $B_5S_8$ ) and the incongruently melting  $3BaO_5SiO_2$  ( $B_3S_5$ ), both in the previously proposed solid solution area. The polymorphic nature of  $BaO_2SiO_2$  was also discovered by Roth and Levin<sup>(13)</sup>, the transformation taking place at 1350 °C. The structure of the low temperature form  $l$ - $BS_2$  was deduced by Douglass<sup>(38)</sup> and is found in nature as the mineral sanbornite. Similarly, the structure of the high form  $h$ - $BS_2$  was described by Katscher et al<sup>(39)</sup>. Full crystal data of all BaO-SiO<sub>2</sub> compounds, including the d-spacings, are given by Oehlschlegel<sup>(40)</sup>. The structure of  $2BaO_3SiO_2$ ,  $5BaO_6SiO_2$  and  $3BaO_5SiO_2$  can be found in references 41, 42 and 43 respectively.

Metastable phase separation in the BaO-SiO<sub>2</sub> system was first suspected

by Greig<sup>(37)</sup> and later by Kracek<sup>(24)</sup> on the basis of the highly sigmoidal liquidus shape. Levin and Cleek<sup>(44)</sup> have linearly extrapolated the consolute curve in the BaO-B<sub>2</sub>O<sub>3</sub>-SiO<sub>2</sub> system from the region of stable immiscibility to the sub-liquidus region of the BaO-SiO<sub>2</sub> binary and estimated the critical point at 8mol% BaO and 1430°C. Cahn and Charles<sup>(45)</sup> have similarly extrapolated the immiscibility data of Toropov et al<sup>(46)</sup> from the ternary system BaO-CaO-SiO<sub>2</sub> to the BaO-SiO<sub>2</sub> binary. Reasonable agreement with the results of Levin and Cleek was found. Calculations by Charles<sup>(47)</sup> of thermodynamic activities in the BaO-SiO<sub>2</sub> system also indicated a critical point at 8mol% BaO but at 1600°C. The experimental investigation of Argyle and Hummel<sup>(48)</sup> suggested immiscibility with a T<sub>c</sub> value of 1655°C. Seward et al<sup>(14)</sup>, using a specially designed rapid quenching apparatus, established a binodal curve with a critical point of 1460°C and 10mol% BaO. The model of Haller et al<sup>(28)</sup>, assuming regular mixing between BaO<sub>2</sub>SiO<sub>2</sub> and (SiO<sub>2</sub>)<sub>8</sub> 'multimers', can be fitted to the data of Seward et al<sup>(14)</sup> very successfully. The data of Seward et al is probably the most reliable to date.

CHAPTER THREE

KINETICS OF PHASE TRANSFORMATIONS IN  
GLASS-FORMING SYSTEMS

CHAPTER THREE - KINETICS OF PHASE TRANSFORMATIONS IN GLASS-FORMING  
SYSTEMS

	<u>Page</u>
3.1 Nucleation in glass-forming systems	15
3.2 Growth of phases in glass-forming systems	32
3.3 Coarsening in glass-forming systems	38
3.4 Crystallisation in baria-silica glasses	41

The decomposition of a phase into one or more phases may generally be divided into three stages: a) formation of nuclei of the new phase, b) growth of the nuclei until mutual impingement or depletion of the matrix, c) coarsening. Depending on thermodynamic considerations stage a) may occur in two ways. If fluctuations in concentration, small in amplitude but large in extent, occur spontaneously, the reaction may proceed by spinodal decomposition with a continuous fall in free energy. If, however, all small fluctuations tend to decay, there is said to be a nucleation barrier. Although unstable, such fluctuations exist and occasionally one becomes so large that it is stable and grows to microscopic dimensions. In this case we are dealing with fluctuations that are large in amplitude and small in extent. It is primarily the purpose of this next section to discuss the kinetics of this latter process of nucleation.

### 3.1 NUCLEATION IN GLASS-FORMING SYSTEMS

#### 3.1.1 The thermodynamic barrier

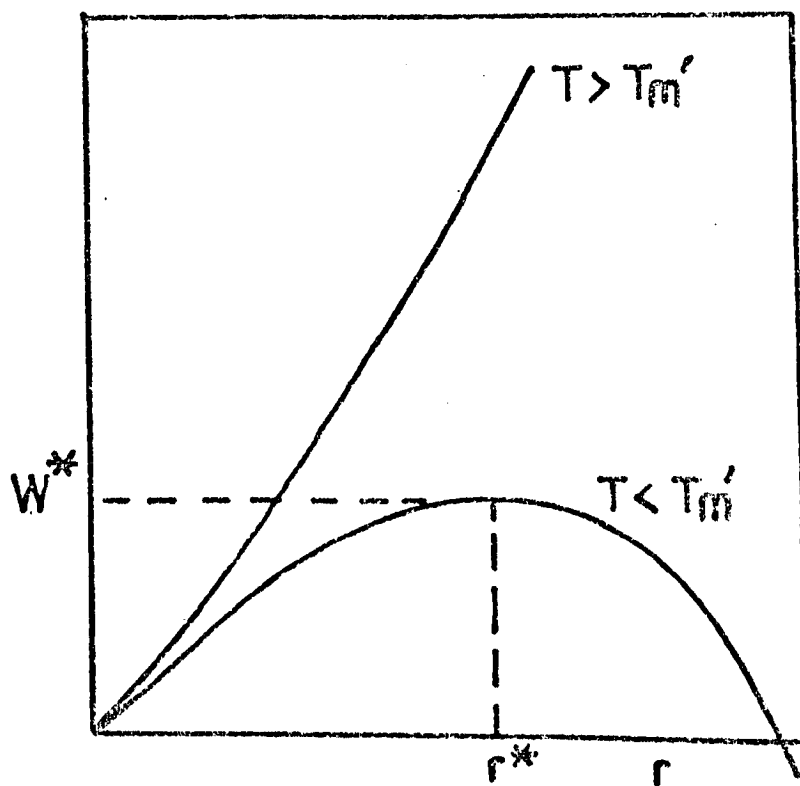
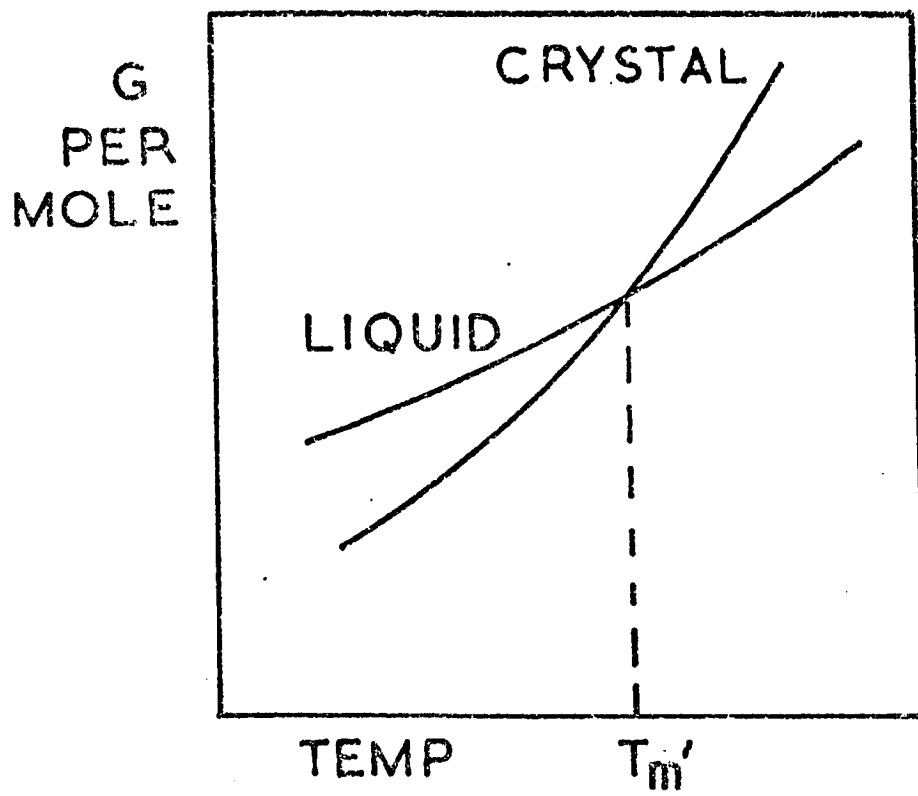
Nucleation theory was first proposed for the condensation of a pure vapour from a liquid but with some modifications it may also be applied to crystal nucleation in glass systems.

The driving force for a liquid to crystal phase transformation in a one component system is given by the difference between the free energies per mole of crystal and liquid, i.e.  $G_{\text{crystal}} - G_{\text{liquid}}$ , henceforth known as  $\Delta G$ , the thermodynamic driving force (see Figure (3.1)). Assuming that a spherical particle of radius  $r$  forms when  $T < T_m$ , where  $T_m$  is the equilibrium melting temperature, then the total free energy change is:

$$\frac{4\pi r^3 \Delta G}{3V_m} + 4\pi r^2 \sigma = W \quad (3.1)$$

**Figure 3.1** Free energy (G) per mole of crystal and liquid phases as a function of temperature

**Figure 3.2** Free energy (W) of formation of a spherical cluster as a function of its radius



where  $\sigma$  is the interfacial energy and  $V_m$  is the molar volume of the precipitating phase. Strain energy may also be involved in condensed systems, but for glasses the flow of the matrix will remove strains induced during transformations.

The theory assumes the presence of homogeneous phases, the existence of a sharp interface between the two phases and a constant value of  $\sigma$  that is identified as  $\sigma_\infty$ , the macroscopic surface energy. The latter assumption may not be justified since  $\sigma$  varies with the size of the droplet, but theory indicates<sup>(49)</sup> that in the extreme case of a closed packed cluster of 13 atoms  $\sigma$  is only 15% less than  $\sigma_\infty$ .

A more rigorous treatment of diffuse interfaces by Cahn and Hilliard<sup>(50,51)</sup> leads to results that are comparable with the classical nucleation theory.

The constant value of  $\sigma$  may be a true representation of conditions during the condensation of a vapour or the separation of a liquid phase but during the crystallization of a glass, surface energy will depend on the crystal plane in contact with the melt. The faceting of a crystal will be controlled to a large extent by the surface energies of the various planes in contact with the melt and as a result the shape of the crystal will deviate from a sphere to favour facets of low surface energy.

The relative magnitude of  $\Delta G$  and  $\sigma$  control the size of the critical nucleus. When  $T < T_m$ ,  $\Delta G < 0$  and a curve of  $W$  against  $r$  will increase to a maximum and then decrease again as shown in Figure (3.2). The position of the maximum is given by  $(\frac{\partial W}{\partial r}) = 0$  and the value of the critical radius is given by:

$$r^* = - 2\sigma V_m / \Delta G \quad (3.2)$$

Particles of radius  $r < r^*$  will tend to dissolve since an increase in size leads to an increase in  $W$ , whilst particles of radius  $r > r^*$  will tend to grow since an increase in radius decreases  $W$ . Particles with  $r < r^*$  are often referred to as embryos and those with  $r > r^*$  as nuclei.

The maximum value of  $W$  is found by substituting (3.2) into (3.1) to give equation (3.3)

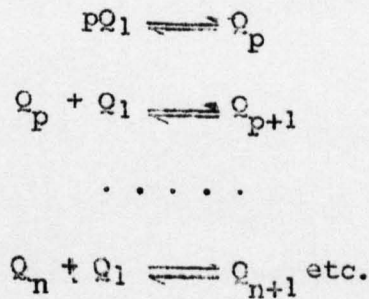
$$W^* = \frac{16\pi\sigma^3 v_m^2}{3\Delta G^2} \quad (3.3)$$

where  $W^*$  is the thermodynamic barrier.

If  $\Delta G > 0$  then  $W$  does not have a maximum value but increases rapidly with  $r$ . Under these conditions all embryos dissolve.

### 3.1.2 The Volmer and Weber theory of nucleation (52)

The formation of a nucleus can be envisaged as a step process where individual molecules or 'formula units' can add on to the embryo thus:



where  $p$  is the smallest possible entity that can be recognised as a new phase.

There is a certain probability per unit time that a 'formula unit' or molecule will add on to the surface of the embryo  $Q_n$  converting it into a

$Q_{n+1}$  embryo. This probability is given by:

$$P = \frac{A_n kT}{h} \exp\left(-\frac{\Delta G_D}{kT}\right)$$

where  $kT/h$  is the atomic vibration factor,  $\Delta G_D$  is the activation energy per 'molecule' or formula unit for motion across the matrix-embryo interface,  $A_n$  is the area of the embryo,  $Q_n$ .

The rate of change of the number of  $Q_n$  embryos to  $Q_{n+1}$  embryos is given by:

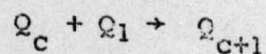
$$R' = \frac{A N_n kT}{h} \exp\left(-\frac{\Delta G_D}{kT}\right)$$

where  $N_n$  is the number of  $Q_n$  embryos and is approximately given by the following equation:

$$N_n = N \exp\left(-\frac{W_n}{kT}\right) \tag{3.4}$$

where  $N$  is the number of molecules in the system and  $W_n$  is the free energy change involved in forming a  $Q_n$  embryo.

Volmer and Weber<sup>(52)</sup> assumed 1) that the distribution of embryos is the same as the equilibrium distribution given by equation (3.4), 2) once the embryo reaches a critical size it is effectively removed from the system and is not considered further. This means that the nucleation rate is governed by the following reaction:



with no consideration given to the reverse reaction. Thus the nucleation rate  $I$  is given by:

$$I = \frac{kTNA^*}{h} \exp\left(-\frac{W^*}{kT}\right) \exp\left(-\frac{\Delta G_D}{kT}\right) \quad (3.5)$$

where  $A^*$  is the surface area of the critically sized embryo  $Q_c$ .

### 3.1.3 The Becker and Doring theory of nucleation <sup>(53)</sup>

The main defects of the Volmer and Weber theory of nucleation are:

1) the assumption that the steady state distribution of embryos is given by equation (3.4), and 2) neglect of the possibility that nuclei greater than the critical size can shrink. The distribution function does not fall to zero at  $N_n = N^*$  but approaches zero when  $N_n$  is very large (Figure 3.3).

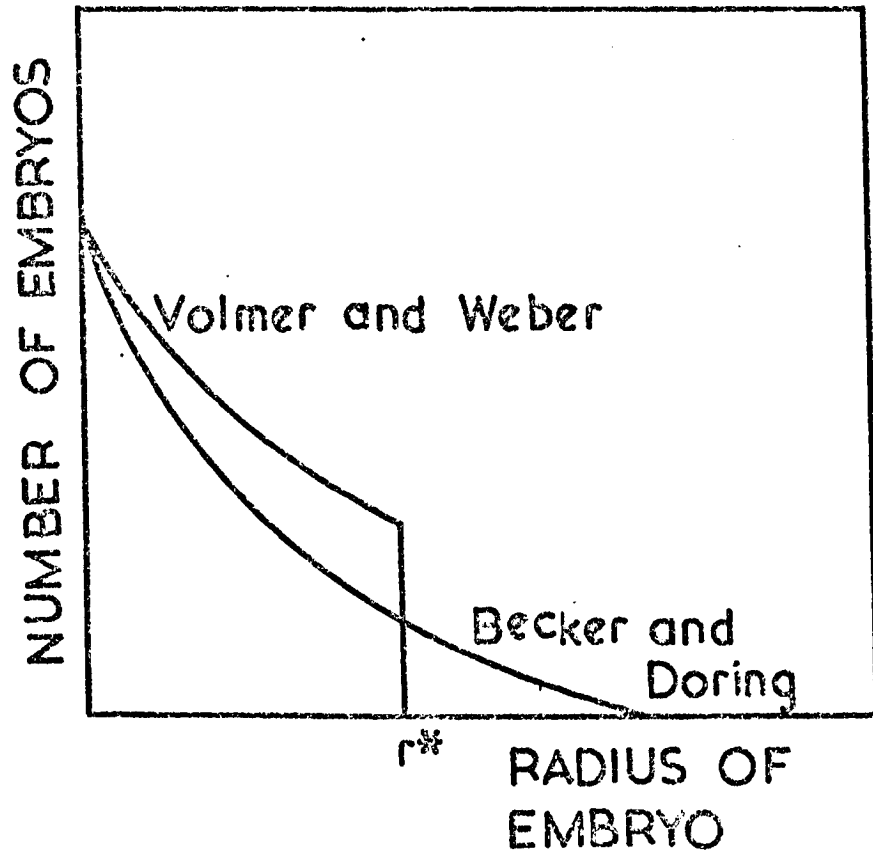
Becker and Doring <sup>(53)</sup> developed a theory that took into account the possibility that critical sized nuclei can decrease in size, (i.e.  $Q_{c+1} - Q_1 \rightarrow Q_c$ ) and avoided the assumption of the equilibrium distribution of embryos given by equation (3.4). The net nucleation rate is given by:

$$I = \frac{kT}{h} (Z^*A^* - Z_{c+1}A_{c+1}) \exp\left(-\frac{\Delta G_D}{kT}\right)$$

where  $Z^*$  is the number of embryos of critical size in the Becker and Doring distribution. The mathematical details involved in evaluating  $I$  and the final equation are given by Christian <sup>(54)</sup>:

$$I = \frac{NkTA^*V_m}{h 4\pi r^{*3}} \left(\frac{3W^*}{\pi kT}\right)^{1/2} \exp\left[-\frac{(W^* + \Delta G_D)}{kT}\right] \quad (3.6)$$

Figure 3.3      Distribution function of embryos  
according to Volmer and Weber<sup>(52)</sup>,  
and Becker and Doring<sup>(53)</sup>



The main effect is to modify the term in the pre-exponential factor by about a hundred. This is not a large factor because values of  $W^*$  in the exponential term are extremely sensitive to very small changes in temperature. For example, Turnbull<sup>(55)</sup> found that the nucleation rate of crystals in liquid mercury varied by  $10^4$  for a temperature drop of  $3^\circ\text{C}$ . Thus equation (3.6) can be approximated as:

$$I \sim \frac{kT}{h} \exp\left[-\frac{(W^* + \Delta G_D)}{kT}\right] \quad (3.7)$$

Other modifications to the theory have been proposed and details are given by Christian<sup>(54)</sup>. None of them change the general form of the equation derived by Volmer and Weber.

#### 3.1.4 Time dependent nucleation rate

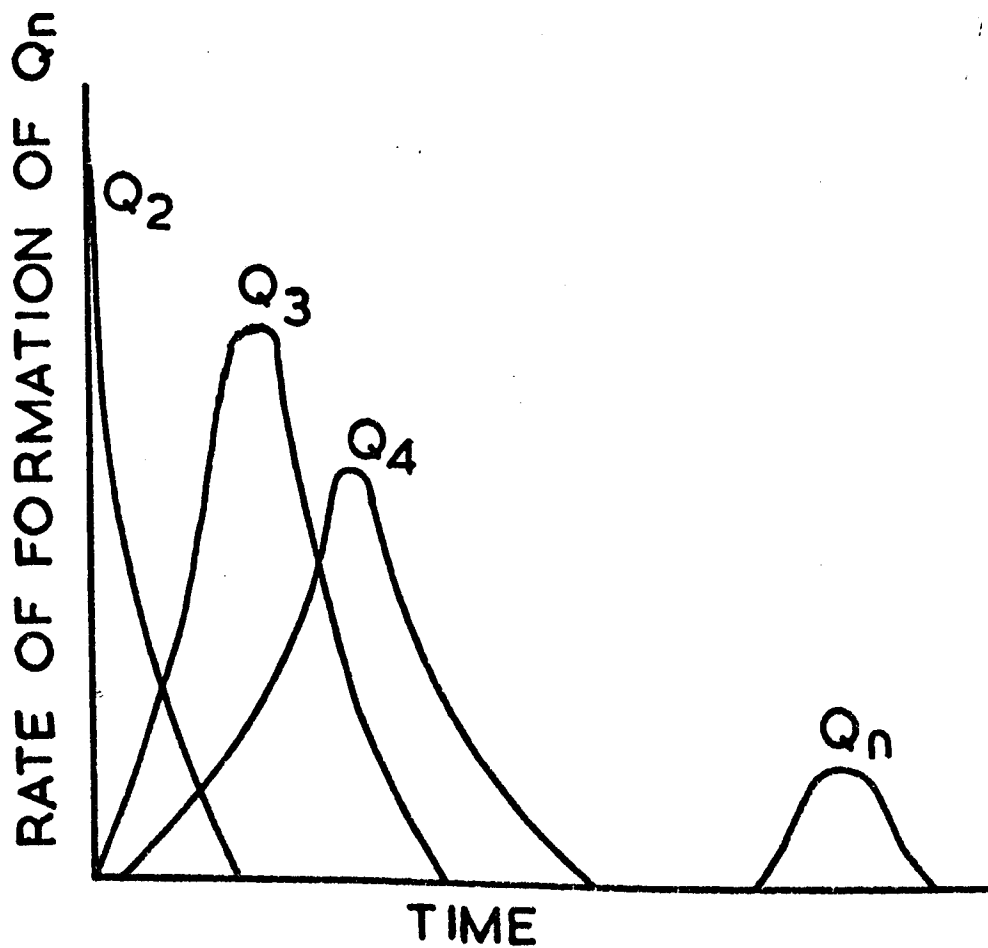
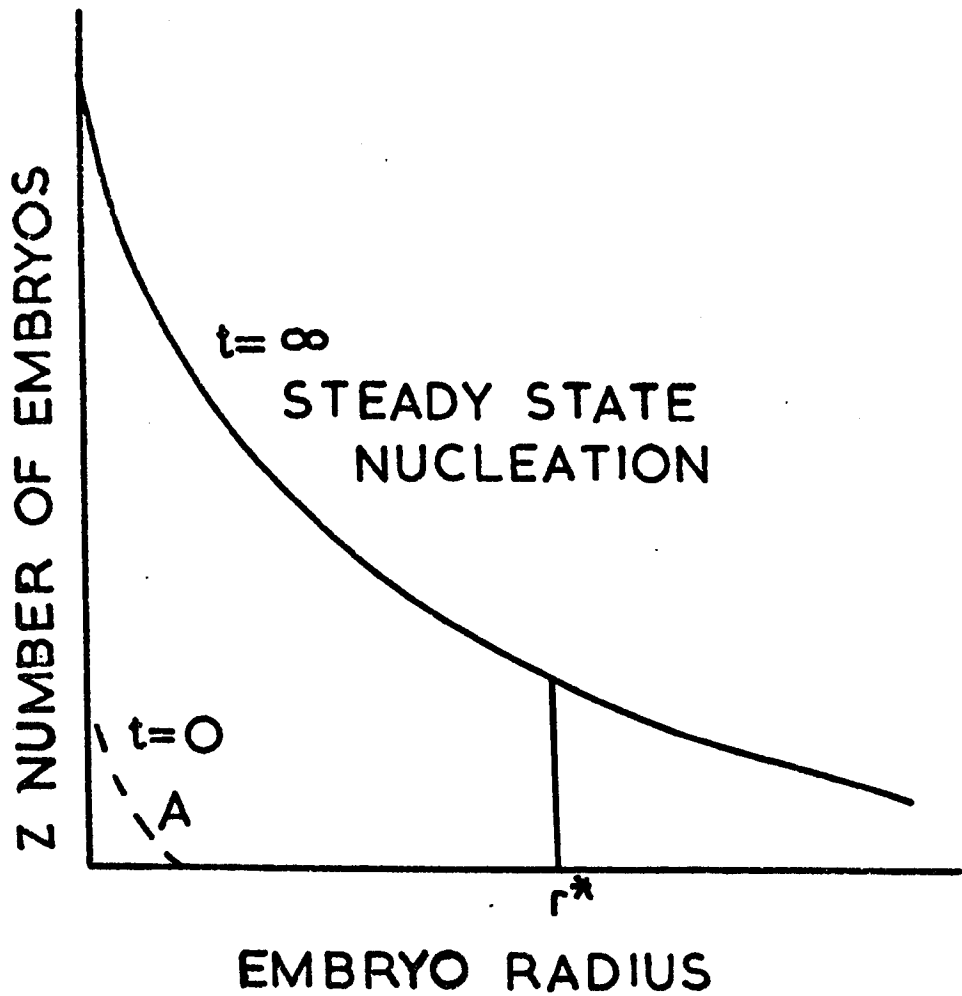
The equations previously derived assume that the nucleation rate is independent of time. This condition is usually valid for vapour-liquid transitions where initial transient effects are of very short duration. In condensed systems however, the existence of an activation energy barrier to the addition and removal of molecules from embryos may mean that the distribution is approached only slowly.

The establishment of a steady state distribution of embryos is shown in Figure (3.4). The initial curve A represents the distribution after the system has been quenched rapidly from above to below the phase transformation temperature. At very short times the rate of formation of small embryos is a maximum. For large critical size embryos the rate of production is small at  $t = 0$ , rises to a maximum and then falls off (see Figure 3.5).

The process is described by a complex partial differential equation known as the Zeldovitch-Frenkel<sup>(54)</sup> equation. A crude approximation to

**Figure 3.4**      Schematic curves to illustrate the change in embryo distribution with time in a quenched sample.

**Figure 3.5**      Rate of formation of embryos as a function of time



the solution of this equation is given in the form of

$$I_t = I_0 \exp\left(-\frac{\tau_1}{t}\right) \quad (3.8)$$

where  $\tau_1$  is a time constant and  $I_0$  is the steady state nucleation rate.

Other approximate solutions by Kantrowitz and Probstein are discussed by Christian<sup>(54)</sup>.

A more rigorous attempt to solve the Zeldovitch-Frenkel equation without involving the assumptions of earlier theories was made by Kaschiev<sup>(56)</sup>. From the solution he obtained a value for the nucleation rate:

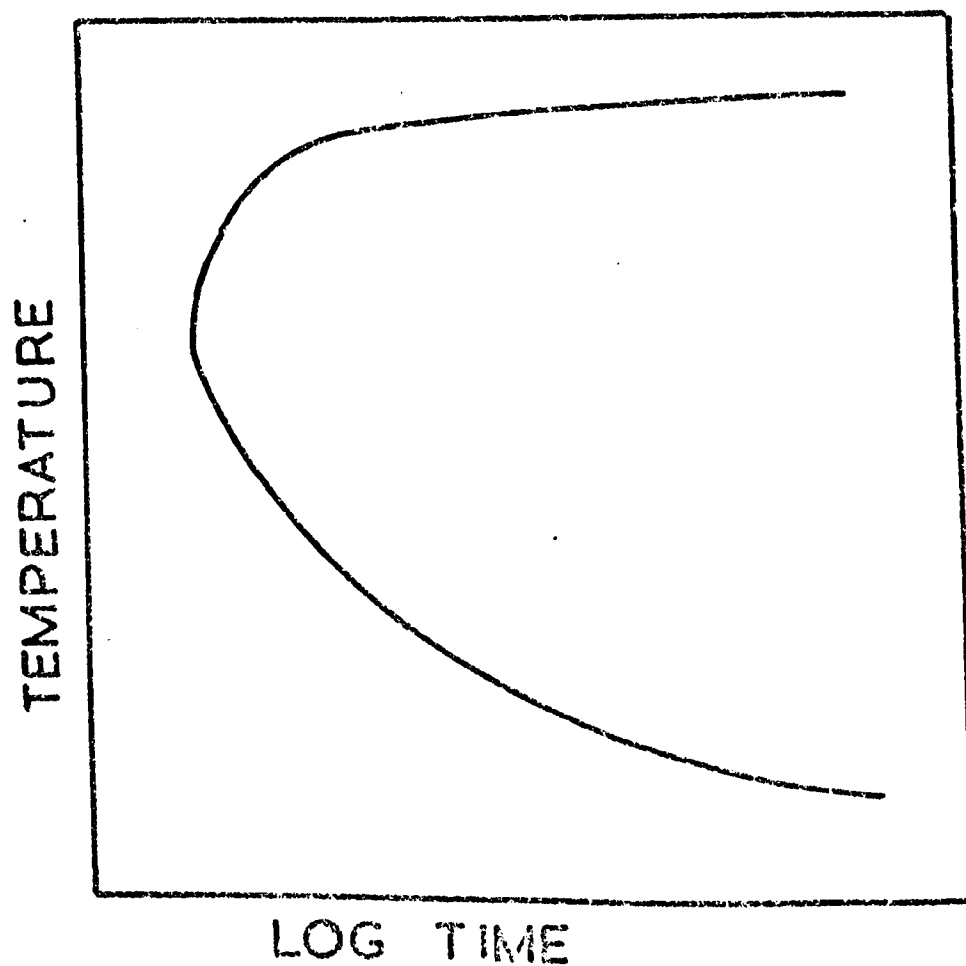
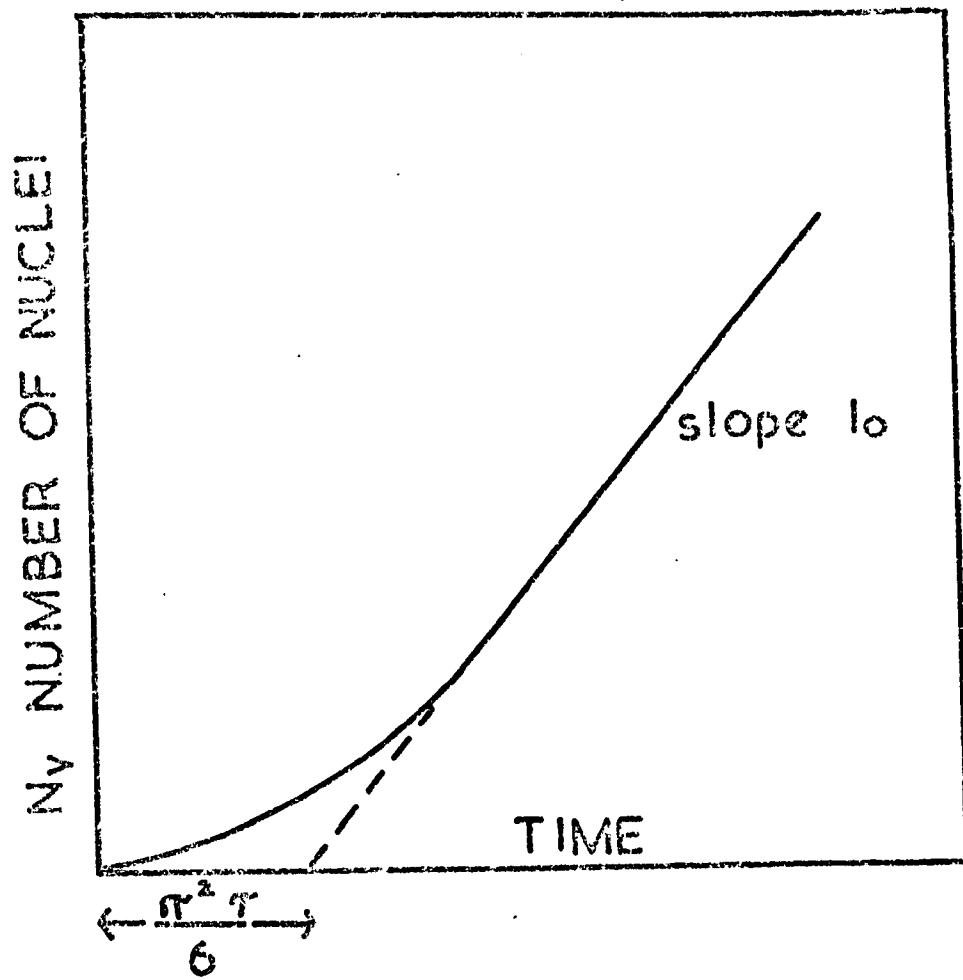
$$I_t = I_0 \left[ 1 + 2 \sum_{n=1}^{\infty} (-1)^n \exp\left(-\frac{n^2 t}{\tau_2}\right) \right] \quad (3.9)$$

where  $\tau_2$  is a time lag or induction time. The nucleation rate equation (3.9) is plotted schematically in Figure (3.6). The plot consists of two parts: (a) an interval where the nucleation rate is slowly increasing as the embryos are created, and (b) a steady state zone. Equation (3.9) represented as a function of temperature is shown schematically in Figure (3.7). The upper limit to nucleation is imposed by the relatively small value of  $\Delta G$ , and the lower limit of nucleation is caused by the ever increasing kinetic barrier for diffusion from matrix to nucleus.

A specific analysis of the induction times for glass systems has been given by Hillig<sup>(57)</sup>. He assumed that a given solute atom behaves as a perfect absorber capturing all other solute atoms that impinge on to it in the course of taking a random walk through the material. The mean time  $\bar{t}$  required to build the radius of the resulting cluster to the critical size  $r^*$  is given approximately by:

Figure 3.6 Schematic representation of number of nuclei formed per unit vol per unit time versus time. Magnitudes of slope and intercept are specific to the solution of equation (3.9) by Kaschiev<sup>(56)</sup>

Figure 3.7 Duration time before nucleation rate exceeds a specified value, as a function of temperature.



$$\bar{t} = \frac{\pi V_L^2 r^{*2}}{4D V_m^2 V_f^2}$$

where  $V_L$  = molar volume of parent glass

$V_m$  = molar volume of A

$D$  = diffusion coefficient of transport of A

$V_f$  = volume fraction of A

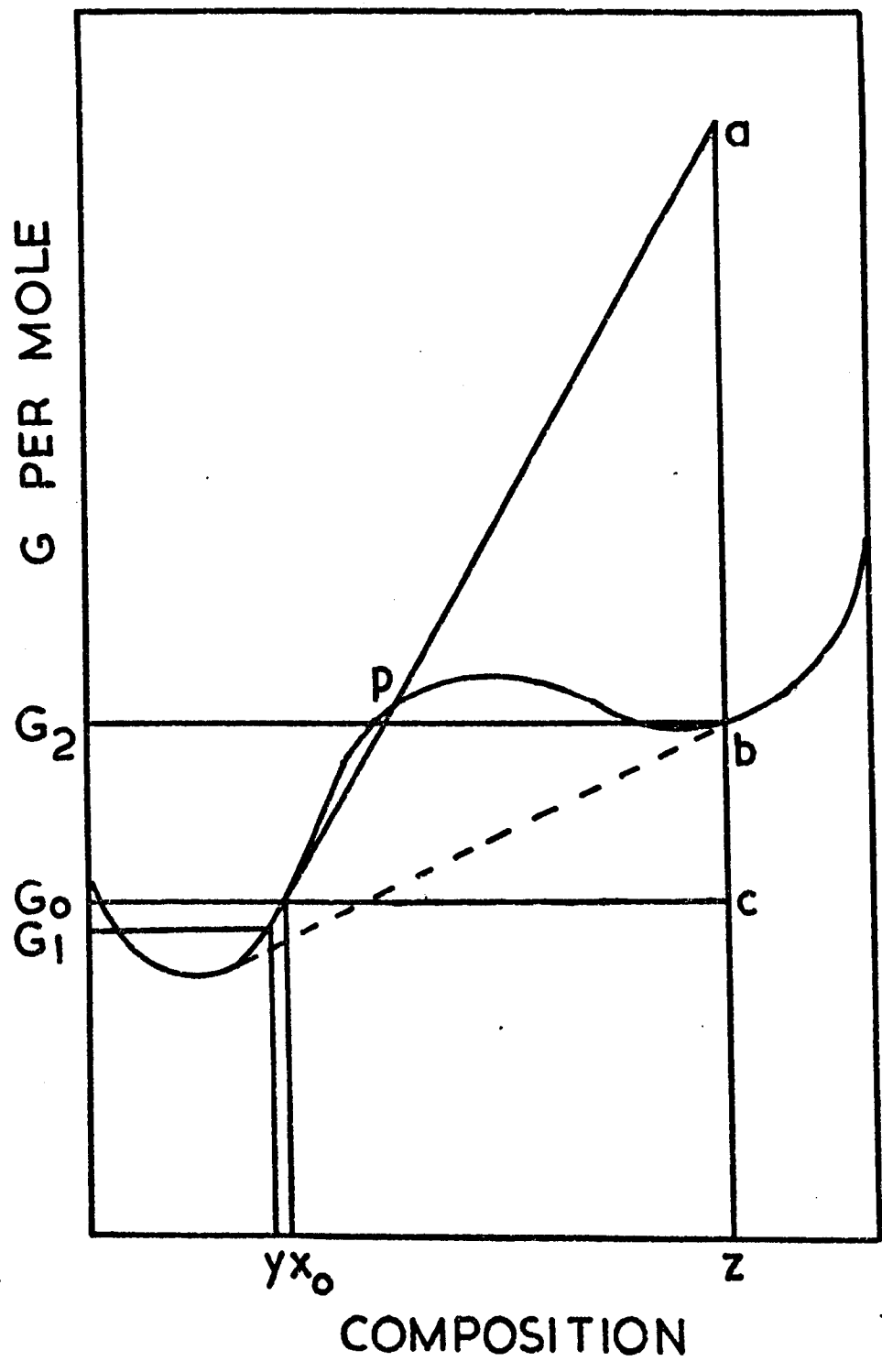
Hillig emphasises that the mean time will be much shorter than the actual time to achieve steady state conditions because of the neglect of the inherent thermodynamic instability of sub-critical embryos.

### 3.1.5 Nucleation in binary systems

With a few modifications the equations previously describing a one component system may be applied to a binary system.

Figure (3.8) shows the free energy-composition curve for a hypothetical binary system. If a homogeneous phase of composition  $x_0'$  consisting of  $M$  moles is present, then it will tend to split into two phases. At a very early stage in the transformation a new phase of  $m$  moles forms of composition  $z$  and the composition of the other phase shifts slightly to  $y$ . Assuming  $m \ll M$  and neglecting surface energies we may write the changes of free energy as:

**Figure 3.8**      **The free energy (G) versus composition curve for a hypothetical binary system**



$$\Delta G = mG_2 + (M - m)G_1 - MG_0 \quad (3.10)$$

From the Lever Rule the proportion of phases are

$$\frac{m}{M-m} = \frac{x_0 - y}{z - x_0}$$

$$\text{and} \quad M = \frac{m(z - y)}{(x_0 - y)} \quad (3.11)$$

From equation (3.10) and (3.11) and assuming that the fraction of precipitated phase is very small

$$\Delta G = m[(G_2 - G_1) - (z - y) \left( \frac{dG}{dx} \right)_{x=x_0}] \quad (3.12)$$

From equation (3.12) it can be seen that the change in free energy per mole to form a phase  $z$  from a homogeneous phase  $x_0$  is given by the value  $-ab$ ; i.e. the vertical distance between the free energy curve at the precipitating composition and the tangent drawn to the free energy curve at the initial composition. The minus sign indicates that the free energy is lowered in the process. As further separation proceeds the tangent rotates as the composition of the matrix shifts to the left. The driving force decreases until equilibrium is attained. Conversely, if the tangent lies below the separating composition the free energy must increase to promote the separation. Thus although the overall energy is lowered by decomposition of  $x_0$ , a free energy barrier must initially be surmounted since the tangent lies below the free energy curve until  $P$  is reached.

One other alteration to the nucleation equation must be considered. This concerns the term  $\Delta G_D$  which was defined previously as the kinetic barrier per molecule for transport across the embryo-matrix interface. For binary systems it is more reasonable to identify  $\Delta G_D$  with the free energy barrier for diffusion of the slowest rate determining species.

Compositions between the points of inflexion do not face a free energy barrier because the tangent to the free energy curve lies above the curve. Consequently only long range diffusion of the rate determining species controls the rate of phase separation.

Liquid phase separation within the two inflexion points ( $\frac{\partial^2 \Delta G}{\partial x^2} = 0$ ) is known as spinodal decomposition. The boundary between the phases is no longer sharp. Within the spinodal the critical nucleus resembles a fluctuation small in degree but large in extent. The decomposition of a matrix within the spinodal necessitates long range diffusional processes because of the scale of the fluctuation, and the transformation may prefer to take place by a nucleation and growth process which will be less favoured energetically but more favoured kinetically.

Within the spinodal the composition is unstable to small fluctuations of wavelength greater than a critical value  $\lambda_c$ . The rate of growth of the fluctuation is greatest when  $\lambda = \lambda_c \sqrt{2}$  (58-60).

Cahn<sup>(61)</sup> has constructed a mathematical model of the process by considering a series of sine waves with the same wavelength but with random phases, amplitudes and orientations in space. He then superimposed the waves and considered two dimensional sections through the structure. The spinodal texture was found to consist of two interpenetrating phases.

The free energy driving force for the precipitation of a crystal phase can also be determined using the tangency rule derived above. However unless solid solution or severely non-stoichiometric compounds

form in the system, crystallization is unlikely to take place by a gradual composition shift as described for liquid immiscibility.

The free energies of two solid solutions  $\alpha$  and  $\beta$  is shown in Figure (3.9). The lowest free energy possible for composition  $C_0$  is  $G_1$  and the composition consists of an  $\alpha$  and  $\beta$  mixture. If for kinetic reasons  $\alpha$  does not form, the free energy of  $C_0$  is given by  $G_2$ . The tangent to the  $\beta$  free energy curve at  $C_0$  intersects the  $\alpha$  curve at  $C'\alpha$ . Using the principles derived above,  $\beta$  can only nucleate a solid solution of compositions left of  $C'\alpha$  (as seen in Figure (3.9)).

Figure (3.10) shows how the formation of a stable phase  $\beta$  can be suppressed in the presence of a metastable phase  $\gamma$ . If for reasons of kinetics  $\alpha$ ,  $\beta$  and  $\delta$  fail to form at composition  $C_0$  then  $\gamma$  will constitute the sole (metastable) phase. A tangent drawn at  $C_0$  illustrates how  $\beta$  is unable to form irrespective of the fact that it is a stable phase. If  $\beta$  was introduced into the system it would dissolve in  $\gamma$ . On the other hand,  $\alpha$  and the metastable phase  $\delta$  can form from  $\gamma$ , and immediately the common tangent to the  $\alpha$  and  $\gamma$  curves intercept the  $\beta$  curve then decomposition to  $\beta$  is favoured thermodynamically,

The monotectic system<sup>(8,62)</sup> illustrates how these principles can be applied to show how phase separation must in some circumstances occur before crystallization is possible. Figure (3.11) shows a monotectic phase diagram and the free energy diagrams at various temperatures. At  $T = T_1$  in region II, the solid is metastable in contact with the single phase liquid and will crystallize from it but will dissolve in the presence of two liquids. When  $T = T_2$  in zone IV, solid cannot form from a single phase liquid and any existing solid will dissolve. However, after phase separation the solid is quite stable. In area V solid is stable with respect to a single liquid but immiscibility can increase the driving force and enhance the solid stability.

**Figure 3.9**      Graphical method of obtaining the  
free energy (G) of a two-phase  
mixture

**Figure 3.10**      In the presence of a single meta-  
stable phase  $\gamma$  of composition  $C_0$ ,  
a stable phase  $\beta$  cannot form

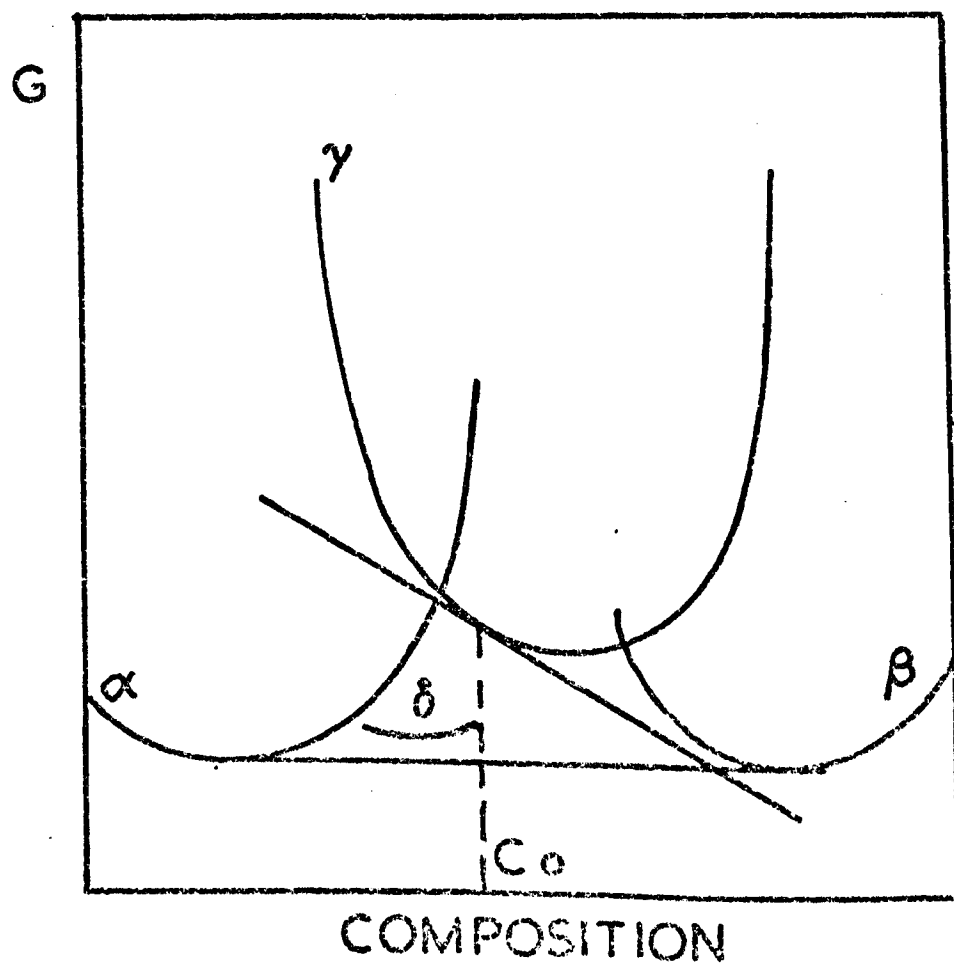
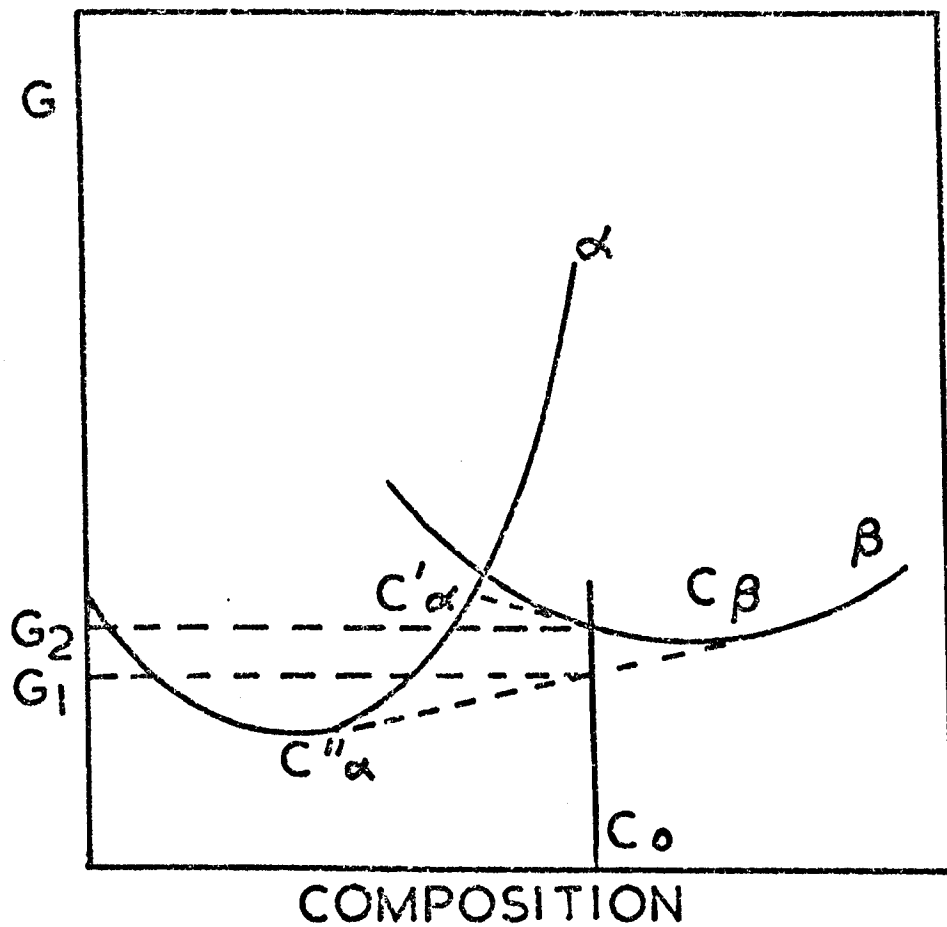
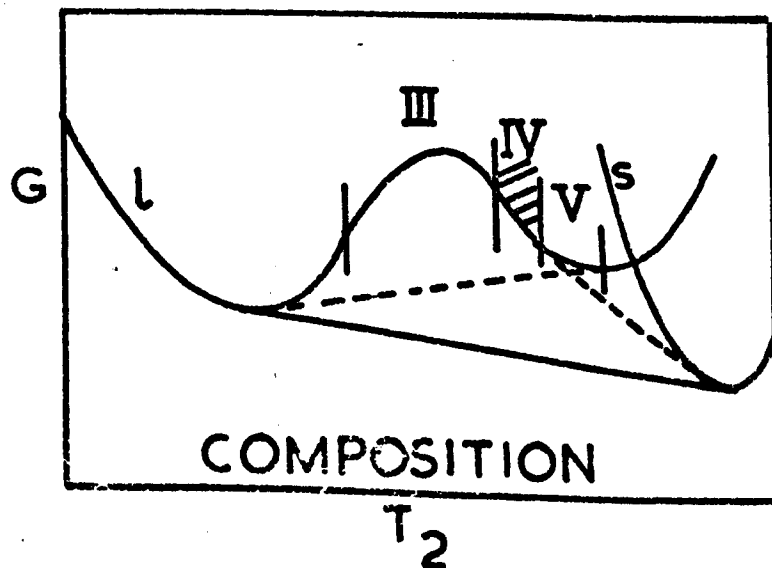
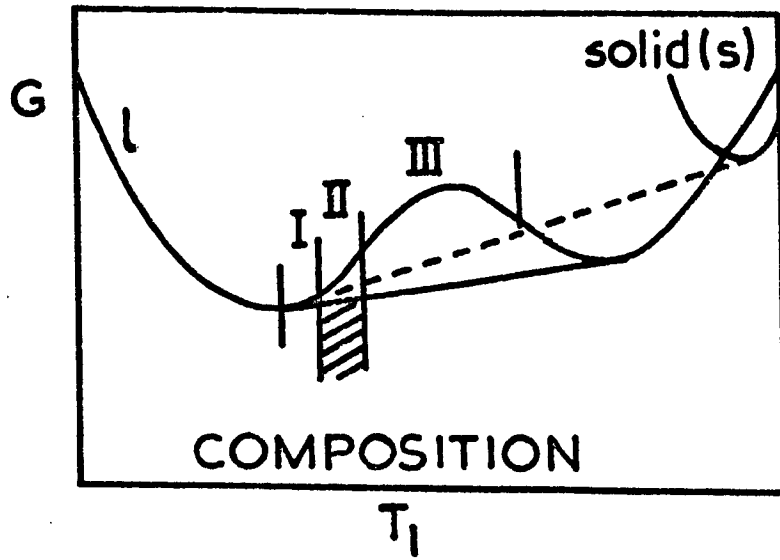
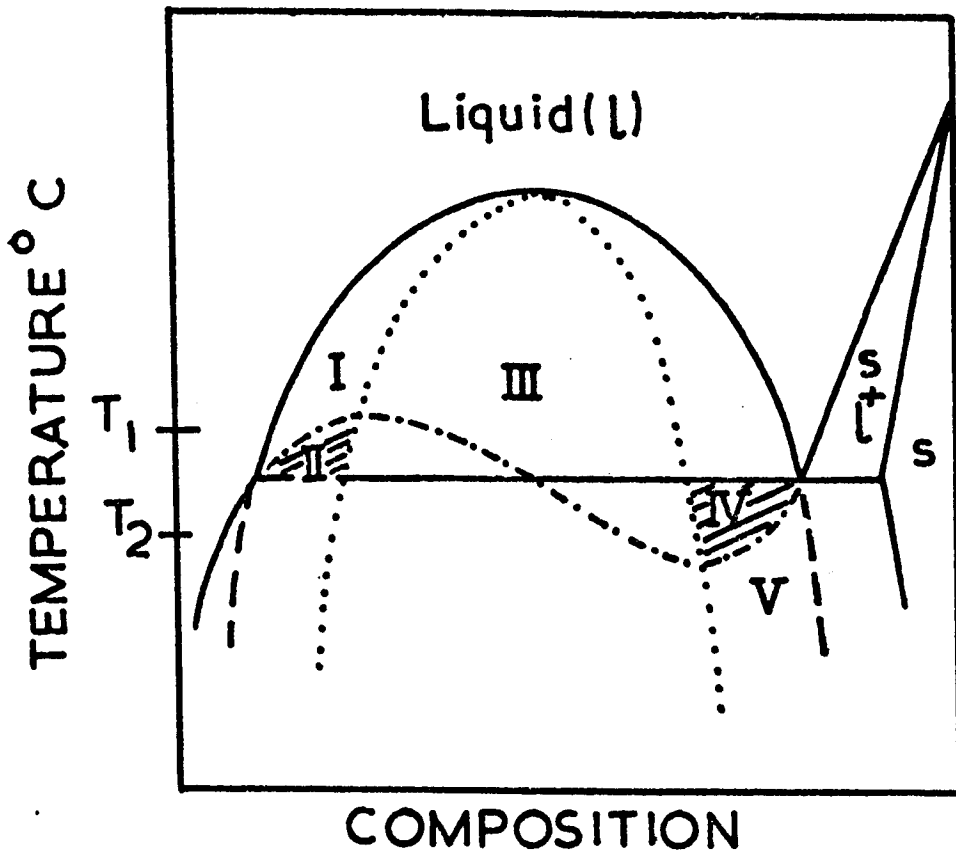


Figure 3.11 Schematic phase diagrams and free energy (G) diagrams of a monotectic system. The dashed tangents defines the metastable liquidus. The continuous tangents define the stable liquidus



### 3.1.6 Applications of nucleation theory to glasses

Both transient and steady state nucleation behaviour have been reported by several workers during the crystallization and liquid phase separation studies on glass-forming systems.

Burnett and Douglas<sup>(15)</sup> have measured the steady state nucleation rate  $I_0$  of  $BaO_2SiO_2$  in a 66.6 wt.%  $SiO_2$ , 16.7%  $BaO$ , 16.7%  $Na_2O$  glass, and demonstrated a very sharp decrease in  $I_0$  at low temperatures where the diffusion term predominates. The simplest equation often quoted to describe transient nucleation (equation (3.8)) was shown to hold approximately for their results.

Several attempts at quantitatively applying the nucleation theory to vapour-liquid transformations have been performed but only a few examples are known of attempts to fit the theory to glass-forming systems (see ref. (64) for a review). Glasses are useful materials for such work because diffusion and viscous flow are slow and phase transformations occur at an experimentally convenient rate.

The earliest attempt to fit the theory to glass-forming systems was due to Hammel<sup>(32)</sup>. He compared the measured nucleation kinetics of liquid droplets in a 76 mol%  $SiO_2$ -13  $Na_2O$ -11  $CaO$  glass specially selected near the binodal where classical theory should apply, with calculated rates given by the nucleation equation.  $\Delta G$  was estimated by fitting a solution model to the experimentally determined immiscibility gap. The free energy curves of the liquid phase could then be plotted. The variation of solubility temperature with particle radius enabled an estimate of  $\sigma$  to be made.  $\Delta G_D$  was found by measuring particle grow rates and assuming that the diffusion mechanisms involved in nucleation and growth were the same. Excellent agreement between experimental and calculated results was obtained when the Lumsden solution model<sup>(31)</sup> was used. However agreement was not

good where the Van der Toorn-Tiedema solution model<sup>(33)</sup> was used.

James<sup>(65)</sup> has studied non-steady state crystal nucleation in two Li<sub>2</sub>O-SiO<sub>2</sub> glass compositions. He has compared the theoretical curve predicted by Kaschiev's equation (3.9) with the experimental curves obtained at short nucleation times by plotting a graph of N<sub>v</sub>/I<sub>0</sub> τ vs t/τ. The close agreement obtained justified the methods he used to estimate I<sub>0</sub> and τ (see Figure (3.6)). The temperature variations of the induction time yielded activation energies that were closely in agreement with those obtained from the viscosity data of Matusita and Tashiro<sup>(66)</sup>. It would appear that the transport processes involved in viscous flow were similar to those involved in the nucleation processes. Estimates of the induction time, using Kaschiev's theory<sup>(56)</sup> and the Stokes-Einstein relation were about an order of magnitude smaller than the experimental values. Very good agreement was obtained with induction times calculated using Hillig's theory<sup>(57)</sup>.

An alternative use of the nucleation equation has been to calculate data from experimental nucleation curves, assuming that the nucleation equation is obeyed. Matusita and Tashiro<sup>(66)</sup> have used the following form of the nucleation equation to compute crystal-glass interfacial energies:

$$\log \eta I = \log K' - \frac{\alpha \sigma^3 V_m^2}{2.3 \Delta G^2 kT}$$

where K' is a constant                      η is the viscosity of the glass  
α is a shape factor                      V<sub>m</sub> is the molar volume of the crystal  
ΔG is the molar free energy  
change in crystallization

By constricting a graph of  $\log I \eta$  against  $1/\Delta G^2 T$  it is possible to obtain  $\sigma$  from the slope of the resulting straight line. The experimental method consisted of measuring the nucleation rates  $I$  and viscosity  $\eta$  for a  $\text{Li}_2\text{O}2\text{SiO}_2$  glass at various temperatures. The free energy changes between liquid and crystal were found from the literature. Substitution of the data into the equation enabled them to estimate the value of  $\sigma$  as  $196 \text{ ergs cm}^{-2}$ . The nucleation of crystals in  $\text{Na}_2\text{O}-2\text{SiO}_2$  and  $\text{K}_2\text{O}-\text{SiO}_2$  was immeasurably small and thus  $\sigma$  could be only approximately calculated. Comparison of the  $\sigma$ ,  $\eta$  and  $\Delta G$  data for  $\text{Li}_2\text{O}2\text{SiO}_2$ ,  $\text{Na}_2\text{O}2\text{SiO}_2$ ,  $\text{K}_2\text{O}2\text{SiO}_2$  enabled them to understand the relative importance of each parameter in controlling the nucleation behaviour for these three glasses.

Nucleation theory has been used by Rowlands<sup>(18)</sup> to determine the unknown parameters  $\bar{\sigma}$ ,  $\Delta H_D$  and  $A_D$ ; the average crystal-liquid surface energy, the activation enthalpy of diffusion and a pre-exponential factor for glasses in the  $\text{Li}_2\text{O}2\text{SiO}_2$ - $\text{BaO}2\text{SiO}_2$  system. Three methods were used, each involving the elimination of one of the three unknown parameters. For example, in method a) the nucleation rates ( $I_1, I_2$ ) at two temperatures ( $T_1, T_2$ ) were used to eliminate  $\Delta H_D$ . The equation obtained was:

$$\frac{T_1 \ln I_1 - T_2 \ln I_2}{T_1 - T_2} = \ln A_D - \frac{k_5 \bar{\sigma}^3}{k(T_1 - T_2)} \left[ \frac{1}{\Delta G_{V1}^2} - \frac{1}{\Delta G_{V2}^2} \right]$$

where  $k_5$  is a crystal shape factor,  $A_D = A \exp\left(-\frac{\Delta S_D}{kT}\right)$ ,  $\Delta S_D$  is the activation entropy for diffusion, and  $\Delta G_{V1}$  and  $\Delta G_{V2}$  are the volume free energies (i.e.  $\frac{\Delta G}{V_m}$ ) for crystallization at  $T_1$  and  $T_2$  respectively. By plotting a suitable graph, a straight line with a slope  $\frac{k_5 \bar{\sigma}^3}{k}$  and an intercept  $\ln A_D$  was obtained for  $T > T_{\text{max}}$ , the temperature of maximum nucleation rate.  $\Delta H_D$ , the eliminated parameter, was calculated by substituting  $\bar{\sigma}$  and  $\Delta S_D$

back into the nucleation equation. Rowlands obtained values of  $\bar{\sigma}$  between the crystal phase and the stoichiometric glass composition as 222 and 132 ergs  $\text{cm}^{-2}$  for  $\text{Li}_2\text{O}_2\text{SiO}_2$  and  $\text{BaO}_2\text{SiO}_2$  respectively. The main assumption of this method is that  $\bar{\sigma}$  and  $\Delta H_D$  are independent of temperature. For  $T < T_{\text{max}}$  (the maximum nucleation rate temperature), straight lines were not obtained and the above equation did not fit experimental data.

In method b) the parameter  $\Delta H_D$  was eliminated by utilising the fact that  $\frac{d \ln I}{dT}$  is zero at  $T_{\text{max}}$ .

Viscosity data was used in the third method to determine  $\Delta G_D$  independent of nucleation measurements.

The nucleation parameters were used to calculate the entire nucleation curve as a function of temperature. Agreement between theory and experiment was good when  $T > T_{\text{max}}$  but for other temperatures the theory predicted nucleation rate values far greater than those measured.

Finally, Rowlands showed that the nucleation kinetics cannot simply be described as two parts obtained by ignoring  $W^*$  and  $\Delta G_D$  at temperatures below and above  $T_{\text{max}}$  respectively.

### 3.1.7 Heterogeneous nucleation

Previously the formation of a nucleus has been regarded as a homogeneous process occurring with equal probability in all parts of the melt. Most phase transformations take place heterogeneously on container walls, impurity particles or structural imperfections. The thermodynamic barrier for this process will be less than for homogeneous nucleation if the activating site is to act as a catalyst.

Consider an interface between phases  $\alpha$  and  $\gamma$ . Assuming that  $\alpha$  is metastable with respect to  $\beta$ , a phase of the same composition; that the  $\alpha$ - $\gamma$  interface is a favourable place for nucleation of  $\beta$  and that the surface

energies are independent of orientation; then if  $r$  is the radius of the sphere circumscribing  $\beta$  (Figure (3.12)) and  $\gamma$  is incompressible, the surface energy to form the  $\beta$  phase is (54):

$$A_{\alpha\beta} r^2 \sigma_{\alpha\beta} + A_{\alpha\gamma} r^2 (\sigma_{\beta\gamma} - \sigma_{\alpha\gamma})$$

where  $A_{\alpha\beta}$ ,  $A_{\alpha\gamma}$ ,  $\sigma_{\alpha\gamma}$ ,  $\sigma_{\alpha\beta}$  are area factors and interfacial energies of the  $\alpha$ - $\beta$  and  $\alpha$ - $\gamma$  interfaces respectively and  $\sigma_{\beta\gamma}$  is the energy of the  $\beta$ - $\gamma$  interface. The free energy of formation of a nucleus may be written:

$$V_{\beta} r^3 \frac{\Delta G}{V_m} + r^2 [A_{\alpha\beta} \sigma_{\alpha\beta} + A_{\alpha\gamma} (\sigma_{\beta\gamma} - \sigma_{\alpha\gamma})] \quad (3.13)$$

where  $V_{\beta}$  is a volume factor for  $\beta$  and  $V_m$  is the molar volume of  $\beta$ .

Differentiating equation (3.13) with respect to  $r$ , equating to zero and solving for  $r$  we obtain:

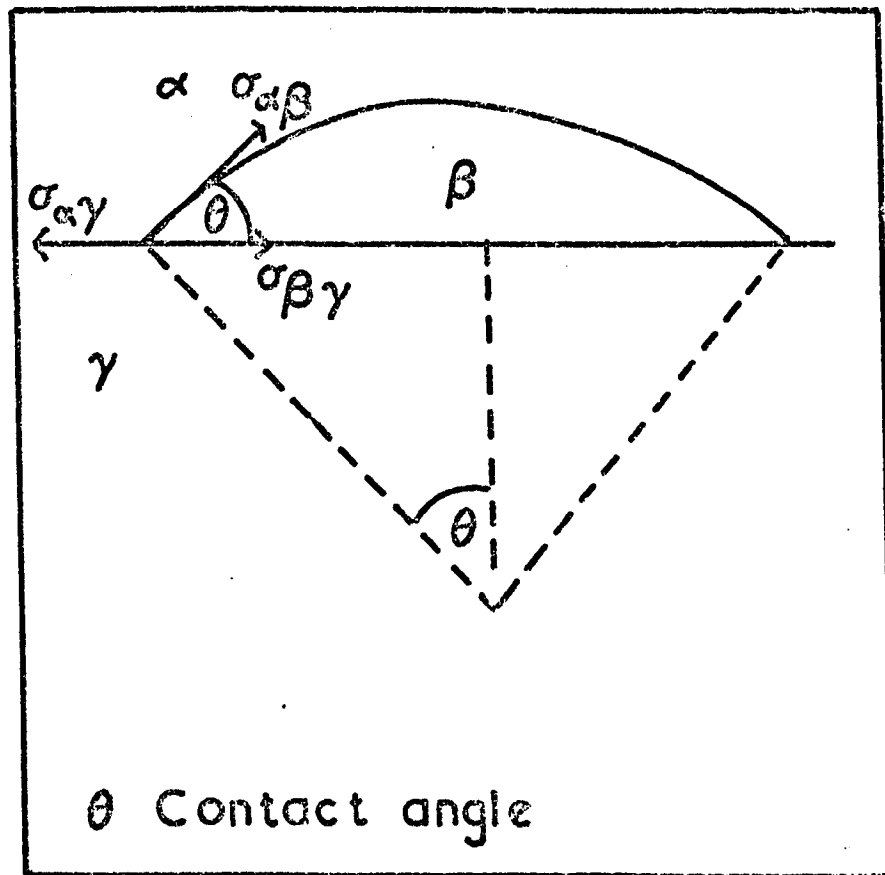
$$r_{\text{het}}^* = \frac{2}{3} \frac{V_m [A_{\alpha\beta} \sigma_{\alpha\beta} + A_{\alpha\gamma} (\sigma_{\beta\gamma} - \sigma_{\alpha\gamma})]}{V_{\beta} \Delta G}$$

Substituting  $r^*$  into equation (3.13) we arrive at:

$$W_{\text{het}}^* = \frac{4}{27} \frac{V_m [A_{\alpha\beta} \sigma_{\alpha\beta} + A_{\alpha\gamma} (\sigma_{\beta\gamma} - \sigma_{\alpha\gamma})]^3}{V_{\beta}^2 \Delta G^2} \quad (3.14)$$

The problem of heterogeneous nucleation becomes one of evaluating  $V_{\beta}$ ,  $A_{\alpha\beta}$  and  $A_{\alpha\gamma}$  for the particular case under consideration. Consider, for example, a spherical cap (Figure (3.12)). From geometry it can be seen that:

**Figure 3.12** Heterogeneous formation of a precipitate  $\beta$  on a substrate  $\gamma$



$$V_{\beta} = \frac{\pi}{3}(2 + \cos\theta)(1 - \cos\theta)^2$$

$$A_{\alpha\beta} = 2\pi(1 - \cos\theta)$$

$$A_{\alpha\gamma} = \pi \sin^2\theta$$

Substituting into equations (3.13) and (3.14):

$$W_{\text{het}}^* = \frac{16\pi}{3} \frac{\sigma_{\alpha\beta}^3}{\Delta G^2} \frac{V_m (2 + \cos\theta)(1 - \cos\theta)^2}{4}$$

and 
$$r_{\text{het}}^* = \frac{2\sigma_{\alpha\beta} V_m}{\Delta G}$$

In fact 
$$W_{\text{heterogeneous}}^* = W_{\text{homogeneous}}^* \times f(\theta) \tag{3.15}$$

where 
$$f(\theta) = \frac{(2 + \cos\theta)(1 - \cos\theta)^2}{4} \tag{3.16}$$

When  $f(\theta) < 1$ , corresponding to  $0 < \theta < \pi/2$ , heterogeneous nucleation takes place in preference to homogeneous nucleation, the action of the catalyst becoming more potent as  $\theta \rightarrow 0$ . The smaller the angle  $\theta$  the greater the ease at which heterogeneous nucleation takes place. A  $\beta$ - $\gamma$  surface of low energy is required where the atomic planes in  $\beta$  facing the planes in  $\gamma$  should have similar arrangements with very small mismatch. The action of a catalyst is now seen to be the replacement of a surface of high energy with a coherent surface of low energy.

The nucleation rates for embryos formed on the surface  $\gamma$  may be found by methods analogous to those used previously for homogeneous nucleation, i.e.

$$N_n = N_s \exp\left(-\frac{WF(\theta)}{kT}\right)$$

where  $N_s$  is the number of molecules of  $\alpha$  in contact with  $\gamma$  per unit area and  $N_n$  is the number of  $\beta$  embryos of size  $Q_n$ . The corresponding steady

state nucleation rate is:

$$I_h \sim \frac{N_s}{h} \exp\left[-\frac{(W^*f(\theta) + \Delta G_D)}{kT}\right] \quad (3.17)$$

where  $I_h$  is the number of nuclei per unit area of  $\gamma$  per unit time. Hence the nucleation rate is proportional to the surface area of  $\gamma$ .

### 3.2 GROWTH OF PHASES IN GLASS-FORMING SYSTEMS

Once a stable nucleus has been formed, crystal growth may proceed by the addition of atoms to the nucleus at a rate which is determined by conditions within the melt and at the interface. The heat of crystallization liberated, as the interface advances, is assumed to be transmitted away from the crystal sufficiently rapidly for growth to occur under isothermal conditions. This assumption is often justified in glass-forming melts of high viscosity where growth rates are relatively slow.

#### 3.2.1 Interface controlled growth

In crystallization of melts not undergoing changes in composition, the growth kinetics and morphology of crystals is dependent on the nature of the interface and on the ways in which the individual atoms can attach themselves to the growing crystal.

Three different growth models have been proposed. In the normal growth model atoms can be added to or taken from any appropriate site on the crystal interface by an activated process. Turnbull and Fisher<sup>(67)</sup> derived the growth rate equation using the theory of reaction rates:

$$u = \lambda v \exp\left(-\frac{\Delta G_D}{RT}\right) \left[1 - \exp\left(-\frac{|\Delta G|}{RT}\right)\right] \quad (3.18)$$

where  $\nu$  is the jump frequency of atoms facing the interface,  $\lambda$  is the jump distance to cross the interface  $\sim 1$  atom layer of new phase,  $\Delta G_D^\ddagger$  is the kinetic barrier to growth per mole of crystal phase (see Figure (3.13)).

Equation (3.18) can be approximated in certain circumstances to yield a much simpler equation. For example, when growth occurs at large undercoolings then  $\Delta G \gg RT$  and

$$u \sim \lambda \nu \exp\left(-\frac{\Delta G_D^\ddagger}{RT}\right) \quad (3.19)$$

$\Delta G_D^\ddagger$  can be expressed as

$$\Delta G_D^\ddagger = \Delta H_D^\ddagger - T\Delta S_D^\ddagger \quad (3.20)$$

where  $\Delta H_D^\ddagger$  and  $\Delta S_D^\ddagger$  are the activation enthalpy and entropy per mole for diffusion respectively. Substituting equation (3.20) into equation (3.19) and assuming the entropy term is independent of temperature:

$$u = A \exp\left(-\frac{\Delta H_D^\ddagger}{RT}\right) \quad (3.21)$$

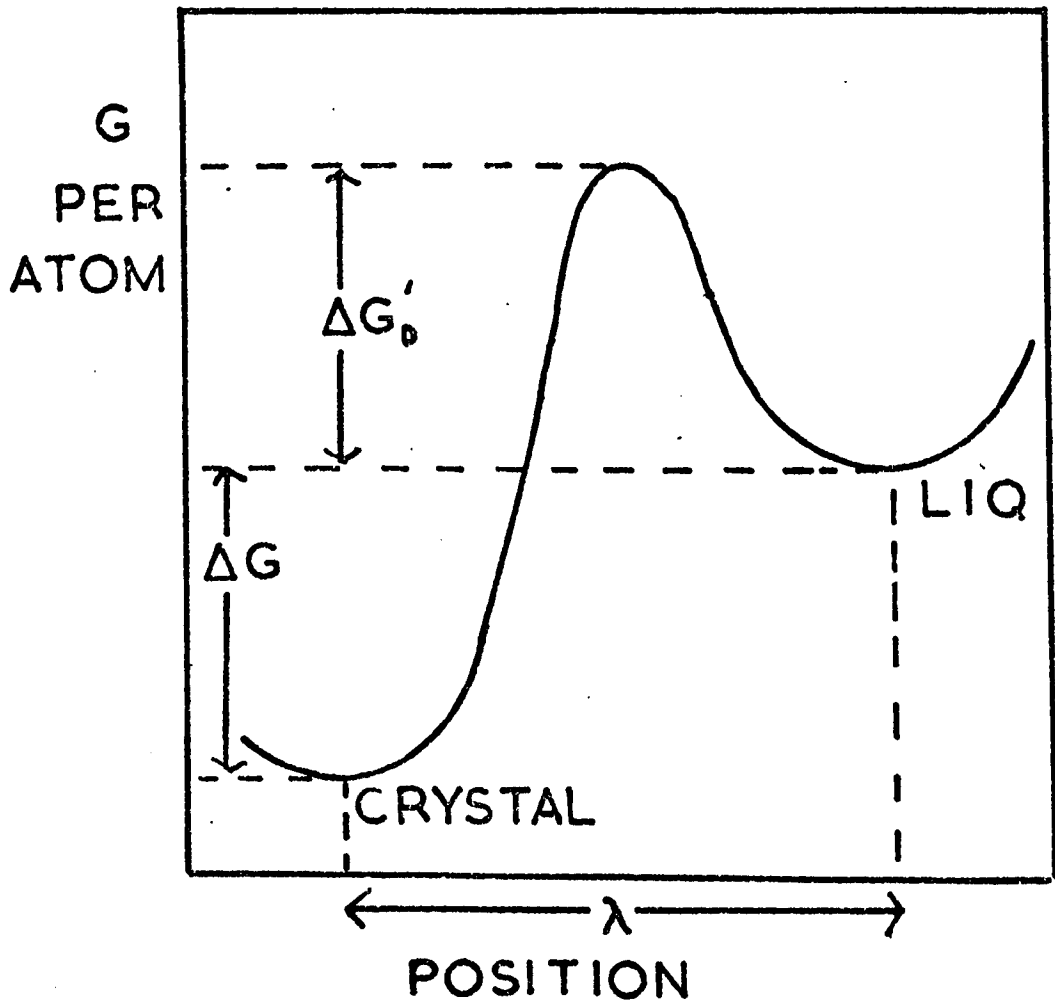
where  $A = \lambda \nu \exp\left(\frac{\Delta S_D^\ddagger}{R}\right)$

A plot of  $\ln u$  against  $1/T$  should yield a straight line whose gradient is  $(\Delta H_D^\ddagger/R)$ .

The diffusion coefficient for transport across the interface can be written as:

$$D = \lambda^2 \nu \exp\left(-\frac{\Delta G_D^\ddagger}{RT}\right) \quad (3.22)$$

**Figure 3.13** Free energy (G) per atom as a function of position relative to a crystal liquid interface



Substituting equation (3.22) into (3.18) we obtain the Hillig-Turnbull equation<sup>(68)</sup>:

$$u = \frac{D}{\lambda} \left[ 1 - \exp\left(-\frac{|\Delta G|}{RT}\right) \right] \quad (3.23)$$

When  $\Delta T$  is small and  $\Delta G \ll RT$ , equation (3.23) becomes:

$$u = \frac{D|\Delta G|}{RT}$$

The free energy of crystallization  $\Delta G$  can be written as:

$$- \frac{\Delta T \Delta H}{T_m}$$

where  $\Delta T$  is the undercooling,  $\Delta H$  is the enthalpy of fusion per mole and  $T_m$  is the melting temperature

$$\text{i.e.} \quad u = \frac{D \Delta T \Delta H}{RT T_m} \quad (3.24)$$

or  $u \propto \Delta T$  when  $\Delta T$  is small.

The screw dislocation model of growth allows atoms to add to step sites provided by a screw dislocation intersecting the interface. Such dislocations would provide a self-perpetuating ledge as atoms are added to the interface. The model describes growth accurately when the interface is smooth on an atomic scale. The equation describing growth rate is similar to (3.24) except for an active site fraction factor  $f$  which must be included in the equation. The growth rate at small  $\Delta T$  is<sup>(68)</sup>:

$$u = \frac{f D \Delta H \Delta T}{RT T_m} \sim \frac{D \Delta H (\Delta T)^2}{2\pi RT T_m^2} \quad (3.25)$$

or  $u \propto (\Delta T)^2$

The third model assumes that the interface is smooth and free of defects, and hence growth can occur only if new layers are nucleated at the surface. The growth rate is<sup>(69)</sup>:

$$u \propto \exp\left(-\frac{B}{T\Delta T}\right) \text{ where } B \text{ is a constant}$$

The surface nucleation model predicts that for small  $\Delta T$  the growth rate is unobservably low due to the nucleation barrier. In fact, due to the presence of screw dislocations, this mechanism is less likely to be observed.

Jackson<sup>(70)</sup> has related a bulk thermodynamic parameter - the entropy of fusion, to the configuration of the interface.

Most materials can be allocated to three classes depending on their entropy of fusion. Class one includes those materials where  $\Delta S_f < 2R$  and all planes are atomically rough. The normal growth model is the most likely mechanism of growth. Only slight anisotropy is expected in the growth and consequently the crystal-liquid surface should be non-faceted.

When  $\Delta S$  is approximately  $4R$  to  $6R$  the most closely packed planes should be smooth, the less closely packed planes should be rough and hence the growth rate anisotropy should be large. The most closely packed planes will be faceted and the growth kinetics should be described by the dislocation model for the close packed planes and the normal growth model for the less closely packed planes.

The third class includes the high  $\Delta S$  materials. At large undercoolings nucleation of new crystals of different orientations may take place on or ahead of the advancing crystal-liquid interface. Such nucleation, which can give rise to spherulitic growth, should be favoured by relatively low molecular mobility and the presence of impurities.

### 3.2.2 Diffusion controlled growth

During the discussion of interface controlled growth we assumed a linear growth law. This assumption is reasonable provided the interface advances into a region of matrix with constant composition. This situation does not always apply when a particle of phase  $\beta$  is growing into phase  $\alpha$  of different composition. If  $\beta$  is richer in solute there may be a region depleted in solute surrounding the  $\beta$  particle. The continued growth of  $\beta$  will then require long range chemical diffusion of constituents across the depleted layer. When the particle is first formed it is likely that processes near the interface will control the growth but eventually diffusion will be the dominant parameter in the growth rate equations. The change of dimension of the  $\beta$  particle may initially be linear with time but should change to a square root of time dependence later.

It can be shown that<sup>(71)</sup>

$$S = \alpha_{\lambda} (Dt)^{\frac{1}{2}}$$

where  $D$  is the atomic diffusion coefficient

$\alpha_{\lambda}$  is the growth coefficient and is a function of concentration

$S$  is a dimension (radius of sphere or cylinder or half width of plate).

The precise dependence of  $\alpha_{\lambda}$  on concentration has been calculated by Zener<sup>(72)</sup>.

In situations where the particle is large compared to the characteristic diffusion distance, the interface should advance at a rate which is independent of time<sup>(92)</sup>. For the specific case of a rod of constant diameter with addition of atoms taking place only near the ends, the length and volume are expected to increase linearly with time. In this example, the end of the rod can be considered to be advancing into a region of constant composition.

### 3.2.3 Applications of growth theory to glasses

In discussing the experimental results obtained in glasses, it will be convenient to define the reduced growth rate  $U_R$  <sup>(73)</sup>

$$U_R = \frac{u\eta}{1 - \exp\left[-\frac{\Delta H \Delta T}{RT T_m}\right]}$$

Using the Stokes-Einstein relation

$$D = kT/3\pi \lambda \eta$$

$$u = \frac{bf}{\lambda \eta} \left[ 1 - \exp\left[-\frac{\Delta H \Delta T}{RT T_m}\right] \right]$$

$$\text{where } b = kT/3\pi \lambda$$

$$\therefore U_R = bf/\lambda$$

and hence  $U_R$  is independent of  $\Delta T$  for normal growth and is proportional to  $\Delta T$  for screw dislocation growth.

The results of experimental studies on the kinetics of growth show good agreement with these predictions. For low entropy of fusion materials, such as  $\text{GeO}_2$  <sup>(73)</sup> and  $\text{SiO}_2$  <sup>(74)</sup>,  $U_R$  was independent of temperature and the interface was non-faceted, whilst for high entropy of fusion materials, such as  $\text{Na}_2\text{O}_2\text{SiO}_2$  <sup>(75)</sup>, O-terphenyl <sup>(76)</sup> and tri- $\alpha$ -naphthybenzene <sup>(77)</sup> and  $\text{PbO}_2\text{B}_2\text{O}_3$  <sup>(78)</sup>, this interface was faceted and  $U_R$  varied according to  $\Delta T$  but not in the way predicted by the screw dislocation mechanism. Thus  $\text{Na}_2\text{O}_2\text{SiO}_2$  showed two definite trends in the curve and the other three materials showed a positive curvature over the whole range of undercooling. The work of Matusita and Tashiro <sup>(79)</sup> on  $\text{Li}_2\text{O}_2\text{SiO}_2$  crystals in a stoichiometric melt revealed that  $f \propto \Delta T$ , indicating that screw dislocations may be important in controlling the growth rates.

The kinetic barrier to growth was found to be equal to that for viscous flow in the melt.

The crystallization studies of other systems, where large changes of composition occur, generally showed a growth rate independent of time (e.g.  $\text{Na}_2\text{O}-\text{B}_2\text{O}_3-\text{SiO}_2$  <sup>(80)</sup>,  $\text{Na}_2\text{O}-\text{SiO}_2$  <sup>(81)</sup>,  $\text{Li}_2\text{O}-\text{SiO}_2$  <sup>(82)</sup> and  $\text{BaO}-\text{Na}_2\text{O}-\text{SiO}_2$  <sup>(83)</sup>). This behaviour was not expected for growth involving long range diffusion except when the crystal was large compared with the mean diffusion path. The growth was spherulitic with fibrils observed to grow from a centre with large length to diameter ratios.

The growth of liquid droplets in a phase separated glass is nearly always controlled by long range diffusion.

Growth kinetics of liquid phase droplets observed by Burnett and Douglas <sup>(84)</sup> in a  $80\text{SiO}_2$   $10\text{Na}_2\text{O}$   $10\text{CaO}$  mole% glass composition, and by Hammel and Ohlberg <sup>(85,86)</sup> in a  $76\text{SiO}_2$   $13\text{Na}_2\text{O}$   $11\text{CaO}$  and  $20\text{CaO}$   $14\text{Al}_2\text{O}_3$   $10\text{B}_2\text{O}_3$   $54\text{SiO}_2$  mole% glasses, were observed to be diffusion controlled with  $r \propto t^{1/3}$ , where  $r$  is the mean particle radius.

### 3.3 COARSENING IN GLASS-FORMING SYSTEMS

The driving force for coarsening is the tendency of the system to reduce its overall surface energy. In liquid immiscibility the large particles grow at the expense of smaller particles and in crystallization, morphological changes that reduce the interfacial area may occur.

The kinetics of coarsening is most conveniently studied in liquid phase separated glasses where variations of  $n_v$  (number of particles),  $S_v$  (surface area of particles) and  $V_f$  (volume fraction) with time can be easily measured.

The solubility of a spherical particle of radius  $r_i$  is given by the Gibbs-Thomson equation:

$$C_r = C_o \exp\left(\frac{2\sigma V_m}{r_i RT}\right)$$

where  $C_r$  is the solubility of a particle radius  $r$

$C_o$  is the equilibrium solubility of a particle of infinite radius

$V_m$  is the molar volume of the particle phase

Following an earlier treatment by Greenwood<sup>(87)</sup>, Lifshitz and Slyozov<sup>(88)</sup> developed a theory of coarsening based on the above equation to obtain for small volume fractions

$$\bar{r}^3 - \bar{r}_o^3 = \frac{8\sigma DC_o V_m^2 t}{9RT}$$

$\bar{r}_o$  is the mean radius at the onset of coarsening

$\bar{r}$  is the mean radius at a time  $t$

$D$  is the diffusion coefficient of solute in the matrix

If  $\bar{r}_o$  is small then  $\bar{r} \propto t^{1/3}$ , and since the volume fraction of the dispersed phase during coarsening must be unchanged, we have  $N_v \propto t^{-1}$ . On the other hand, coarsening by an interface mechanism occurring in systems where diffusion is rapid compared with the incorporation of the species into the droplet will, according to Wagner<sup>(89)</sup>, be characterized by the relations:

$$\bar{r} \propto t^{1/2}, N_v \propto t^{-3/2} \quad V_f = \text{constant.}$$

Haller<sup>(90)</sup> has shown theoretically for a highly interconnected system that  $S_v \propto t^{-1/3}$  when coarsening is diffusion controlled and  $S_v \propto t^{-1/2}$  for interface controlled coarsening.

Most investigators have observed a diffusion controlled mechanism in the coarsening process using replica techniques<sup>(91,26)</sup> and thin sections<sup>(93)</sup>. James and McMillan<sup>(93)</sup> employed a three dimensional stereo

micrograph technique in their calculations of  $\bar{r}, n_v$  and  $V_f$ . Reasonable agreement with the Lifshitz-Slyozov theory was obtained.

Diffusion controlled particle coarsening has also been followed by small angle X-ray scattering by Zarzycki and Naudin<sup>(94)</sup> in the PbO-B<sub>2</sub>O<sub>3</sub> system and Neilson<sup>(95)</sup> in the Na<sub>2</sub>O-SiO<sub>2</sub> system.

The coarsening of a highly interconnected structure has been studied by Mahoney et al<sup>(96)</sup> on a sodium borosilicate glass. They defined a correlation length  $\Lambda$  which is related to the average distance between boundaries  $\bar{r}_1$  on the electron micrograph by  $\Lambda = 0.63 \bar{r}_1$ . They found that  $\bar{r}_1$  (and  $\Lambda$ )  $\propto t^{1/3}$  thus indicating that the coarsening was diffusion controlled.

Burnett and Douglas<sup>(84)</sup> studied the coarsening kinetics of liquid-liquid immiscibility in two glasses - glass 75 (75 mol% SiO<sub>2</sub>, 12.5% Na<sub>2</sub>O, 12.5% CaO) and glass 80 (80 mol% SiO<sub>2</sub>, 10% CaO, 10% Na<sub>2</sub>O). At temperatures just below  $T_m$  glass 80 separated rapidly into droplets which grew by a coarsening mechanism. No evidence of the initial growth before coarsening could be found.  $V_f$  was constant with time and  $S_v \propto t^{-1/3}$ , as expected for diffusion controlled coarsening. Glass 75 was characterised by a temperature range, just below  $T_m$  where growth of the droplets could occur but nucleation was absent. This was utilised to estimate the nucleation rate at a particular temperature. The results showed that the nucleation rate was not constant with time at a given temperature but required a finite period before a steady state constant value was achieved - a behaviour which was in agreement with nucleation theory. The number of particles  $n_v$  increased initially due to nucleation, but reached a maximum and then decreased due to coarsening. Over the same period of time the particles grew initially with  $\bar{r} \propto t^{1/2}$  and later changed to  $\bar{r} \propto t^{1/3}$ .

### 3.4 CRYSTALLIZATION OF BARIA-SILICA GLASSES

We have described the phase diagram, liquid-liquid immiscibility and crystal nucleation studies in baria-silica glasses. The results of other work in this system will now be briefly described.

The first comprehensive study of the crystallization of baria-silica was made by MacDowell<sup>(16)</sup>, using X-ray diffraction and electron microscopy, in the composition range  $\text{BaO}_2\text{SiO}_2$  to  $2\text{BaO}_3\text{SiO}_2$ . The region of good glass formation using conventional quenching, extended from 41 mol% to 29 mol% BaO. Outside these compositions either crystallization or liquid phase separation took place. All the glasses nucleated crystals internally without addition of nucleating agents. The first crystalline particles to appear were small radial spherulites at  $750^\circ\text{C}$  and these grew until impinge- at  $850^\circ\text{C}$ . At  $1000^\circ\text{C}$  the morphology resembled block or lath-shaped crystals, although X-ray diffraction did not indicate any change in phase. The spherulite to lath transformation was followed by DTA where an exothermic reaction at  $975^\circ\text{C}$  occurred.

Rowlands<sup>(18)</sup> confirmed the observations of MacDowell in  $\text{BaO}_2\text{SiO}_2$  glasses. An X-ray diffraction pattern of the crystallized glass, consisting of broad diffuse peaks resembling poorly crystallized  $\text{BaO}_2\text{SiO}_2$ , was obtained at temperatures below the spherulite-lath transformation, whilst at temperatures exceeding this transformation the apparent degree of crystallinity was greater.

Rowlands<sup>(18)</sup> also investigated the crystal growth mechanisms in the  $\text{BaO}_2\text{SiO}_2\text{-Li}_2\text{O}_2\text{SiO}_2$  and  $\text{BaO}_2\text{SiO}_2\text{-Na}_2\text{O}_2\text{SiO}_2$  systems. A eutectic growth model was fitted to the data from glasses in the  $\text{Li}_2\text{O}$  system exhibiting eutectic crystals. A screw dislocation model was fitted to the data from glasses in the  $\text{Na}_2\text{O}$  system. Only slight variations of activation enthalpy were found as a function of composition, except near  $\text{BaO}_2\text{SiO}_2$  where a marked increase



occurred. This was reflected in a decrease in the growth rates. The activation enthalpy of crystal growth was calculated as 115 kcal mole<sup>-1</sup> over a temperature range 749 to 868°C.

Burnett and Douglas<sup>(15)</sup> have described in detail the growth of BaO<sub>2</sub>SiO<sub>2</sub> spherulites in a 70 mol% SiO<sub>2</sub>, 20BaO, 10Na<sub>2</sub>O glass at a temperature of 600°C. Small spheres of h-BS<sub>2</sub> were first to appear. These nucleated needles of l-BS<sub>2</sub> and the characteristic spherulitic appearance began to take shape. After a long period of heating the spherulites transformed into laths and the remaining h-BS<sub>2</sub> reverted to l-BS<sub>2</sub>. Slow heating rates during a DTA run enabled the exothermic effects of the crystallization of h and l-BS<sub>2</sub> to be separated.

Freiman et al<sup>(17)</sup> have observed similar changes in microstructure from spherulite to laths in a 3BaO5SiO<sub>2</sub> glass. The transformation was accompanied by sharp changes in the electrical resistivity and heat evolution. The growth rate was independent of time except during the onset of impingement when a parabolic law was followed. They described four stages of crystallization, 1) classical nucleation, 2) spherulitic growth, 3) secondary crystallization in which glassy remnants crystallize, 4) spherulite to lath crystal transformations.

Oehlschlegel<sup>(97)</sup> has also reported the presence of a four stage crystallization process in the 3BaO5SiO<sub>2</sub> composition. According to his results the third stage mentioned above corresponds to the crystallization of h-BS<sub>2</sub>, and at stage 4) 3BaO5SiO<sub>2</sub> decomposes to l-BaO<sub>2</sub>SiO<sub>2</sub> and l-5BaO8SiO<sub>2</sub>. For BaO<sub>2</sub>SiO<sub>2</sub> glass, stage 3) represents the conversion of h to l-BaO<sub>2</sub>SiO<sub>2</sub>.

Tanikawa and Tanaka<sup>(98)</sup> followed the nucleation and crystallization processes by density change, permittivity measurements, DTA, X-ray analysis and electron microscope observations. Although early stage crystallization could not be identified, the eventual crystal form corresponded to l-BaO<sub>2</sub>SiO<sub>2</sub>. The transformation to lath crystals was also noted.

**CHAPTER FOUR**

**THE RELATION BETWEEN LIQUID-LIQUID  
IMMISCIBILITY AND CRYSTALLIZATION**

CHAPTER FOUR - THE RELATION BETWEEN LIQUID-LIQUID IMMISCIBILITY AND  
CRYSTALLIZATION

	<u>Page</u>
4.1 Introduction	43
4.2 Experimental observations of liquid-liquid immiscibility and crystal nucleation	44
4.3 Summary of Chapter Four	50

#### 4.1 INTRODUCTION

According to nucleation theory discussed in section (3.1) the rate of nucleation is a sensitive function of the thermodynamic driving force  $\Delta G$  (which is related to undercooling  $\Delta T$ ),  $\sigma$  the interfacial free energy between crystal and melt and  $\Delta G_D$  the kinetic barrier to nucleation. If liquid phase separation is to influence crystal nucleation then at least one of these parameters must be altered during or after the process of separation. Similarly, crystal growth rates may be increased or decreased if phase separation causes a change in  $\Delta G$  or  $\Delta G_D'$ , the kinetic barrier to crystal growth.

The most obvious way in which liquid phase separation may influence nucleation and growth is by producing local changes in composition which in turn may result in changes in  $\Delta G$ ,  $\sigma$ ,  $\Delta G_D$  and  $\Delta G_D'$ .

According to Uhlmann<sup>(9)</sup>, four mechanisms could control the relation between liquid immiscibility and crystal nucleation:

- "a) The separation can result in a driving force for nucleation of a crystalline phase where none existed with the homogeneous liquid. ....
- b) The separation results in interfaces between the phases and the associated interfacial energy can result in the interfaces being preferred sites for the nucleation of the crystalline phases.
- c) The separation can result in one of the liquid phases having appreciably higher atomic mobilities in the range of large undercooling than in the parent homogeneous phase.
- d) The interfacial regions between the separated phases may be enriched in some component providing a locally larger driving force for nucleation or a locally higher mobility."

Uhlmann expresses the opinion that mobility changes induced by liquid phase separation is the most important factor.

The relevance of the above mentioned four points to the results presented in this thesis on the BaO-SiO<sub>2</sub> system will be discussed later (Chapter Six).

#### 4.2 EXPERIMENTAL OBSERVATIONS OF LIQUID-LIQUID IMMISCIBILITY AND CRYSTAL NUCLEATION

Many examples are known of oxides (particularly TiO<sub>2</sub>) that enhance crystal nucleation<sup>(2,99)</sup>. The addition of oxides can result in the precipitation of small colloidal particles of the oxides. These can act as heterogeneous nucleation sites that initiate bulk crystallization. Hillig<sup>(57)</sup> has shown that crystal nucleation of BaO<sub>2</sub>SiO<sub>2</sub> in the system BaO-SiO<sub>2</sub>-TiO<sub>2</sub> can be explained satisfactorily in terms of the liquidus temperatures and viscosity. A simple analysis of heterogeneous nucleation demonstrated that a readily nucleating precursor phase was expected to be a poor catalyst for a more difficult nucleating phase. However, liquid unmixing<sup>(99,100,101)</sup>, caused by the addition of a catalyst, could encourage crystal nucleation by changing the thermodynamic driving force, viscosity or crystal-liquid interfacial energy.

The appearance of liquid phase separation before crystallization has prompted several workers to conclude that immiscibility is a pre-requisite for crystallization. For example, Kalinina et al<sup>(102)</sup> observed a hazy blue opalescence in a Li<sub>2</sub>O-SiO<sub>2</sub> glass although X-rays could detect no crystallinity at the early stages of heat treatments. Buzhinskii et al<sup>(103)</sup> have observed three stages in the crystallization of a Li<sub>2</sub>O-Al<sub>2</sub>O<sub>3</sub>-SiO<sub>2</sub> glass. The first stage was attributed to liquid immiscibility and the second stage was characterized by the appearance of  $\beta$  eucryptite. Although they concluded

that the liquid phase separation and crystallization process were related, no specific experiment to test this hypothesis was undertaken.

The work of Vogel and Gerth<sup>(7,104-6)</sup> has included studies of liquid phase separation and crystallization in the following glasses:  $\text{LiF-BeF}_2$ ,  $\text{Li}_2\text{O-SiO}_2$ ,  $\text{MgO-P}_2\text{O}_5\text{-TiO}_2$  and  $\text{SiO}_2\text{-Al}_2\text{O}_3\text{-TiO}_2\text{-Li}_2\text{O-MgO-ZnO}$ . Electron micrographs showed crystals growing on the interfaces or in the matrix or within the droplets. It was deduced that phase separation may promote crystal nucleation heterogeneously or homogeneously.

Ohlberg, Golob and Strickler<sup>(6)</sup> studied liquid phase separation and crystallization in  $\text{MgO-Al}_2\text{O}_3\text{-SiO}_2\text{-TiO}_2$ ,  $\text{Li}_2\text{O-CaO-SiO}_2\text{-TiO}_2$  and  $\text{Li}_2\text{O-MgO-Al}_2\text{O}_3\text{-SiO}_2$  glasses, They suggested from their results that the internal crystal nucleation was the result of liquid phase separation and that crystallization was initiated at the droplet-matrix interfaces.

Maurer<sup>(107,108)</sup> made light scattering studies on a  $\text{SiO}_2\text{-MgO-Al}_2\text{O}_3\text{-TiO}_2$  glass heat treated at different temperatures and found that the scattering centres became increasingly anisotropic. This was interpreted as a crystallization of liquid droplets.

Direct observations of crystallization in thin sections of a  $\text{Li}_2\text{O-Al}_2\text{O}_3\text{-SiO}_2$  glass containing  $\text{TiO}_2$  was made by Doherty et al<sup>(109)</sup>. Their results indicated that liquid phase separation preceded the crystallization of an unknown phase containing Ti and Al. This in turn nucleated  $\beta$ -eucryptite. The base composition without  $\text{TiO}_2$  phase separated but did not internally nucleate. Thus the  $\text{TiO}_2$  was probably responsible for the internal nucleation rather than the liquid-liquid immiscibility.

There are other observations of phase droplets initiating crystallization heterogeneously. These include  $\text{Na}_2\text{O-SiO}_2\text{-TiO}_2$ <sup>(110)</sup>, fluor-richterite<sup>(111)</sup>, alkaline earth alumino-silicates<sup>(112)</sup>, fluorine additions in a  $\text{CaO-MgO-P}_2\text{O}_5\text{-SiO}_2$  glass<sup>(113)</sup> and an unspecified crystal in a  $\text{SiO}_2\text{-TiO}_2\text{-CaO-Li}_2\text{O}$ <sup>(114)</sup> glass.

The catalytic effect of  $P_2O_5$  on the crystal nucleation rate in  $Li_2O-SiO_2$  glasses was first reported by Partridge and McMillan<sup>(115)</sup>. Phillips and McMillan<sup>(116)</sup> also found the addition of  $P_2O_5$  to several  $Li_2O-SiO_2$  glasses promoted liquid phase separation. Their results suggested that  $P_2O_5$  enhanced crystal nucleation by increasing the tendency of the glasses to phase separate. However, their work was not conclusive since the influence of  $P_2O_5$  on the nucleation kinetics may be due to its effect on liquidus temperature, viscosity and glass-crystal surface energy.

James<sup>(117)</sup> has obtained evidence indicating the increase in nucleation rates is due solely to  $P_2O_5$  additives and is not connected directly with the occurrence of liquid phase separation.

Harper et al<sup>(118)</sup> have suggested that liquid phase separation affects the nucleation kinetics by shifting the composition of the  $Li_2O$ -rich phase closer to the more rapidly nucleating  $Li_2O \cdot 2SiO_2$  composition. They studied the liquid-liquid immiscibility and internal crystallization in two glasses : glass 1  $30Li_2O, 70SiO_2$ , glass 2  $30Li_2O, 69SiO_2, 1 P_2O_5$  mol%. Both glasses phase separated but with fairly similar morphologies (and similar values of interfacial areas). Thus the crystal nucleation was probably not dependent on interface morphology. To explain the very large effect of  $P_2O_5$  on the nucleation rates (the crystal nucleation rate is increased 200 times), it was further suggested that in addition to the compositional shift, nucleation may also be enhanced, either by precipitation of phosphate crystals that act as heterogeneous sites, or by a lowering of the crystal-liquid interfacial energy.

Heterogeneous nucleation by phosphate crystals was also suggested by Harper and McMillan<sup>(119)</sup>.

Nakagawa and Izumitani<sup>(120)</sup> have studied the liquid immiscibility effect on crystal nucleation in a  $Li_2O-SiO_2$  and a  $Li_2O-SiO_2-TiO_2$  glass.

They obtained evidence that in the latter glass liquid immiscibility can increase the crystal nucleation rate. Micrographs were published showing crystals of lithium titanate forming heterogeneously at the liquid droplets. These crystals acted as nucleation sites for the main crystal phases. Titania free glass with the same  $\text{Li}_2\text{O}:\text{SiO}_2$  ratio showed less tendency to nucleate. It was probable that liquid phase separation stimulated the nucleation of the titanate phase and thus indirectly enhanced crystal nucleation of  $\text{Li}_2\text{O}_2\text{SiO}_2$ .

Tomozawa<sup>(121)</sup> compared the kinetics of liquid phase separation for  $\text{Li}_2\text{O}-\text{SiO}_2$  glasses with crystal nucleation as a function of temperature and time. The nucleation rate in a glass outside the immiscibility gap was constant with time but for glasses that phase separated and underwent crystal nucleation at the same time, a temporary but marked increase in nucleation rate was observed. This phenomenon was related to the commencement of phase separation. The number of crystals in the phase separated glass eventually exceeded that in the homogeneous glass outside the immiscibility gap. The temporary increase in crystal nucleation was attributed to the presence of a diffusion zone (depleted in silica) surrounding the silica-rich droplets which acted as a favourable site for crystal nucleation by lowering the effective surface energy. Tomozawa was unable to explain the results in terms of a compositional change in the matrix brought about by the liquid phase separation, which would give changes in the driving force, in surface energy and diffusion rate. However, it may be noted that apart from the heterogeneous mechanism suggested by Tomozawa, depletion of silica around the droplets (as envisaged by Tomozawa) could also provide a locally higher driving force (and larger mobility) for crystal nucleation. Further work in this system is needed to test these ideas.

Matusita and Tashiro<sup>(122)</sup> determined the effect of a series of oxide additives on the crystal nucleation and growth of a  $\text{Li}_2\text{O}_2\text{SiO}_2$  glass. They

showed that changes in nucleation rate caused by the additives (except  $P_2O_5$  and  $V_2O_5$ ) were due to changes in viscosity. Their results suggested that  $P_2O_5$  and  $V_2O_5$  additives influenced the nucleation kinetics by inducing liquid phase separation.

Matusita et al.<sup>(123)</sup> have also examined the effect of oxide additions ( $RO_n$ ) on the crystal nucleation and growth kinetics of  $Li_2O_2SiO_2$  in  $Li_2O_3SiO_2 \cdot RO_n$  glasses. The ratios of the number of nuclei between glasses  $Li_2O_3SiO_2 \cdot RO_n$  and  $Li_2O_2SiO_2 \cdot RO_n$  and also the ratios of the crystal growth rates were shown to increase with  $T_m$ , the immiscibility temperatures of  $Li_2O_3SiO_2 \cdot RO_n$ . The results were partly explainable on the basis that liquid immiscibility in the higher  $T_m$  glasses produced a liquid phase closer to the  $Li_2O_2SiO_2$  composition. However, the ratios of the growth rates between the two glasses were always less than the nucleation rates ratio. From nucleation theory they showed that nucleation rates were more sensitive than the growth rates to composition shifts in the matrix phase produced by phase separation. Thus the nucleation ratios should be less than the growth ratios. It was suggested that the nucleation ratios in the phase separated glass were higher than expected because crystals nucleated heterogeneously on the phase droplets.

The influence of fluorides on the nucleation of crystallization in soda-lime-silica glasses was determined quantitatively by Mukherjee and Rogers<sup>(124)</sup>. Two systems were chosen for study, 1)  $CaO-Na_2O-Al_2O_3-SiO_2$  and  $CaF_2$  2)  $Na_2O-CaO-SiO_2$  and  $CaF_2$ . The base glass in the first series nucleated only with difficulty but  $CaF_2$  containing glasses readily nucleated and phase separated at the holding temperature. The second series of glasses nucleated with difficulty despite extensive phase separation. The activation energy for nucleation in the first series was similar to the sodium ion diffusion activation energy in a  $Na_2O-CaO-SiO_2$  glass. Since sodium ion

diffusion is essential during phase separation they suggested that phase separation controlled the nucleation kinetics. Their results were based on the assumption that the nucleation kinetics at the low temperature end can be represented thus:

$$I \propto \exp\left(-\frac{\Delta G_D}{RT}\right)$$

where  $\Delta G_D$  is a diffusion activation energy. Rowlands analysis<sup>(18)</sup> of the nucleation kinetics shows that this approximation is probably inaccurate for silicate systems. Thus the effect of liquid immiscibility on the nucleation kinetics in this series may be open to question.

The role of fluorides in the crystallization of  $\text{Na}_2\text{O}-\text{CaO}-\text{MgO}-\text{Al}_2\text{O}_3-\text{SiO}_2$  glasses was studied by Lyng<sup>(125)</sup>. DTA data suggested that fluorides increased nucleation rates. All glasses showed liquid phase separation but only in a fluoride glass with MgO content less than 5 wt% did crystals appear to grow from the interfaces.

Kokubo et al<sup>(126)</sup> have studied the effects of additions of  $\text{Al}_2\text{O}_3$  and the occurrence of phase separation on the crystal products in two glasses:  $40\text{PbO}, 25\text{TiO}_2, 35\text{SiO}_2$  (glass 1),  $40\text{PbO}, 25\text{TiO}_2, 10\text{Al}_2\text{O}_3, 25\text{SiO}_2$  (glass 2).

Glass 1 crystallized metastable lead titanate followed by the transformation to perovskite. Glass 2 decomposed into a silica-rich matrix and droplets rich in  $\text{PbOTiO}_2$ . The latter precipitated perovskite. The  $\text{Al}_2\text{O}_3$  component in glass 2 induced liquid phase separation which stimulated perovskite formation.

Some examples of systems that do not exhibit phase separation and yet crystallize on a fine scale are  $\text{Li}_2\text{O}-\text{Al}_2\text{O}_3-\text{SiO}_2$ ,  $\text{MgO}-\text{Al}_2\text{O}_3-\text{SiO}_2$ ,  $\text{Li}_2\text{O}-\text{Ga}_2\text{O}_3-\text{SiO}_2$  and  $\text{Li}_2\text{O}-\text{Al}_2\text{O}_3-\text{GeO}_2$  with  $\text{TiO}_2$ <sup>(127)</sup>. Phase separation is also not essential for fine internal crystallization to occur in several simple binary systems, such as  $\text{Li}_2\text{O}-\text{SiO}_2$  and  $\text{BaO}-\text{SiO}_2$ .

Barry et al<sup>(128)</sup> have investigated the role of titania and liquid immiscibility in the crystallization of  $\text{Li}_2\text{O}\cdot\text{Al}_2\text{O}_3\text{-SiO}_2$  glasses. No sign of liquid immiscibility was detected in the  $\text{Li}_2\text{O-SiO}_2\text{-}\beta$  spodumene and  $\text{Li}_2\text{OSiO}_2\text{-}\beta$  eucryptite joins and yet some compositions were highly nucleating. They showed that titania acted to modify the kinetics of crystal growth by preferentially concentrating on particular faces of  $\beta$  eucryptite and inhibiting growth at these faces. It was also shown that titania could enhance crystal nucleation kinetics by acting as a surface active agent (i.e. reducing  $\sigma$ ) and inducing a redistribution of non-bridging oxygen ions to the periphery of completely bridged network regions.

#### 4.3 SUMMARY OF CHAPTER FOUR

The precise nature of the liquid phase separation effect on crystal nucleation has still not been clearly resolved. The influence of phase separation is probably specific to different glass systems. Theoretically, liquid phase separation should influence crystal nucleation in one or more of the ways according to the points discussed by Uhlmann. In practice it is difficult to determine which mechanism is involved. The apparent observation, in some cases, of heterogeneous nucleation of crystals on the surface of droplets could imply that crystals prefer to form here either due to concentration of components near the interface, which locally increase the driving force, or the mobility. There is a possibility that interfaces may migrate during heat treatment, and any relation between the interface and the crystals they nucleate may be lost. However, the dependence of the nucleation rate on the parameters describing phase separation morphology would still be retained, and hence it should be possible to study experimentally the importance of interfaces in nucleating crystals.

It is clear that in many cases phase separation can produce another liquid phase which can undergo crystal nucleation much more easily than the original composition before separation. (See for example the work of Burnett and Douglas<sup>(15)</sup> on  $\text{Na}_2\text{O}-\text{BaO}-\text{SiO}_2$  glasses). In this sense phase separation can be very useful since it effectively increases the range of compositions which can be crystallized to form glass ceramics.

The coincidence of liquid phase separation with crystal nucleation, as reported by several workers, does not provide sufficient evidence to conclude that the two are directly related as for example, by a heterogeneous nucleation process. Only nucleation experiments carried out on phase separated and homogeneous glasses of similar compositions can show if, and how phase separation influences crystal nucleation. In the case of nucleation catalysts it is probable that large additions of catalyst can increase nucleation rates on the basis of altering the liquidus temperature, diffusion rates and surface energies rather than causing liquid immiscibility to occur.

Thus although numerous experiments have been performed, the effects of phase separation on crystal nucleation and growth have by no means been clearly established.

**CHAPTER FIVE**

**EXPERIMENTAL METHODS**

## CHAPTER FIVE - EXPERIMENTAL METHODS

	<u>Page</u>
5.1 Preparation of the glasses	52
5.2 Chemical analysis of the glasses	53
5.3 Heat treatments	57
5.4 Optical microscopy	59
5.5 Electron microscopy	60
5.6 X-ray diffraction	62
5.7 Differential thermal analysis	62
5.8 Description of experiments to study the effect of liquid-liquid immiscibility on crystal nucleation.	63
5.9 Measurements of crystal growth rates in phase separated and non-phase separated glasses.	68
5.10 Early crystal development in baria-silica glasses.	69
5.11 Calculation of the morphological characteristics.	70

### 5.1 PREPARATION OF THE GLASSES

Eight binary BaO-SiO<sub>2</sub> glasses were melted with nominal batch compositions of 37, 35, 33, 32, 31, 30, 28 and 26 mol% BaO. The batch materials used to prepare the glasses were analar BaCO<sub>3</sub>, manufactured by Fisons, with a total impurity level not greater than 0.2 wt%, and acid washed Belgian sand with an iron content of less than 0.01 wt%. Accurately weighed quantities of the two materials were very thoroughly mixed. The blending action was achieved by a prolonged manual grinding process. Automatic mixing was not satisfactory because aggregation of the BaCO<sub>3</sub> occurred. The batch was sintered in a mullite crucible in an electric furnace at 1300°C for 16 hours to encourage reaction between SiO<sub>2</sub> and BaCO<sub>3</sub> and to facilitate homogenization. The material was ground to pass a 30 mesh sieve and after further mixing the batch was melted in a platinum crucible in a gas furnace at 1550-1600°C.

Ten minutes after the batch had completely melted, a platinum blade was introduced into the melt and stirring was immediately commenced. After six hours of stirring, the blade was withdrawn and within five minutes the glass was cast on a corrugated stainless steel plate. The resultant rods were allowed to cool to room temperature without an annealing treatment. The glass was crushed in a mortar and pestle until it passed a 30 mesh sieve and the melting schedule (excluding sintering) was repeated twice. It was necessary to follow this process closely in order to obtain reasonably homogeneous glasses. Omission of the sintering process produced a glass containing a solid surface layer of unmelted batch. This glass could not be stirred and consequently the final product was inhomogeneous.

The opalescent appearance of the two most baria-rich glasses (designated glasses 26 and 28) indicated the presence of liquid phase separation. Since the aim of the project was to study the influence of liquid phase separation on crystallization, it was necessary to quench glasses 26 and 28 more rapidly

between two cold stainless steel plates to prevent phase separation from occurring. The 'milky' was largely removed by the rapid quenching. However, a slight blue haze was still retained in some areas of glass 26.

The nucleation results, to be described later, showed a variation with composition and heat treatment. As a successful interpretation of the experiments depended on comparing nucleation rates in different glass samples, it was vital that representative sections of homogeneous glass should be obtained.

Each glass was tested by nucleating six to eight samples, taken from widely different regions of the glass, at 700°C for one hour, followed by a growth treatment at 840°C for a suitable time (usually about 10 mins to 30 mins). Visual observation of the microstructure in the optical microscope enabled quite small differences (about 20-30%) in the number of crystals to be detected. If a large variation was found in the number of crystals per unit volume measured in different parts of the same glass melt (for example a variation by a factor of two), the glass was deemed to be unsatisfactory and was remelted. Generally one or two premeltings were sufficient to obtain a satisfactory homogeneous glass with only a small variation in nucleation density (no more than 20-30% maximum variation). In order to standardise melting procedure, all glasses were melted a total of three times.

## 5.2 CHEMICAL ANALYSIS OF THE GLASSES

A prolonged treatment of sintering, melting and crushing was required to prepare the glasses, and this can cause changes in overall composition to occur. Estimates of BaO content and the level of impurities were carried out on all glasses.

### 5.2.1 Estimates of baria

Two chips of glass were fractured from different regions and tested individually. The glass was ground thoroughly in an agate mortar and pestle and the resulting powder dried in an oven and weighed in a platinum dish. A small amount of distilled water was added to moisten the powder, followed by aliquots of 40% HF and HClO<sub>4</sub>. The SiO<sub>2</sub> content combines with HF to form the volatile SiF<sub>4</sub> (boiling point -90°C), the reaction being catalysed by HClO<sub>4</sub>. Remnants of SiF<sub>4</sub> were removed on a steam bath and HClO<sub>4</sub> (boiling point 180°C) was fumed on a hot plate. The chemical treatment was repeated to remove all traces of SiO<sub>2</sub>. The BaO component was precipitated as BaSO<sub>4</sub> by addition of excess concentrated H<sub>2</sub>SO<sub>4</sub>. All remaining liquids were fumed on a hot plate and then evaporated in a muffle furnace at 500°C. The precipitate was weighed and BaO was calculated as BaSO<sub>4</sub>. This method had an accuracy of about ±0.5 mol% BaO at the compositions analysed, and all results for each pair of samples were within this error.

### 5.2.2 Estimate of alumina

Silica was removed by HF, as preciously described, and the barium-rich precipitate dried on a hot plate. This was dissolved in distilled water and reprecipitated as BaSO<sub>4</sub> on adding H<sub>2</sub>SO<sub>4</sub>. The Al<sub>2</sub>O<sub>3</sub> and iron compounds remained in solution. The mixture was filtered and the residue washed. The resulting filtrate was analysed for Al<sub>2</sub>O<sub>3</sub> content. Excess 0.01 M EDTA solution was used to complex the aluminium. The pH of the solution was adjusted by adding 18N ammonia solution with methyl orange as indicator until neutrality was achieved. This was buffered at 5.6 pH with ammonium acetate solution. A short boiling treatment ensured that

all aluminium was complexed with EDTA. On cooling, the excess EDTA was combined with zinc by titration against a standard 0.01M ZnSO<sub>4</sub> solution using xylenol orange as indicator. Boiling for two minutes with excess NaF released the EDTA combined with Al<sub>2</sub>O<sub>3</sub>, and this was titrated against ZnSO<sub>4</sub> solution. The difference between the two titration readings was a measure of the Al<sub>2</sub>O<sub>3</sub> content according to the relation:

$$1 \text{ ml of } 0.01 \text{ M EDTA} \equiv 0.0005 \text{ g of Al}_2\text{O}_3$$

### 5.2.3 Estimate of total iron

Another sample of filtrate was boiled down to 50 mls and poured into a 100 ml flask. 5 mls of 25% tartaric acid prevented aluminium from complexing with the indicator. The solution was buffered at a pH of 2.9 as follows: 2-3 drops of p nitrophenol and then 0.88N ammonia solution were added until the solution was slightly yellow. On cooling, the pH was adjusted with 3N HCl until the solution was colourless. The transfer of ferric to ferrous was achieved by first adding 2 mls of 10% hydroxy-ammonium chloride and then complexing with 10 mls of 0.1% orthophenanthroline. After standing, a red colour characteristic of the complex was developed. The solution was made up to 100 mls and the intensity of its colour was measured with an Evans electroselenium colorimeter at a wavelength of 510 nm. The iron content was found by contrasting the colour absorption with standard solutions of iron.

The chemical analysis revealed significant changes in the composition of the glass during the melting procedure (see Table 5.1). A possible explanation for the loss of baria from the original batch composition was the tendency of baria-rich glass to sink towards the bottom of the crucible during stirring. Since some glass was inevitably left in the crucible after pouring, the poured glass tended to be slightly silica-rich.

TABLE 5.1

GLASS COMPOSITIONS

Nominal Composition mol% BaO	Glass Designation	General Appearance of cast rods	BaO mol%	Al <sub>2</sub> O <sub>3</sub> mol% (Analysed)	Total Fe mol%
26	26	Opalescent	25.3	.15	.030
28	28	Opalescent	25.7	.48	.068
30	30	Clear	28.5	.34	.030
31	31	Clear	27.4	.02	.025
32	32	Clear	30.4	.19	.046
33	33	Clear	28.7	.03	.016
35	35	Clear	34.0		no values
37	37	Clear	35.4		no values

The amount of alumina detected in some of the glasses was larger than expected. Subsequently, it was found that the crystallization and liquid phase separation were affected noticeably by relatively small changes in the alumina impurity levels in the different glasses. It was, therefore, important to know the levels accurately to successfully interpret the results. It should be noted that the first four glasses to be melted (26, 28, 30, 32) contain higher levels of Al<sub>2</sub>O<sub>3</sub> than the rest. The main cause of alumina contamination was probably the sintering stage in the mullite crucible. Although great care was taken after sintering to reject batch immediately in contact with the mullite crucible, this precaution was

not sufficient to exclude all impurity. However, the contamination problem for the last four glasses to be melted (31, 33, 35, 37) was considerably reduced by only using sintered batch from the very central zone of the crucible for subsequent melting. Sintering in platinum was not a viable alternative to sintering in mullite or alumina since the sintering caused pitting of the crucible.

### 5.3 HEAT TREATMENTS

#### 5.3.1 Nucleation and growth

Small slices of glass rods 3 mm in thickness were cut using a diamond saw. Samples of each glass were given nucleation treatments at appropriate temperatures and times. The heat treatments necessary to grow the crystals to sizes that just avoided impingement within reasonable times, (10 mins to 1 hour) were carried out at 840°C. It was possible to determine when sufficient growth had occurred by noting the point at which the appearance of the glass began to change from transparent to translucent. This could be ascertained by shining a light through the sample while still in the furnace. When the glass started to appear 'frosty' the growth treatment was stopped.

Ideally the glass should not nucleate at the growth temperature. In practice it was sometimes necessary to allow for the relatively small amount of nucleation occurring at the growth temperature, and also to allow for some nucleation which occurred during the initial cooling down of the original glass melt and during the subsequent heating up and cooling. A correction for the nucleation at the growth temperature (840°C) was made by plotting a graph of number of crystals per unit volume ( $N_V$ ) versus time for glass samples heated at 840°C. However, in most cases the nucleation occurring at 840°C was negligible compared with that at the first stage nucleation treatment.

There is also a possibility that nuclei, having exceeded the critical size during the nucleation treatment, might redissolve at the growth temperature. The error was experimentally determined to be negligible for  $\text{Li}_2\text{O-SiO}_2$  glasses<sup>(65)</sup>. This was expected because growth at the nucleation temperature, although small, was sufficient for most crystals to exceed the critical size at the growth temperature.

The samples were nucleated in a Kanthal wound tubular furnace controlled to within  $\pm 1^\circ\text{C}$  using a Eurotherm temperature controller type 072. The gradient in the constant zone varied by less than  $1^\circ\text{C}$  over 2 cms. The glass samples were positioned in the middle of the constant zone. This was achieved by pushing them to a stop inserted at the appropriate place. A platinum wound furnace, also controlled by a Eurotherm controller, was used to grow the samples.

The specimens were supported in the furnace in pre-heated mullite boats. About three minutes or less elapsed before the samples attained the temperature of the furnace, and this was considered negligible when compared with the duration of the heat treatments. The temperature was measured with a Pt/Pt 13% Rh thermocouple inserted adjacent to the samples, the emf being accurately measured by a potentiometer using a mixture of ice and water as the cold junction. Continuous monitoring of the temperature was carried out on a Cambridge Chart Recorder.

### 5.3.2 Liquid-liquid immiscibility temperature measurements

Small chips of glass were heat treated at a sufficiently high temperature to cause opalescence within a reasonable time. They were then reheated at a series of higher temperatures. The maximum temperature above which the glasses visibly cleared was taken as the immiscibility temperature  $T_m$ , and could be obtained with an accuracy of about  $\pm 5^\circ\text{C}$  by this method. Electron

micrographs of the glasses heat-treated according to the 'clearing' method revealed liquid droplets in the opalescent glass and no evidence of separation in the transparent glass.

Some measurements were also carried out by noting the temperature at which opalescence first appeared in an initially clear glass. However, this 'opalescence' method was not considered to be as reliable as the clearing method. In general, the 'opalescent' method will tend to underestimate  $T_m$  due to the very slow kinetics of phase separation at temperatures just below the binodal - a finite undercooling being required for detectable nucleation to occur. However, droplets redissolve very rapidly at temperatures just above  $T_m$  and no evidence of phase separation was detected by electron microscopy (i.e. the 'clearing' method is expected to give the more accurate estimate of  $T_m$ ).

For compositions with lower miscibility temperature accurate measurements of  $T_m$  became impossible due to the occurrence of rapid internal crystallization (for example glass 32). Thus no liquid phase separation could be observed.

Difficulty was found in measuring  $T_m$  for glass 26 because rapid crystallization curtailed the time of heat treatment to a period of two or three minutes. Temperature equilibrium was not reached in such short times and hence the  $T_m$  for this glass may have been overestimated.

#### 5.4 OPTICAL MICROSCOPY

After heat treatment each glass sample was ground flat with 220 carborundum grit and several specimens were mounted together on a glass slide with pitch. Grinding was carried out on a lap wheel with successively finer carborundum grit (220, 440 and 600 grades) and finally polished thoroughly on a cerium oxide (cerirouge) felt wheel.

The glass samples were etched in a 0.2 HCl 0.5 vol% HF solution for the minimum time consistent with reasonable contrast. Usually ten seconds were sufficient to reveal the microstructure in detail. The etching procedure must necessarily dissolve one phase preferentially and this will modify the flatness assumed when calculating nucleation rates. This error was found by James<sup>(65)</sup> to be negligible in  $\text{Li}_2\text{O}_2\text{SiO}_2$  glass even for a quite heavy etch. Moreover, any error introduced by etching will be approximately the same for all glasses and the relative values will remain unchanged.

The microstructure was observed and photographed on a Leitz metallux microscope using reflected light. This method was used since a large number of crystals per unit volume  $N_v$  could be measured (and hence higher nucleation rates) than were possible using thin sections in transmission. With thin sections the overlapping of crystals more severely limited the maximum  $N_v$  that could be measured. In certain cases the insertion of a graticule in one of the eyepieces permitted the dimensions of any object to be directly determined without using photography.

## 5.5 ELECTRON MICROSCOPY

The electron microscope was a powerful tool for examining liquid phase separation morphology and early stage crystal development in the glasses. Thus thin glass films and carbon-platinum replicas of etched surfaces were prepared for detailed observation in the electron microscope.

The replicas were deposited by evaporation of carbon-platinum on to an etched glass surface mounted on a water repellent silicone rubber. The angle of shadow was  $10^\circ$ . A porcelain chip partly covered with silicone oil provided a method of estimating the thickness of the deposited film. A thin replica was preferable for maximum contrast. The replica was separated from the surface by scoring areas of  $1 \text{ mm}^2$  and then immersing the

glass in HF solution. Specimens of replica were scooped on to a copper grid and dried by evaporation. Observations of the replicas were carried out in an Hitachi HU 11A instrument at 75 kV.

The morphology of phase separation and crystallization were studied with replicas. More detailed information of the internal microstructure of crystals was obtained when thin films of glass were used. Selected area diffraction has been used <sup>(129)</sup> to identify the crystals and determine the mechanisms of the early stages of crystal growth in  $\text{Li}_2\text{O-SiO}_2$  glasses.

For the purpose of identifying crystals it was necessary to determine the camera constant ( $L\lambda$ ) of the electron microscope.  $L$  is the length from the objective lens to the SAD pattern and  $\lambda$  is the wavelength of the electron beam. The following relation was used

$$rd = L\lambda$$

where  $r$  is the distance separating a diffracted spot from the central spot and  $d$  is the interplanar distance of the planes responsible for the diffracted spot.  $\text{MoO}_3$  crystals of known unit cell dimensions were used to calculate  $L\lambda$ . It was thus possible to calculate  $d$  for any spot on the selected area diffraction pattern of any unknown crystal.

James and Kecwa <sup>(129)</sup> were able to study the early stages of spherulitic crystallization in a  $\text{Li}_2\text{O}.2\text{SiO}_2$  glass using a chemical thinning technique developed by James and McMillan <sup>(130)</sup>. Although chemical thinning was also applied successfully to the partially crystallized  $\text{BaO-SiO}_2$  glasses, it was found that somewhat better results were obtained for these glasses using ion beam thinning.

Specimens for ion beam thinning were prepared as follows. A flat piece of glass was cut into circular cross sections 3mm in diameter and 1 mm thick using an ultrasonic drill. These were mounted on a slide with

Canada Balsam and both sides ground with successively finer carborundum grit and polished with 6 $\mu$  and 3 $\mu$  diamond dust pads until the thickness had been reduced to 20-25 $\mu$ . Dissolution of the Canada Balsam in methanol separated the sample from the slide. The thin section was attached to a copper grid with lacomit.

The final thinning process was carried out in an Edwards IBMA2 ion beam thinning apparatus. The sample was bombarded by argon ions using a potential difference of 5kV. An angle of 20° was sufficient to thin the sample within a reasonable time limit and yet still retain large areas of uniformly thin sample transparent to an electron beam. A Phillips 301 electron microscope was used to examine and photograph the microstructure.

#### 5.6 X-RAY DIFFRACTION

The major crystal phases formed when the glasses had been heat treated, were identified by conventional X-ray diffraction techniques using Cu K $\alpha$  radiation on a Phillips powder diffractometer. The output was in the form of a trace that recorded the intensity of radiation diffracted as a function of angle of rotation. The 'd' spacings corresponding to the intensity peaks were collated and the identification of phases made with the ASTM index.

#### 5.7 DIFFERENTIAL THERMAL ANALYSIS

Changes in heat content that are characteristic of glasses when they crystallize or undergo relaxation at the glass transformation temperature T<sub>g</sub> were recorded on a Standata differential thermal analysis (DTA) apparatus. The output was in the form of a trace consisting of an endothermic dip produced by structural relaxation and an exothermic peak produced by

crystallization or crystal transformation. Hence the interpretation of the thermograms yielded values of  $T_g$  and crystallization or transformation temperatures. Figure (5.1) shows how these are obtained from a schematic thermogram.

The DTA compares heat absorption and evolution of a finely divided glass powder with a reference standard (AR calcined alumina powder) as a function of temperature. The powders were held in two small platinum crucibles surrounded by a sintered alumina block. Pt/Pt 13% Rh thermocouples measured the temperature of the ceramic block and the differential temperature of the two samples. A platinum wound furnace surrounding the DTA 'head' was heated at a rate of  $10^\circ\text{C}$  per minute using a programmed temperature controller.

It must be noted that the dynamic estimate of  $T_g$  described above will give a higher value (usually about  $30^\circ\text{C}$ ) than a static determination. Static measurements of  $T_g$  usually correspond to a temperature where the viscosity is  $10^{13}$  poise. The DTA estimate of  $T_g$  determined in this work (using a heating rate of  $10^\circ\text{C}$  per min) will be referred to as 'DTA  $T_g$ '.

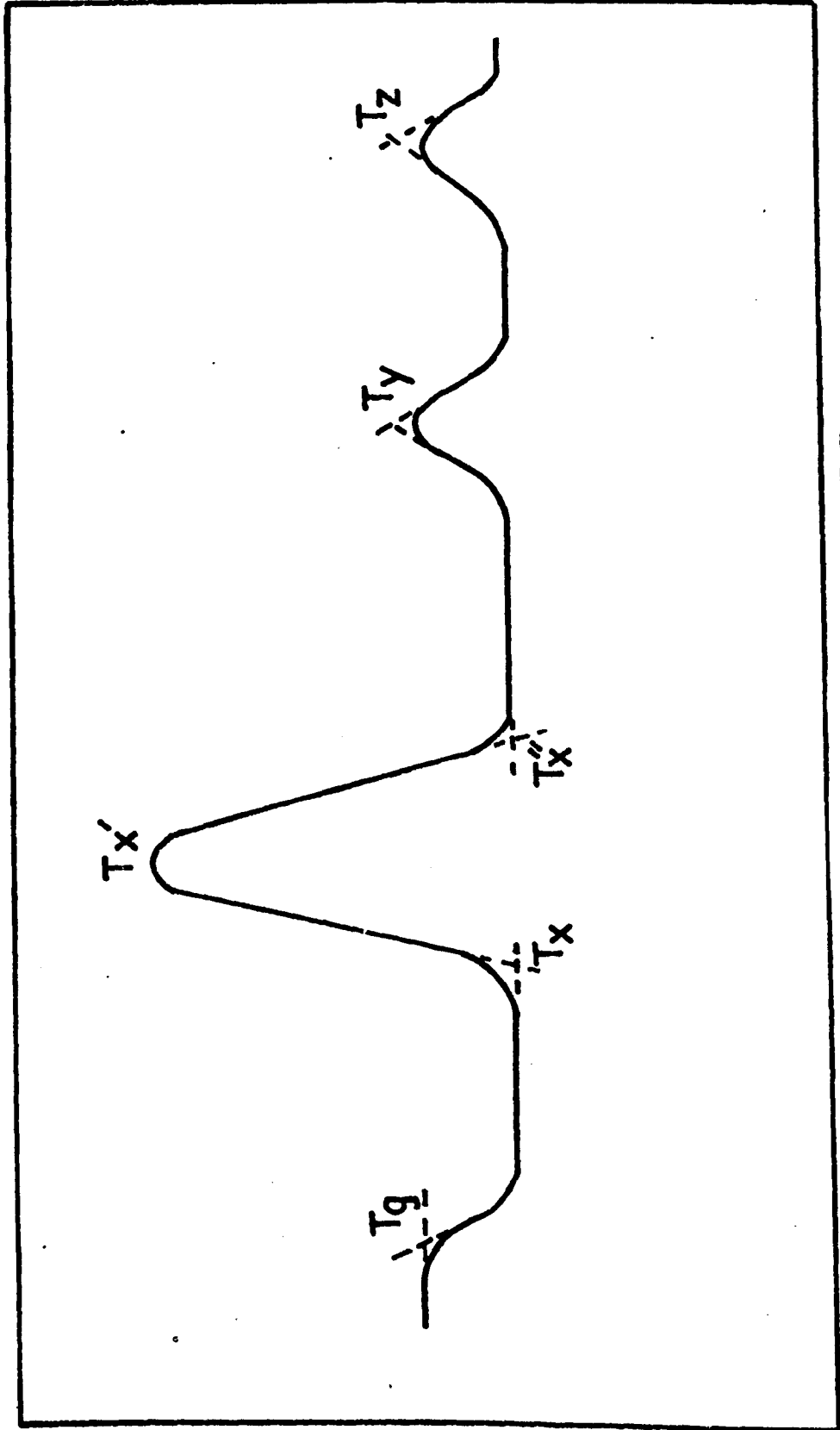
## 5.8 EXPERIMENTS TO STUDY THE EFFECT OF LIQUID-LIQUID IMMISCIBILITY ON CRYSTAL NUCLEATION

Glasses 33, 32, 31, 30, 28 and 26 occupy an interesting area of the phase diagram extending from outside the immiscibility zone to regions well within the zone.

Two types of experiments were devised to study the effects of liquid-liquid immiscibility on crystal nucleation kinetics. In the first type of experiment all the glasses, including those compositions capable of phase separating and those which could not, were given heat treatments at a series of temperatures from  $673^\circ\text{C}$  to  $807^\circ\text{C}$  for a constant time (1 hour). Nucleation

**Figure 5.1** Schematic DTA thermogram showing how  $T_g$ ,  $T_x$ ,  $T_x'$ ,  $T_x''$ ,  $T_y$  and  $T_z$  were determined.

$\Delta T$  is the difference in temperature between the sample and the  $Al_2O_3$  reference



SAMPLE TEMPERATURE

of the barium disilicate crystalline phase occurred in this temperature range. After the nucleation heat treatment, each glass was given a growth treatment at 840°C to grow the crystals to observable dimensions for the optical microscope. The values of  $N_v$  were determined and compared for the various glasses. The morphology of liquid-liquid immiscibility in the glasses given only a crystal nucleation treatment was also studied and compared with the nucleation results (the growth stage was omitted in this case).

Interpretation of the results for the first type of experiment was subsequently found to be complicated by the presence of small amounts of alumina impurity which made direct comparison of the glasses more difficult. However, some useful conclusions were obtained as will be described later.

In the second type of experiment, studies were carried out on single compositions (26 and 30) in which the morphology and extent of liquid phase separation were varied systematically and the effects on nucleation kinetics determined. Thus the problem of alumina contamination was not important. Slight opalescence in glass 26 indicated the presence of liquid phase separation and some samples were reheated to above  $T_m$  and then rapidly quenched into silicone oil to remove phase separation. Samples quenched in silicone oil and samples rapidly cooled in air were given a crystal nucleation heat treatment at 700°C and a growth treatment at 840°C. These were compared with samples that had been given heat treatments designed to fully phase separate the glasses, followed again by nucleation at 700°C and growth.

The temperatures and times chosen to induce liquid-liquid immiscibility (900°C 10 mins; 800°C 1 hour) were chosen to satisfy the requirements of negligible or very low crystal nucleation rates, since it was desired to have negligible crystal nucleation present prior to the main nucleation treatment at 700°C. Also, it was necessary for these heat treatments to produce microstructures of separation on quite different scales, thus

enabling any relation between  $N_v$  and the phase separation morphology to be determined.

The nucleation times at 700°C were from 0.5 hours to 17 hours. As well as taking samples for growth treatment to determine crystal nucleation densities  $N_v$  for the different times, samples of the glass heated only at 700°C (not grown) for identical times were used to study the liquid phase separation quantitatively. Carbon replicas were made from these samples and photographed in the electron microscope to determine the various parameters characterising the phase morphology, i.e. number of particles of liquid separation per unit volume  $N_v$ , volume fraction of dispersed phase  $V_f$  and interfacial area  $S_v$ . This work was carried out to monitor the development of liquid phase separation quantitatively at the same time as determining the crystal nucleation kinetics. These experiments were designed to a) reveal the consequences of phase separation occurring at the same temperature as nucleation, b) to assess whether the morphology of phase separation influenced nucleation.

The experiment described is illustrated schematically in Figure (5.2), which shows the relations between the heat treatments at 700°, 800°, 900°C and the composition of the equilibrium phases that form at each initial temperature for an initial composition C.

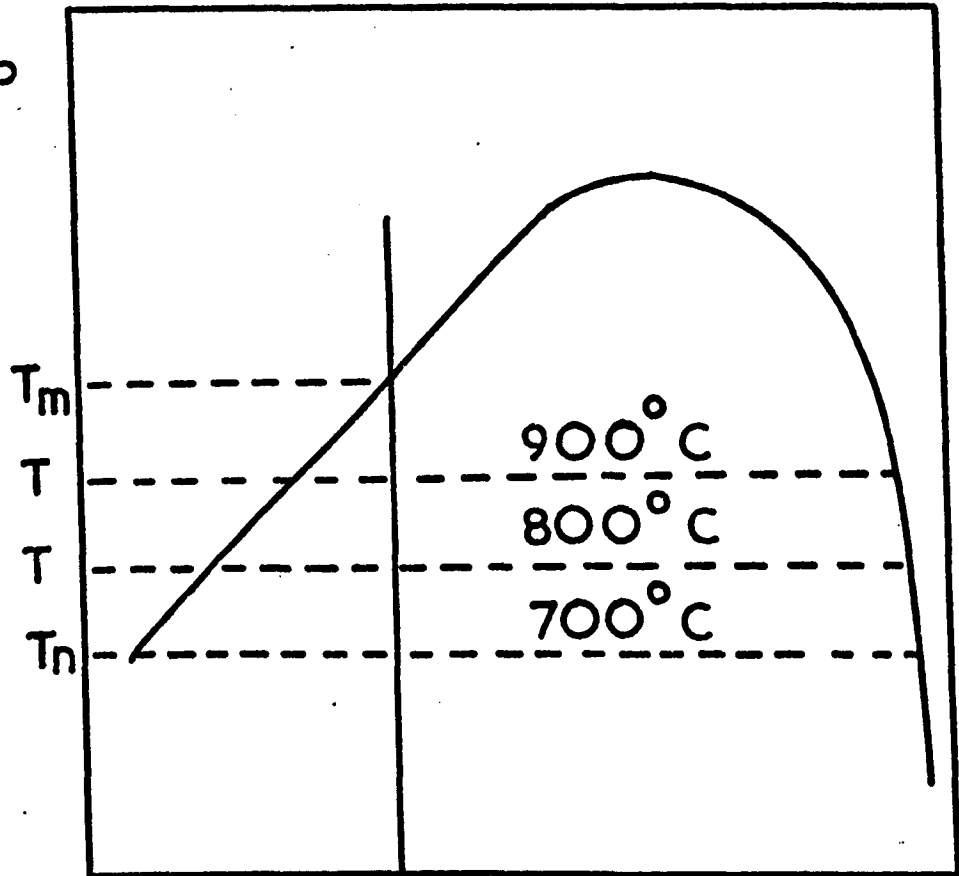
The crystal nucleation temperature  $T_N$  (700°C) was selected to satisfy the following requirements:

a)  $T_N$  was near the maximum nucleation rate temperatures for the glass. In practice, use of this temperature enabled greater accuracy of  $n_v$  measurements to be obtained since almost negligible nucleation occurred during heating or cooling compared with the nucleation produced at  $T_N$ .

b) Liquid phase separation had to proceed gradually over a period of several hours before the coarsening stage began. This criterion was necessary in order to sustain over a long period the differences in

**Figure 5.2.** Diagram showing relation between composition of phases separating from a glass of composition C, as a function of temperature

TEMP



C COMPOSITION

nucleation behaviour between the initially homogeneous samples and the initially phase separated samples. On the other hand, if coarsening was delayed too long then any changes associated with continued phase separation would have involved determining an  $N_v$  that exceeded the limits of the optical microscopic method ( $\sim 2 \times 10^{10} \text{ cm}^{-3}$ ). The  $T_N$  of  $700^\circ\text{C}$  satisfied these conditions.

The pre-heat treatment temperature  $T_H$  (used for some of the samples) was chosen on the grounds of a) very low or negligible nucleation rate for crystals, b) very rapid phase separation, c) non-proximity to  $T_m$  the immiscibility temperature. For glass 26 the range of temperatures satisfying these conditions were wide. However, for glass 30 where  $T_m$  was  $905^\circ\text{C}$ , for temperatures approaching  $T_m$  liquid phase separation occurred on a coarse scale with only small changes in composition between the equilibrium phases. Two  $T_H$  temperatures were chosen for experiments on glass 26, but for glass 30 the low  $T_m$ , allowed only one value to be selected ( $780^\circ\text{C}$ ). Each temperature of heat treatment for 26 and 30 produced a quite different phase separation morphology. This was, of course, intended so that the crystal nucleation behaviour of glasses of widely different values of  $S_v$ ,  $n_v$  and  $V_f$  for phase separation could be directly compared.

In the case of glass 30, pairs of samples of the as-poured glass were taken. One of each pair was given a liquid phase separation treatment to equilibrium at  $780^\circ\text{C}$  for one hour while the other was given no heat treatment. The pairs of samples were then nucleated for crystals at  $700^\circ\text{C}$  for a series of times ranging from 2 to 60 hours. In this way the nucleation behaviour of the initially separated glass could be compared with the as-cooled glass. The normal air quenching method was sufficient to suppress phase separation and no rapid quenching technique was employed.

Summarising, the second type of experiment compares the crystal

nucleation behaviour of samples of the same glass composition in the following initial states: a) a homogeneous sample that had been oil quenched (little or no phase separation), b) a very fine scale but incompletely separated sample that had been cooled rapidly in air and c), d) samples completely phase separated at two different temperatures designed to produce a medium and a coarse 'droplet' microstructure. For glass 30 the crystal nucleation behaviour of the following were compared, a) an air cooled initially homogeneous glass and b) a completely phase separated glass.

Control samples were used to estimate the nucleation (if any) during the prior heat treatment and growth procedures.

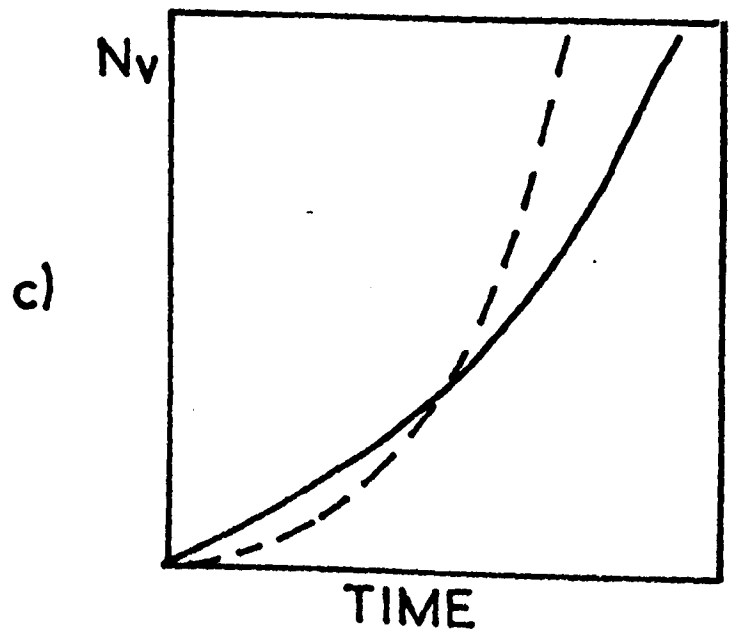
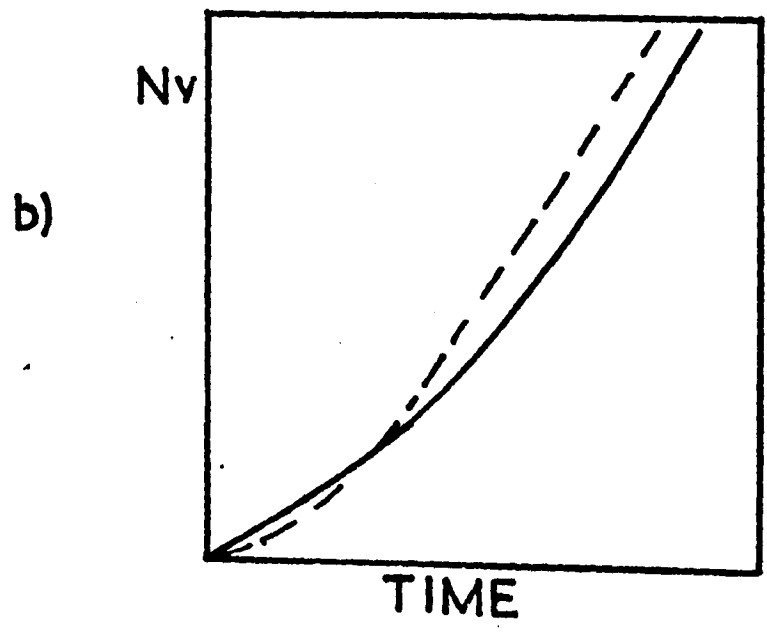
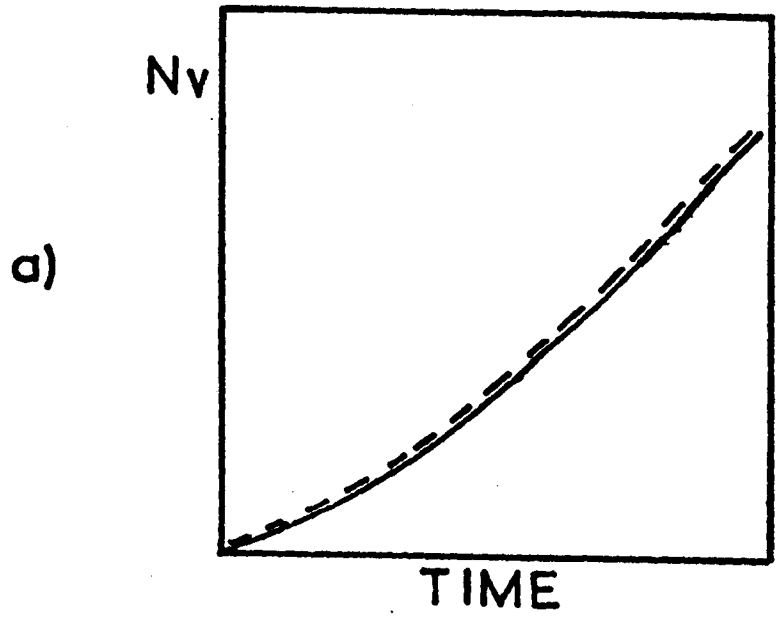
There are many ways in which liquid phase separation might affect the  $N_v$  versus time plots for crystal nucleation. Although it is not proposed to discuss all of these ways in this chapter, it will be useful to consider a few of the possibilities before detailed results are presented later. These are represented schematically in Figure (5.3). For simplicity only two curves are considered: the as-cooled glass sample and the glass prior heat treated to induce initial phase separation. If the curves are coincidental as in a), then phase separation has had no effect on the crystal nucleation at temperature  $T_N$ . The case represented by b) where the curves are eventually parallel, is the result of compositional changes being of paramount importance. Figure (5.3(c)) illustrates a continual and permanent divergence between the curves. This observation would imply that the morphology is exerting a considerable influence on crystal nucleation. If, for example, crystals nucleated on the surface of the liquid droplets then  $S_v$ , the interfacial area, would be important, and as this factor is different for the various glass samples, the overall tendency would be for the glasses to nucleate at different rates.

**Figure 5.3** Schematic representation of the effect of liquid-liquid immiscibility on crystal nucleation

- a) Liquid-liquid immiscibility has no effect on crystal nucleation
- b) Liquid-liquid immiscibility affects crystal nucleation only by causing compositional shifts in the nucleating phase
- c) Crystals prefer to nucleate on interface between phases.

————— initially phase separated

----- initially non-phase separated



## 5.9 MEASUREMENTS OF CRYSTAL GROWTH RATES IN PHASE SEPARATED AND NON-PHASE SEPARATED GLASSES

In general it was not possible to carry out experiments designed to compare the growth rates in phase separated and non-phase separated samples of a glass of a given composition, because of the very rapid development of liquid-liquid immiscibility at the temperatures where crystal growth rates could be measured conveniently by optical microscopy. An exception was glass 30 in a specific temperature zone just below the immiscibility boundary. Here the nucleation of phase separation was very slow and samples opalesced only if they were given a prior heat treatment at lower temperatures.

From theoretical considerations the Arrhenius plot of  $\ln$  (growth rate) versus  $1/T$  is expected at high undercoolings below the liquidus temperature, to be approximately a straight line with a constant activation enthalpy of growth.

The compositions selected for the growth experiments consisted of glasses 26, 28, 30 and 32. Glasses 26 and 28 had immiscibility temperatures  $T_m$  well above the range of temperatures used for crystal growth measurements. For glass 32 the  $T_m$  was lower than the growth range, and for glass 30 the  $T_m$  was in the middle of the growth range.

Six quenched samples of each glass were heat treated at specified temperatures for different periods of time. The temperature range utilised for the growth experiments usually extended from about 750°C to 900-950°C. At the low temperature end the nucleation rates were high, and due to impingement, crystals were prevented from growing to sizes convenient for measurement in the optical microscope. At the high temperature end measurements were limited by furnace temperature stabilisation during short growth times (< 3 mins). The average of the radii of ten of the largest spherulites

was measured and plotted as a function of time. The slope of the graph gave the crystal growth rate at the particular temperature. If only a few spherulites were available for measurement the experiment was repeated on a pre-nucleated glass sample. This ensured that the polished section passed through the centres of a reasonable number of the spherulites. Thus several of the maximum size spherulite sections could be measured with little scatter in the radii values.

A thin glass sample was ground and polished on both sides and the growth of the spherulites was determined using transmitted light. These results were entirely in agreement with the method described above using surface reflected light. Thus when the microstructure contained many large spherulites the techniques described produced satisfactory measurements of the crystal growth rate.

The growth rates calculated according to the largest diameter spherulites on the polished section, gave more consistent results than those taken from the thickness of surface growth. In fact the layer thickness was apparently very dependent on the nature of the surface that initiated crystal growth. The surface formed by the glass in contact with the steel mould during casting was rough and the glass-air interface was usually smooth. In addition, the angle that the surface made with the cross-section under examination also affected the layer thickness. Since there was no accurate control over these factors, it was decided to use the internal spherulites when measuring growth rates.

#### 5.10 EARLY CRYSTAL DEVELOPMENT IN BARIA-SILICA GLASSES

The techniques of X-ray diffraction, replica and thin film electron microscopy were used to provide additional information on the crystals nucleated internally, particularly the morphology of the development and the

crystallographic mechanism of the growth processes.

A particularly high internally nucleating glass containing nominally 35 mol% BaO was prepared. The chemical analysis indicated that the final composition was 34.0 mol% BaO and was very close to the stoichiometric disilicate composition. Thus this glass possessed a very high nucleation rate for the BaO<sub>2</sub>SiO<sub>2</sub> crystal phase. Heat treatment at 700°C - close to the maximum nucleation temperature, was carried out for a series of times until crystal impingement occurred (~ 160 hours). The samples were slowly heated and cooled to prevent stresses from shattering the glass. The time of heating and cooling was approximately ten minutes in each case and was considered to be negligible compared with the period of heat treatment at 700°C. The nucleation was so high that a reasonable number of crystals was visible in the glass in the electron microscope and the crystal development could be traced back to the very early stages.

## 5.11 CALCULATION OF THE MORPHOLOGICAL CHARACTERISTICS

### 5.11.1 Nucleation measurements

The crystal nucleation rate was calculated from the slope of the number of crystals per unit volume ( $N_v$ ) versus time (t) plot. The equations derived by Fullman<sup>(131)</sup> and Dehoff and Rhines<sup>(132,133)</sup> were used to calculate  $N_v$  from micrographs of plane sections of the glass. The particle intersections were close to circular in shape and, therefore, the particles were assumed to be spherical.

Fullman's formula is based on the probability of a random plane intersecting particles of different sizes and shapes. The number of particles intersected per unit area  $N_A$  is related to  $N_v$  by the equation:

$$N_A = N_v \overline{D_v}$$

where  $\overline{D}_v$  is the mean perpendicular distance between tangent planes for each particle under consideration. The formula is valid for any particle shape and size distribution.  $\overline{D}_v$  can be determined if a function  $Z$  is introduced so that

$$\overline{D}_{v_i} \overline{Z}_i = C$$

where  $C$  is a constant defining particle shape but not size and  $\overline{D}_{v_i}$  is the average value of  $D_v$  for particles in the size interval  $i$ . The particle number can now be written as

$$N_v = \frac{N_A \overline{Z}}{C}$$

$Z$  must be a unit of dimension (length)<sup>-1</sup> and is the reciprocal of the intersection diameter. For a sphere,  $C$  has the value of  $2/\pi$  and

$$N_v = \frac{2N_A \overline{Z}}{\pi}$$

Since

$$\overline{Z} = \frac{\sum_i N_{A_i} \overline{Z}_i}{\sum_i N_{A_i}}$$

$$\therefore N_v = \frac{2 \sum_i N_{A_i} \overline{Z}_i}{\pi} \quad (5.1)$$

The main problem was to evaluate  $\sum_i N_{A_i} \overline{Z}_i$ . This was done by measuring the diameters of 300-400 particles on enlarged prints from optical micrographs to within 0.25 mm using an accurately calibrated graticule. All the particles were consigned to one of ten or more groups depending on their size. The value of  $N_{A_i} \overline{Z}_i$  was calculated for each group and then summed. A sample calculation is given in Appendix (5.1).

The interpretation of the results required the careful comparison of nucleation rates between glasses of different compositions and identical glasses subjected to varying thermal histories. The errors probably arise from two main sources: the random sampling error (purely statistical in nature), and errors due to small compositional variations in the glass from one region to another. The latter could, for example, cause small systematic variations in the number of crystals nucleated in the glass in different regions. It was possible to assess the total effect of these sources of errors by analysing the results from different areas of the same glass sample. Appendix (5.2) shows that a count of 300-400 particles gave  $N_v$  with 95% confidence limits of about  $\pm 15\%$ .

For the crystal growth measurements the best values of the slopes of  $\log_{10}(\text{growth rate})$  versus  $1/(T^\circ\text{K})$  and crystal thickness versus time were obtained by the method of least squares. A sample calculation is given in Appendix (5.5).

#### 5.11.2 Determination of stereological parameters for the phase separated glasses

The volume fraction can be used to characterise the stage of development of liquid-liquid immiscibility. According to other workers<sup>(84)</sup> the volume fraction in phase separated glasses varies sigmoidally with time until a constant value is attained. At this stage phase separation is complete and coarsening commences.

A convenient property of a system containing a large number of phase particles is that the volume fraction of the phase constituting the particles is equal to the area fraction of the phase on any plane provided that the depth of etch is not great<sup>(133,134)</sup>. The area fraction was estimated by determining the fractional number of points in an array that fell within

the boundaries of the dispersed phase. The points were distributed at the corners of a square lattice. This method provided a more accurate result for a given number of counts than any other method of area or linear point counting. The optimum density of points corresponded to approximately one point for each particle. Two sets of four lines were inscribed on a sheet of perspex at right angles to each other at a suitable distance apart. The intersection of the lines provided a sixteen point grid which was applied randomly to the micrographs. The proportion of the points lying in one phase was the volume fraction  $V_f$  of that phase. A point falling within the dark boundary surrounding each particle was considered to belong equally to either phase and counted as one half. After the completion of a few trials the mean value of  $V_f$  was substituted into the equation:

$$P = \frac{1}{\sigma^2} [V_f(1 - V_f)] \quad (5.2)$$

where  $P$  is the total number of points needed to attain 95% confidence limits within an error of  $\pm 10\%$  of the mean value and  $\sigma$  is the appropriate standard deviation of the normally distributed  $V_f$  values. The point counting process was continued for  $P/16$  times and the average value of  $V_f$  was computed. An example of the calculations is given in Appendix (5.3) and shows that sixty trials on a phase separated structure with a volume fraction of about 30% gives 95% confidence limits within  $\pm 10\%$ .

The surface areas of internal boundaries were calculated by the Smith and Guttman method<sup>(133,135)</sup>. The interfacial area of the dispersed phase per unit volume  $S_v$  is given in terms of the number of intersections per unit length of a test line with the interface  $N_L$  by

$$S_v = 2 N_L \quad (5.3)$$

A straight line of 10 cm length was scored on a thin perspex sheet and placed randomly across the print of the microstructure. From the number of intersections per unit length,  $S_v$  was calculated.

In the case of two particles that apparently coalesced the convergence of the dark outline was assumed to indicate a close approach but not a contact between the two particles. The disappearance of the outline was taken to represent a true joining together of the droplets.

About 40 trials were required to obtain  $S_v$  with 95% confidence limits within  $\pm 8\%$  of the mean. An example of the calculation of  $S_v$  and the 95% confidence limits is supplied in Appendix (5.4).

**CHAPTER SIX**

**CRYSTAL NUCLEATION AND LIQUID-LIQUID IMMISCIBILITY**

**RESULTS AND DISCUSSION**

CHAPTER SIX - CRYSTAL NUCLEATION AND LIQUID-LIQUID IMMISCIBILITY

RESULTS AND DISCUSSION

	<u>Page</u>
6.1 Crystal nucleation and liquid-liquid immiscibility in glasses 33, 32, 31, 30, 28 and 26 - Experiment 1	75
6.2 Crystal nucleation and liquid-liquid immiscibility in glass 26 - Experiment 2	94
6.3 Crystal nucleation and liquid-liquid immiscibility in glass 30 - Experiment 3	110
6.4 Further discussion	116

## 6.1 CRYSTAL NUCLEATION AND LIQUID-LIQUID IMMISCIBILITY IN GLASSES

### (33, 32, 31, 30, 28, 26) - EXPERIMENT 1

#### 6.1.1 Crystal nucleation results

Samples of glasses 33, 32, 31, 30, 28 and 26 were nucleated over a temperature range from 650°C to 807°C for one hour and given a growth treatment at 840°C or 902°C for a suitable time. The nucleation results, expressed as the number of crystals per cm<sup>3</sup>, are given in Table (6.1).

The letters below each entry symbolise the visual appearance of the glass samples after a nucleation. For instance, C denotes that the glass was clear, SO slightly opalescent, VO very opalescent.

Plots of  $\log_{10}N_v$  versus temperature are shown in Figures (6.1) and (6.2). For clarity the glasses are subdivided into two groups: 1) 26, 31, 32,33 with an alumina content less than 0.2 mol%, and 2) 30, 28 with an alumina content greater than 0.2 mol%. The results labelled 35G are extrapolated from data supplied by Rowlands<sup>(18)</sup> for a glass containing nominally 33<sup>1/3</sup> mol% BaO. This date (Table (6.2)) gives the number of crystals formed after one hour of heat treatment as a function of temperature. The BaO<sub>2</sub>SiO<sub>2</sub> (35G) results, as given by Rowlands, were in the form of an  $N_v$  (number of crystals) versus time (t) plot for each temperature. At high temperatures the  $N_v$  versus time plot was linear and data could be easily extrapolated. However, at lower temperatures, where induction times were considerable, the plot was no longer linear, and estimation of values by extrapolation was less reliable.

The nucleation results for glasses 26 to 33 are more dispersed at the low temperature end (see Figures (6.1) and (6.2)). For example, the gap of nearly 1.5 orders of magnitude at 693°C that spans the results for glasses 26, 31 and 32 is reduced to 0.5 orders at 773°C. Similar observations can be made for glasses 30 and 28. It should also be noted that there is a

**Figure 6.1** Plot of  $\log_{10} N_v$  ( $\text{cm}^{-3}$ ) versus temperature ( $^{\circ}\text{C}$ ) for glasses containing less than 0.2 mol%  $\text{Al}_2\text{O}_3$  (i.e. glasses 26, 31, 32 and 33)

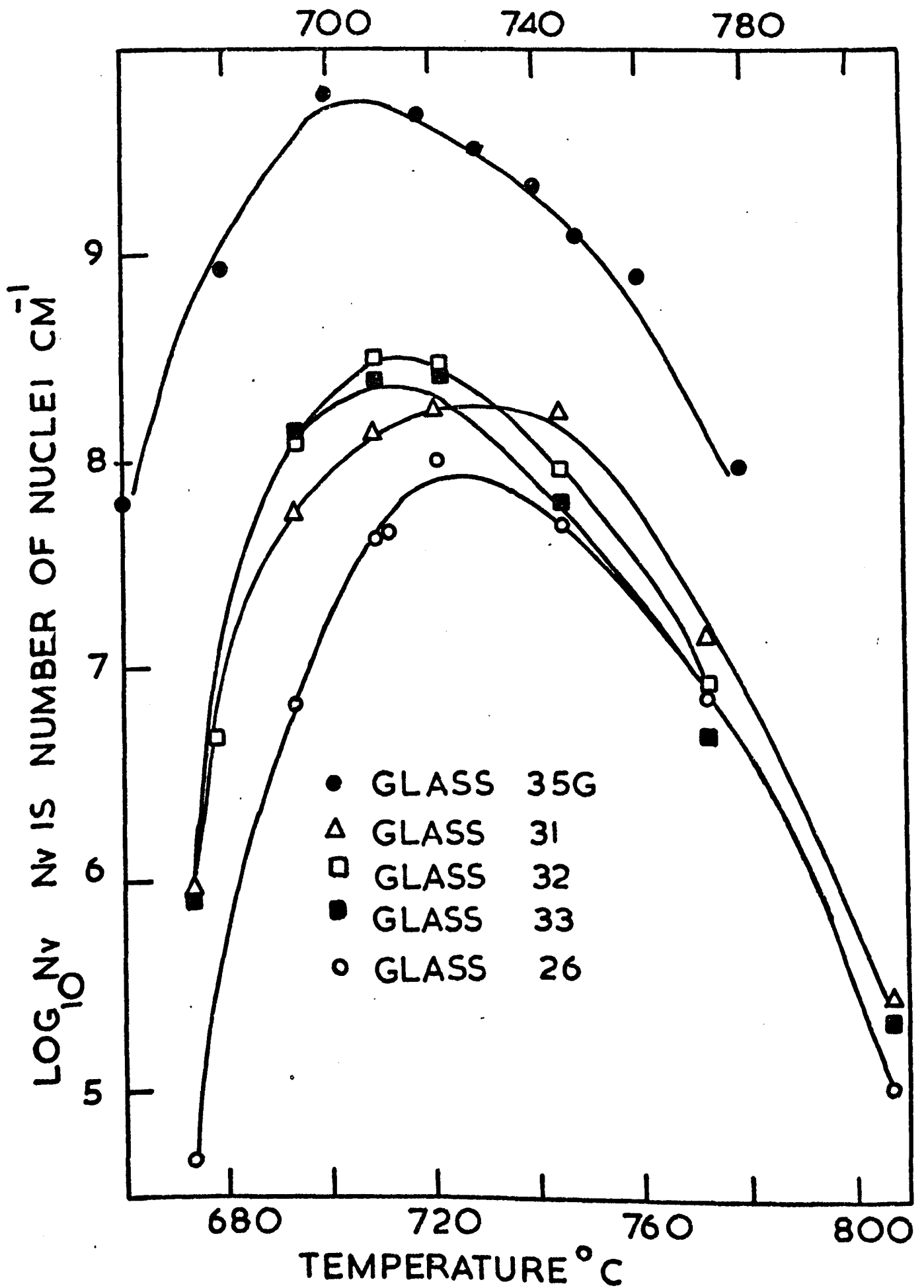


Figure 6.2 Plot of  $\log_{10} N_v$  ( $\text{cm}^{-3}$ ) versus temperature ( $^{\circ}\text{C}$ ) for glasses containing more than 0.2 mol%  $\text{Al}_2\text{O}_3$  (i.e. glasses 28 and 30)

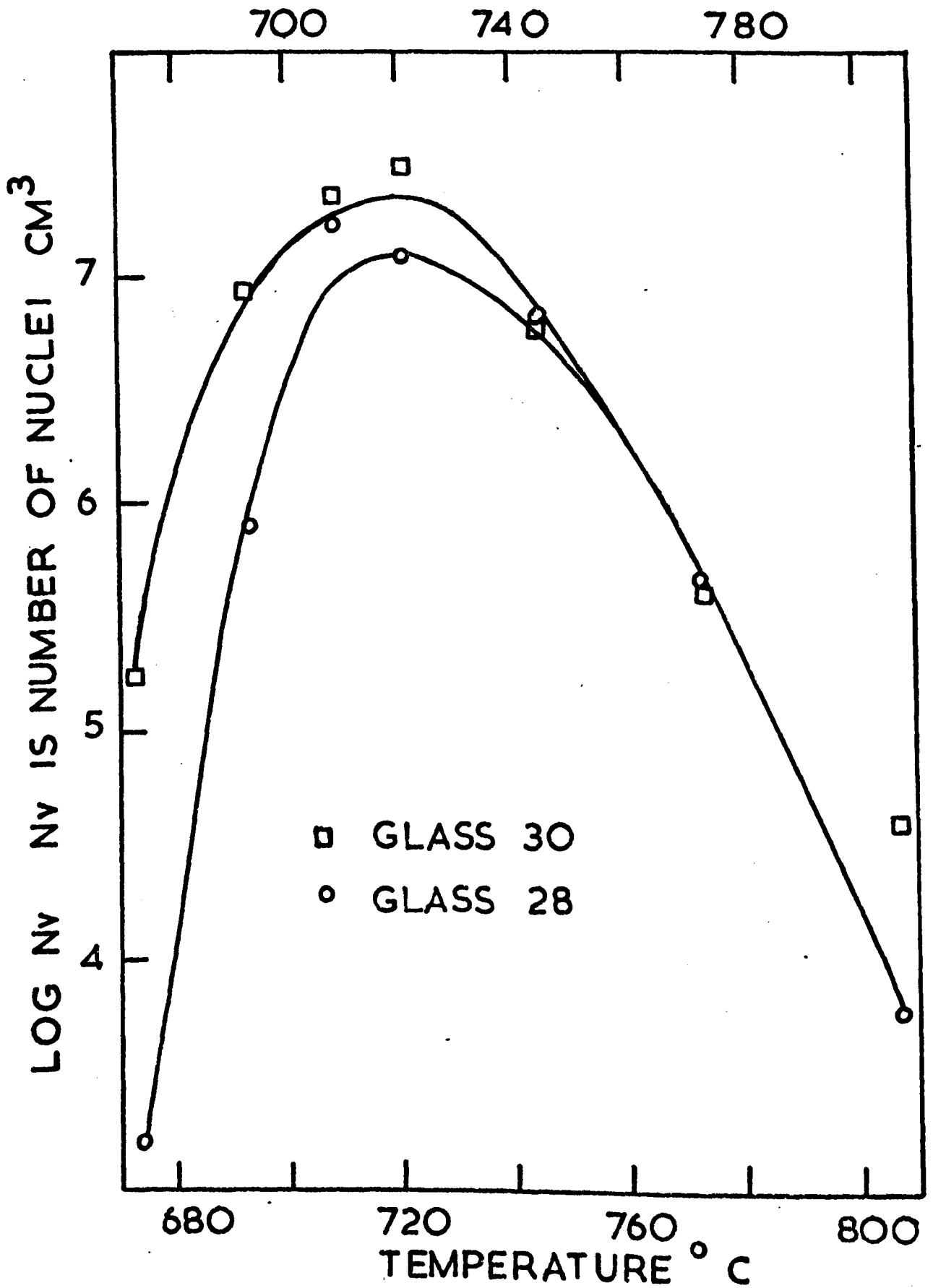


TABLE 6.1

NUMBER OF CRYSTALS ( $N_v$ )  $\text{cm}^{-3}$  IN GLASSES 26, 28, 30, 31, 32  
AND 33 AFTER A NUCLEATION TREATMENT OF ONE HOUR  
AS A FUNCTION OF TEMPERATURE

Nucleation Temperature °C	Glass					
	26	28	30	31	32	33
650	$7.91 \times 10^3$ C	negligible C	$2.57 \times 10^4$ C	$1.37 \times 10^4$ C	$9.95 \times 10^4$ C	$7.80 \times 10^4$ C
673	$4.44 \times 10^4$ C	$1.58 \times 10^3$ C	$1.70 \times 10^5$ C	$8.42 \times 10^5$ C	$4.78 \times 10^6$ C	$8.15 \times 10^5$ C
693	$6.61 \times 10^6$ C	$7.69 \times 10^5$ C	$8.57 \times 10^6$ C	$5.80 \times 10^7$ C	$1.28 \times 10^8$ C	$1.38 \times 10^8$ C
709	$4.13 \times 10^7$ C	$1.70 \times 10^7$ C	$2.28 \times 10^7$ C	$1.38 \times 10^8$ C	$3.24 \times 10^8$ C	$2.53 \times 10^8$ C
721	$1.02 \times 10^8$ C	$1.21 \times 10^7$ C	$3.00 \times 10^7$ C	$1.87 \times 10^8$ C	$2.90 \times 10^8$ C	$2.92 \times 10^8$ C
745	$4.91 \times 10^7$ C	$6.37 \times 10^6$ C	$6.34 \times 10^6$ C	$1.67 \times 10^8$ C	$9.48 \times 10^7$ C	$6.45 \times 10^7$ SO
773	$7.21 \times 10^6$ C	$4.47 \times 10^5$ C	$4.19 \times 10^5$ O	$1.38 \times 10^7$ O	$8.52 \times 10^6$ C	$4.68 \times 10^6$ O
807	$1.11 \times 10^5$ O	$5.86 \times 10^3$ O	$4.12 \times 10^4$ VO	$2.81 \times 10^5$ VO	na C	$2.21 \times 10^5$ C

na , not available

TABLE 6.2

NUMBER OF CRYSTALS ( $N_v$ )  $\text{cm}^{-3}$  FORMED IN  $\text{BaO}_2\text{SiO}_2$  GLASS (35G)  
AT ONE HOUR (EXTRAPOLATED FROM DATA GIVEN IN REF. 18)

Temperature °C	660	680	700	715	
$N_v$ $\text{cm}^{-3}$	$5.89 \times 10^7$	$8.32 \times 10^8$	$5.89 \times 10^9$	$4.79 \times 10^9$	
Temperature °C	729	740	748	760	780
$N_v$ $\text{cm}^{-3}$	$3.16 \times 10^9$	$2.09 \times 10^9$	$1.20 \times 10^9$	$7.59 \times 10^8$	$9.33 \times 10^7$

constant difference (about an order of magnitude) in the number of crystals nucleated in glasses 32 and 35G over a temperature range 693 to 773°C (i.e. the nucleation curves for these two glasses do not converge at high temperatures).

Figure (6.3) compares visually the number of crystals nucleated at one hour for glasses 26 and 32 at 709, 721, 745, 773°C.

### 6.1.2 The DTA results

The values of 'DTA Tg',  $T_x$ ,  $T_x'$ ,  $T_x''$ ,  $T_y$  and  $T_z$  (see Figure 5.1) are given in Table (6.3).

The crystallization peak X does not show any systematic variation between the glass compositions. This shows that the crystallization peaks are mainly influenced by the growth rates since the nucleation rates vary between the glasses.

The origin of the peaks Y and Z was not investigated. However, it should be noted that Z is absent in 35 and becomes increasingly prominent with silica content. Thus it is likely that Z identifies precipitation of cristobalite. Also, the position of Y is almost identical to the spherulite-lath transformation reported by Rowlands<sup>(18)</sup>.

The glass transformation temperature is generally considered to correspond to a constant viscosity value. ( $10^{13}$  poise, although the DTA Tg corresponds to a somewhat lower value than this). If the Stokes-Einstein relation is valid for crystal growth (Chapter 3), the kinetic term involving  $\Delta G_D^*$  in the crystal growth equation should be proportional to  $1/\text{viscosity}$ . Now, at large supercoolings the crystal growth rates are controlled by the kinetic term (Chapter 3). Thus growth rates might be expected to depend on the value of Tg for similar compositions, higher Tg values indicating lower growth rates at a given temperature and vice versa.

Figure 6.3  
(two pages)

Optical micrographs from experiment 1  
comparing nucleation behaviour of glasses  
32 and 26.

This page:

Top left: glass 32 nucleated 709°C for 1 hour  
Mag x240

Top right: glass 26 nucleated 709°C for 1 hour  
Mag x240

Bottom left: glass 32 nucleated 721°C for 1 hour  
Mag x240

Bottom right: glass 26 nucleated 721°C for 1 hour  
Mag x240

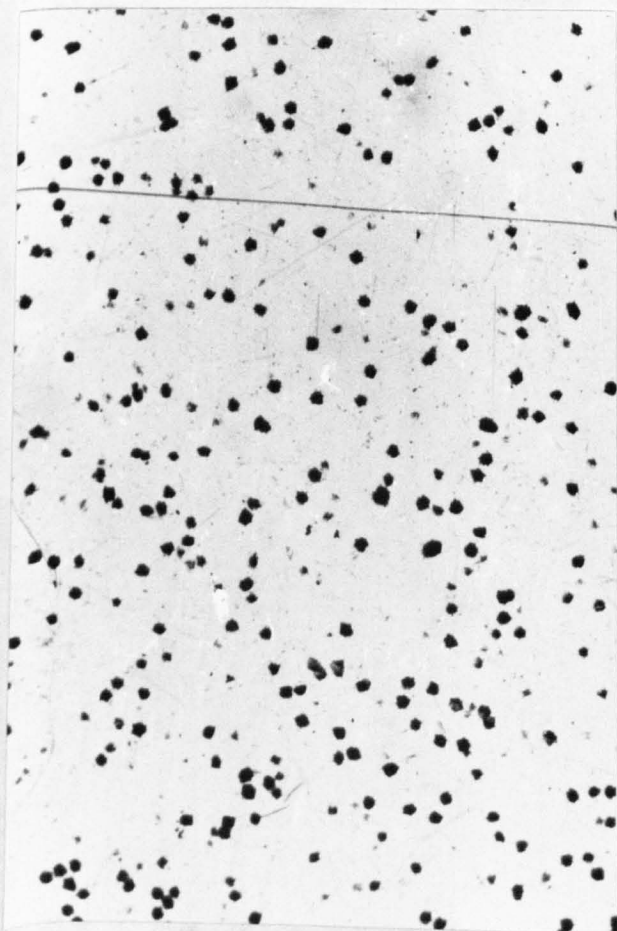
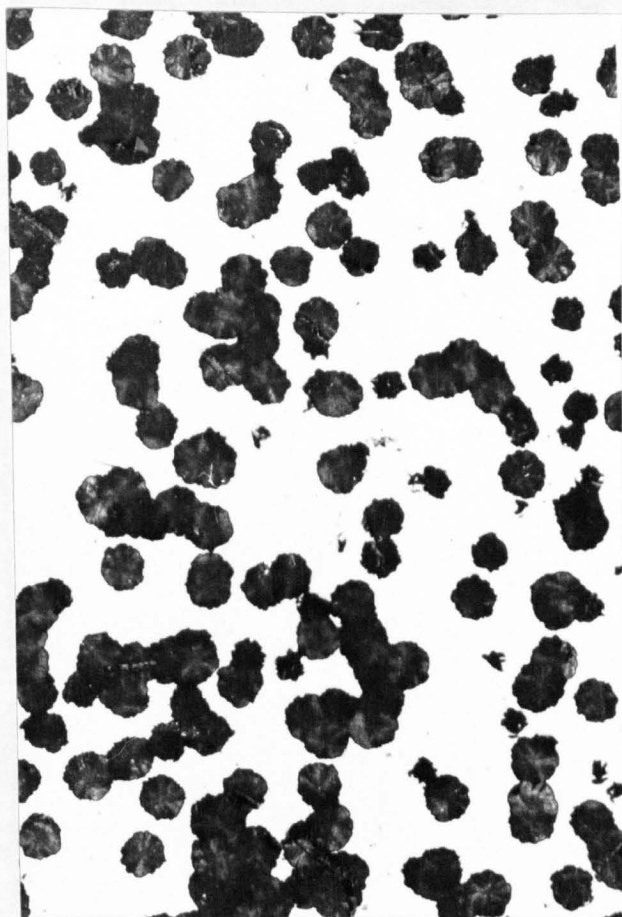
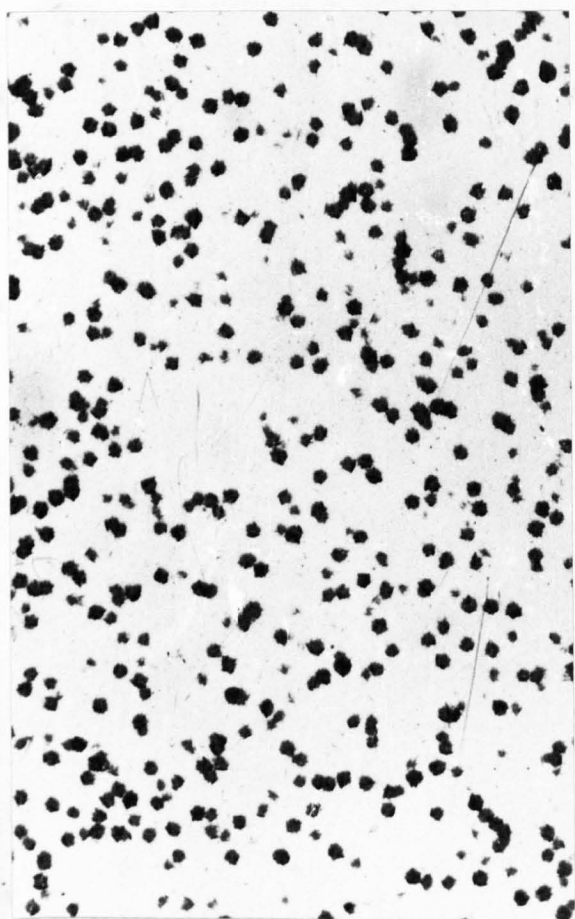
Second page:

Top left: glass 32 nucleated 745°C for 1 hour  
Mag x240

Top right: glass 26 nucleated 745°C for 1 hour  
Mag x240

Bottom left: glass 32 nucleated 773°C for 1 hour  
Mag x120

Bottom right: glass 26 nucleated 773°C for 1 hour  
Mag x120



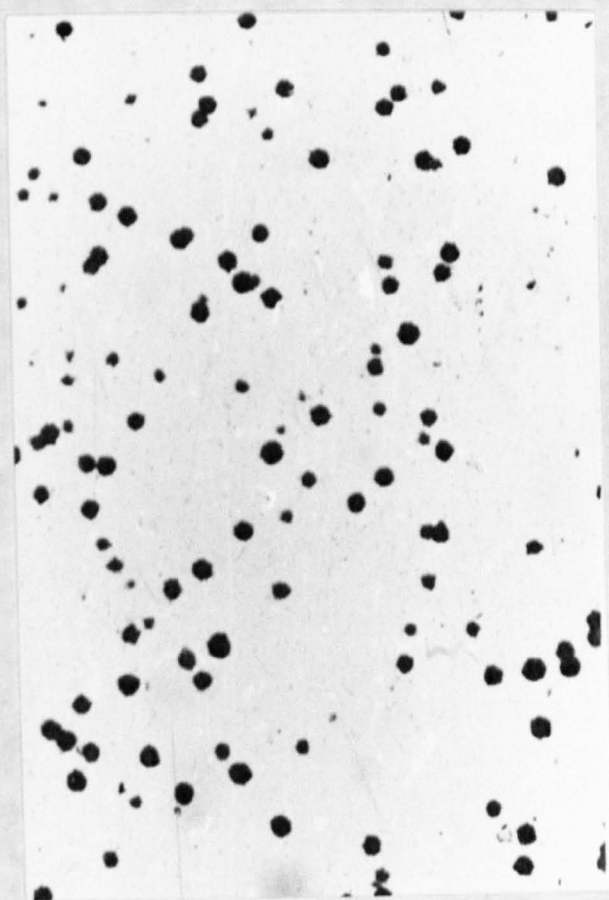
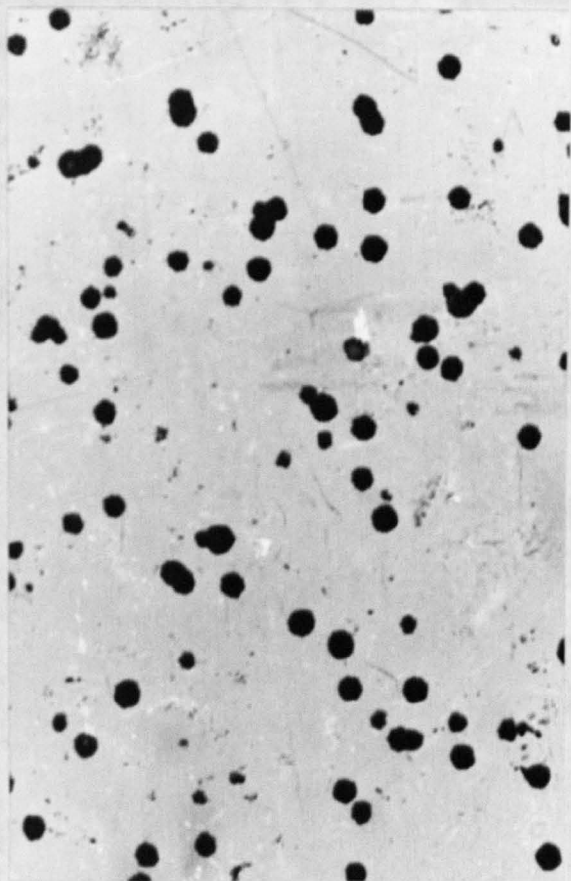


TABLE 6.3

DTA DATA FOR BARIA-SILICA GLASSES

Glass Designation	Analysed BaO content	Heat Treatment	T <sub>g</sub> °C	T <sub>x</sub> <sup>x</sup> °C	T <sub>x</sub> <sup>'</sup> °C	T <sub>x</sub> <sup>''</sup> °C	T <sub>y</sub> °C	T <sub>z</sub> °C
35	34.0	as poured	691	833	861	887	1001	ncne
33	28.7	as poured	691	834	862	937	1046	1179
32	30.4	as poured	694	847	877	893	1032	none
31	27.4	as poured	691	835	862	902	1021	na
30	28.5	as poured	683	853	883	931	1017	na
30	28.5	as poured and phase separated 780°C 1 hr	683	na	864	933	1033	1079
28	25.7	as poured	684	853	866	938	1031	1075
26	25.3	as poured	690	840	870	913	1014	na
26	25.3	as poured and phase 800°C 1 hr	681	838	869	914	1023	1161

na, not available

From the results (Table (6.3)) there is no systematic variation in DTA T<sub>g</sub> for the glasses for an overall variation in BaO content from 25 to 34 mol%. Also the maximum variation in DTA T<sub>g</sub> observed is only 10°C. Since phase separation will not have time to take place during the DTA run at temperatures below T<sub>g</sub>, the values listed should correspond to the 'as-poured' non-phase separated glasses. We will refer again to these results in Section (6.4) when discussing the causes of change in the nucleation behaviour.

### 6.1.3 Liquid-Liquid immiscibility results

The location of the actual glass compositions relative to the liquid immiscibility dome is shown in Figure (6.4). The numbers along the base of the figure refer to the glasses (26, 28, 30, 31, 32 and 33) positioned at the appropriate compositions. The solid curve delineates the boundary of liquid immiscibility and is calculated from the equations (2.5) derived by Haller et al<sup>(28)</sup>.

The experimentally determined immiscibility temperatures for the present work are given in Table (6.4) and plotted in Figure (6.4) as squares if the glass contained very low quantities of Al<sub>2</sub>O<sub>3</sub> (26, 31, 32, 33), or triangles for slightly higher Al<sub>2</sub>O<sub>3</sub> containing glasses (28 and 30).

The six glasses (26 - 33) are within the immiscibility dome at some of the nucleation temperatures while 35G, melted by Rowlands, is outside. In the case of glass 32, T<sub>m</sub> was theoretically determined to be 760°C. However, no trace of liquid immiscibility could be detected below 760°C. This glass is an example of the phenomenon mentioned earlier, whereby crystallization occurs before liquid immiscibility. The driving force for liquid phase separation is so small at temperatures between T<sub>g</sub> and 760°C that liquid unmixing is extremely slow.

Carbon replicas of freshly etched glass surfaces were examined in the electron microscope. Micrographs of the phase separation morphology of glasses 26 and 31 nucleated at temperatures 773, 745, 721 and 709°C are shown in Figure (6.5). A brief description of the morphology of liquid phase separation for each glass after a crystal nucleation treatment of one hour at temperatures 807, 773, 745, 721, 709°C is given in Table (6.5). Glasses 26 and 28 were shown to have phase separated in the as-cast state although little or no trace of opalescence was present.

The slight scattering that produces the characteristic milkiness is dependent on the size of the droplets and the refractive indices of the

Figure 6.4      The immiscibility dome of baria-silica glasses calculated from the equations of Haller et al <sup>(28)</sup>. Also included are the experimentally determined immiscibility temperatures for glasses 33, 31, 30, 28 and 26. The symbols along the base of the figure represent the following glasses:  
a (35G), b (32), c (33), d (30), e (31),  
f (28), g (26)

○ Calculated immiscibility data ref(28)

□ Experimental immiscibility data for glasses

containing less than 0.2 mole %  $\text{Al}_2\text{O}_3$

● Experimental immiscibility data for glasses containing more than 0.2 mole %  $\text{Al}_2\text{O}_3$

○ 0.2 mole %  $\text{Al}_2\text{O}_3$

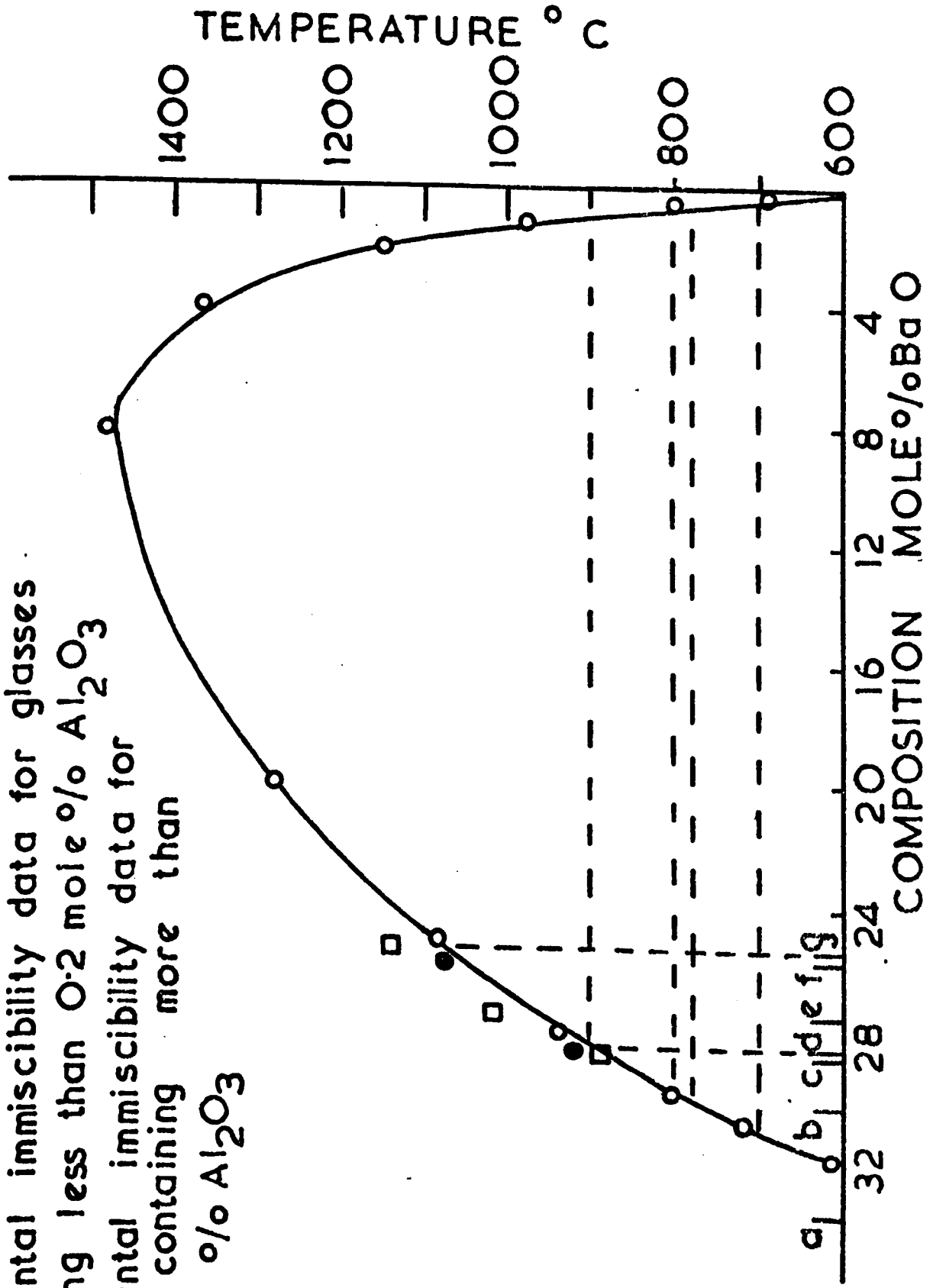


Figure 6.5 Electron micrographs of phase separation morphology of glasses 31 and 26 in experiment 1.

This page:

Top left: glass 31, air quenched.  
Mag x 46000

Top right: glass 26, air quenched  
Mag x79000

Bottom left: glass 31, heated 722°C, 1 hour  
Mag x46000

Bottom right: glass 26, heated 722°C, 1 hour  
Mag x 46000

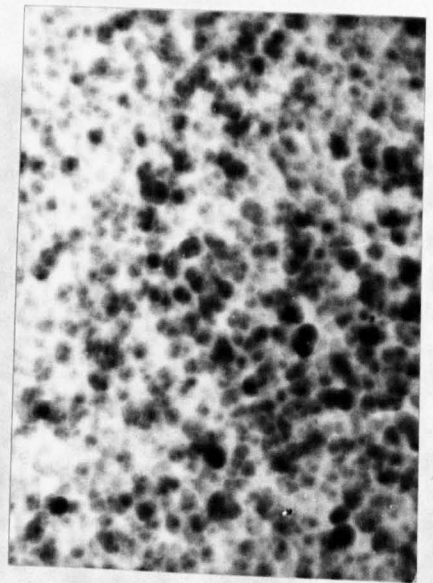
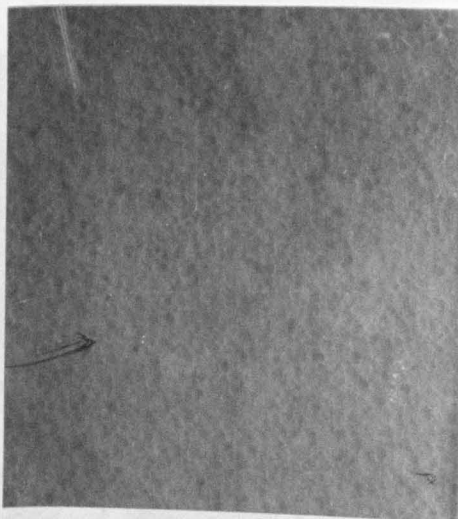
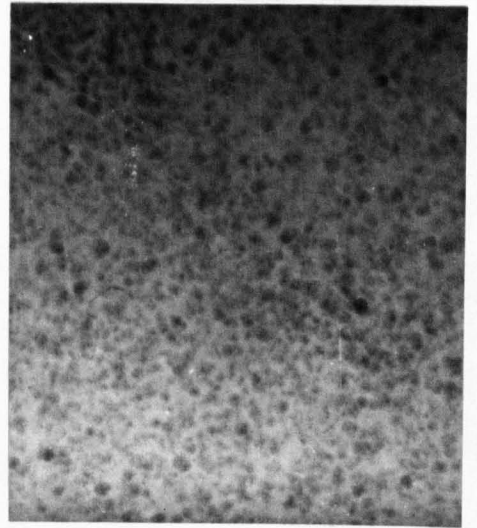
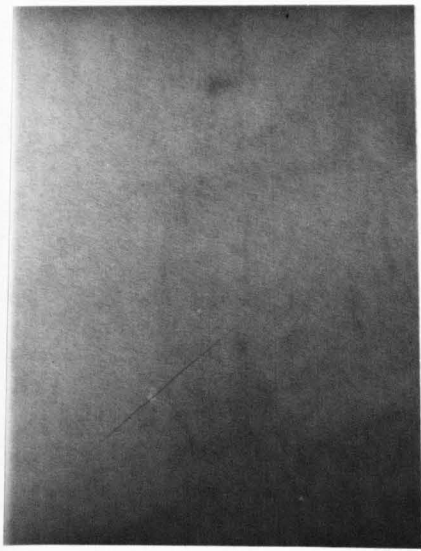
Second page:

Top left: glass 31, heated 745°C, 1 hour  
Mag x 46000

Top right: glass 26, heated 745°C, 1 hour  
Mag x46000

Bottom left: glass 31, heated 773°C, 1 hour  
Mag x46000

Bottom right: glass 26, heated 773°C, 1 hour  
Mag x46000



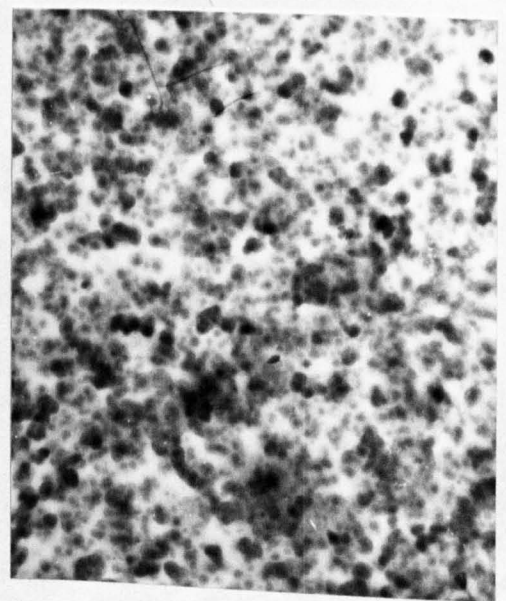
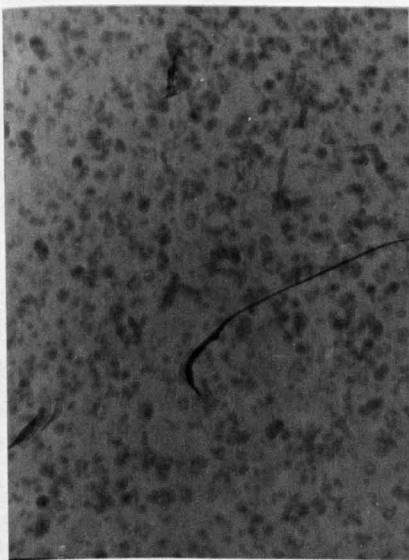
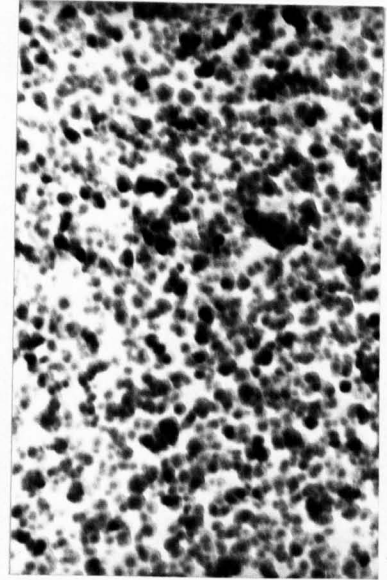
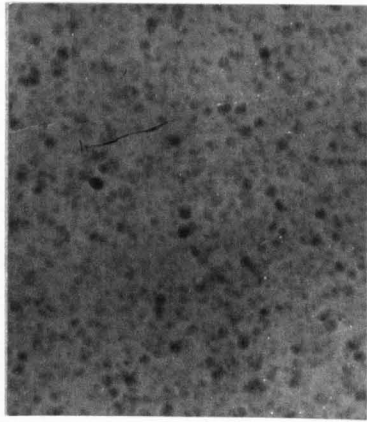


TABLE 6.4

IMMISCIBILITY DATA OF BARIA-SILICA GLASSES

Glass	Experimentally determined $T_m$ °C	Theoretically calculated $T_m$ (using equations of Haller et al (28)) °C
33	890	890
32	No immiscibility detected	760
31	1010	960
30	905	900
28	1070	1050
26	1140	1070

TABLE 6.5

DESCRIPTION OF PHASE SEPARATION MORPHOLOGY OF FIVE  
GLASSES HEAT TREATED FOR ONE HOUR AT SEVERAL TEMPERATURES

(FROM ELECTRON MICROSCOPE REPLICAS)

Temp °C	Glass					
	26	28	30	31	32	33
807	overlapping particles	discrete particles	as 28	discrete particles	no structure	no structure
773	"	"	"	"	"	discrete particles
745	"	"	"	"	"	"
721	"	"	"	"	"	no structure
709	"	"	no structure	"	"	"
As cast	"	"	"	no structure	"	"

two phases present. Certain glasses when quenched from the melt do not have sufficient time to phase separate fully during the brief time that the temperature exceeds  $T_g$  (i.e. the volume fraction and phase compositions have not reached equilibrium). This was the case for 26 as later results will show and probably also for 28. Thus the separation was on a very fine scale and in addition the separated phases were probably quite close in composition (and hence refractive index), so that there was no visible opalescence in the rapidly quenched samples.

In some of the other glasses the rate of liquid unmixing was sufficiently slow for the homogeneous (i.e. non phase separated) structure to be 'frozen-in', when using normal air quenches. Thus glasses 30 and 31 phase separated readily on heating but showed no evidence of liquid immiscibility in the quenched state.

The experimental determination of  $T_m$  for glass 33 yielded a value of  $890^\circ\text{C}$ . However, no liquid immiscibility could be detected for this glass when heated at  $807^\circ\text{C}$  for one hour, whereas at lower temperatures (e.g.  $773$ - $745^\circ\text{C}$ ) the occurrence of phase separation was obvious. It is likely that at  $807^\circ\text{C}$  the thermodynamic driving force for immiscibility (which will be referred to as  $\Delta g$ ) was insufficient to produce classical nucleation of phase droplets after only one hour, whereas at lower temperature nucleation became more rapid.

Burnett and Douglas<sup>(84)</sup> also reported the existence of a similar temperature gap for a  $\text{Na}_2\text{O}-\text{CaO}-\text{SiO}_2$  glass where liquid immiscibility could not be induced to occur. In their case  $T_m$  was about  $690^\circ\text{C}$  and phase separation was observed over a temperature range  $580$ - $670^\circ\text{C}$ .

In general, it was found that for the compositions studied, the greater the silica content of the glass, the more rapidly nucleation of liquid phase droplets occurred at any given temperature. Glass 31, for example, was

observed to nucleate liquid phase droplets at 709°C, whereas for 33 there was no evidence of liquid droplets after one hour at temperatures below 745°C (Table 6.5). This is probably due to the increased driving force for nucleation of liquid immiscibility ( $\Delta g$ ) in the silica-rich glasses which is illustrated in Figure (6.6). At temperature T (say 700°C) the composition of the separated liquid phases is E and H. The driving force inducing liquid immiscibility is least for glass 32 (equal to  $\Delta g_1$ ) but increases for glasses nearer the spinodal. According to Haller et al.<sup>(28)</sup> and Seward et al.<sup>(14)</sup>, the spinodal at 700°C is 24 mol% BaO. The composition of glass 26 lies just outside the spinodal (see S in Figure 6.6)). Hence glass 26 has the greatest driving force which indicates a higher nucleation rate of silica rich droplets on the basis of the classical theory.

This is a somewhat oversimplified picture since we have assumed that the equilibrium silica-rich phase precipitates initially according to classical theory. Strictly we should consider the more comprehensive theory due to Cahn and Hilliard<sup>(50,51)</sup>. However, the above picture is sufficient for present purposes.

#### 6.1.4 General discussion of the influences of liquid-liquid immiscibility on crystal nucleation kinetics

Before discussing the results of experiment 1 in detail let us consider the possible effects of liquid-liquid immiscibility on crystal nucleation.

Uhlmann<sup>(9)</sup> has described four ways that liquid phase separation can influence nucleation rates (see Section 4.2). Considering point (a), Figure (6.7) illustrates schematically how  $\Delta G$  for crystallization depends on whether liquid immiscibility occurs for a system A-B similar to BaO<sub>2</sub>SiO<sub>2</sub>-SiO<sub>2</sub>. Nucleation of phase A, which is very sensitive to the driving force,

Figure 6.6 Schematic free energy diagram of liquid  
in the  $\text{SiO}_2\text{-BaO}_2\text{SiO}_2$  system at an  
arbitrary temperature

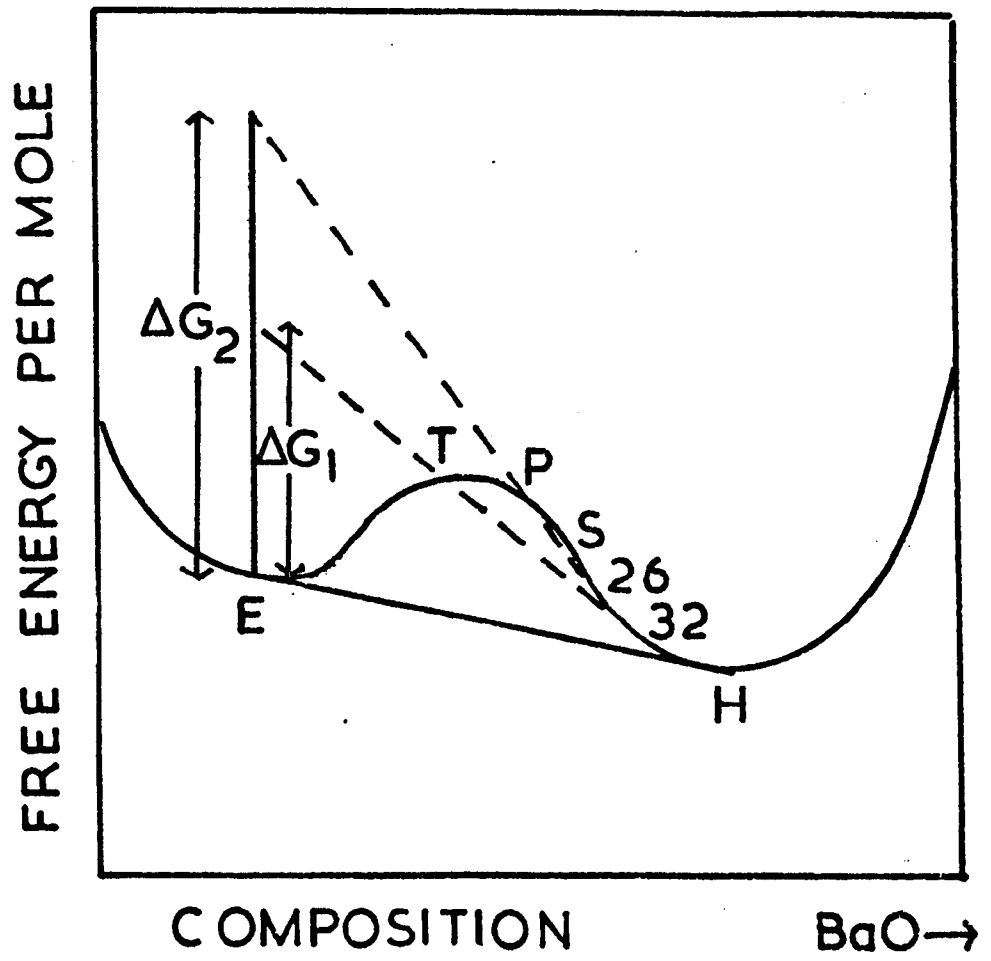


Figure 6.7

a) Schematic phase diagram for a system similar to  $\text{BaO}_2\text{SiO}_2\text{-SiO}_2$ :

..... unstable liquidus of A

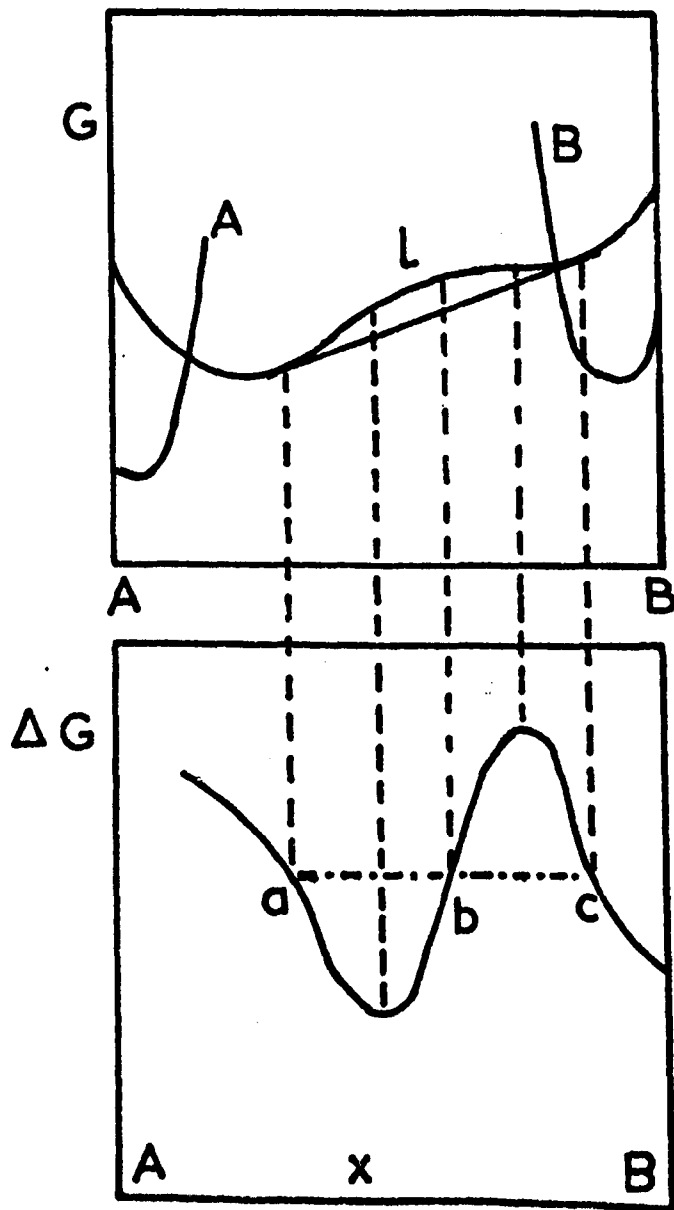
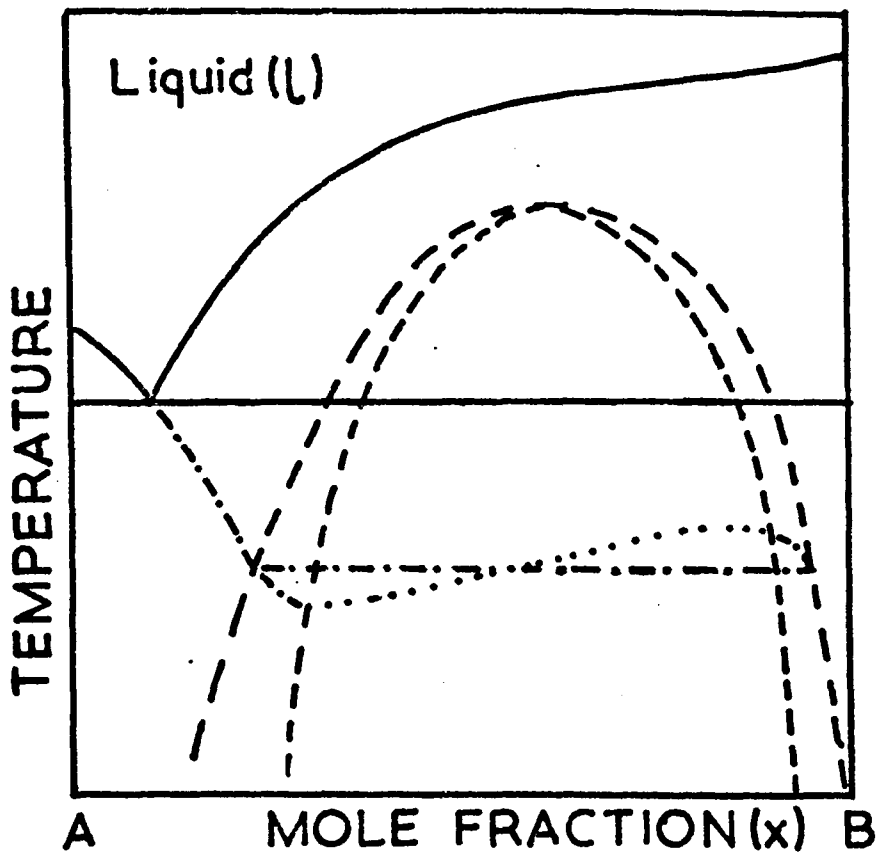
-.-.-.-.- metastable liquidus of A

b) Free energy diagram for a system similar to  $\text{BaO}_2\text{SiO}_2\text{-SiO}_2$  at temperature T,

c) Diagram illustrating thermodynamic driving force ( $\Delta G$ ) as a function of composition for a system similar to  $\text{BaO}_2\text{SiO}_2\text{-SiO}_2$  at

temperature T. The solid line between a, b, c denotes  $\Delta G$  for a non-phase separated glass.

The dot dash line between a, b, c represents  $\Delta G$  for a phase separated glass.



will be enhanced by liquid phase separation between a and b but retarded between c and b.

The interface between the two liquids might act as a heterogeneous nucleating site for the crystals (point b). This mechanism will be effective only if the crystals can form a low energy interface with one of the liquids. Effective heterogeneous action by liquid-liquid interfaces is not likely to be significant in BaO-SiO glasses. This can be demonstrated as follows.

The thermodynamic barrier for heterogeneous nucleation  $W_{het}^*$  is related to the homogeneous nucleation thermodynamic barrier  $W_{homo}^*$  by the relation:

$$W_{het}^* = W_{homo}^* f(\theta)$$

Thus  $f(\theta)$  is a measure of the potency of the nucleation catalyst and for the case illustrated in Figure (6.8):

$$\cos\theta = \frac{\sigma_{\alpha\gamma} - \sigma_{\beta\gamma}}{\sigma_{\alpha\beta}}$$

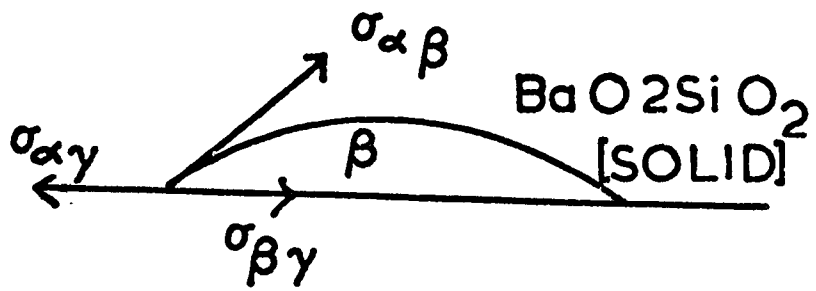
Consider in (Figure 6.8) the nucleation of a spherical cap of crystalline  $BaO_2SiO_2(\beta)$  on a droplet of silica rich phase ( $\gamma$ ) in a matrix of baria rich phase ( $\alpha$ ). For simplicity assume that  $\gamma$  is pure  $SiO_2$  liquid and  $\alpha$  is pure  $BaO_2SiO_2$  liquid. From Rowlands<sup>(18)</sup>  $\sigma_{\alpha\beta} \sim 132$  ergs  $cm^{-2}$  and probably  $\sigma_{\alpha\beta} < \sigma_{\beta\gamma}$ . Also Hammel's work on the  $Na_2O-CaO-SiO_2$  system suggests that the interfacial energy between liquid phases is likely to be small compared with that between crystal and liquid phases (less than 5 ergs  $cm^{-2}$ ), i.e.

$\sigma_{\alpha\gamma} \ll \sigma_{\beta\gamma}$ . Thus  $\cos\theta$  will be approximately -1 and  $f(\theta) \sim +1$  and  $W_{het}^* \sim W_{homo}^*$ , i.e. the heterogeneous mechanism is not significant.

In other glass-forming systems examples are known of crystals growing on the interfaces of droplets. However, Tomozawa<sup>(121)</sup> comments that after a long nucleation treatment the interfaces may migrate considerably away from

**Figure 6.8**      **Diagram of a crystal ( $\beta$ ) nucleating on  
an interface separating two liquids  
( $\alpha$  and  $\gamma$ )**

$\alpha$  BaO<sub>2</sub>SiO<sub>2</sub> [LIQUID]



$\gamma$  SiO<sub>2</sub> [LIQUID]

the crystals they initiated and thus the relation between heterogeneously nucleated crystals and the interfaces may become difficult to detect.

One way of solving the difficulty of determining the relation between crystal nucleation and phase separation morphology is to plot the nucleation rates as a function of a parameter that defines the scale of phase separation, such as  $n_v$ ,  $S_v$  or  $V_f$ . In the present case (experiment 1) it was not possible to analyse the results in this way because we only have one nucleation value at one time for a specific temperature, and any non-linear effects similar to the transient time lag phenomena in phase separation and crystal nucleation kinetics, may be present and complicate the analysis. However, in the later experiments to be described, where heat treatments were carried out at one temperature for a series of times, it was possible to examine the effects of interfacial areas on crystal nucleation.

A factor that Uhlmann<sup>(9)</sup> neglected to mention was the variation of crystal-liquid surface energy with composition. Surface energy values are available only for one composition in the BaO-SiO<sub>2</sub> system, i.e. BaO<sub>2</sub>SiO<sub>2</sub><sup>(18)</sup>. However it is reasonable to suppose that the surface energy between the liquid and primary phase is at a minimum at the stoichiometric composition of this phase and increases as other components are added. This is suggested by some data in the Li<sub>2</sub>O-BaO-SiO<sub>2</sub> system<sup>(18)</sup>. Thus it can be tentatively assumed that the surface energy between BaO<sub>2</sub>SiO<sub>2</sub> and liquid is at a minimum (132 ergs cm<sup>-2</sup>) at the composition 33 $\frac{1}{3}$  mole% BaO and increases with silica content. The nucleation rate is partly governed by the surface energy and irrespective of driving force considerations the nucleation rate of BaO<sub>2</sub>SiO<sub>2</sub> should decrease with addition of SiO<sub>2</sub>. Liquid immiscibility can stimulate crystal nucleation by producing a phase near the BaO<sub>2</sub>SiO<sub>2</sub> composition with smaller interfacial energy with the crystal.

By considering surface energy and  $\Delta G$  variations with composition, it can be seen that the occurrence of liquid phase separation will probably

stimulate crystal nucleation by shifting the composition of the matrix phase nearer to  $\text{BaO}_2\text{SiO}_2$ .

The shift of composition of the matrix phase due to phase separation may also affect the kinetic barrier to crystal nucleation  $\Delta G_D$ , which is related to the mobilities of the atomic species involved in nucleation (mechanism c), p.43. According to Uhlmann<sup>(9)</sup> this is likely to be of paramount importance in affecting crystal nucleation.

In the  $\text{BaO-SiO}_2$  system phase separation results in a matrix phase richer in baria with a lower viscosity and probably of more rapid mobility<sup>(136)</sup>. Hence this would also result in more rapid crystal nucleation.

Mechanism d) mentioned above involves the diffusion of impurities to the interfaces.

Scholes<sup>(137)</sup> has described how a sparingly soluble component in a complex glass may concentrate at the interface and eventually precipitate as heterogeneous nuclei for bulk crystallization. In practice this mechanism will not function if rapid diffusion of impurities away from the interface occurs before nucleation can occur.

Also, impurities concentrating at the interface could modify locally  $\Delta G$  and  $\sigma$  for homogeneous nucleation. In many cases this would result in a decrease in nucleation in these regions and since the remainder of the matrix would exhibit higher nucleation kinetics, the overall effect would be small and difficult to detect. Also, if an increase in nucleation occurred in these regions, the effect would have to be very large for the overall effect to be detectable.

In other cases the concentration of impurities at the interface could locally decrease viscosity and thus encourage crystal nucleation of the major phase. Matusita and Tashiro<sup>(122)</sup>, for example, attributed their results to this effect.

Also, the existence of compositional gradients around the small liquid

droplets (of the major components, not impurities) may cause  $\Delta G$  and  $\sigma$  to be altered locally in the zone around the interface. Thus a local smaller proportion of silica around the growing silica-rich droplets undergoing diffusion controlled growth might give, in the case of the BaO-SiO<sub>2</sub> system, a locally higher  $\Delta G$  (in the depleted zone) and a lower  $\sigma$ , thereby enhancing the crystal nucleation kinetics.

There is also the possibility of heterogeneous nucleation occurring in the 'depleted zone' around the droplets, as suggested by Tomozawa<sup>(121)</sup> and discussed in Chapter 4.

Thus we have three mechanisms associated with interfaces that could enhance or inhibit nucleation.

- i) The heterogeneous catalysing mechanism at the interface itself (mechanism b), p.43. This assumes the existence of a 'sharp' interface as distinct from iii) below.
- ii) Diffusion of impurities or surface active agents to the boundaries between liquid phases, causing local changes in  $\Delta G$  and  $\sigma$  for homogeneous crystal nucleation or precipitating as heterogeneous nuclei.
- iii) The existence of compositional gradients of the main components in the glass around small liquid droplets, again causing local changes in  $\Delta G$  or  $\sigma$  for homogeneous crystal nucleation, or promoting heterogeneous nucleation.

In practice it would be difficult to distinguish between these mechanisms since the dependence of crystal nucleation rate on the phase morphology would in all cases be similar. In particular, a large interfacial area  $S_v$  and number of droplets  $n_v$  would be in all cases very important, as present, for example, in the early stages of phase separation when the scale of separation is very fine. Since both  $S_v$  and  $n_v$  decrease progressively with time at a given temperature due to Ostwald ripening all these mechanisms

would become less potent as time increases.

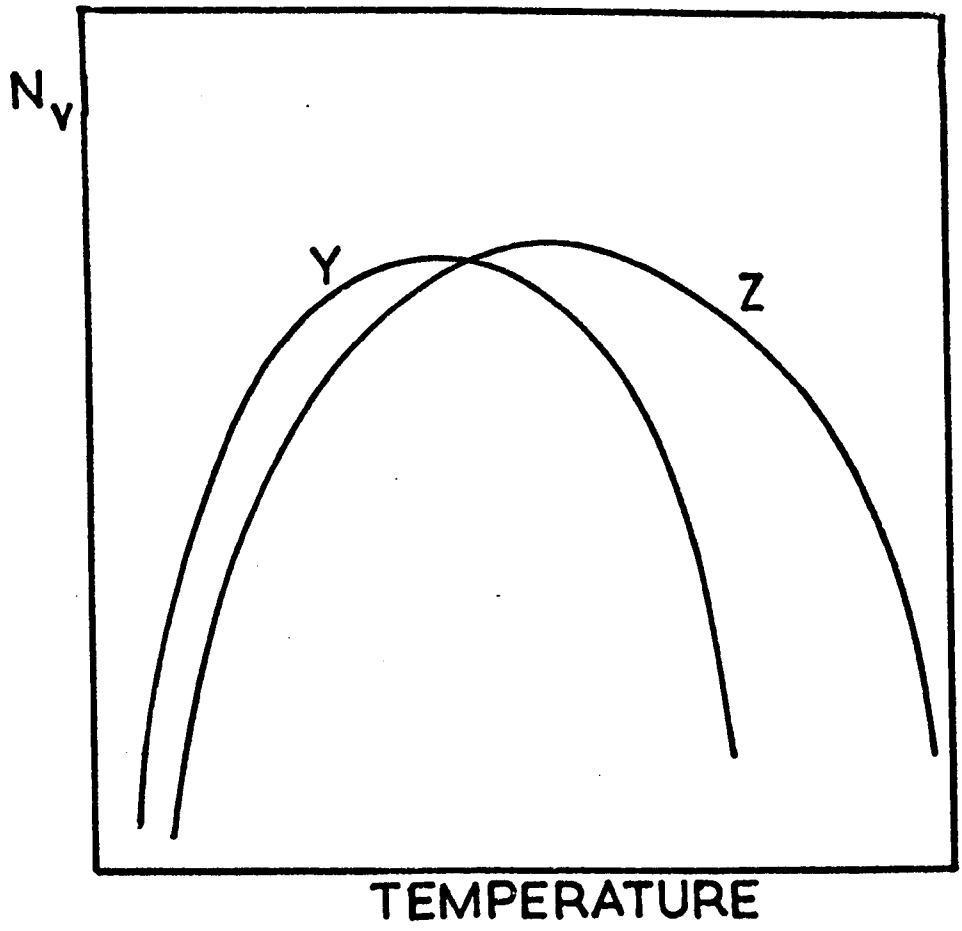
In addition, if the crystal nuclei formed preferentially near the interface they would need to form rapidly and grow rapidly to avoid being overtaken and absorbed by the growing liquid droplet. Thus in cases where crystal growth is not particularly rapid compared with droplet growth, the 'interface' mechanisms are not expected to be effective.

#### 6.1.5 Further discussion of results for Experiment 1

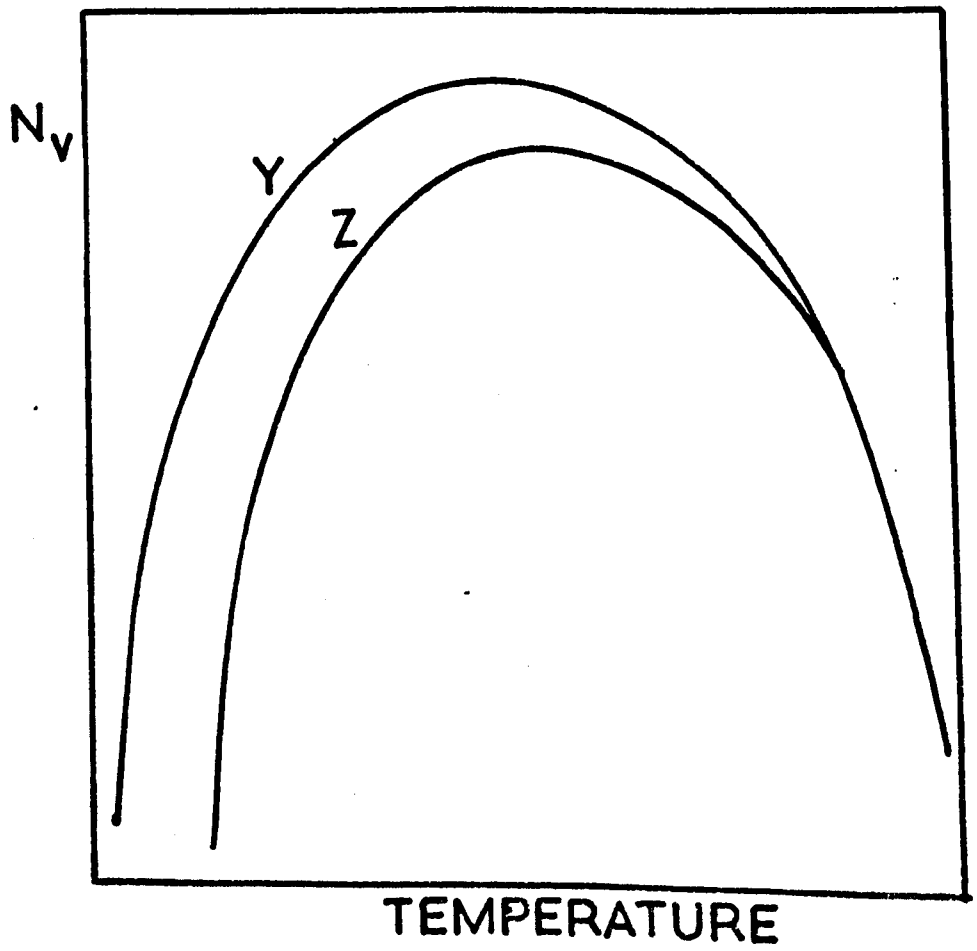
Schematic nucleation curves for two glasses of different BaO contents, both of which phase separate in the range of temperatures used for crystal nucleation, we illustrated in Figure (6.9). A) represents a situation where interfaces nucleate crystals. The values of  $N_v$  will partly reflect the values of  $S_v$  for each glass. The interfacial areas will depend on the  $V_f$  and the nucleation rate of the liquid immiscibility, so glasses containing the most silica would be expected to have the highest  $S_v$  and consequently the highest  $N_v$ . It is assumed in Figure (6.9A) that phase separation occurs more rapidly at higher temperature so that the curves would diverge as shown.

In Figure (6.9B) the interfaces do not nucleate crystals significantly. After immiscibility, the crystals nucleate in a phase of the same composition for both glasses and the curves are expected to converge at higher temperature. At the lower temperatures, particularly below the maximum in crystal nucleation rate, liquid phase separation would be slower or would not occur at all after one hour, and the nucleation curves for the different glasses would be expected to show more pronounced differences due to their different compositions. The same behaviour at lower temperatures would be also expected for Figure (6.9A) if phase separation does not occur appreciably. In this case 'cross-over' of the curves might occur as shown.

Figure 6.9 Schematic representation of  $N_v$  (number of crystals) versus temperature curves of two glasses (Y and Z) containing different quantities of baria. Both Y and Z phase separate at high temperatures, however, Y contains more baria than Z.



a)



b)

Thus at the lower temperatures the glasses higher in silica have a smaller  $\Delta G$  (driving force for crystal nucleation) and probably have a larger  $\sigma$  and smaller diffusion rates, leading to smaller crystal nucleation rates. On this basis at lower temperatures the compositions studied can be tentatively arranged in order of decreasing nucleation rate (and increasing silica content) as follows: 32, 33, 30, 31, 28 and 26. From Figure (6.1) and (6.2) the observed order is 32 and 33 (close together), 31, 30, 26 and 28, which is in fairly close agreement. The deviations from exact agreement are probably due to the small levels of alumina impurity affecting the nucleation rates. Methods of compensating for the impurity are described later.

If it is assumed that interfaces heterogeneously nucleate crystals, then it is interesting to derive how the nucleation curves might diverge. It has already been indicated that the interfacial area and the number of droplets are greater for glasses whose compositions are deeper within the liquid immiscibility dome. In general, for the same heat treatment, glasses that are well within the immiscibility dome will tend to have a higher volume fraction, a more connected microstructure and probably a larger interfacial area per unit volume  $S_v$ , as was in fact qualitatively observed on the electron microscope replicas (see also section (6.2.2) and (6.3.2)). On this basis glass 26 would nucleate crystals the most readily, followed by 31, 33 then 32. Also, of the two glasses higher in alumina impurity, 28 might be expected to have the higher nucleation rate since the composition of this glass is further inside the immiscibility dome than glass 30 (but both glasses have similar alumina impurity levels).

From Figures (6.1) and (6.2) at the high temperatures where phase separation occurred the order, in decreasing number of nuclei, was 31 followed by 32 and then the other glasses (33, and 26), which were approximately

coincidental. For the two glasses higher in alumina impurity, 30 was followed by 28. Thus it can be concluded that interfacial areas do not effectively nucleate crystals.

In the case of glasses that do not phase separate (32 and 35G), no marked convergence would be expected at higher temperatures and in fact this was observed.

Thus, in general, good agreement was obtained between the present results and the predictions based on the theory represented schematically by B in Figure (6.9). Nevertheless, the curves for the glasses that phase separate do not coincide as closely as might be expected at higher temperatures. Reasons for this behaviour are now examined.

One correction must be made to the nucleation densities for the fact that the values refer to a unit volume of the glass (whether phase separated or not), whereas the values should refer to a unit volume of the baria-rich phase in which nucleation is assumed to occur. Hence each value of  $N_v$  must be multiplied by the reciprocal of the volume fraction of the baria-rich (major) phase. The volume fractions of the phases were calculated at 745, 773 and 807°C for each glass assuming that the immiscibility dome predicted from the equation given by Haller et al<sup>(28)</sup> was correct. The mole fractions obtained by the Lever Rule from the molar phase diagram were converted into weight fractions and then volume fractions using the density data of BaO-SiO<sub>2</sub> glasses supplied by MacDowell<sup>(16)</sup>. The new results are shown in Table (6.6) for these three temperatures, where liquid phase separation was most likely to be complete in a very short time. However, this correction made only a relatively small difference to the values as plotted in Figure (6.2) and (6.1) and no significant relative changes in the curves.

TABLE 6.6

NUCLEATION RESULTS CORRECTED FOR VOLUME FRACTION

OF PHASE SEPARATION  $N_v$   $\text{cm}^{-3}$

	Temperature °C	745	773	807
Glass	33	$6.93 \times 10^7$	$4.97 \times 10^6$	$2.31 \times 10^5$
	32	$9.48 \times 10^7$	$8.52 \times 10^6$	not available
	31	$1.89 \times 10^8$	$1.54 \times 10^7$	$3.10 \times 10^5$
	30	$6.86 \times 10^6$	$4.49 \times 10^5$	$4.35 \times 10^4$
	28	$7.78 \times 10^6$	$5.36 \times 10^5$	$6.93 \times 10^3$
	26	$6.09 \times 10^7$	$8.84 \times 10^6$	$1.34 \times 10^5$

TABLE 6.7

NUCLEATION RESULTS CORRECTED FOR EFFECT OF ALUMINA

ON VOLUME FRACTION OF PHASE SEPARATION  $N_v$   $\text{cm}^{-3}$

	Temperature °C	745	773	807
Glass	31	$1.95 \times 10^8$	$1.59 \times 10^7$	$3.21 \times 10^5$
	28	$7.87 \times 10^6$	$5.46 \times 10^5$	$7.06 \times 10^3$
	26	$6.46 \times 10^7$	$9.39 \times 10^6$	$1.43 \times 10^5$

Glass 32 shows no immiscibility; glasses 33 and 30 coincide with immiscibility boundary calculated using the equations derived by Haller et al<sup>(28)</sup>, and thus the values are identical in these three glasses to values in Table (6.6).

An important factor which could cause additional variation to occur in  $N_v$  between glasses is the  $Al_2O_3$  impurity level. This is apart from any differences due to the phase separation itself. Alumina may have two possible effects: 1) it can depress crystal nucleation directly, for example, by lowering  $\Delta G$ , 2) alumina can have an indirect effect by depressing the immiscibility temperature  $T_m$ , (i.e. lowering the tendency to phase separate and hence reducing the volume fraction of silica-rich phase). The composition of the baria-rich phase shifts away from  $BaO_2SiO_2$ , and thus the nucleation rate of this phase will probably fall slightly. Some attempt to calculate the latter effect was made for the present results. The volume fractions were calculated for the baria-rich phase by drawing curves that passed through the experimentally determined immiscibility temperatures and were parallel to the overall curve plotted in Figure (6.4). This procedure produced little change in the values of  $N_v$ , showing that the correction was a small one (see Table (6.7)).

To check the direct effect alumina can exert on the nucleation kinetics, a  $BaO_2SiO_2$  glass containing 1 mol% alumina (henceforth called  $ABS_2$ ) was prepared. Figure (6.10) and Table (6.8) show the extent that one mol%  $Al_2O_3$  can depress nucleation in a  $BaO_2SiO_2$  glass. This figure and the analysed  $Al_2O_3$  contents of the glasses were used to estimate the depression of the nucleation due to the alumina impurity and thus to 'correct' the results. The following equation was employed for this purpose:

$$\ln I_1 = \ln I_2 + B Y_A \quad (6.1)$$

where  $B$  is a constant for a given temperature,  $Y_A$  is the mole fraction of  $Al_2O_3$ ,  $I_2$  is the nucleation rate in a glass containing  $Al_2O_3$ ,  $I_1$  is the nucleation rate in a glass of the same  $BaO-SiO_2$  ratio but containing no  $Al_2O_3$ . The  $N_v$  values for a given time can be employed instead of  $I_1$  and  $I_2$

Figure 6.10 Effect of one mol%  $\text{Al}_2\text{O}_3$  on the nucleation behaviour of  $\text{BaO}2\text{SiO}_2$

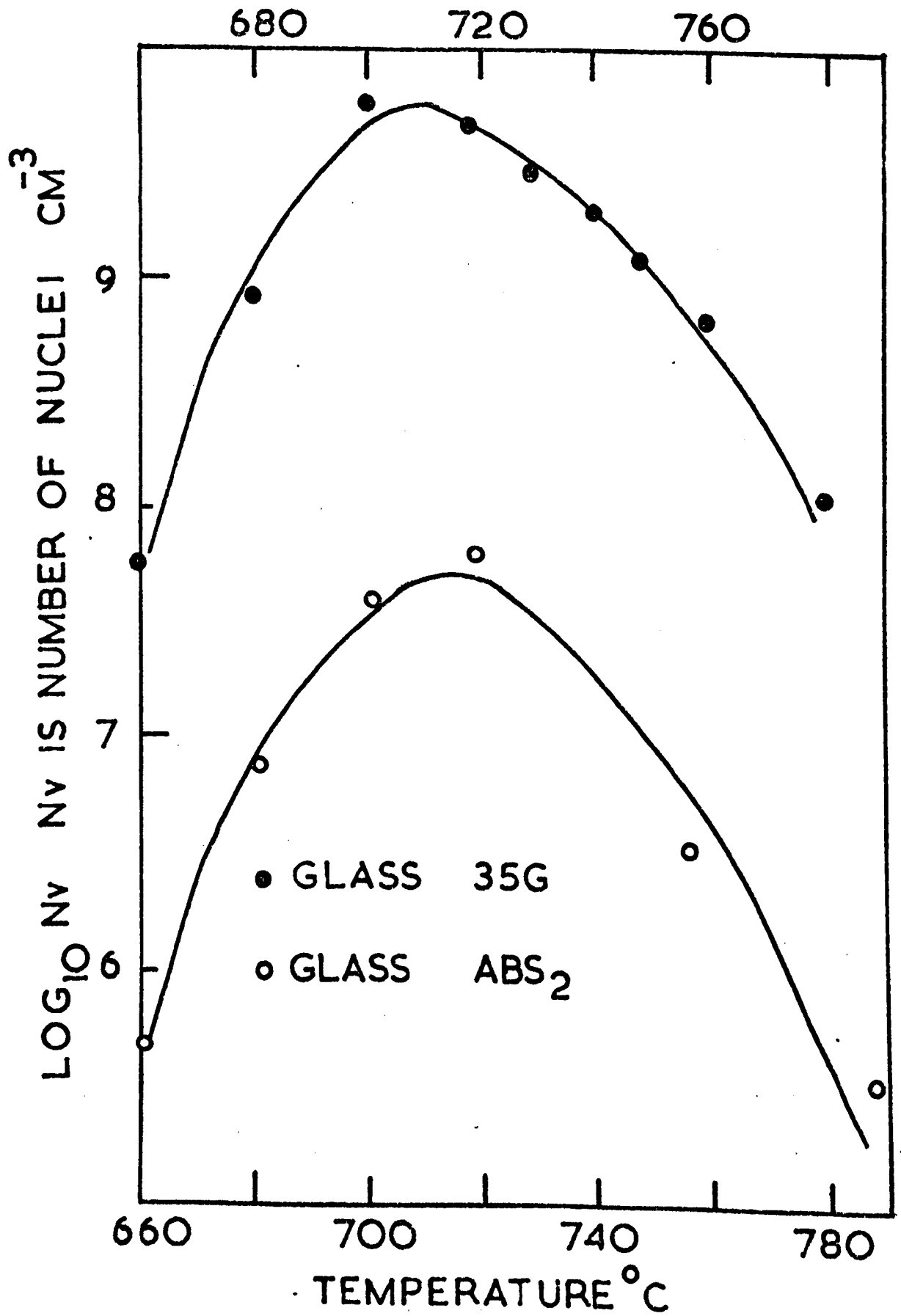


TABLE 6.8

NUCLEATION RESULTS CORRECTED FOR EFFECT OF ALUMINA ON  
NUCLEATION KINETICS (USING EQUATION (6.1))  $\log_{10} N_v$  ( $\text{cm}^{-3}$ )

Temperature °C	Glass					
	32	33	30	31	28	26
807	na	5.41	5.30	5.49	4.76	5.36
773	7.36	6.74	6.32	7.19	6.63	7.16
745	8.41	7.86	7.50	8.27	7.78	7.98
721	8.88	8.51	8.17	8.32	8.06	8.31
709	8.93	8.46	8.05	8.19	8.21	7.93
693	8.53	8.21	7.62	7.79	6.86	7.13
673	7.21	5.96	5.92	5.97	4.18	4.96
650	5.43	4.96	5.10	4.17	-	4.21

na, not available

TABLE 6.9

NUCLEATION RESULTS CORRECTED FOR EFFECT OF ALUMINA AND  
VOLUME FRACTION OF PHASE SEPARATION,  $\log_{10} N_v$  ( $\text{cm}^{-3}$ )

Temperature °C	Glass				
	33	30	31	28	26
807	5.41	5.34	5.50	4.94	5.42
773	6.74	6.37	7.20	6.83	7.23
745	7.87	7.55	8.27	8.00	8.06

in equation (6.1) provided non steady state effects can be neglected. The derivation of this equation and the assumptions used are given in Appendix (6.1). The equation was used empirically and the constant B was calibrated from nucleation data of  $ABS_2$  and the  $BaO_2SiO_2$  glasses. The value of B was calculated at each temperature and was used to calculate the number of crystals that glasses 26, 28, 30, 31, 32, 33 would nucleate if they contained no alumina impurity. The new results are shown in Table (6.8) and plotted in Figures (6.11) and (6.12) as  $\log_{10}N_v$  versus temperature. Similarly the number of crystals that the baria-rich phase in glasses 26, 28, 30, 31, 33 would nucleate if it contained no alumina, were also calculated at temperatures where liquid phase separation was most likely to be complete in a very short time (viz. 745, 773, 807°C, see Table (6.9)). The volume fraction of the separated phase after a one hour heat treatment at lower temperatures was unknown and the volume fraction correction could not be applied. However, at these lower temperatures the glasses nucleate at very different rates and since the volume fraction correction, when applied, does not greatly alter the results, (see Table (6.9) and (6.7)) it can be assumed that the interpretation of the results at the lower temperatures is not greatly affected by the neglect of the volume fraction factor.

Consider first the glasses of lower impurity levels (Figure (6.11)). At the higher temperatures (particularly 773 and 807°C) glasses, 32, 31 and 26 coincide more closely than before correction (Figure 6.1)). At lower temperatures below the maximum, a larger spread of values still exist. The order in decreasing nucleation was 32, 33, 31 and 26, almost the same as before correction and in good agreement with the expected order according to the silica contents as described before.

In the case of the glass 28 and 30, containing higher levels of alumina impurity (Figure (6.12)), the  $N_v$  values are much closer to the other glasses than before correction, particularly at higher temperatures as can be seen

**Figure 6.11** Plot of  $\log_{10} N_v$  ( $\text{cm}^{-3}$ ) versus temperature ( $^{\circ}\text{C}$ ) for glasses 33, 32, 31 and 26, corrected for  $\text{Al}_2\text{O}_3$  and liquid-liquid immiscibility

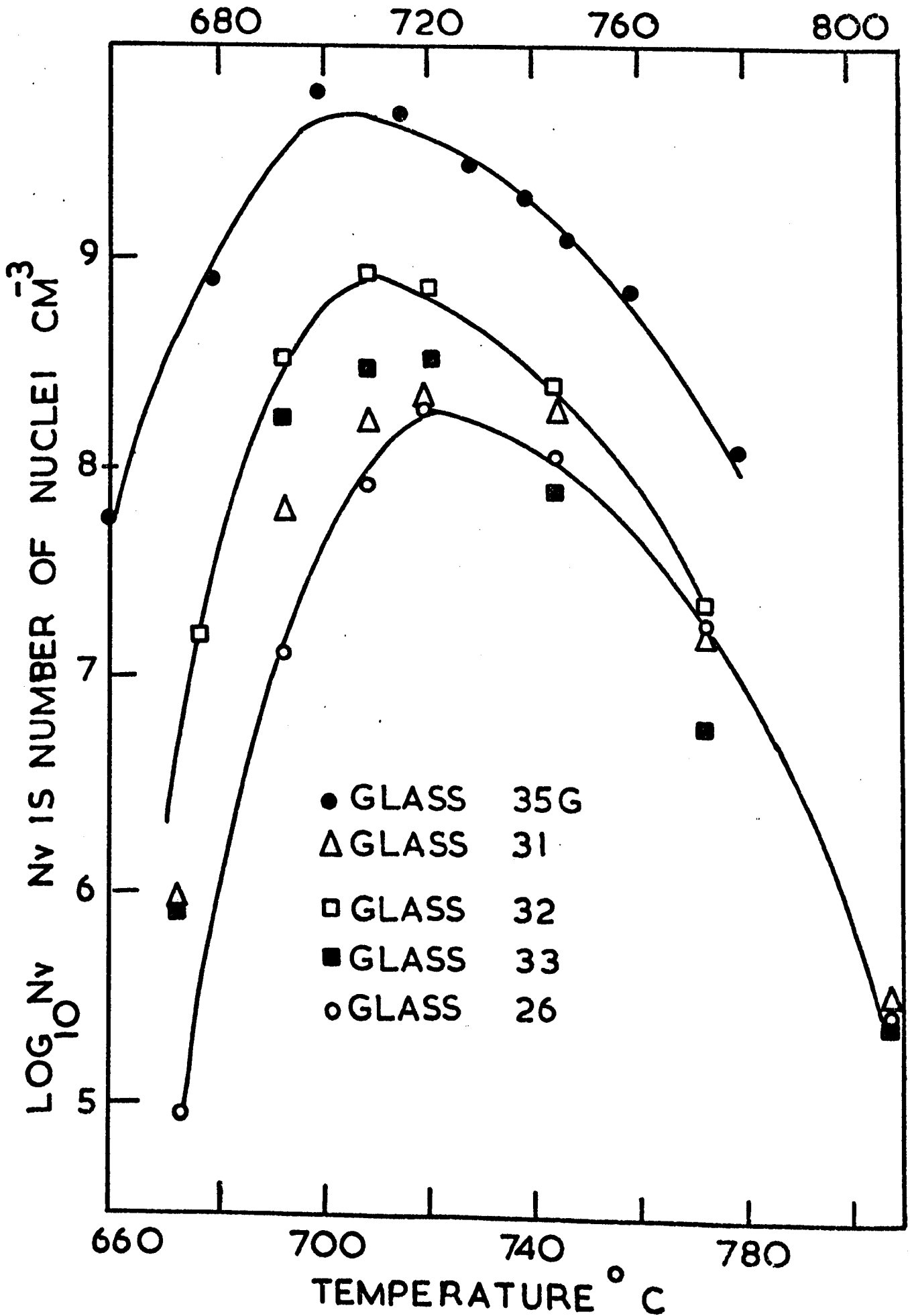
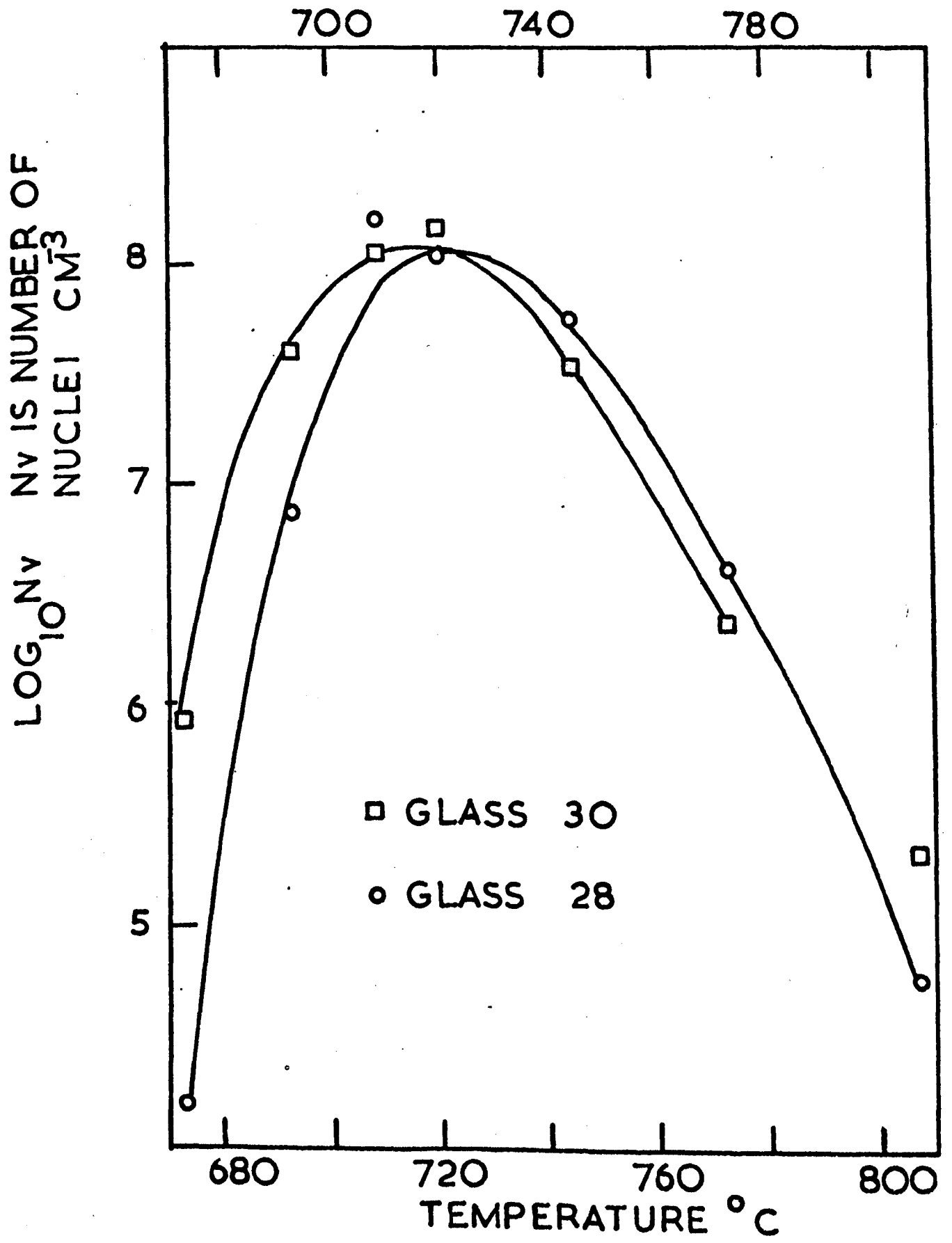


Figure 6.12 Plot of  $\log_{10} N_v$  ( $\text{cm}^{-3}$ ) versus temperature for glasses 28 and 30 corrected for  $\text{Al}_2\text{O}_3$  and liquid-liquid immiscibility.



by comparing Figures (6.11) (6.12) and (6.2) (6.1).

The results corrected for both alumina and volume fractions show closer convergence at the higher temperatures (viz. 745, 773 and 807°C). The failure to obtain even closer coincidence of the values may be attributed to a) experimental errors in estimating the alumina content, b) uncertainty in using the correction formula, particularly for the higher impurity levels in 28 and 30.

It may be concluded that correction of the nucleation curves explains some of the discrepancies present in the "uncorrected" curves. In general, the results are more consistent with the 'composition' mechanism (Figure 6.9B) than the 'interface' mechanism (Figure 6.9A)).

## 6.2 CRYSTAL NUCLEATION AND LIQUID-LIQUID IMMISCIBILITY IN GLASS 26

### EXPERIMENT 2

#### 6.2.1 Crystal nucleation in glass 26 - Results

The problems associated with minor impurity levels when comparing glasses of different overall compositions, as in experiment 1, were avoided by investigating crystal nucleation trends and their dependence on liquid phase separation as a function of time at a constant temperature for a particular glass.

Two glasses (30 and 26) were selected on the basis of their high degree of homogeneity. The results on glass 30 will be discussed later and attention is focussed in this section on glass 26. Small samples of glass 26 having quite different thermal histories or initial heat treatments were subsequently given a crystal nucleation and growth treatment to study their crystal nucleation kinetics. It will be recalled that 26 has a measured  $T_m$  of 1140°C and was already showing slight immiscibility on cooling from the melt. Efforts were made to produce a non-phase separated glass by heating

samples at  $1250^{\circ}\text{C}$  (above  $T_m$ ) for one minute and immediately quenching into silicone oil. This is referred to as glass A. Also, comparison between two different phase morphologies was effected by heating a sample at  $800^{\circ}\text{C}$  for one hour (glass C) and another at  $900^{\circ}\text{C}$  for ten minutes (glass D). Phase separation was developed fully in both samples and at these temperatures crystal nucleation was negligible (i.e. less than 0.1% of the total  $N_v$  subsequently nucleated during the heat treatment). The three specimens with different initial treatments were given a crystal nucleation treatment at  $700^{\circ}\text{C}$  alongside a typical 'as-cooled' sample (glass B) for several periods of time. This was the important crystal nucleation heat treatment that showed up any differences between the nucleation ability of the different samples. It will be remembered that  $700^{\circ}\text{C}$  was a convenient temperature for the study since the maximum nucleation rate occurred at about  $700^{\circ}\text{C}$ . The growth treatment to 'develop' the crystals for quantitative measurements was carried out at  $840^{\circ}\text{C}$  and the nucleation characteristics ( $N_v$ ) obtained are tabulated in Table (6.10).

The nucleation results are shown in figures (6.13-6.15) where  $N_v$  is plotted against time. For clarity the early and later stages are plotted separately. The results are expressed to some extent more conveniently in the form of nucleation rates because these are characteristic of the glass at the particular time under consideration (see figure (6.16)) whilst the cumulative number of nuclei in figures (6.13-6.15) depend on the conditions previously existing in the glasses.

Returning to figures (6.13-6.15) the relative differences between the four glasses are more pronounced in the earlier stage of nucleation. A pronounced curve is present in plots of three of the glasses, 26A, B and D, whilst the fourth glass 26C is much straighter particularly at longer times (i.e. nucleation rate is more constant). The nucleation curves of glasses 26A and B are very similar for all times with 26B always slightly above 26A. This testifies to the accuracy of the method for determining  $N_v$  because a slight difference is maintained consistently over a long period of time. The  $N_v$  curve for glass 26C was consistently much higher than the other curves.

Figure 6.13 Plot of  $N_v$  (number of crystals  $\text{cm}^{-3}$ )  
versus time (hrs) for glass 26

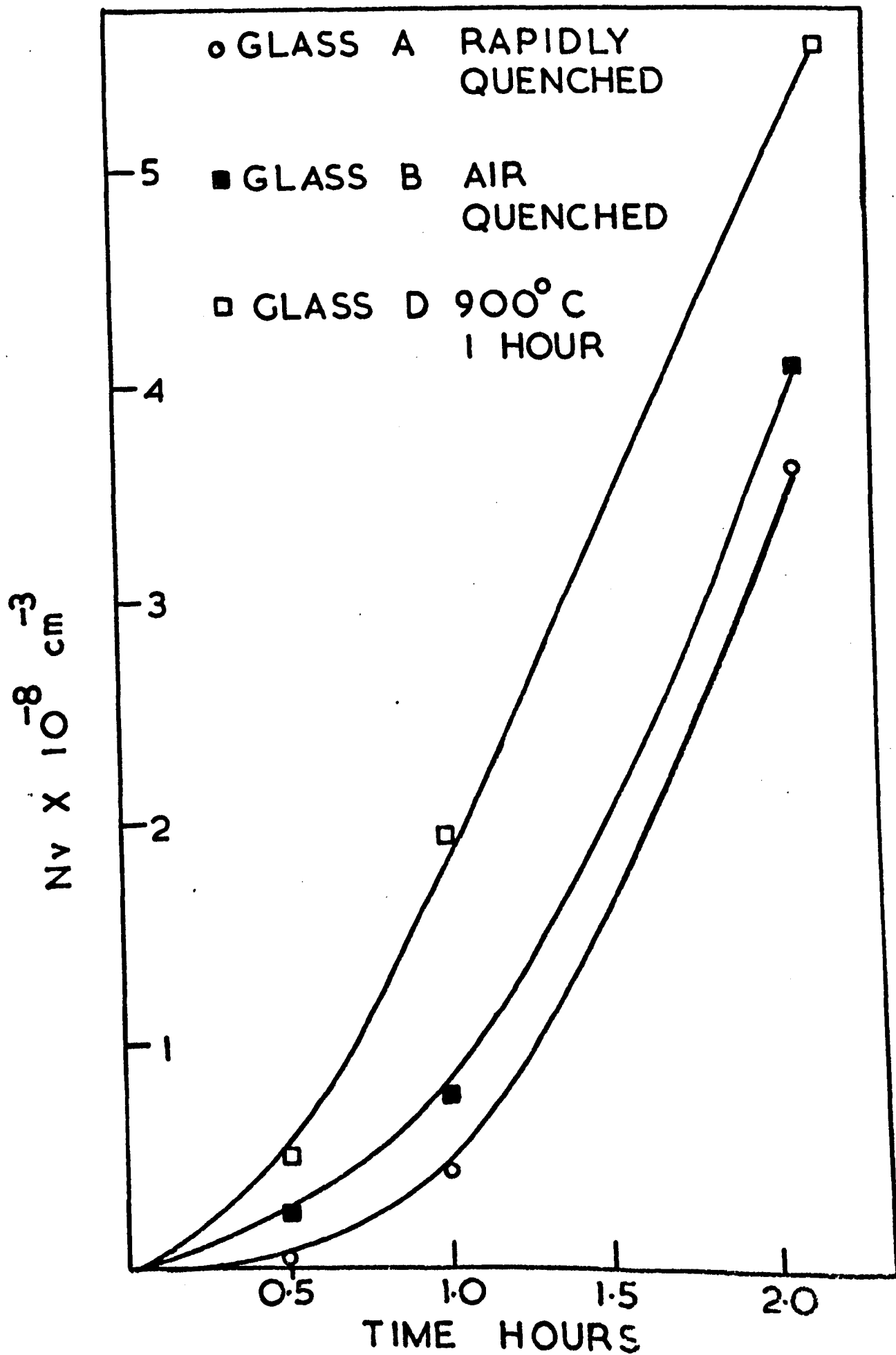


Figure 6.14 Plot of  $N_v$  (number of crystals  $\text{cm}^{-3}$ )  
versus time (hrs) for glass 26

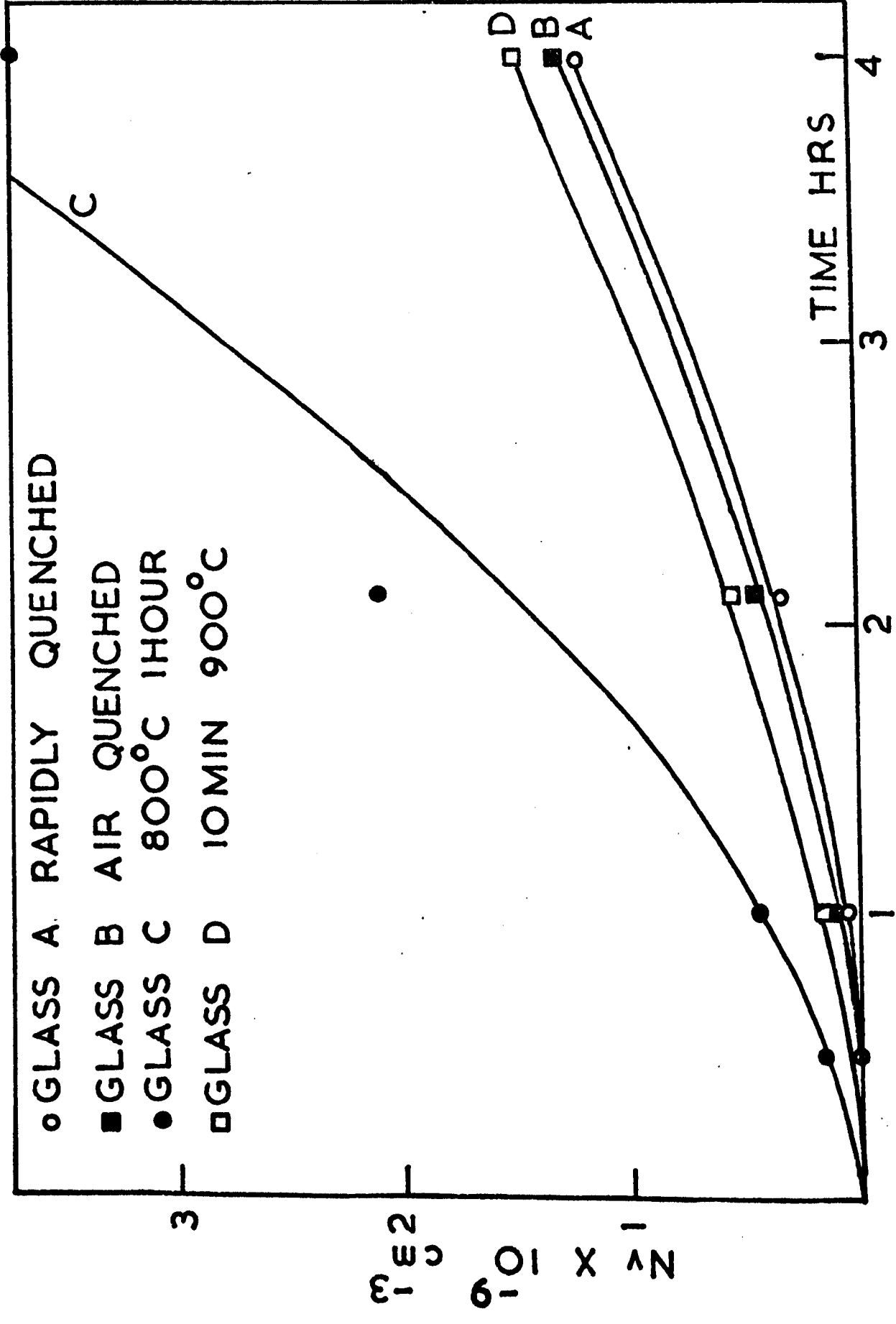


Figure 6.15 Plot of  $N_v$  (number of crystals  $\text{cm}^{-3}$ ) versus time (hrs) for glass 26

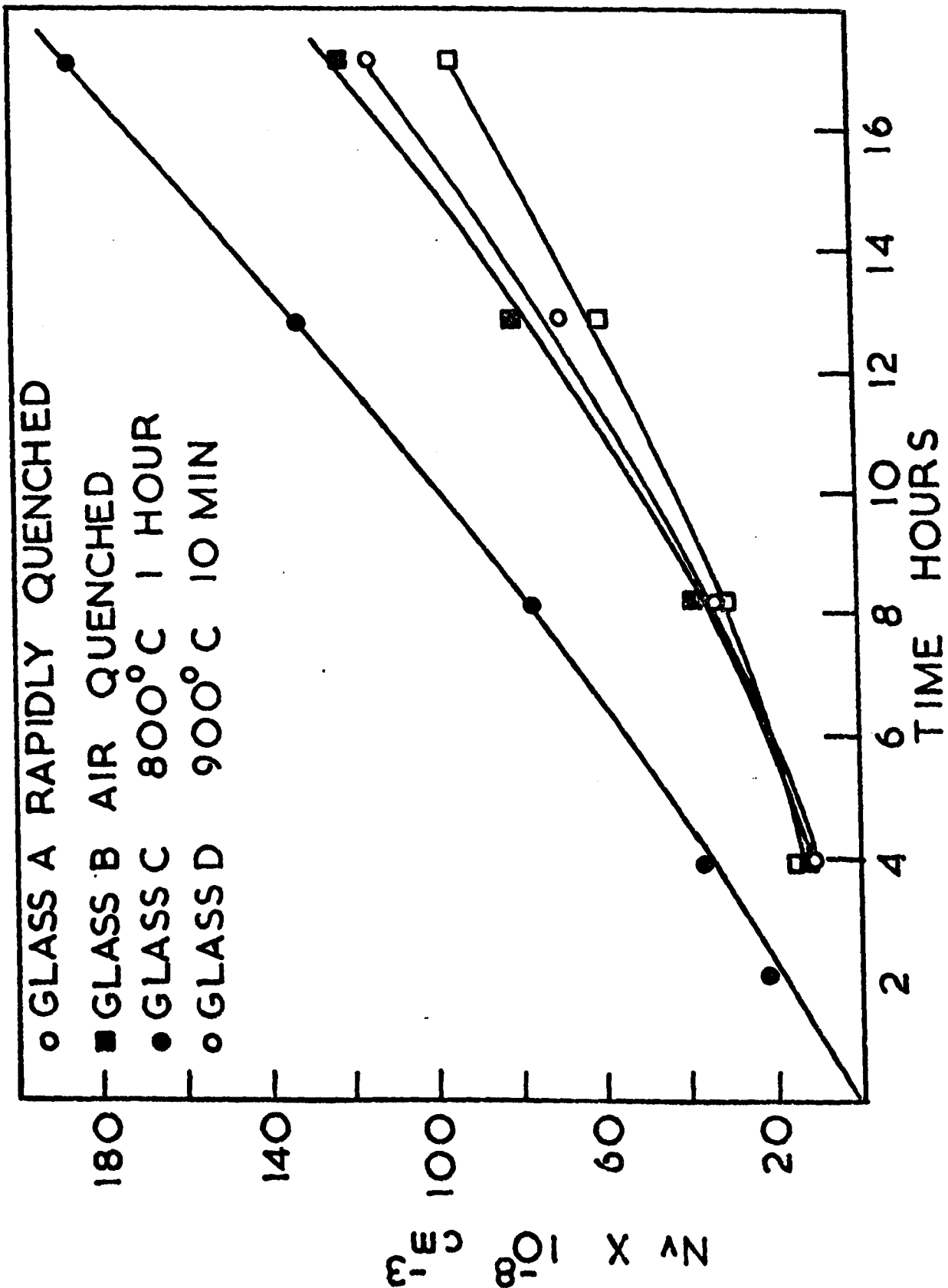


Figure 6.16 Plot of nucleation rate  $\left(\frac{dN_v}{dt}\right)$  versus time (hrs) for glass 26

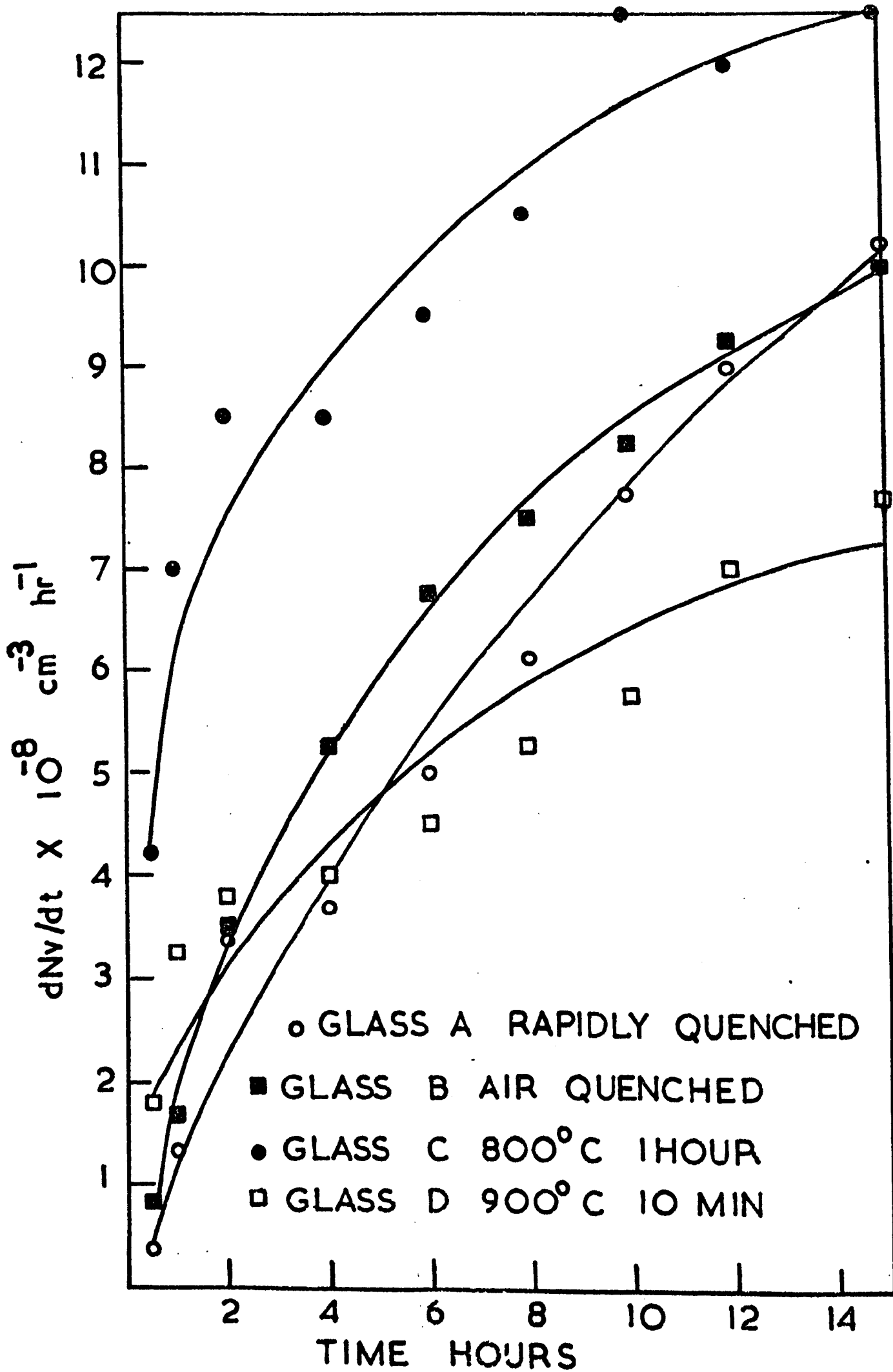


TABLE 6.10

NUCLEATION DATA FOR GLASS 26 AT 700°C. ( $N_v$  in  $\text{cm}^{-3}$ )

Class	Time							
	0.5 hrs	1 hr	2 hrs 6 mins	4 hrs	8 hrs 7 mins	12 hrs 55 mins	17 hrs 7 mins	
A	$4.77 \times 10^6$	$4.3 \times 10^7$	$3.61 \times 10^8$	$1.19 \times 10^9$	$3.18 \times 10^9$	$6.92 \times 10^9$	$1.14 \times 10^{10}$	
B	$2.19 \times 10^7$	$7.8 \times 10^7$	$4.07 \times 10^8$	$1.29 \times 10^9$	$3.83 \times 10^9$	$8.18 \times 10^9$	$1.22 \times 10^{10}$	
C	$1.47 \times 10^8$	$4.34 \times 10^8$	$2.09 \times 10^9$	$3.73 \times 10^9$	$7.6 \times 10^9$	$1.32 \times 10^{10}$	$1.86 \times 10^{10}$	
D	$5.13 \times 10^7$	$1.96 \times 10^8$	$5.58 \times 10^8$	$1.47 \times 10^9$	$3.07 \times 10^9$	$6.05 \times 10^9$	$9.59 \times 10^9$	

Glass A = glass 26 rapidly quenched into silicone oil

Glass B = glass 26 as cooled from the melt

Glass C = glass 26 heat treated at 800°C for one hour

Glass D = glass 26 heat treated at 900°C for ten minutes

TABLE 6.11

NUCLEATION DATA FOR GLASS 32 AT 677°C

Time (hrs)	$N_v$ ( $\text{cm}^{-3}$ )
1	$4.78 \times 10$
2	$4.96 \times 10$
4	$2.59 \times 10$
8	$2.35 \times 10$
16	$9.2 \times 10$

Between four and eight hours the  $N_v$  curves for 26A and B cross the curve for glass 26D. Although at short times glass D has a small but significantly greater  $N_v$  than 26A or B, at longer times glass 26D has a smaller  $N_v$  than 26A or B.

The relative differences in  $N_v$  for all glasses tend to become less pronounced at longer times. Figure (6.16) clearly depicts the tendencies in nucleation rates and how they vary with time. It shows for example that the nucleation rates are steadily approaching one another after 17 hours.

Figure (6.17) is optical micrographs of glasses 26A, B, C and D, heat treated at 700°C for  $\frac{1}{2}$ , 1 and 2 hours. They show the contrasting nucleation behaviour between the specimens given different initial heat treatments.

No nucleation measurements were carried out beyond 17 hours due to the difficulties in measuring the high values of  $N_v$  accurately using the optical microscopy technique although the range of times studies was sufficient for the experiment.

The initial strong curvature of the  $N_v$  plots for 26A and B may be

Figure 6.17 Optical micrographs from experiment 2  
(three pages) comparing nucleation behaviour of glasses  
26A, B, C and D at 700°C

This page:

Top left glass 26A, nucleated at 700°C, ½ hour  
Mag x60

Top right: glass 26B, nucleated at 700°C, ½ hour  
Mag x120

Bottom glass 26D, nucleated at 700°C, ½ hour  
left: Mag x240

Bottom glass 26C, nucleated at 700°C, ½ hour  
right: Mag x240

Second page:

Top left glass 26A, nucleated at 700°C, 1 hour  
Mag x240

Top right: glass 26B, nucleated at 700°C, 1 hour  
Mag x 240

Bottom glass 26D, nucleated at 700°C, 1 hour  
left: Mag x600

Bottom glass 26C, nucleated at 700°C, 1 hour  
right: Mag x600

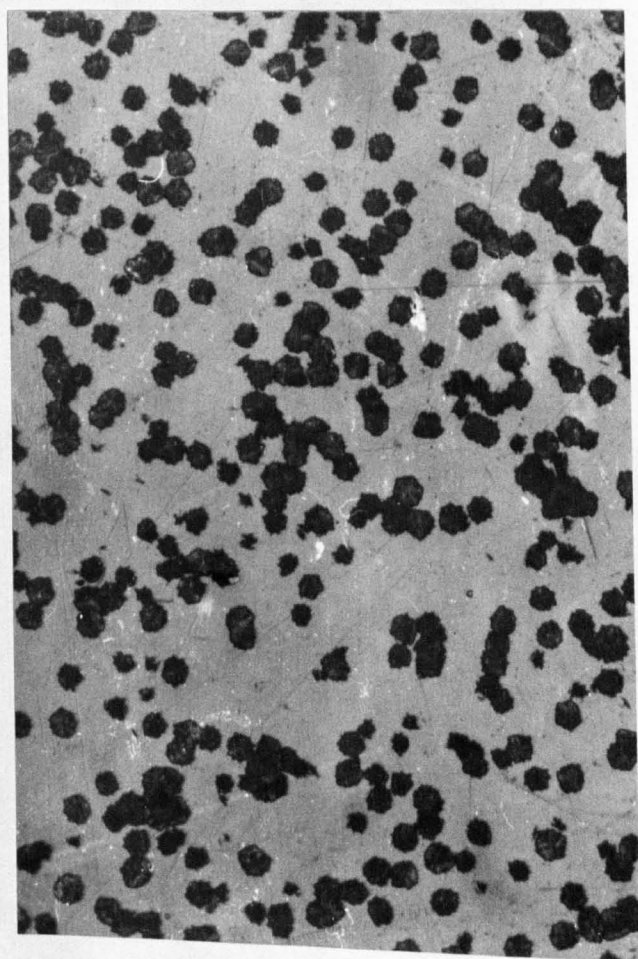
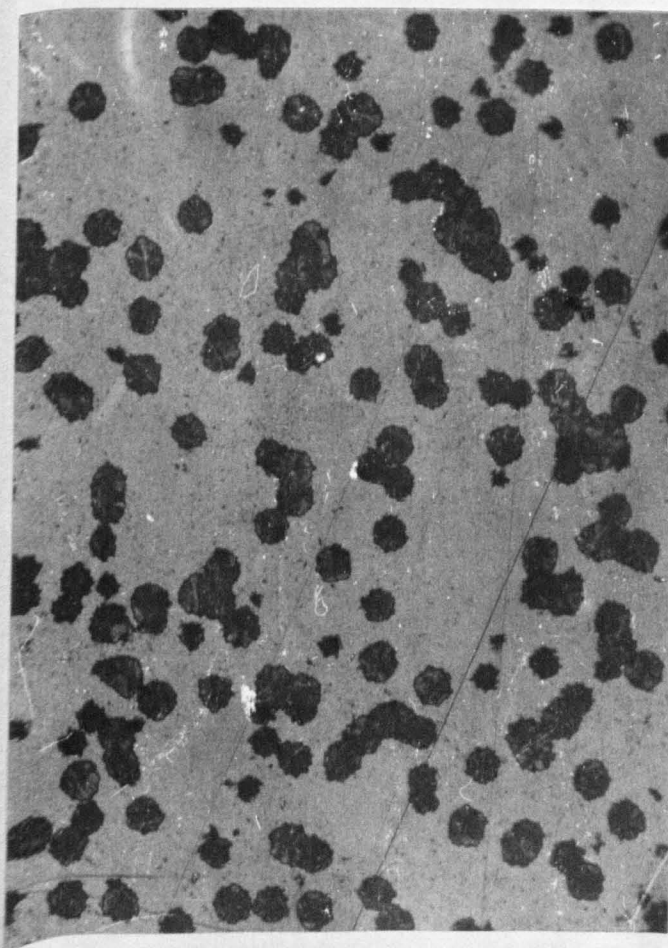
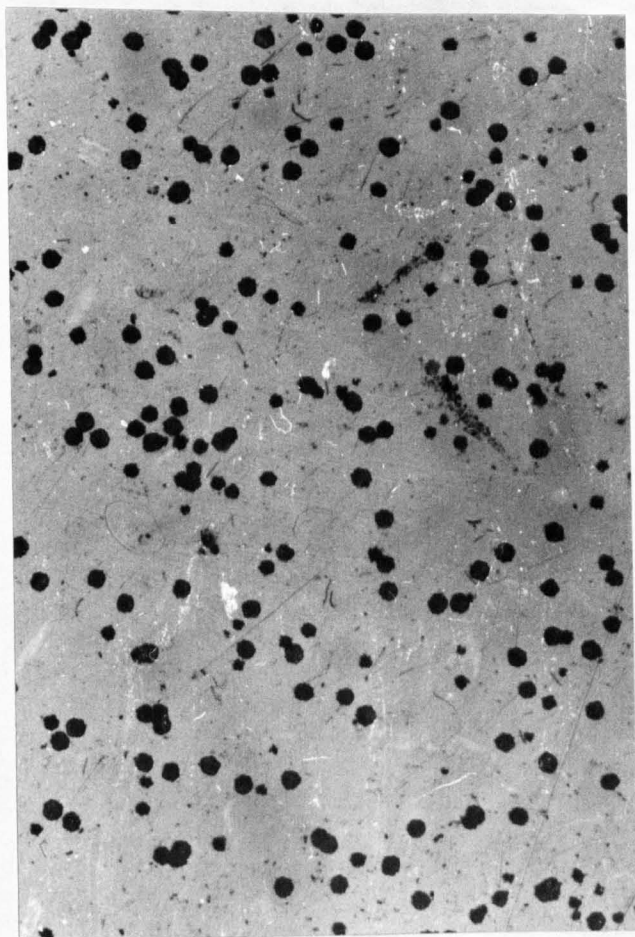
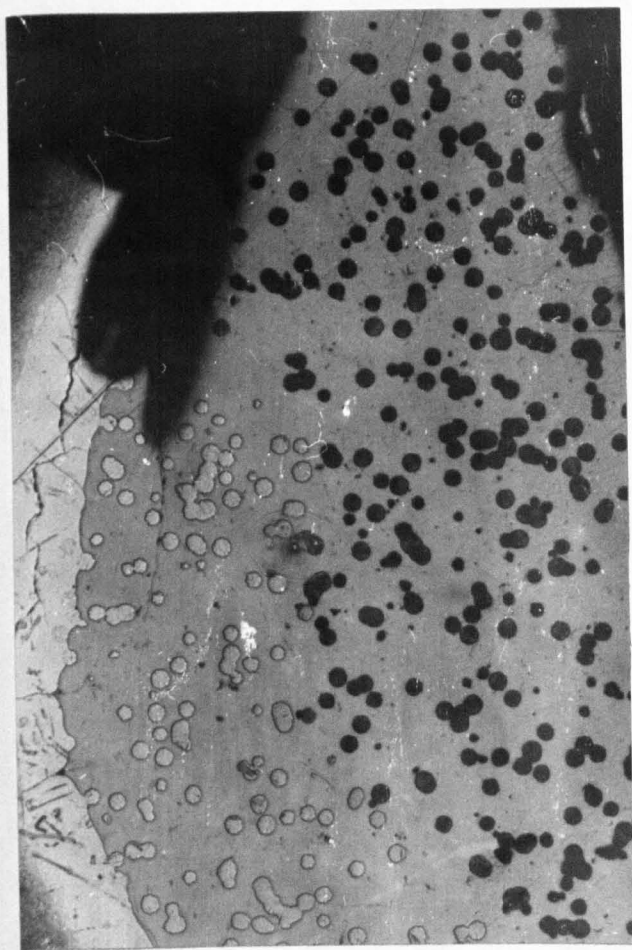
Third page:

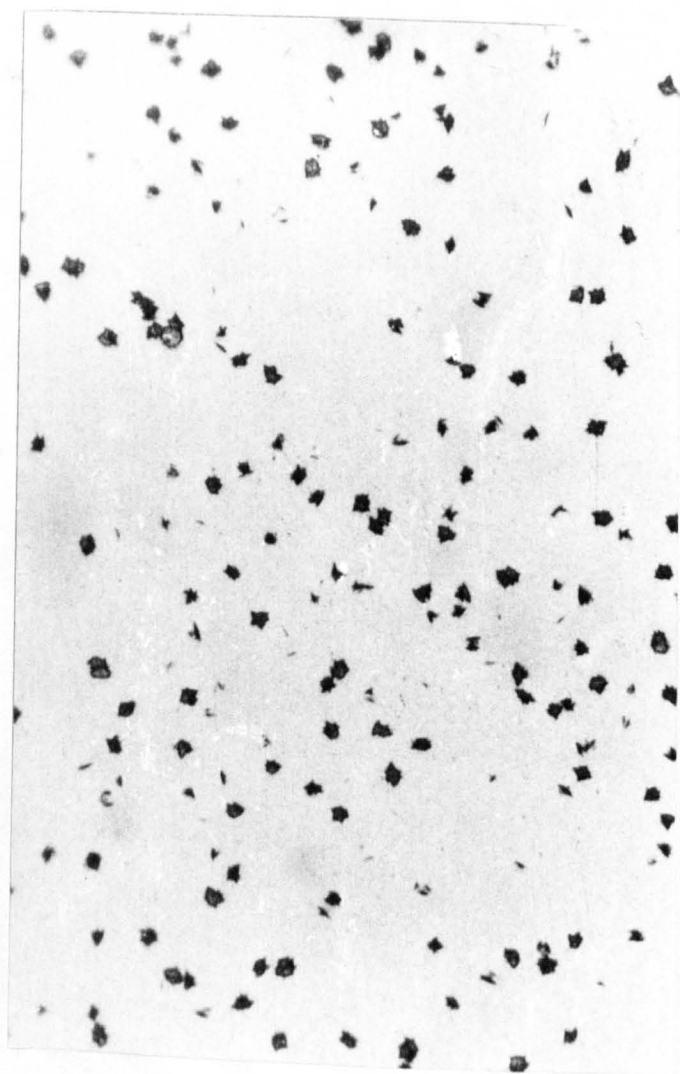
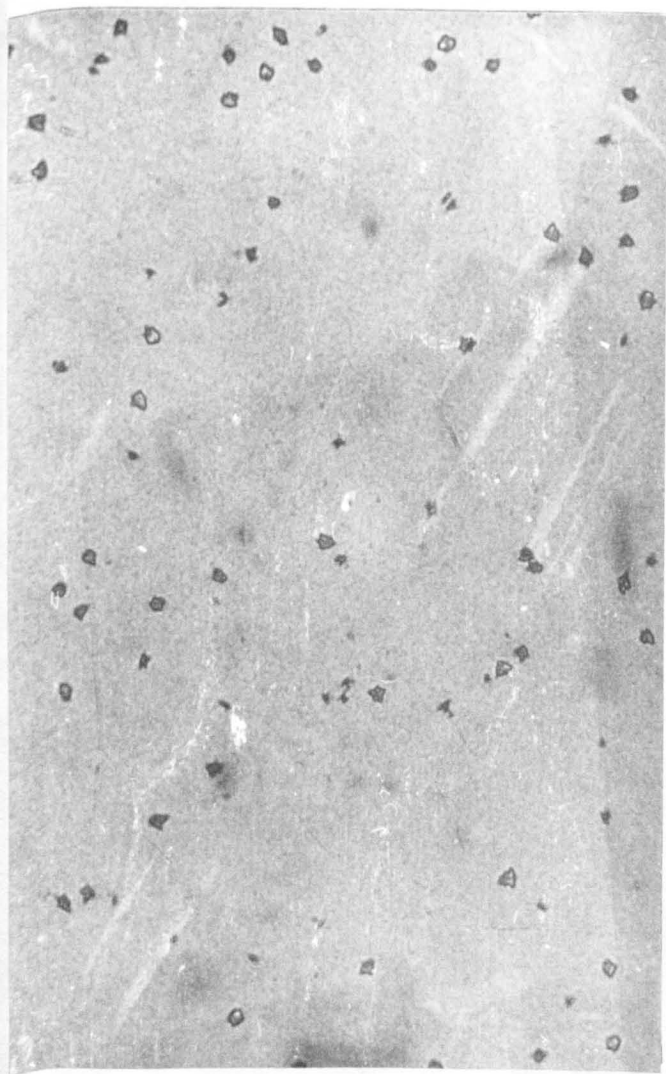
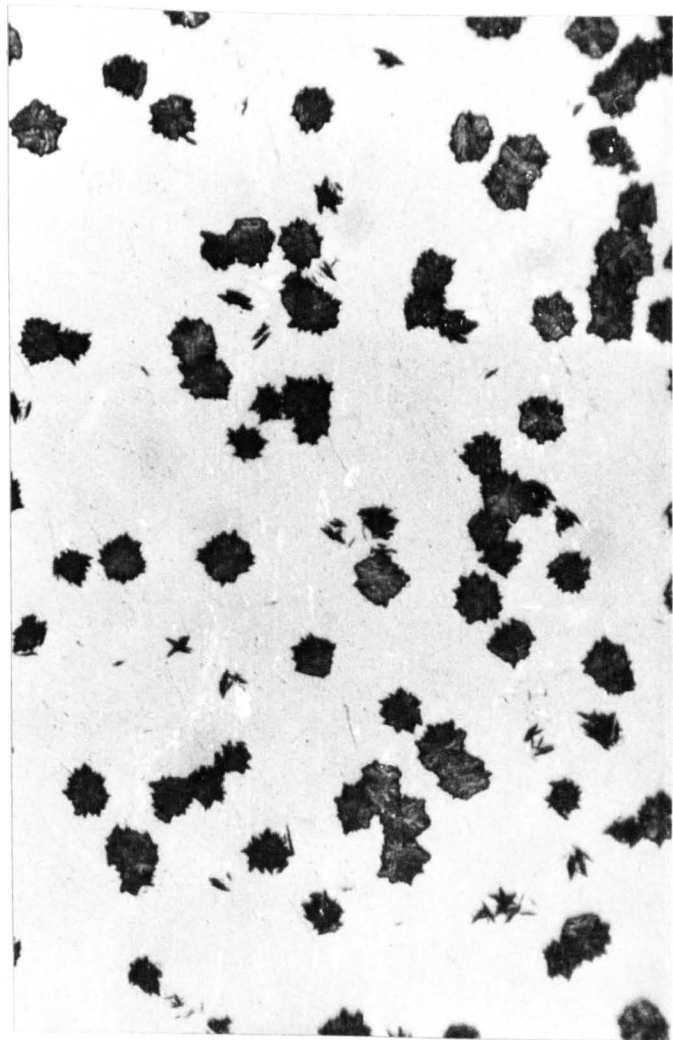
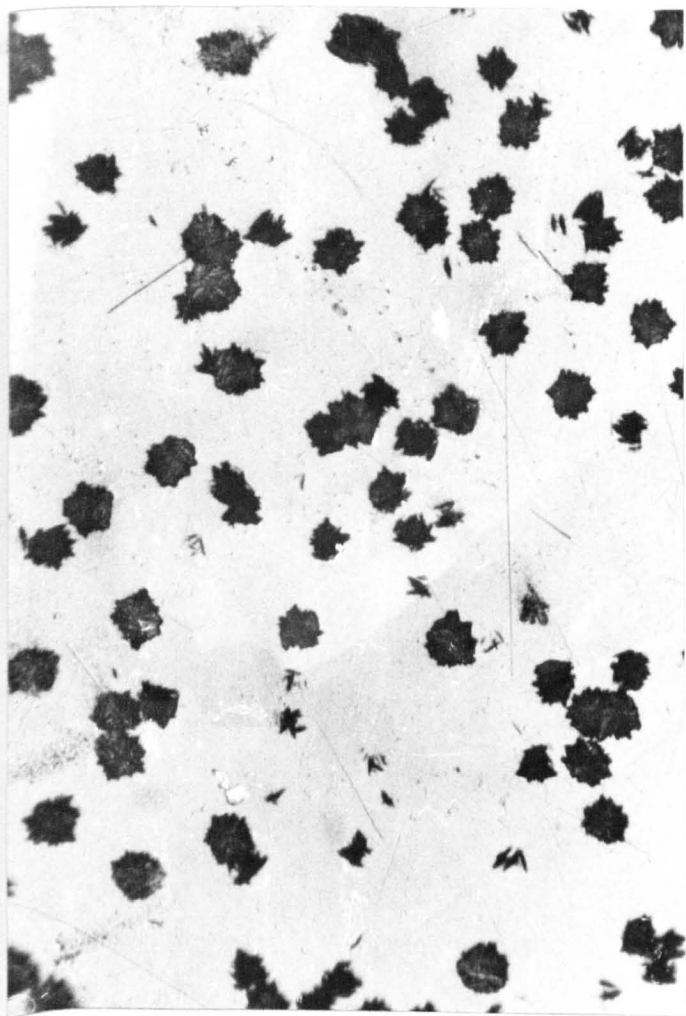
Top left: glass 26A, nucleated at 700°C, 2 hrs  
6 mins, Mag x600

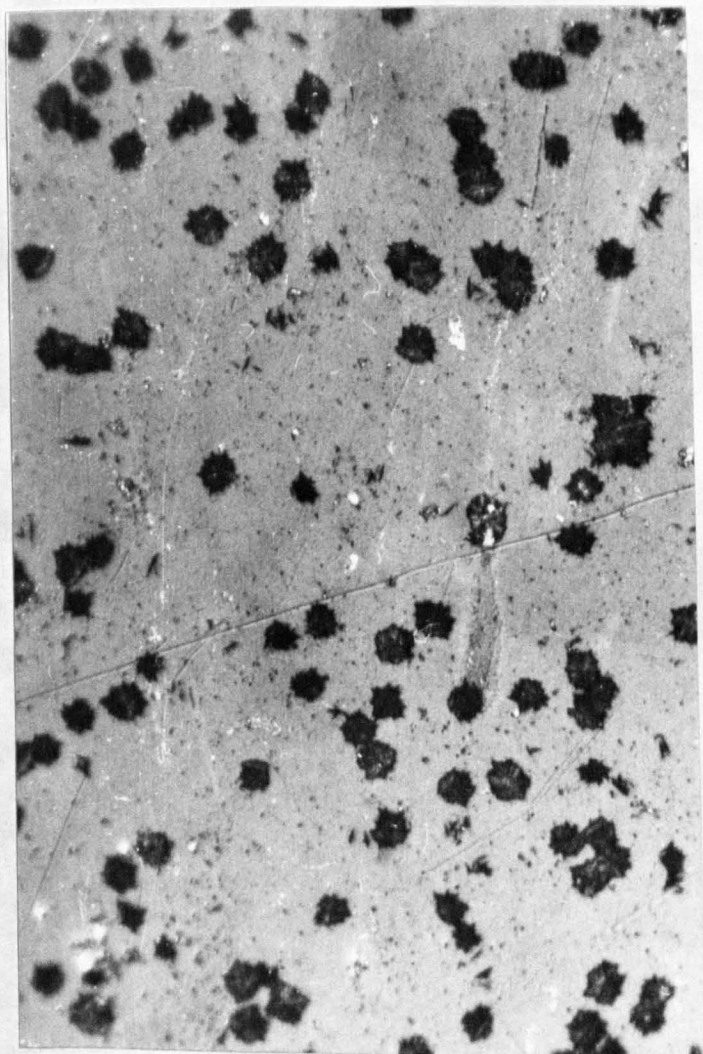
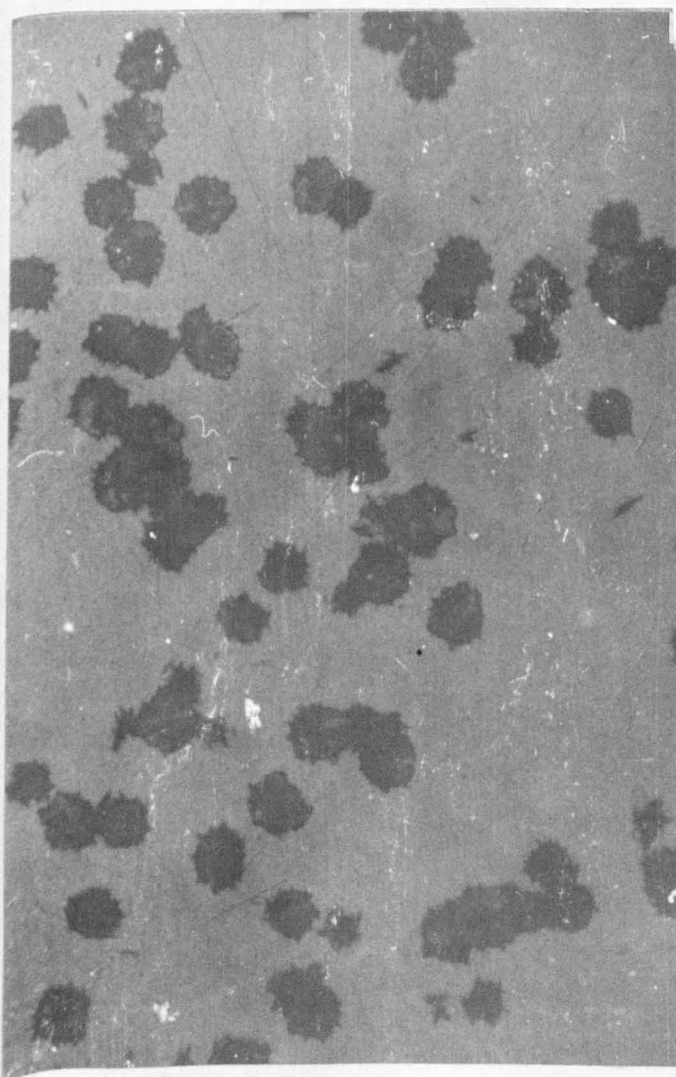
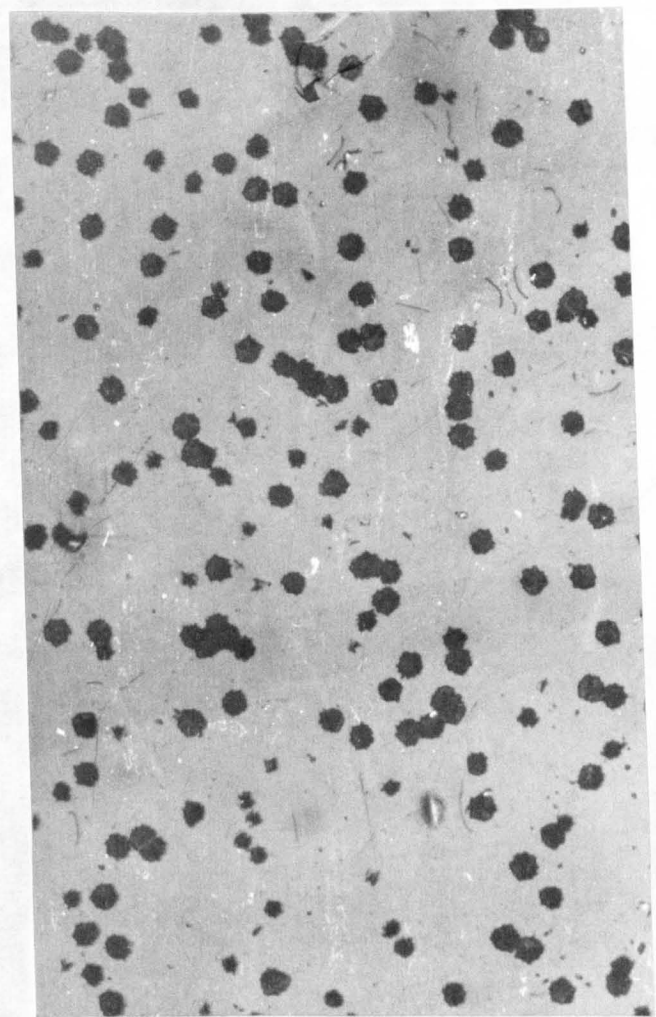
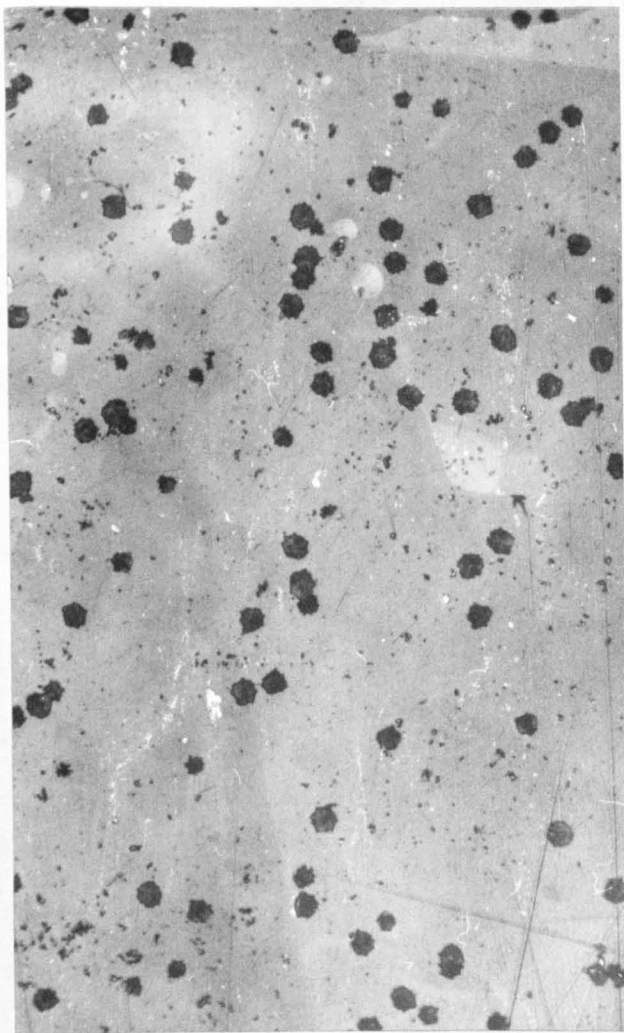
Top right: glass 26B, nucleated at 700°C, 2 hrs  
6 mins, Mag x600

Bottom glass 26D, nucleated at 700°C, 2 hrs  
left: 6 mins, Mag x600

Bottom glass 26C, nucleated at 700°C, 2 hrs  
right: 6 mins, Mag x600







attributed to liquid phase separation occurring in the glasses at the same time as crystal nucleation (Figures (6.13-6.15)). Thus 26A and B are initially non-separated or only slightly phase separated quenched glasses. Phase separation then occurs over an extended period during which a silica-rich phase is precipitated and the composition of the baria-rich matrix phase changes gradually until the equilibrium compositions are eventually reached. Even after this stage the morphology of separation may continue to change due to coarsening, as explained previously. As the composition of the matrix changes and becomes closer to (but not equal to) the barium disilicate composition, the nucleation rate of crystals increases, as in fact observed. The changes in nucleation rates for 26C and D may also be explained generally in the same way, although to explain the precise details the kinetics of phase separation must also be considered. This will be discussed shortly. The higher  $N_v$  values and higher nucleation rates in glass 26C are due to the more extensive degree of phase separation initially present in this glass.

An alternative explanation of the curvatures of the  $N_v$  plots is that they are caused by transient (non steady state) nucleation, characteristic of nucleation at lower temperatures. It will be remembered from section (3.1) that initially the number of crystal embryos in the glass is zero but increases with time until the number of embryos attaining the critical size reaches a steady state. Consequently the rate of formation of nuclei must be zero at  $t = 0$  and will gradually rise to a steady state constant value. This explains the curvature of experimental  $N_v$  versus time plots in certain glasses.

However, the transient process is unlikely to apply to glass 26 at  $700^\circ\text{C}$  since the number of crystals counted in a glass of similar composition that does not phase separate (glass 32) showed no sign of any such transient effects at  $700^\circ\text{C}$  (see Figure (6.18 and Table 6.12). However, if the

Figure 6.18 Plot of number of nuclei ( $N_v \text{ cm}^{-3}$ ) versus time (hrs) for glass 32 at  $700^\circ\text{C}$

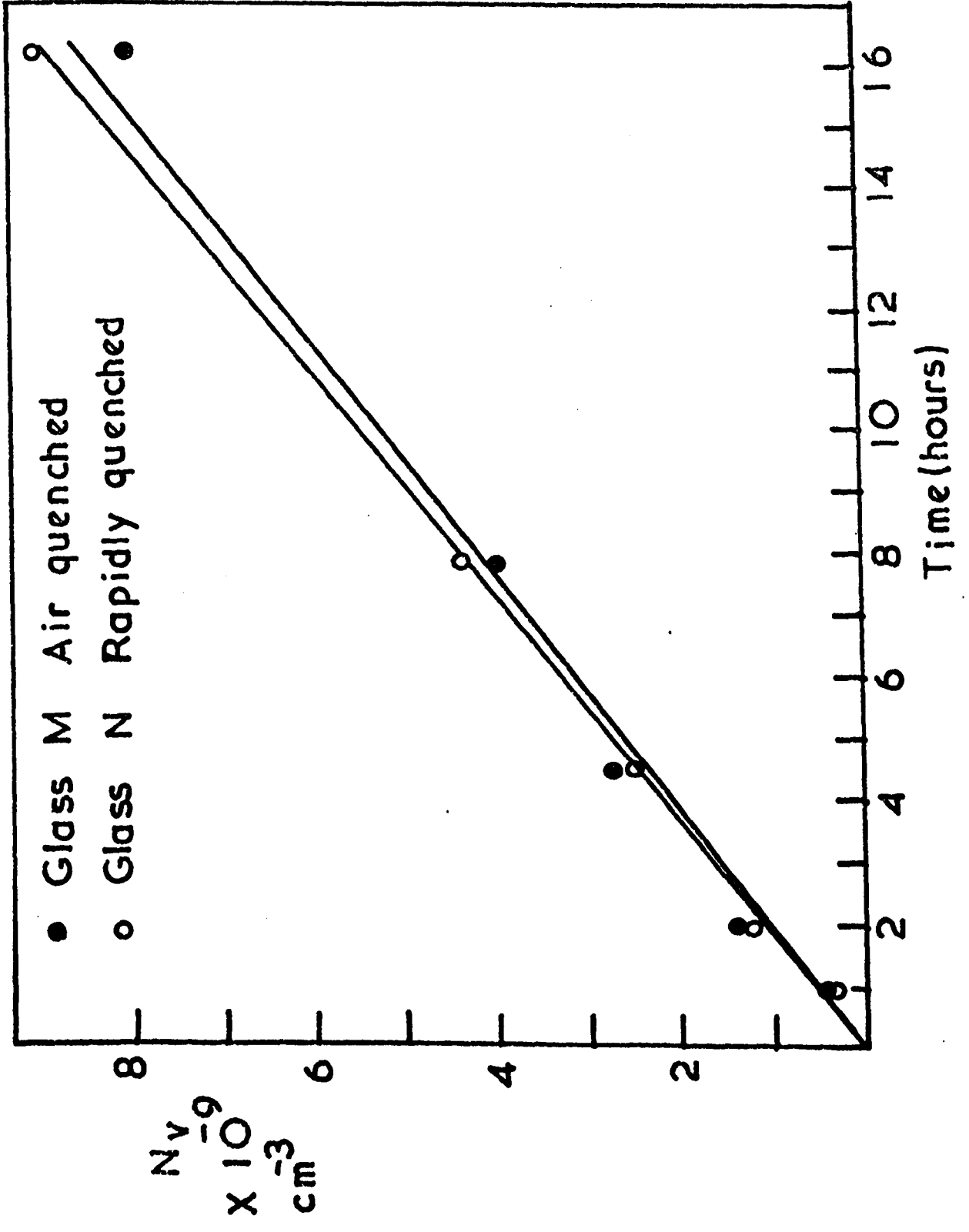


TABLE 6.12

NUCLEATION DATA FOR GLASS 32 AT 700°C

Time	$N_V \text{ cm}^{-3}$	Time	$N_V \text{ cm}^{-3}$
1 hr	M $4.08 \times 10^8$	7 hrs 45 mins	M $3.96 \times 10^9$
	N $3.83 \times 10^8$		N $4.37 \times 10^9$
2 hrs	M $1.35 \times 10^9$	16 hrs 15 mins	M $8.02 \times 10^9$
	N $1.28 \times 10^9$		N $9.04 \times 10^9$
4 hrs 30 mins	M $2.71 \times 10^9$		
	N $2.48 \times 10^9$		

Glass M  $\equiv$  glass 32 heat treated at 1050°C for  $\frac{3}{4}$  min and quenched in silicone oil.

Glass N  $\equiv$  glass 32 as-cooled from the melt

TABLE 6.13

CALCULATED VOLUME FRACTION DATA FOR GLASS 26

Temperature °C	$V_f$ (Haller)	$V_f$ (Present Work)
900	13.2%	18.6%
800	17.2%	22.1%
700	20.4%	25.0%

nucleation temperature is lowered to 677°C, a pronounced time delay does appear for 32 (see Figure (6.19)) and Table (6.11)). These induction times are due to the lower diffusion rates at lower temperatures. Thus at 700°C the time delay is small for glass 26 and 30 and the curvature is caused primarily by liquid immiscibility occurring within the glasses.

To check the possibility that thermal history (i.e. quenching rate) might in some way influence the nucleation behaviour, even in a glass incapable of liquid phase separation, the following subsidiary experiment was carried out. Glass 32 was rapidly quenched into silicone oil after heating at 1050° for  $\frac{3}{4}$  minute. However, no significant changes in nucleation behaviour compared with the normal air-cooled samples were observed (see Table (6.12), Figure (6.18)).

#### 6.2.2 The liquid-liquid immiscibility in glass 26 - Results and discussion

The composition of glass 26 is shown on the phase diagram (Figure (6.4)) and the heat treatments at 700, 800 and 900°C are indicated by the dashed lines. The equilibrium volume fractions of the phases are calculated from the mole fractions using the Lever Rule and density data of MacDowell<sup>(16)</sup>. The first column in Table (6.13) is the volume fraction of the silica rich phase computed by assuming that the curve obtained by Haller et al<sup>(28)</sup> is correct. This assumes a  $T_m$  for 26 of 1080°C. If we assume that the experimentally determined  $T_m$  of 1140°C is more accurate and drawing the immiscibility curve through this point and parallel to the curve of Haller et al, another estimate of  $V_f$  is obtained (column two in Table (6.13)).

The experimentally determined values of the volume fractions obtained from replica electron micrographs for glasses 26B, C and D held at 700°C for various times are given in Table (6.14). No values describing phase separation morphology for 26A are available because the replication technique

Figure 6.19 Plot of number of nuclei ( $N_v \text{ cm}^{-3}$ ) versus time (hrs) for glass 32 at  $677^\circ\text{C}$

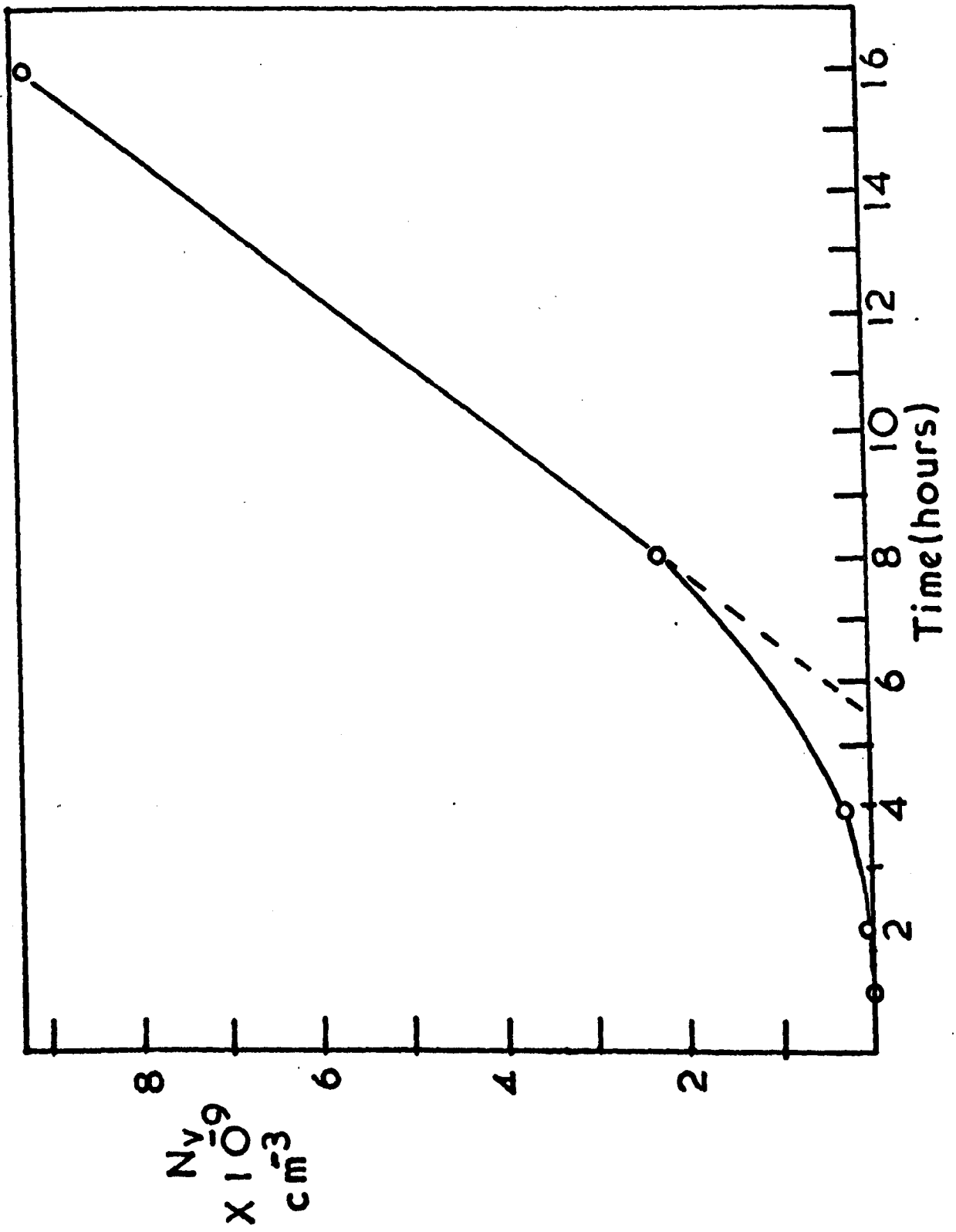


TABLE 6.14

EXPERIMENTALLY DETERMINED VOLUME FRACTIONS OF SILICA

RICH PHASE FOR GLASSES 26B, C AND D

Glass	26D	26C	26B
Times of heat treatment at 700°C			
0	32.0%	42.7%	33.8%
1 hr	33.5%	41.4%	35.5%
2 hrs	29.8%	38.3%	45.0%
		(2 hrs 05 mins)	
4 hrs		39.9%	
7 hrs 35 mins	32.6%		45.6%
			(8 hrs 42 mins)
11 hrs 25 mins	33.1%	42.6%	
		12 hrs 15 mins)	
16 hrs 37 mins			46.8%

could not produce satisfactory replicas.

The 95% confidence limits of a typical  $V_f$  result have been estimated in Appendix (5.3). The estimate of volume fractions was expected to be fairly accurate for phase separated glasses 26 (C and D) but in glass 26B (air quenched) the phase separation structure was fine and faint and calculations of  $V_f$  were subject to large errors. The figures are suitable for comparative purposes but on an absolute scale these values are much higher than expected (see Table (6.13)) and are an approximate guide only. This is probably because heavy etching was needed to reveal the structure

sufficiently clearly for measurement. This effect is well known and has been studied systematically by Burnett and Douglas<sup>(84)</sup>. They were able to improve the accuracy of the method by plotting measured  $V_f$  values against etching time and extrapolating back to zero time. This was also attempted with the present glasses but was impractical since accurate estimates of  $V_f$  could not be obtained for very light etches.

Exactly the same etching treatment was employed for each glass at all times and so the results are still useful as a comparative guide. For example, the  $V_f$  values do provide some evidence of the extent to which phase separation has occurred for a given time series at constant temperature.

If criterion b) or d) of Uhlmann's four points is applicable in affecting nucleation kinetics, it should be possible to detect differences in crystal nucleation characteristics that are dependent on the relative values of the interfacial areas of liquid phase separation. If the phase morphology resembles isolated droplets then the number of droplet particles also becomes of importance because two or more crystals nucleating around a droplet will eventually coalesce and be recorded as one crystal. Hence each droplet will not give rise to more than one crystal. This will occur whatever the size of the droplets. Thus the number of droplets will in this case be more important than  $S_v$ . The statistics on the number of droplets  $n_v$  and the interfacial area  $S_v$  for glasses 26B, C and D heat treated at 700°C for various times are recorded in Tables (6.15) and (6.16).

Representative areas illustrating phase morphologies of glasses 26B, C and D heat treated at 700°C are shown in Figure (6.20). It can be seen that pronounced changes occurred in the phase separation morphology of 26B on heating at 700°C. This was also reflected in changes in  $n_v$ ,  $S_v$  and  $V_f$  (see Tables (6.14 - 6.16)). However, changes in 26C and D were slight. The phase morphologies of glass 26C and D are isolated droplets after all

Figure 6.20 Electron micrographs of development of  
(three pages) phase separation morphology of glasses  
26B, C and D at 700°C.

This page: Glass 26B, air quenched

From the top, Air quenched, no heat treatment

Mag x47000

1 hr 3 mins at 700°C, Mag x47000

2 hr at 700°C, Mag x47000

8 hr 42 mins at 700°C, Mag x47000

16 hr 37 mins at 700°C, Mag x47000

Second page: Glass 26C, 800°C, 1 hour

Top left: No further heat treatment.

Mag x47000

Top right: 1 hr at 700°C, Mag x47000

Middle left: 2 hr 5 mins at 700°C, Mag x47000

Middle right: 4 hr 10 mins at 700°C, Mag x47000

Bottom left: 12 hr 15 mins at 700°C, Mag x47000

Bottom right: 17 hr at 700°C, Mag x47000

Third page: Glass 26D, 900°C, 10 mins

From the top: No further heat treatment.

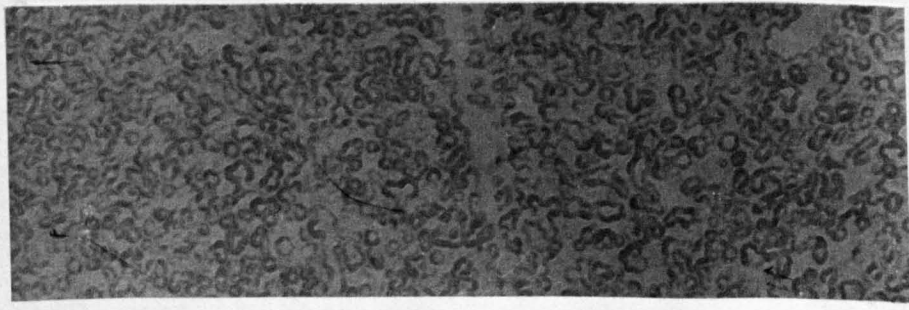
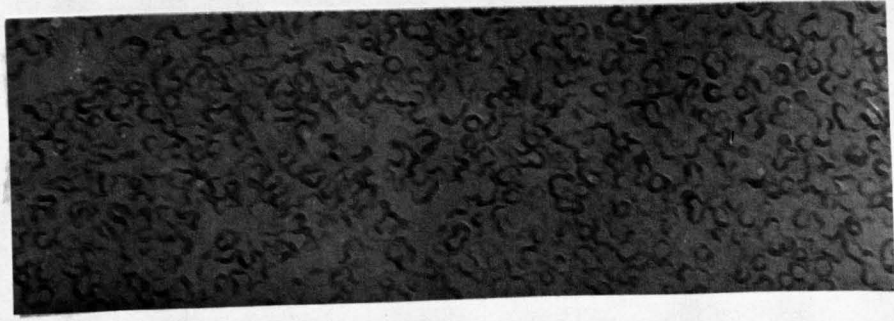
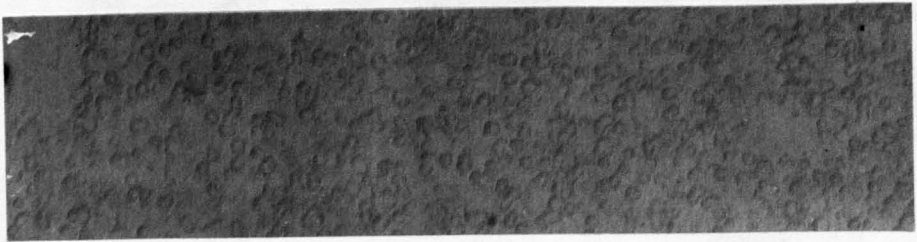
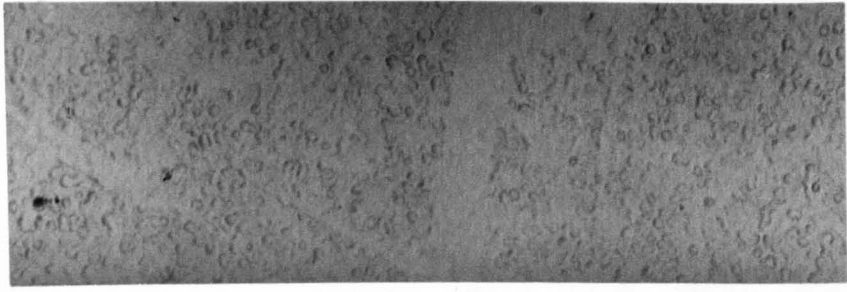
Mag x47000

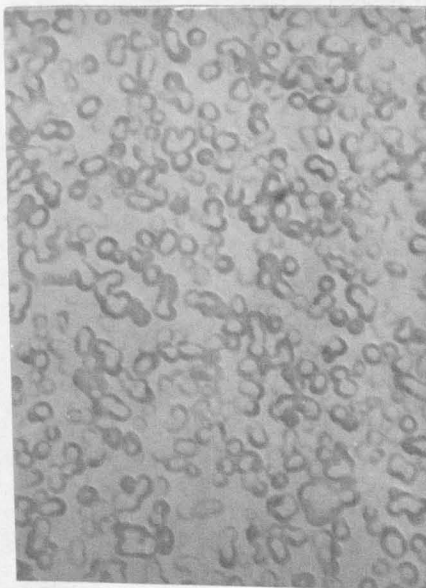
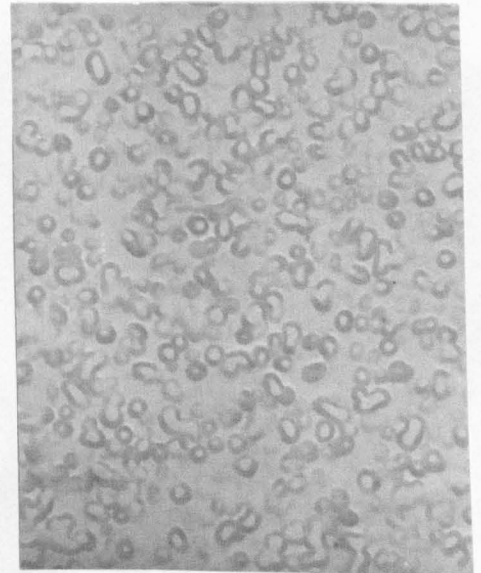
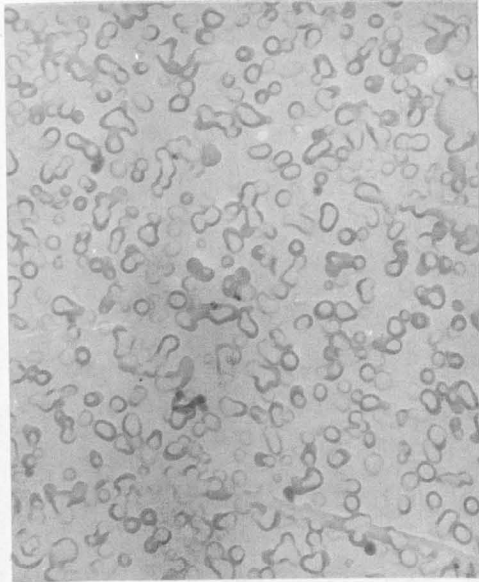
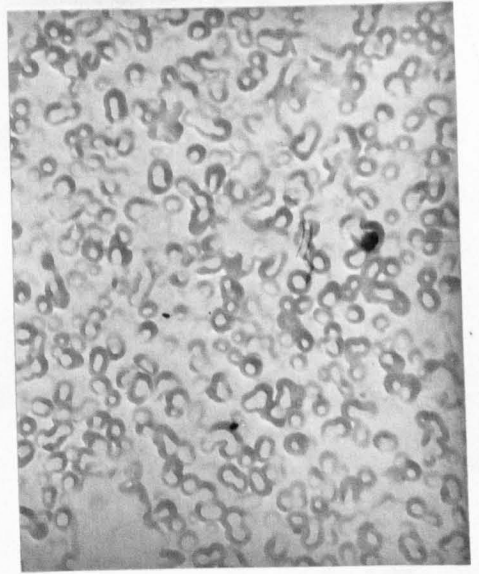
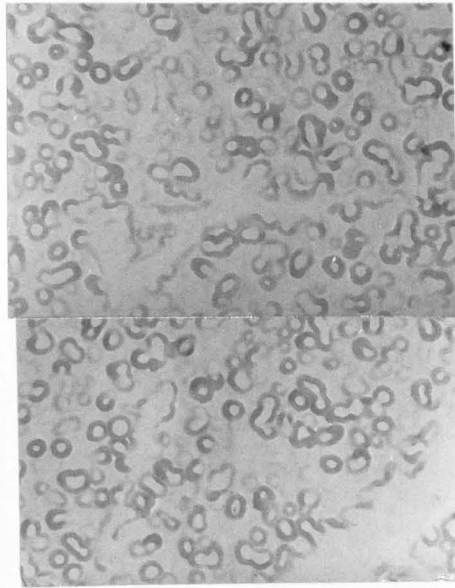
1 hr at 700°C, Mag x47000

2 hr at 700°C, Mag x47000

7 hr 35 mins at 700°C, Mag x47000

16 hr 11 mins at 700°C, Mag x47000





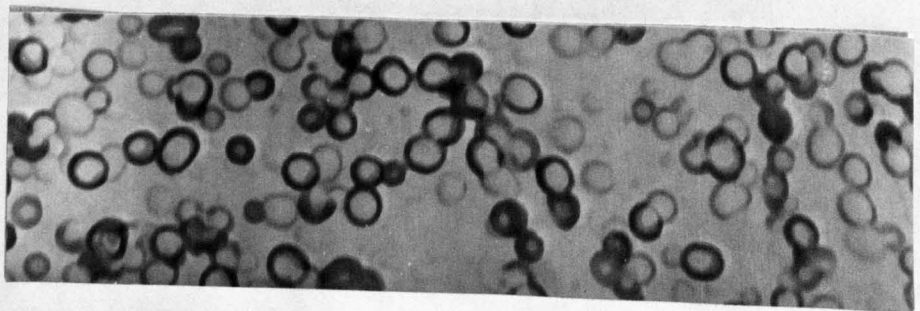
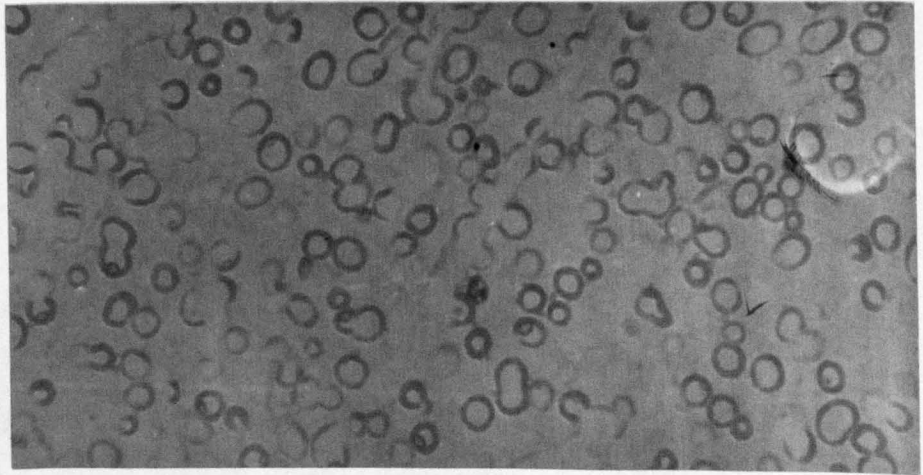
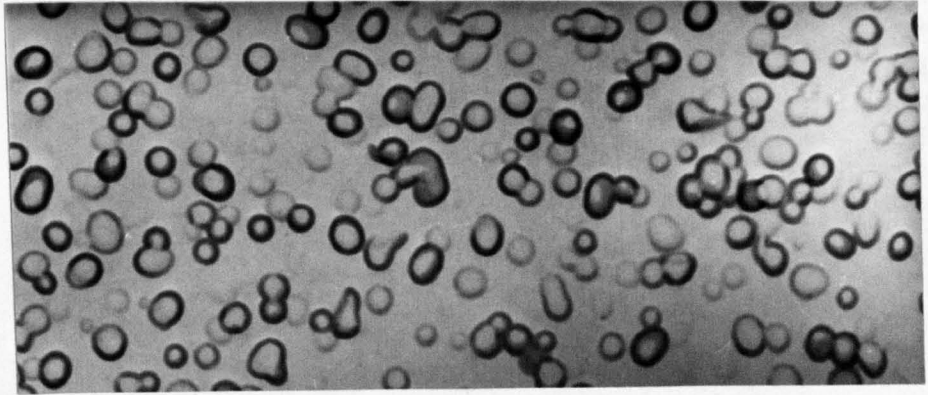
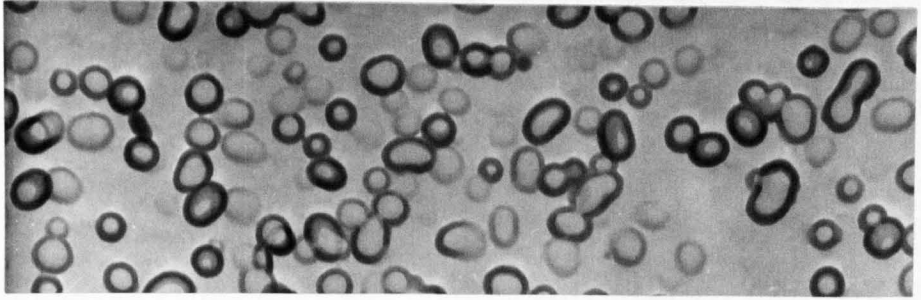
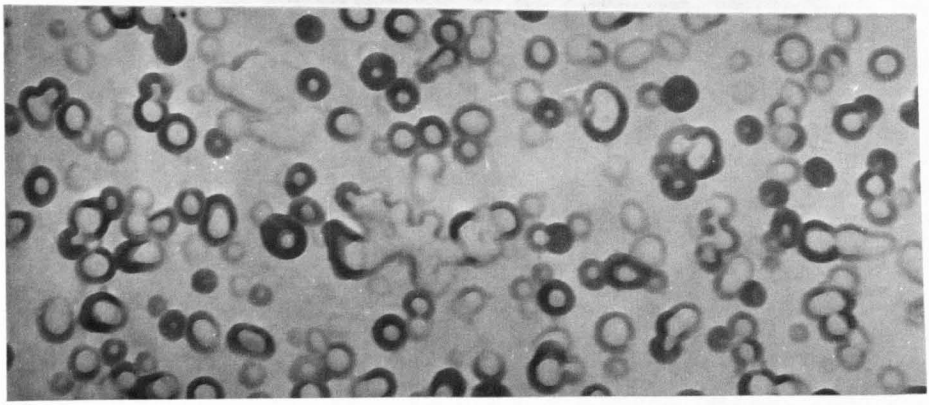


TABLE 6.15

EXPERIMENTALLY DETERMINED INTERFACIAL AREAS OF GLASSES 26B

C AND D HEAT TREATED AT 700°C (cm<sup>2</sup>/cm<sup>3</sup>)

Glass	26D	26C	26B
Times of heat treatment at 700°C			
0	2.04 x 10 <sup>5</sup>	3.0 x 10 <sup>5</sup>	4.12 x 10 <sup>5</sup>
1 hr	2.03 x 10 <sup>5</sup>	3.64 x 10 <sup>5</sup>	4.46 x 10 <sup>5</sup> (1 hr 03 mins)
2 hrs	1.99 x 10 <sup>5</sup>	3.74 x 10 <sup>5</sup> (2 hrs 05 mins)	5.26 x 10 <sup>5</sup>
4 hrs		3.69 x 10 <sup>5</sup> (4 hrs 10 mins)	4.98 x 10 <sup>5</sup>
7 hrs 35 mins	1.94 x 10 <sup>5</sup>		4.96 x 10 <sup>5</sup> (8 hrs 42 mins)
11 hrs 25 mins	1.97 x 10 <sup>5</sup>	4.17 x 10 <sup>5</sup> (12 hrs 15 mins)	
16 hrs 37 mins			5.03 x 10 <sup>5</sup>

TABLE 6.16

EXPERIMENTALLY DETERMINED DROPLET NUMBERS (n<sub>v</sub>) IN GLASSES

26B, C AND D HEAT TREATED AT 700°C

Glass	Time of heat treatment at 700°C	Number of droplets n <sub>v</sub> cm <sup>-3</sup>
26D	2 hrs 01 mins	8.18 x 10 <sup>14</sup>
	7 hrs 35 mins	8.16 x 10 <sup>14</sup>
26C	2 hrs 05 mins	5.00 x 10 <sup>15</sup>
	1 hr	4.85 x 10 <sup>15</sup>
26B	0	9.97 x 10 <sup>15</sup>
	1 hr 03 mins	9.95 x 10 <sup>15</sup>
	2 hrs	9.00 x 10 <sup>15</sup>
	8 hrs 42 mins	1.36 x 10 <sup>16</sup>
	16 hrs 37 mins	9.2 x 10 <sup>15</sup>

the heat treatments. However, after glass 26B had been heat treated at 700°C for 8 hours or more, the structure became interconnected and the  $n_v$  parameter was difficult to assess. Only two  $n_v$  measurements were taken on glass 26C and D because the nearly constant values of  $V_f$  and  $S_v$  with time implied a nearly constant  $n_v$ .

It is a common occurrence for a glass given a two stage heat treatment in the phase separated zone to undergo secondary phase separation during the final heating procedure. This occurs because the composition of one of the phases itself can phase separate on cooling to the second heat treatment temperature. The matrix between the large particles separates into many fine droplets. The size of these droplets is limited by the slower kinetics at the lower heat treatment temperatures. Alternatively, secondary phase separation can involve simply growth of the large droplets of silica present after the first stage treatment without additional precipitation of finer scale droplets. It is feasible in other systems for the minor phase to separate but in BaO-SiO<sub>2</sub> glasses for the temperatures used in the present study (800-900°C) the silica-rich phase is already nearly pure silica and is unlikely to phase separate further. Burnett<sup>(30)</sup> has found examples of secondary liquid immiscibility in one phase for a Na<sub>2</sub>O-CaO-SiO<sub>2</sub> glass. Seward et al<sup>(14)</sup> have observed secondary phase separation in both phases in a BaO-SiO<sub>2</sub> glass near the critical composition and consolute temperature.

The compositions of the baria rich phases were found by extending the horizontal line at the phase separation temperature to the liquid immiscibility boundaries. In the case of glass C at 800°C, the baria-rich phase contained 30 mol% BaO if 'Hallers curve' was assumed to represent the immiscibility dome. Alternatively, by drawing a curve through the experimentally determined immiscibility temperature  $T_m$  (1140°C) parallel to 'Hallers curve', the baria rich phase were found to consist of 31.6 mol% BaO.

A glass of this composition would probably not undergo secondary phase separation easily at 700°C because the driving force  $\Delta G$  for the nucleation of fine scale droplets would be small. This is probably why glass 32 containing 30.4 mol% BaO and a  $T_m$  of 760°C was not observed to phase separate. Thus glass 26C heat treated at 800°C for one hour and then heated at 700°C will undergo a slow additional phase separation probably by the growth of the droplets already present in the glass. This was reflected indirectly in the nucleation kinetics as an almost straight line relationship between the number of crystals and time.

### 6.2.3 Further discussion of results for glass 26

In this section we compare and examine critically the differences in the number of crystals nucleated in glasses 26A, B, C and D and comment on the possible reasons for these differences.

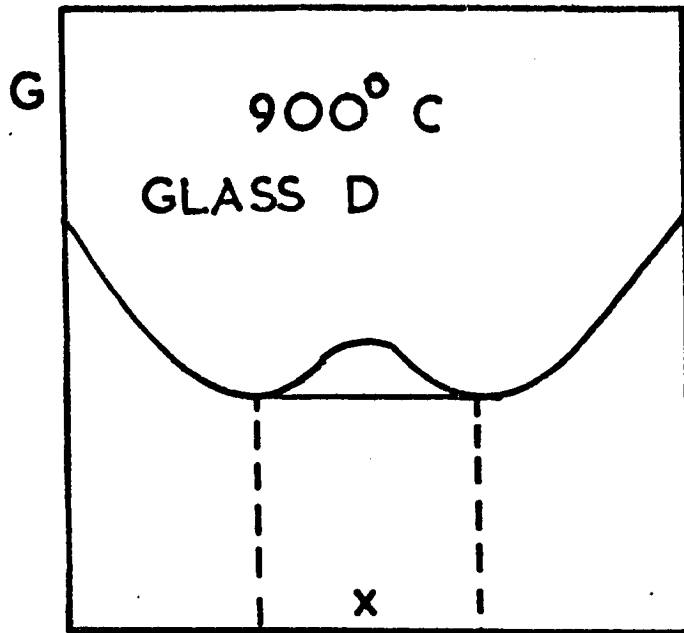
It will be shown that all the nucleation behaviour can be explained in terms of changes in the composition of the baria-rich matrix phase with time. Some of the behaviour has already been explained in this way above. Comparing the results for glasses 26A, B, C and D, it is noted that C has the highest nucleation rate and  $N_v$  value for all times at 700°C due to the matrix phase being closest to the barium disilicate composition throughout. This resulted from the initial phase separation treatment at 800°C. For short nucleation times at 700°C, 26D has a higher nucleation rate than 26A and B, also due to its initial separation treatment.

The curvatures in the  $N_v$  plots are due to phase separation taking place at 700°C at the same time as crystal nucleation. The evidence from quantitative phase separation measurements and examination of the replica micrographs shows that phase separation at 700°C is taking place slowly and results in a gradual shift in composition of the two phases without

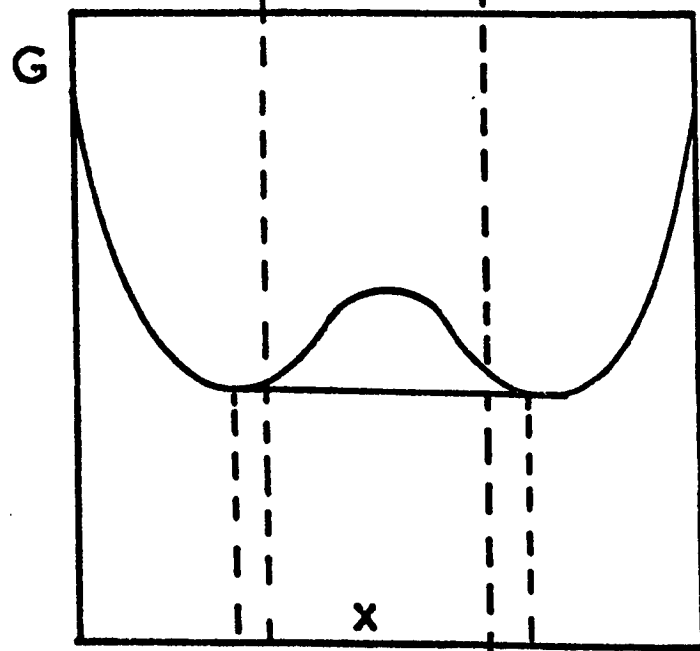
altering very significantly the morphological parameters ( $V_f, n_v, S_v$ ). Comparing 26C and D, 26D has a more pronounced initial curvature ( $N_v$  versus time) at 700°C. This can be related to the occurrence of additional liquid phase separation at 700°C after the primary separation at 900°C. The driving forces for phase separation in B, C and D are shown schematically in Figure (6.21). It is clear that the driving force for nucleation of phase droplets is greatest in B (this corresponds to primary phase separation). The driving forces for secondary nucleation in C and D are much smaller. This probably accounts for the fact that no sign of secondary phase separation was observed for C or D at 700°C. The additional phase separation must therefore, take the form of growth of the existing droplets present after the pre-phase separation treatments. During this growth process the composition of the baria-rich phase will shift gradually, causing the nucleation rate to rise and the  $N_v$  versus time plot to become curved.

Both glasses 26A and B were quenched from above  $T_m$ . The replicas showed that very fine scale phase separation occurred during the quenching process (thus glass 26B has approximately ten times as many droplets as glass 26D). This may be attributed to the greater driving force  $\Delta g$  for nucleation of phase separation in 26A and B during rapid cooling (illustrated in Figure (6.21)), causing a higher nucleation rate for liquid droplets. However, the droplets are very fine and the amount of phase precipitated is probably smaller than for 26C and 26D. Also, the overall shift in the matrix composition is probably smaller than in the case of 26C and D. Hence, initially at 700°C, crystal nucleation rates are less in 26A and B than in C and D. Although liquid separation still occurs slowly at 700°C, there are many more potential growth sites in glass A and B than in C or D. Assuming diffusion controlled parabolic growth to occur, the precipitation rate will be

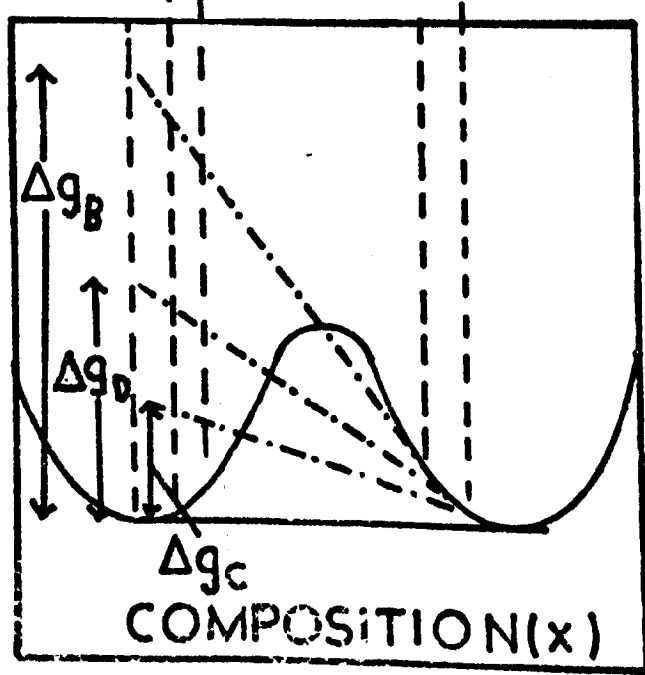
**Figure 6.21** Schematic diagrams illustrating thermodynamic driving force for liquid-liquid immiscibility ( $\Delta g$ ) in glasses B, C and D.



a)



b)  
800° C  
GLASS C



c)  
700° C  
 $\Delta g_B > \Delta g_D > \Delta g_C$

more rapid in A and B. The greater driving force  $\Delta g$  may also encourage more rapid precipitation. Consequently the matrix composition will undergo a more rapid shift. Eventually the matrix composition in A or B becomes richer in baria than D so that the crystal nucleation rate becomes greater. Thus the crystal nucleation rates for B and D coincide after about one hour and thereafter are greater for B (figure (6.16)). Also, a cross-over in the  $N_v$  versus time plots occurs with 26A and B overtaking 26D between 4 and 8 hours. In the course of the experiment the crystal nucleation in 26A and B is always less than in 26C due to the large initial shift in composition of this glass.

It should also be noted that the  $N_v$  for 26A is always slightly less than 26B probably due to the more rapid initial quench given to 26A producing less phase separation in this glass.

The above explanation depends on the phase separation occurring slowly at 700°C, causing gradual changes in matrix composition. Since the process is slow, the values of  $V_f$ ,  $S_v$  and  $n_v$  show very little change with time for 26C or 26D. However, there is some evidence that  $V_f$  and  $S_v$  show a small increase for 26B, notwithstanding the difficulties in accurate measurement of these quantities (Tables 6.14-6.16) and Figure (6.20)).

The possible influence of crystal nucleation heterogeneously catalysed by interfaces will now be considered. It has been observed that at 700°C  $S_v$  is changing only slightly for 26B and C or not at all for 26D (Table (6.15)). Yet nucleation rates for D are changing considerably with time (by up to a factor of four times, Figure (6.16)). This suggests the interfacial area is not affecting crystal nucleation directly. Also, although glass 26B has a larger  $S_v$  than 26C, B has the lower nucleation rate. This is the opposite to the results expected if interfaces nucleate crystals. Comparing 26D and C, it would be expected that D would have a lower nucleation

rate due to its coarser morphology. Figure (6.16) shows that although 26D has a lower nucleation rate, the gap between the rates of nucleation is steadily closing and this is not expected if interfaces are important. Instead the rates would parallel one another, the remaining gap between them being due to the large sustained difference in the morphology.

Considering the arguments from the perspective of the number of droplets, ( $n_v$ ) the conclusion reached above becomes even more obvious. For example, glass 26B has ten times more droplets than glass 26D and more than glass 26C, but initially 26B has a crystal nucleation rate similar to that of 26D and much less than 26C.

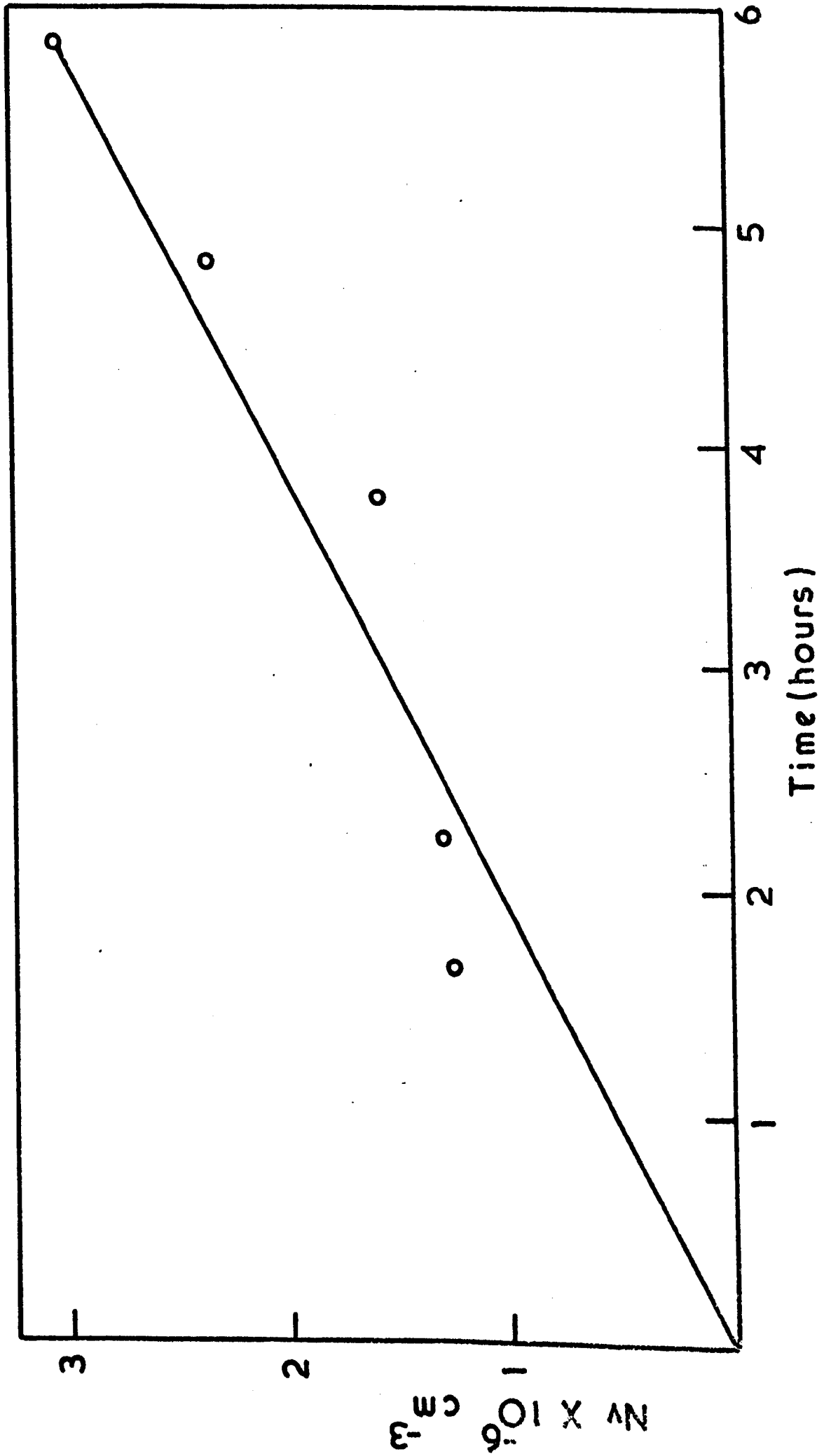
It may be concluded that the crystal nucleation observations are not explainable in terms of the phase separation morphology alone.

A final experiment on glass 26 involved heating the 'as-cooled' glass at a temperature where both crystal nucleation and growth and also the growth and coarsening of liquid phase separation took place concurrently. By relating  $V_f$ ,  $S_v$  and  $n_v$  with the crystal nucleation rate it was hoped to study further the effect (if any) of the morphology during the periods of growth and coarsening of phase separation (when  $S_v$  and  $n_v$  fall off with time).

Five specimens were given a heat treatment to nucleate and grow the crystals at 785°C for times indicated in Table (6.17) and the number of crystals counted. The results are plotted in Figure (6.22).

Although the points show some scatter, (precise nucleation measurements are more difficult at higher temperatures where the nucleation rates are much lower) the number of crystals show a general linear increase with time. On the other hand, the number of liquid droplets and the interfacial area

Figure 6.22 Plot of number of nuclei ( $N_v \text{ cm}^{-3}$ )  
versus time (hrs) in glass 26 at 785°C.



decreased over the same period due to coarsening or Ostwald ripening (see Table (6.18)). The results suggest that the crystal nucleation rate is not related to coarsening of phase separation.

TABLE 6.17

NUMBER OF CRYSTALS NUCLEATED AT 785°C

Time	Number of crystals $N_v \text{ cm}^{-3}$
1 hr 40 mins	$1.26 \times 10^6$
2 hrs 15 mins	$1.30 \times 10^6$
3 hrs 46 mins	$1.58 \times 10^6$
4 hrs 51 mins	$2.36 \times 10^6$
5 hrs 51 mins	$3.06 \times 10^6$

TABLE 6.18

EXPERIMENTALLY DETERMINED MORPHOLOGICAL PARAMETERS OF

LIQUID-LIQUID IMMISCIBILITY IN GLASS 26

HEAT TREATED AT 785°C

Time of heat treatment	$V_f \%$	$S_v \text{ cm}^2/\text{cm}^3$	$N_v \text{ cm}^{-3}$
1 hr 41 mins	44.5	$3.7 \times 10^5$	$4.1 \times 10^{15}$
2 hrs 15 mins	45.5	$3.4 \times 10^5$	$3.4 \times 10^{15}$
3 hrs 47 mins	39.8	$2.5 \times 10^5$	$1.9 \times 10^{15}$
4 hrs 51 mins	39.5	$2.8 \times 10^5$	$2.2 \times 10^{15}$

### 6.3 CRYSTAL NUCLEATION AND LIQUID-LIQUID IMMISCIBILITY RESULTS

#### IN GLASS 30 - EXPERIMENT 3

##### 6.3.1 Crystal nucleation in glass 30 - Results

Further experiments on crystal nucleation kinetics were carried out on glass 30. This composition was chosen for detailed study because it had a lower immiscibility temperature (905°C) than glass 26 and also a higher baria content (26.5 mol%). As a result, glass 30 phase separated less easily than glass 26 and produced a more 'droplet-like' and less interconnected phase microstructure than glass 26. The presence of a small amount of Al<sub>2</sub>O<sub>3</sub> impurity had the effect of depressing the crystal nucleation kinetics to a significant degree, but this was unimportant since comparisons were made between a phase separated and non-phase separated glass of the same overall composition. The lower nucleation rates at 700°C compared with glass 26 was also an advantage since longer times (up to sixty hours) could be employed in the experiments without reaching the limit of the quantitative optical microscope techniques.

The as-cooled glass 30 was free from liquid phase separation and the use of rapid quenching was, therefore, unnecessary. A sample of glass was phase separated at 780°C for one hour to fully develop liquid immiscibility within the glass (glass F). This was nucleated alongside the as-cooled glass (glass E) for various periods at 700°C.

The nucleation results are given in Table (6.19) and plotted as a function of time in Figures (6.23-6.25). The comparative numbers of crystals for specific times are expressed as a ratio and these are shown in Figure (6.26) whilst the rates are shown in Figure (6.27).

Typical micrographs comparing the nucleation behaviour between glasses E and F heat treated at 700°C for 1, 4, 8 and 10 hours are shown in Figure (6.28).

**Figure 6.23** Plot of number of crystals ( $N_v \text{ cm}^{-3}$ ) versus time (hours) for glass 30 at 700°C.

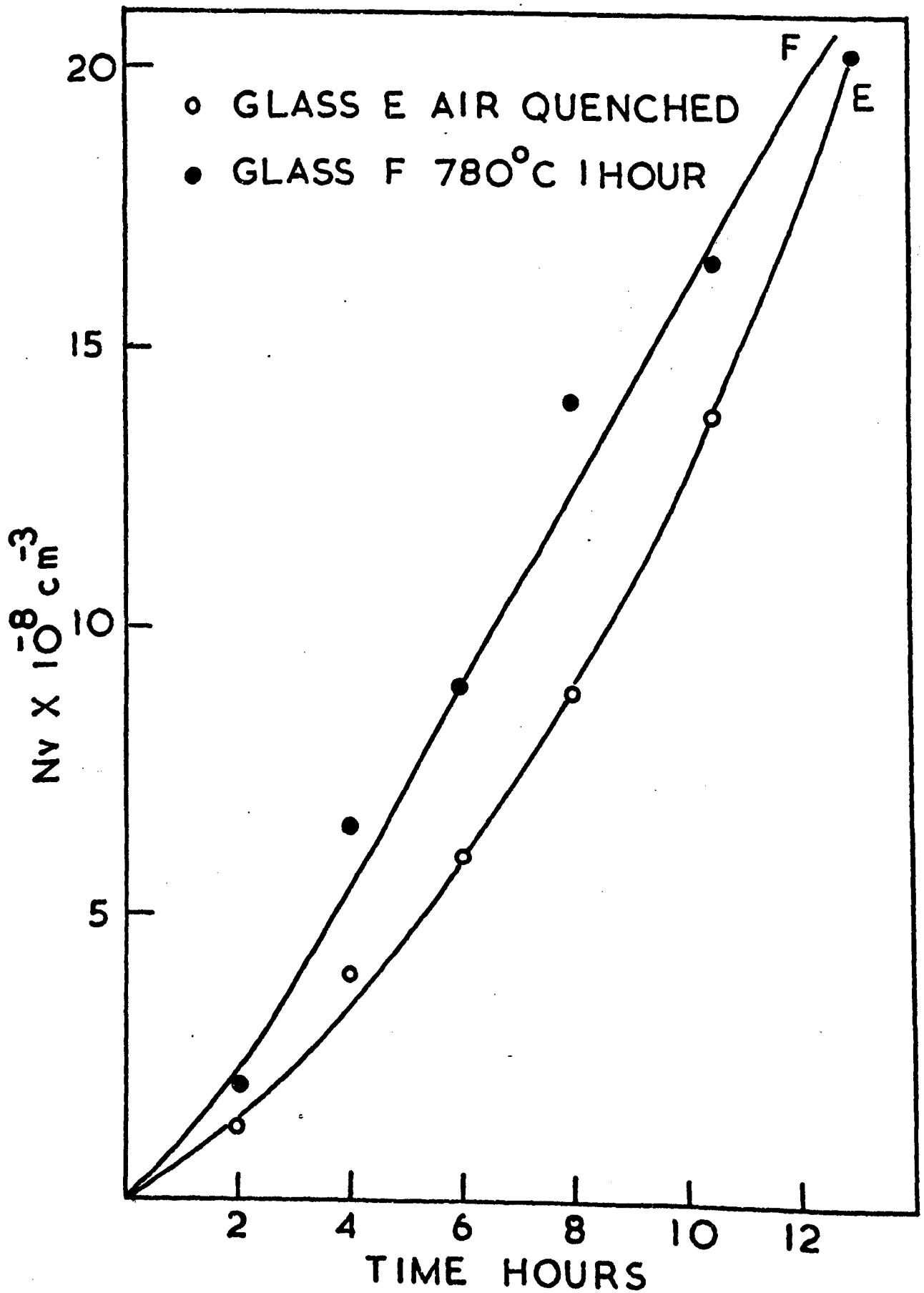
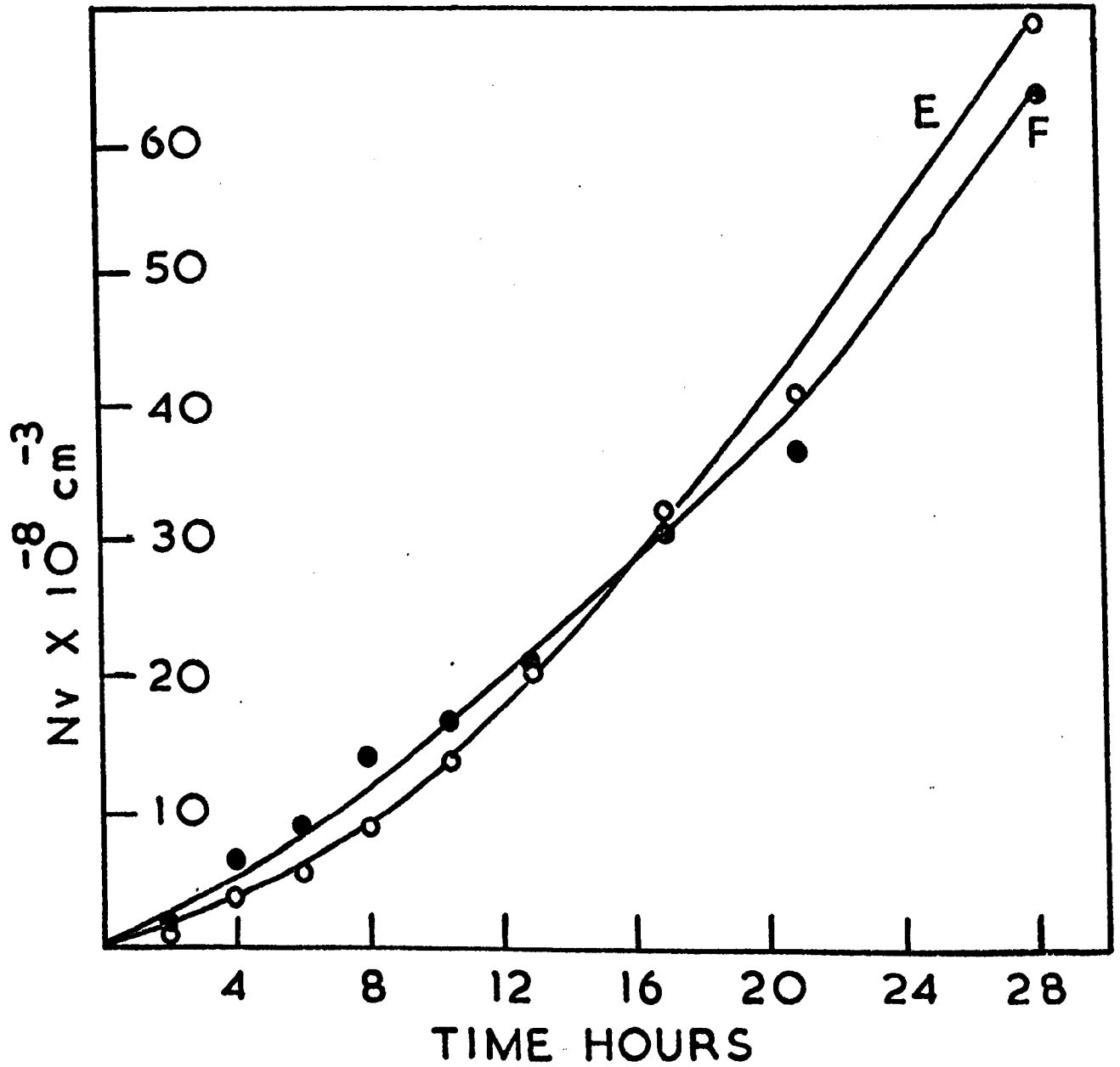


Figure 6.24 Plot of number of crystals ( $N_v$  cm<sup>-3</sup>)  
versus time (hours) for glass 30 at 700°C



○ GLASS E AS QUENCHED

● GLASS F 780°C 1 HOUR

Figure 6.25 Plot of number of crystals ( $N_v \text{ cm}^{-3}$ ) versus time (hours) for glass 30 at  $700^\circ\text{C}$ .

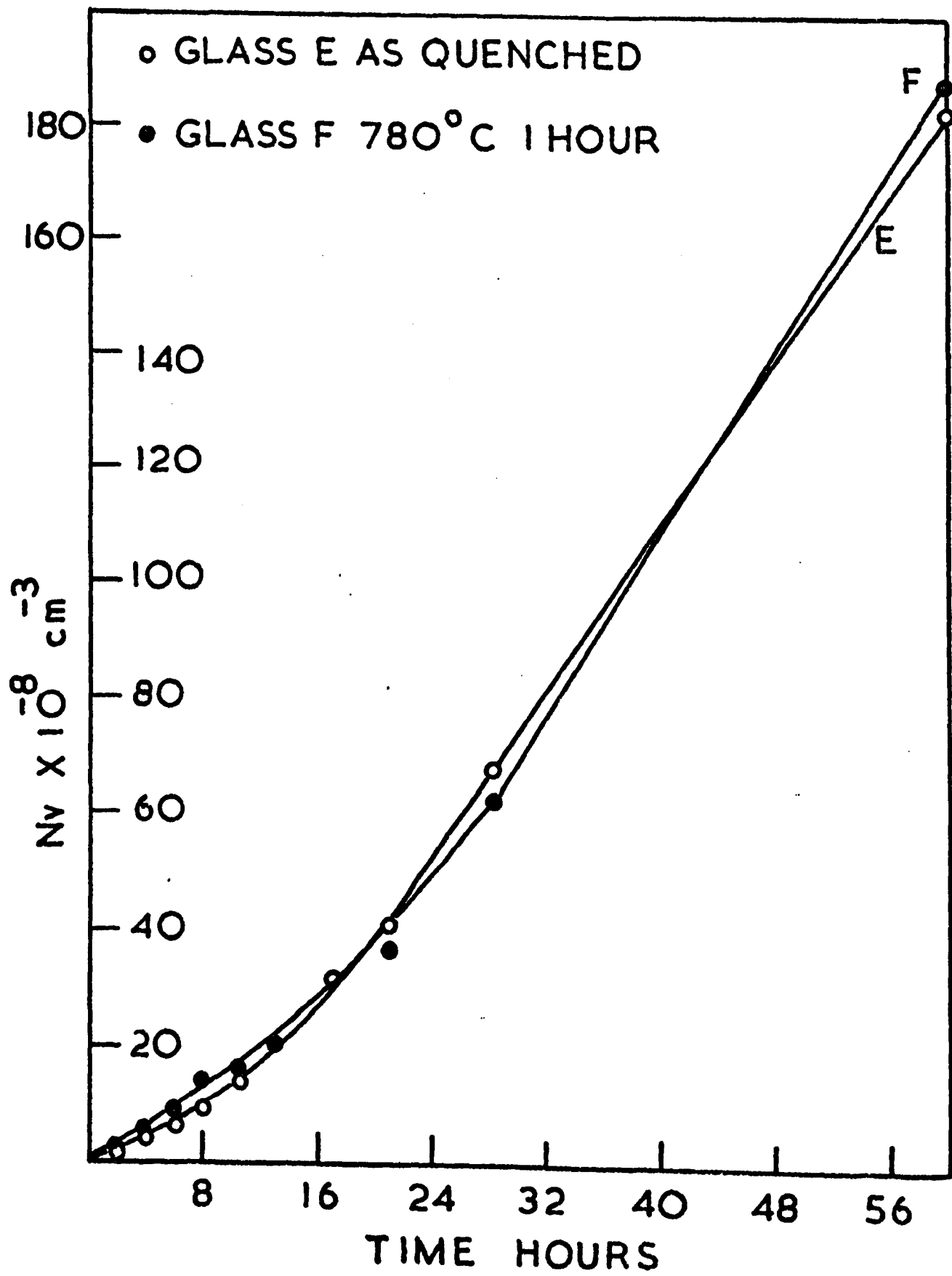


Figure 6.26 Plot of ratio of number of crystals in glasses 30E and F [ $N_v(E)/N_v(F)$ ] versus time (hours) for glass 30 at 700°C.

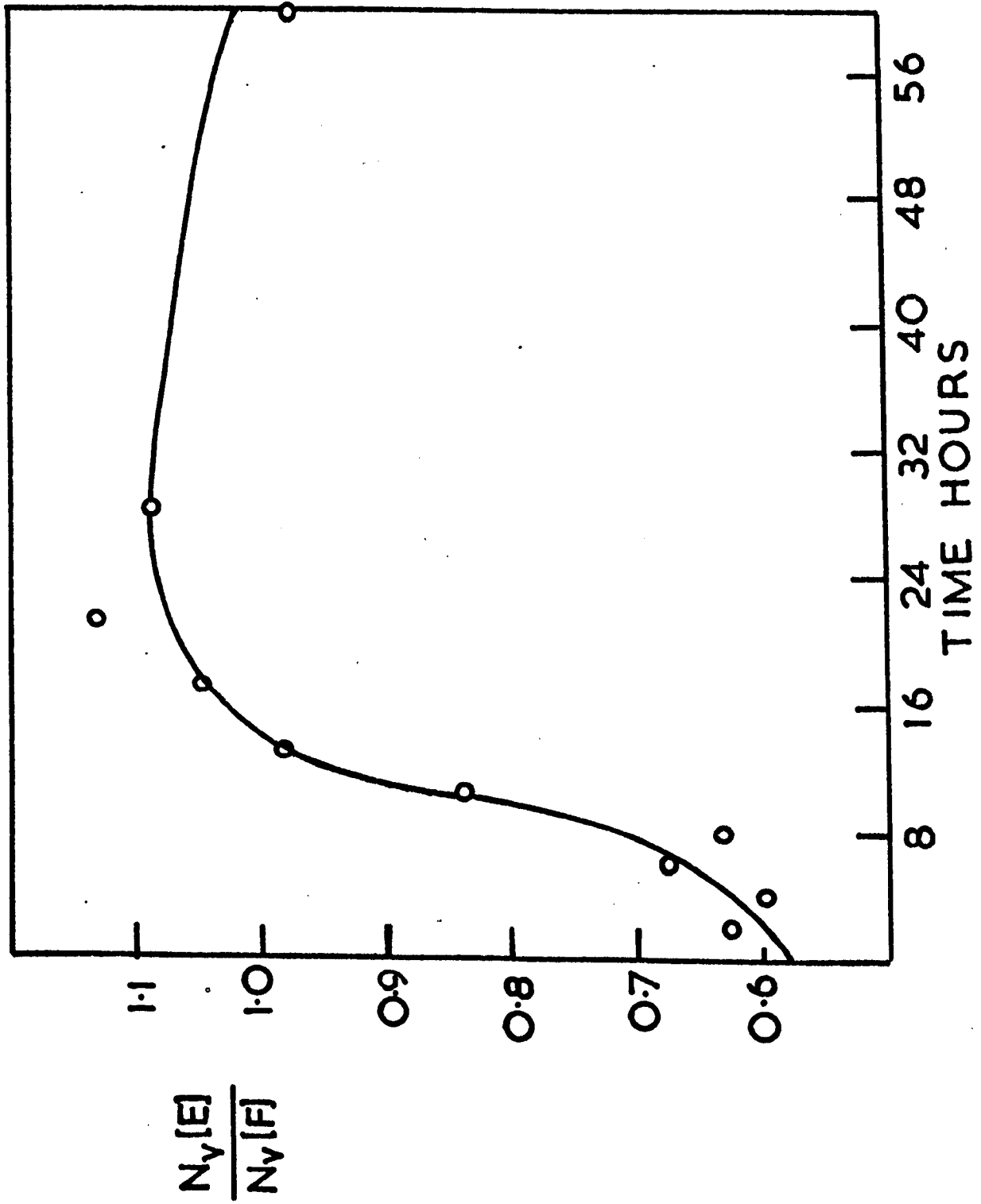
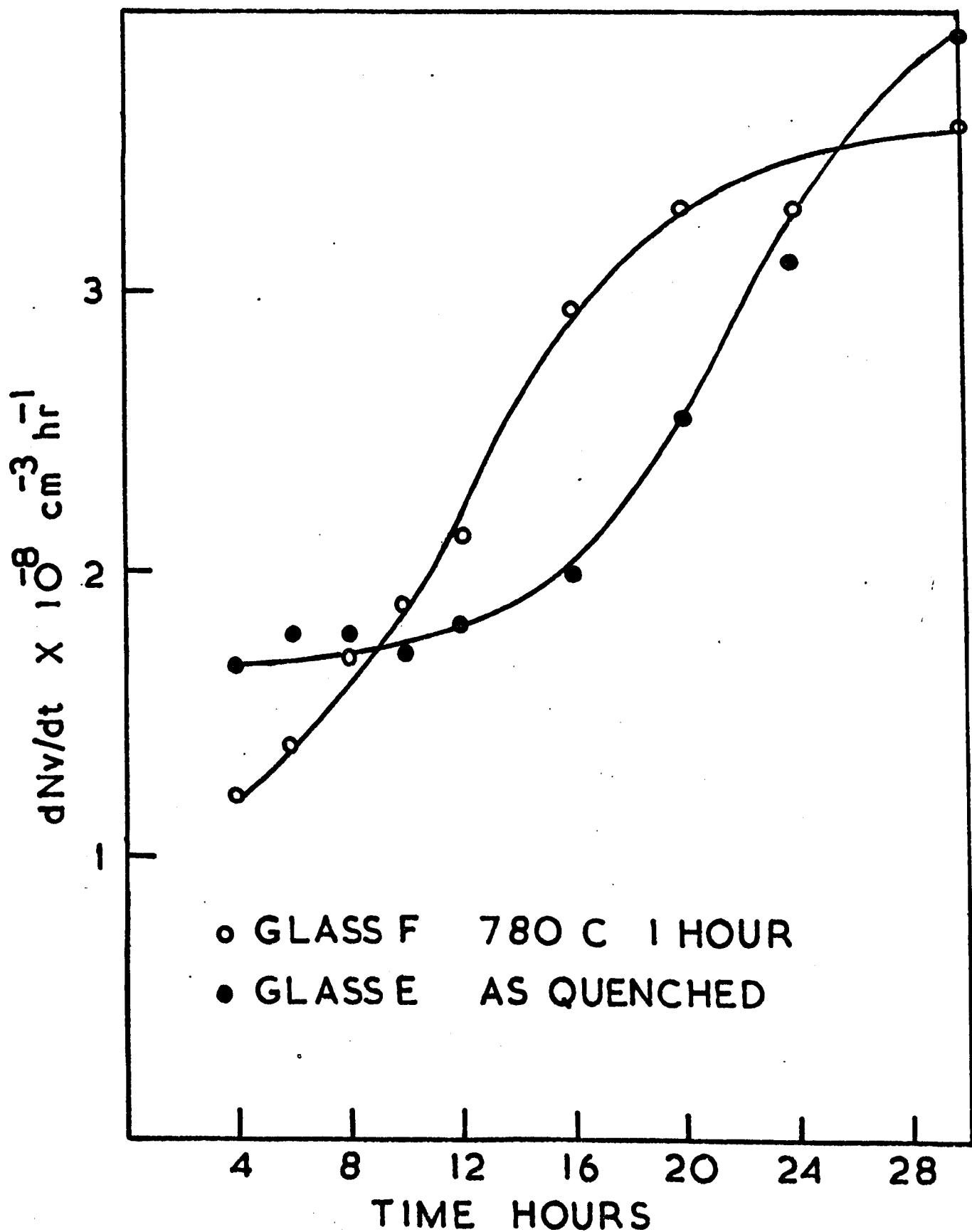
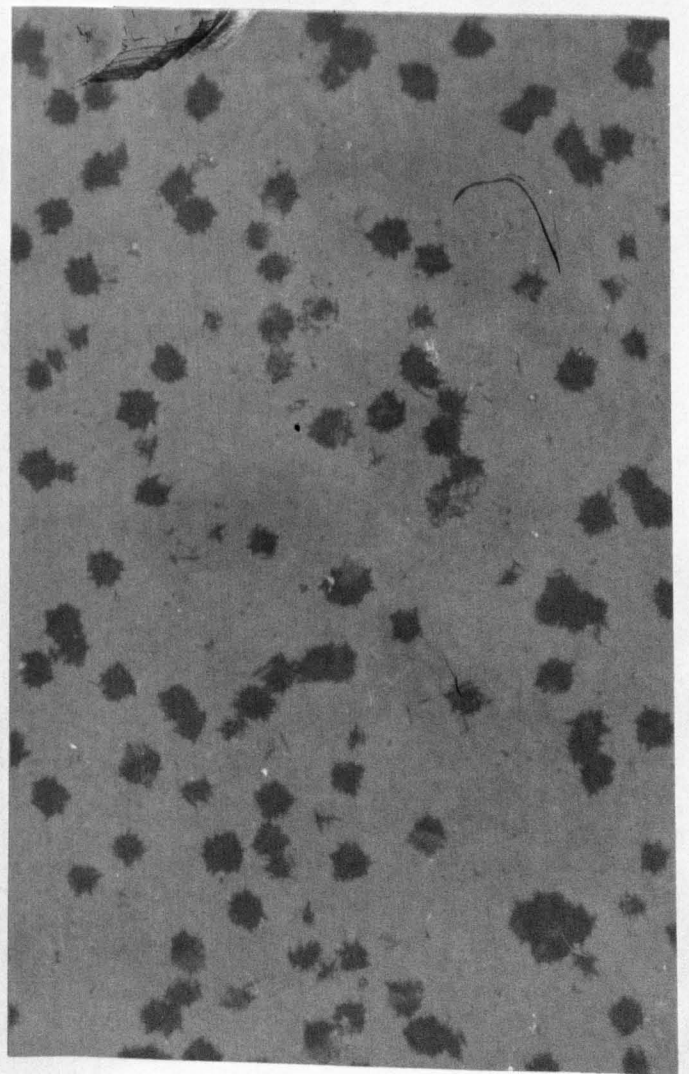
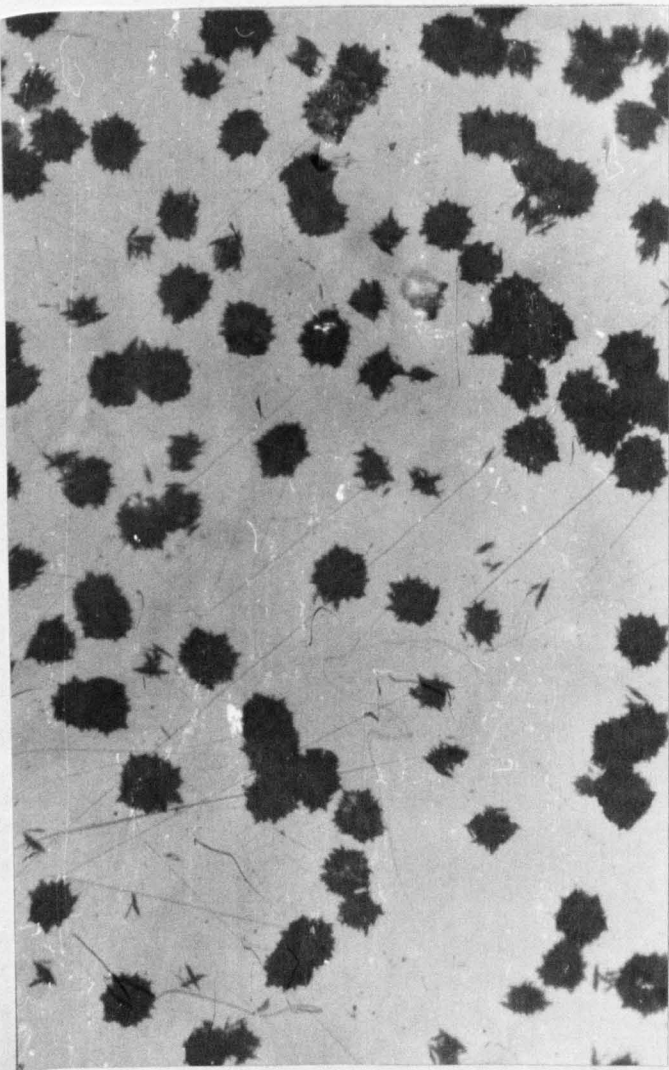
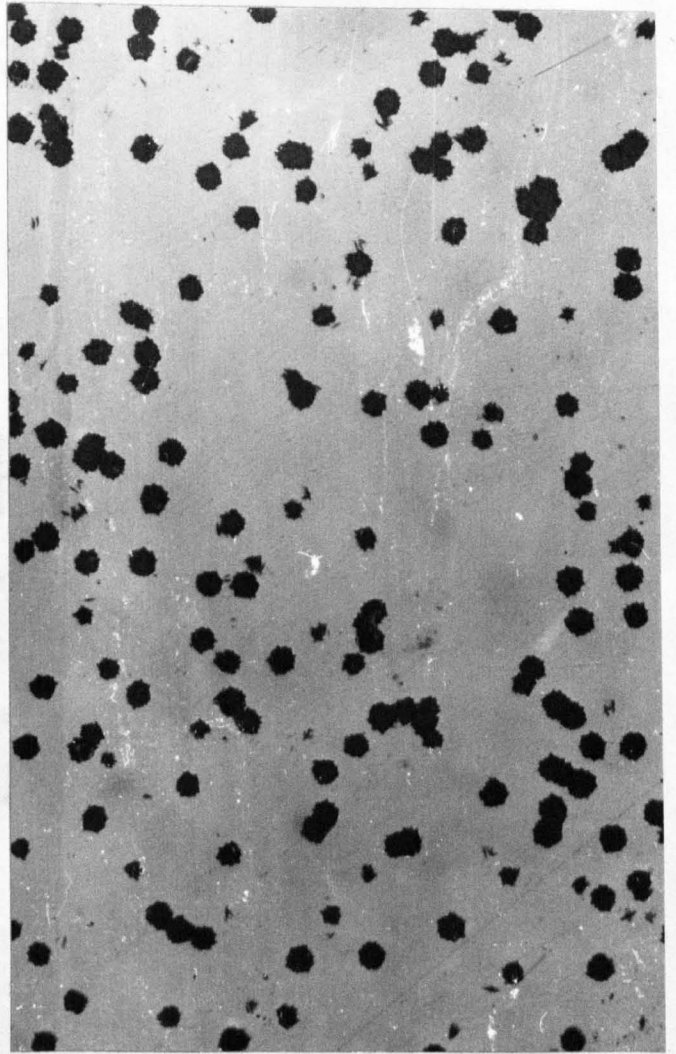
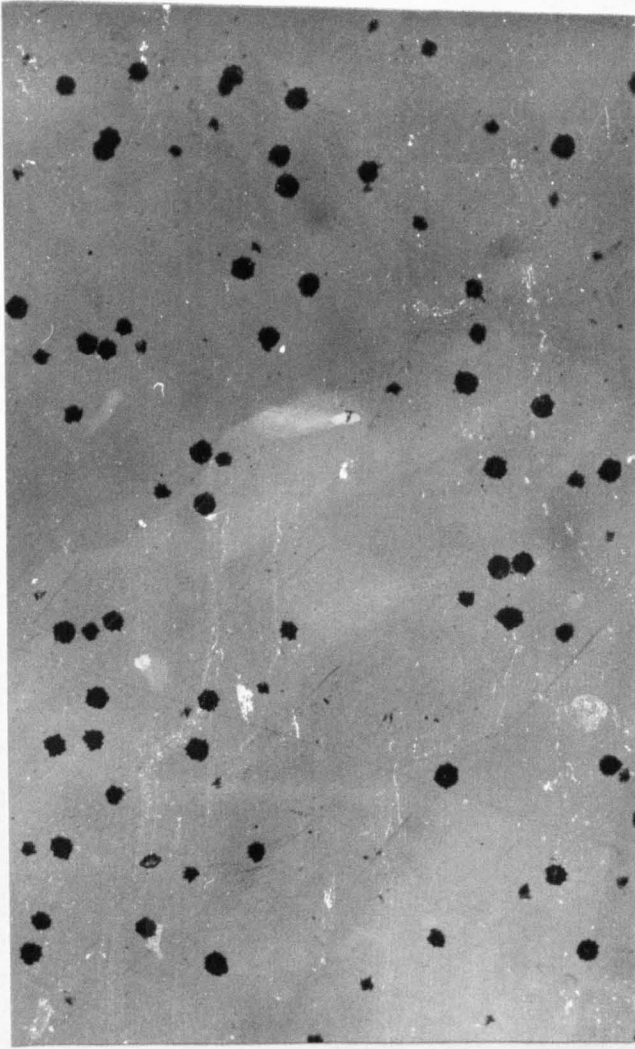


Figure 6.27 Plot of nucleation rates  $\left(\frac{dN_v}{dt}\right) \text{ cm}^{-3}$   
 $\text{hr}^{-1}$  versus time (hours) for glasses  
3OE and F at  $700^\circ\text{C}$







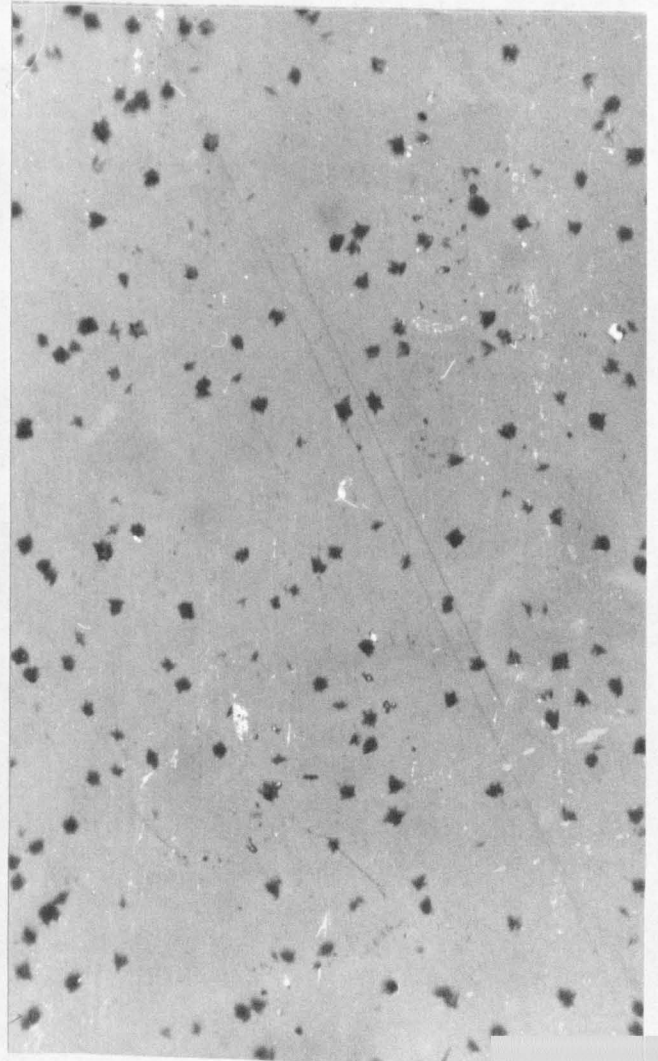
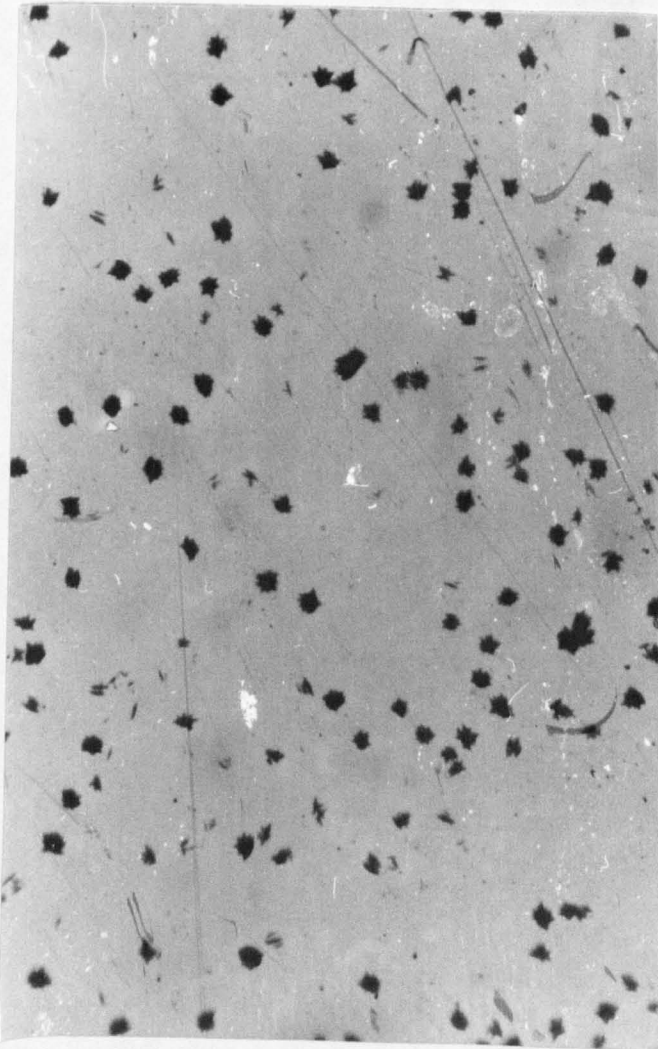
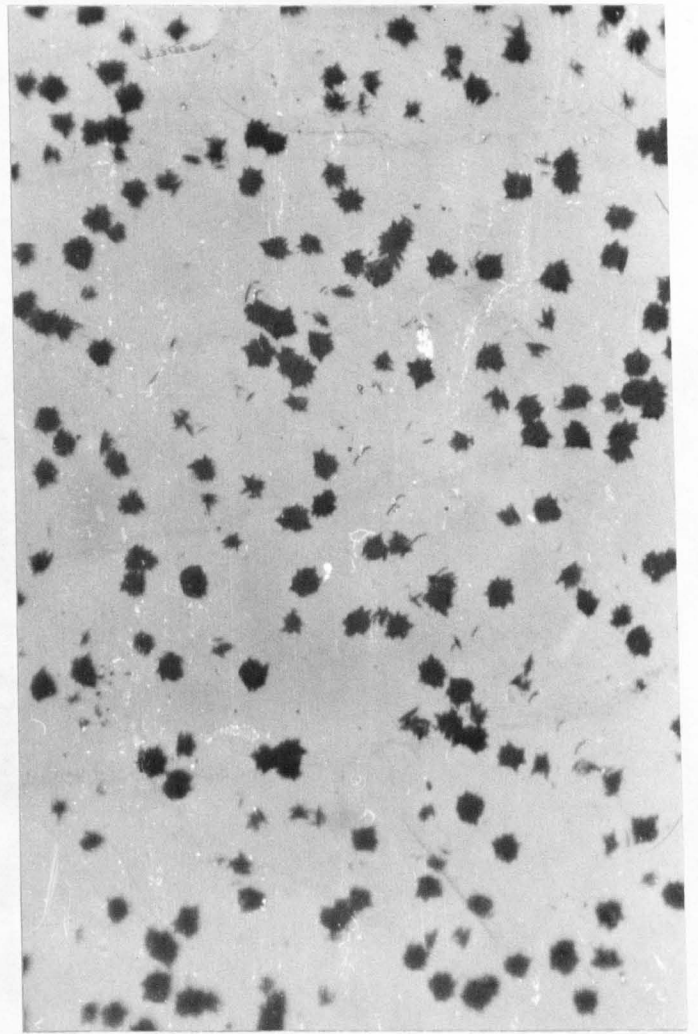
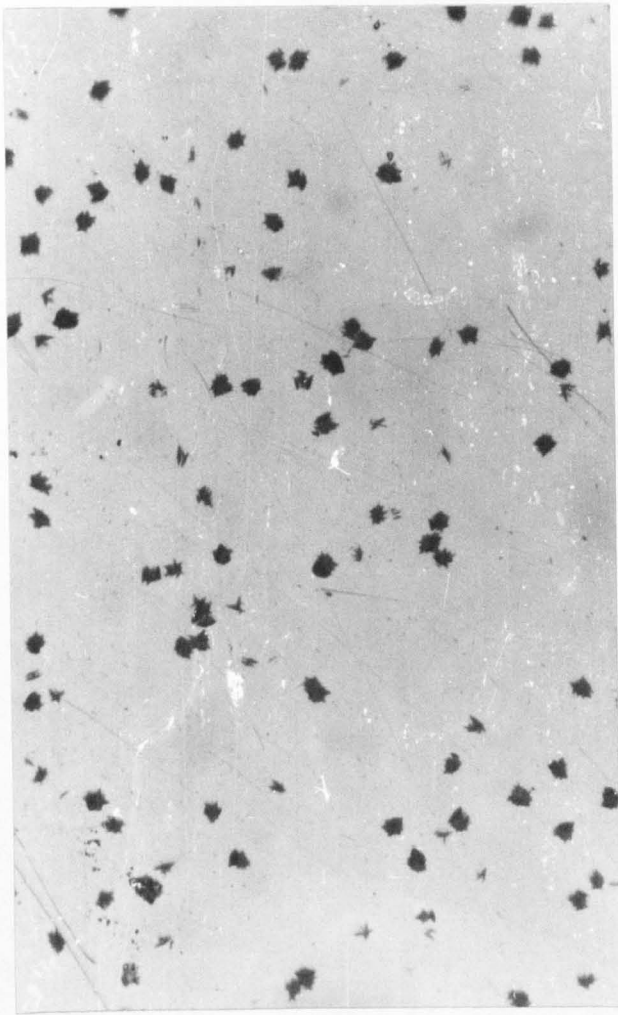


TABLE 6.19

NUMBER OF CRYSTALS  $N_v$  ( $\text{cm}^{-3}$ ) FORMED IN  
GLASS 30 AT 700°C

	Time	2 hrs	4 hrs	6 hrs	8 hrs	10 hrs 32 mins
glass	E	$1.24 \times 10^8$	$3.89 \times 10^8$	$5.98 \times 10^8$	$8.85 \times 10^8$	$1.38 \times 10^9$
	F	$1.99 \times 10^8$	$6.50 \times 10^8$	$8.95 \times 10^8$	$1.40 \times 10^9$	$1.65 \times 10^9$
	Time	13 hrs	17 hrs	21 hrs	28 hrs 16 mins	60 hrs
glass	E	$1.99 \times 10^9$	$3.19 \times 10^9$	$4.11 \times 10^9$	$6.86 \times 10^9$	$1.83 \times 10^{10}$
	F	$2.03 \times 10^9$	$3.05 \times 10^9$	$3.64 \times 10^9$	$6.30 \times 10^9$	$1.88 \times 10^{10}$

E is the as-cooled glass 30

F is glass 30 phase separated at 780°C for one hour

The general behaviour is similar to that observed in glass 26. For example, there is a curved portion in the  $N_v$  versus time plots for both E and F. Both curved portions are followed by a straight line portion. As we shall see the strong curvature can be related to phase separation occurring within the glass during heat treatment at 700°C. At short times the  $N_v$  values for glass 30F are significantly greater than for glass 30E. For example, the number of crystals nucleated at times of eight hours or less in E is consistently about 30-40% less than that in F. Since the 95% confidence limits are within  $\pm 15\%$  of the mean, this difference between E and F is significant. Also, the nucleation rates given by the slopes of the  $N_v$  plots (Figure (6.27)) are greater for glass 30F.

However, a reversal occurs after about 9 hrs when the as-poured glass 30E shows a higher nucleation rate. The  $N_v$  values also show a reversal after about

16 hrs. At much longer times the relative difference between 30E and 30F is only slight and within experimental error they have identical values of  $N_v$ . Although there is some experimental error associated with all the points, the general trends described are considered to be significant.

### 6.3.2 Liquid-liquid immiscibility in glass 30 - Results and discussion

The composition of glass 30 can be located on the phase diagram and the heat treatment temperatures at 780 and 700°C are indicated (see Figure (6.4)). The volume fraction of silica-rich liquid was calculated according to the method described in section (6.1.5). The morphological parameters for liquid immiscibility are displayed in Tables (6.20-6.22).

Electron micrographs showing the development of liquid immiscibility are given in Figure (6.29).

All estimates of volume fraction are significantly higher than expected and this is probably the result of heavy etching necessary to reveal the structure. Again, as mentioned previously, these values are mainly useful for comparative purposes and are intended only to serve as a rough guide. Nevertheless, if the etching conditions are kept constant trends, in the development of phase separation can be monitored.

The values of  $n_v$ ,  $S_v$  and  $V_f$  are plotted in Figure (6.30) for glass 30E. The results show that glass 30E commences phase separation within the first few hours of heat treatment. After six hours the liquid immiscibility is sufficiently developed to be measured with ease. The volume fraction for 30E is approaching an equilibrium (maximum) value after approximately 13 hours. Both  $S_v$  and  $n_v$  appear to peak at about 13 hours whilst  $V_f$  approaches a steady value at approximately the same time. This indicates that the early stage processes of nucleation and growth are followed by a coarsening process or Ostwald ripening which begins to predominate after about 13 hours.

**Figure 6.29** Electron micrographs of development of phase separation morphology of glasses 30E and F at 700°C. (two pages)

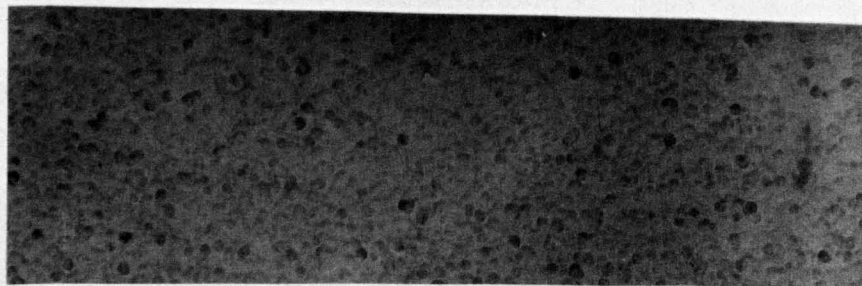
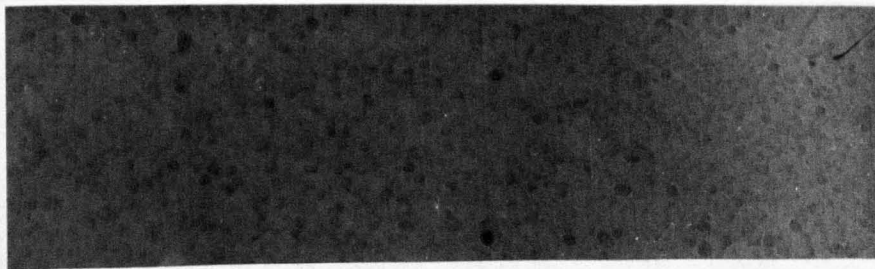
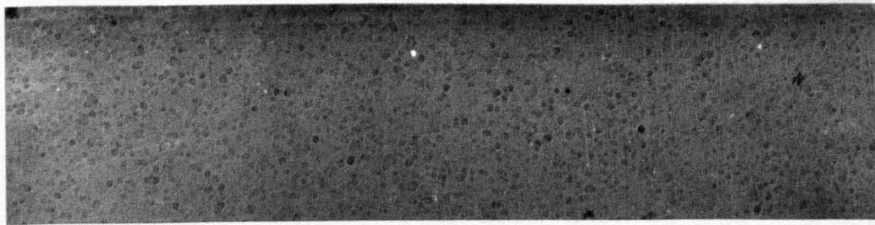
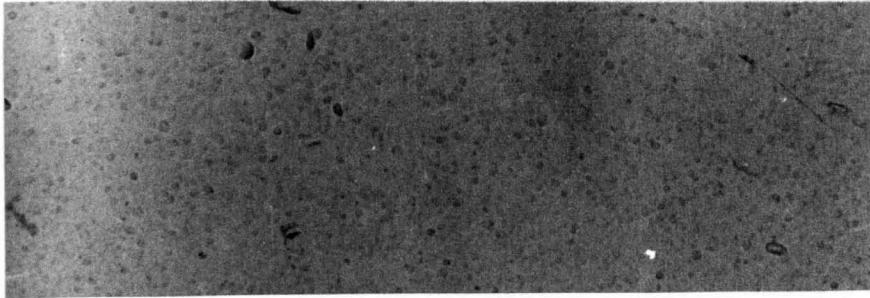
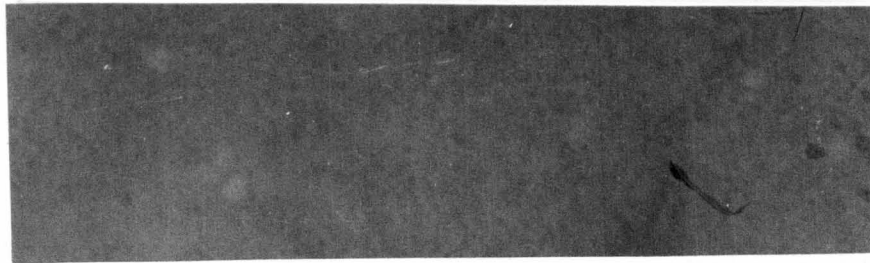
**This page: Glass 30E, Air cooled.**

**From the top:**

2 hours 700°C, Mag x51000  
6 hours 700°C, Mag x51000  
8 hours 700°C, Mag x51000  
17 hours 700°C, Mag x51000  
21 hours 700°C, Mag x51000

**Second page: Glass 30F, 780°C, 1 hour**

2 hours 700°C, Mag x51000  
6 hours 700°C, Mag x51000  
8 hours 700°C, Mag x51000  
13 hours 700°C, Mag x51000  
21 hours 700°C, Mag x51000



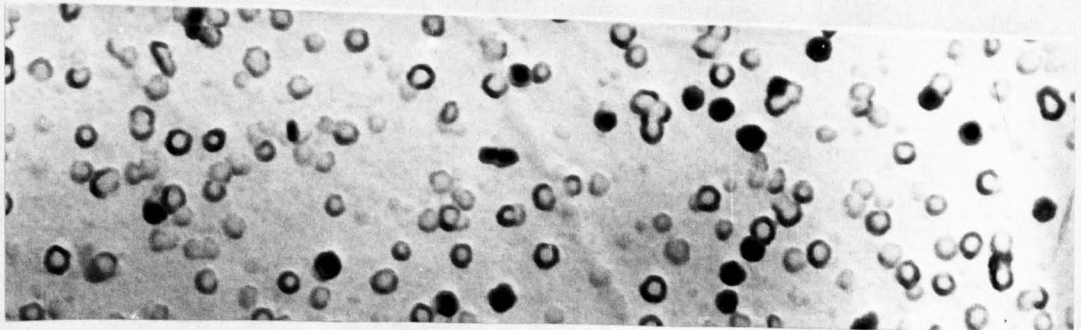
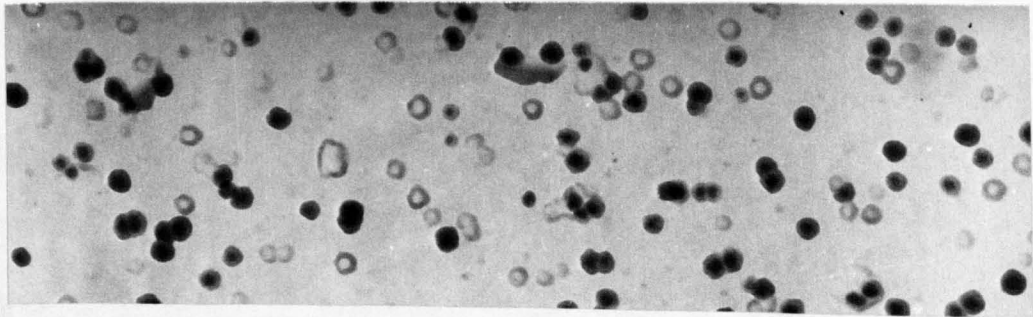
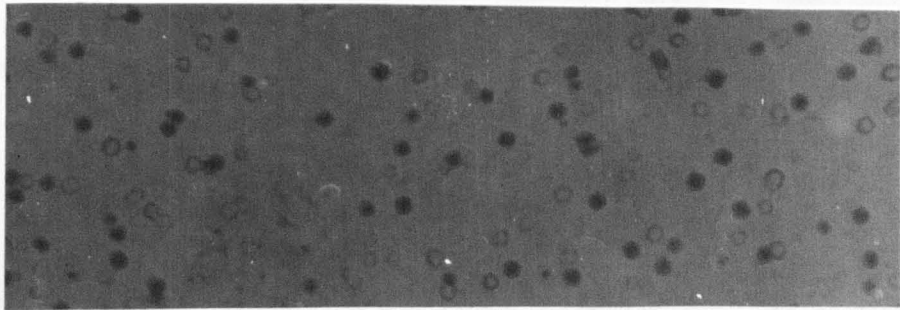
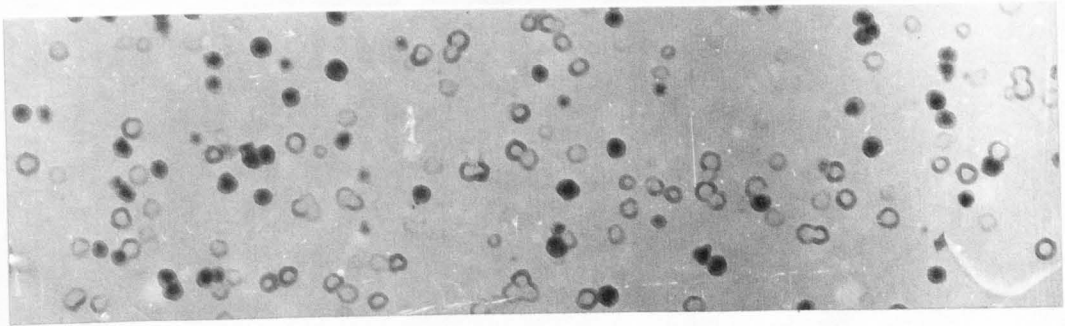
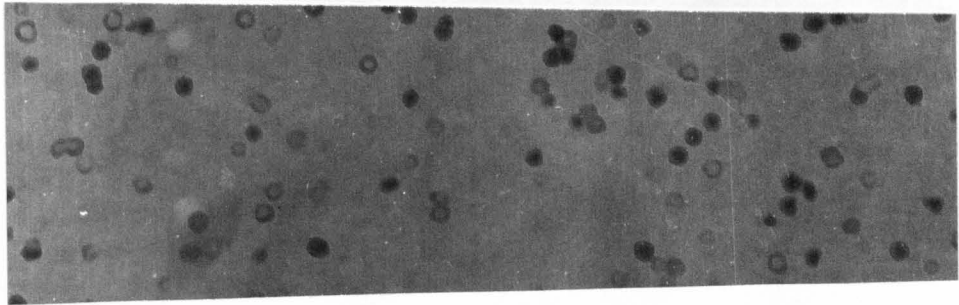
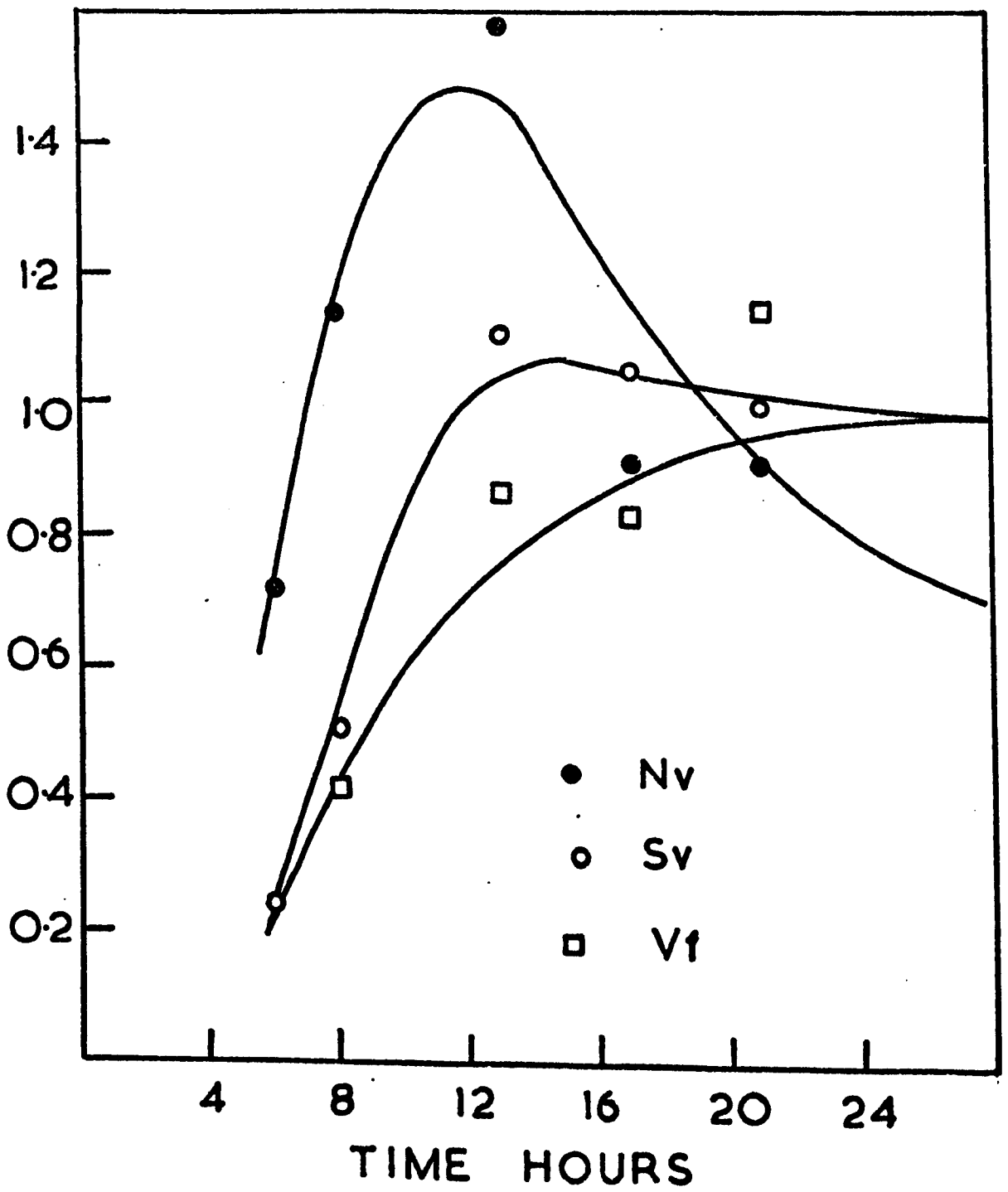


Figure 6.30 Plot of ratios of  $V_f$ ,  $S_v$  and  $n_v$  for  
Glass JOE versus time (hours) at 700°C

RATIO OF  $V_f$   $S_v$   $N_v$  RELATIVE TO THEIR  
VALUES AT 28 HOURS



During a similar study on  $\text{Na}_2\text{O}-\text{CaO}-\text{SiO}_2$  glasses Burnett and Douglas<sup>(84)</sup> found that the onset of coarsening was characterised by a peak in  $n_v$  and  $S_v$  and an asymptotic approach to constancy of  $V_f$ . In the present case the boundary delineating the coarsening stage approximately coincides with the establishment of a constant rate of crystal nucleation.

It is clear from Tables (6.20 - 6.22) and Figure (6.30) that the parameters  $n_v$ ,  $S_v$  and  $V_f$  are changing more rapidly in the early stages for glass 30E than for glass 30F. This is because in the case of 30E rapid primary separation is occurring but in 30F secondary separation is taking place. At the same time the compositions of the dispersed and matrix phases shift gradually in composition. The results for  $n_v$  suggest that some further nucleation of fine droplets is occurring at  $700^\circ\text{C}$  for glass 30F although further growth in size of the existing droplets (produced at  $780^\circ\text{C}$ ) is also probably taking place.

The results also suggest that the coarsening stage starts to pre-dominate for glass 30F at about 14 hours, as in the case of 30E, although there is less certainty in the results for 30F due to the smaller changes in the parameters involved.

### 6.3.3 Further discussion of results for glass 30

The explanation of the results for glass 30 follows closely the arguments used for glass 26.

No liquid immiscibility was detected in the as-cooled glass 30 before heat treatment at  $700^\circ\text{C}$ . Thus the composition of the matrix in the pre-phase separated glass 30F was nearer the  $\text{BaO}_2\text{SiO}_2$  composition than the homogeneous glass 30E. Hence 30F initially nucleated crystals more rapidly than 30E. However, glass 30E underwent a more rapid phase separation (see Table (6.21)) than 30F because the  $\Delta g$  for phase separation was greater.

TABLE 6.20

CALCULATED VOLUME FRACTIONS FOR GLASS 30

Temperature	700°C	780°C
$v_f$ %	9.5	6.2

TABLE 6.21

EXPERIMENTALLY DETERMINED MORPHOLOGICAL PARAMETERS

FOR LIQUID-LIQUID IMMISCIBILITY IN GLASS 30E

Time (hrs)	6	8	13	17	21	28
$n_v$ (cm <sup>-3</sup> )	$1.5 \times 10^{16}$	$2.4 \times 10^{16}$	$3.3 \times 10^{16}$	$1.9 \times 10^{16}$	$1.9 \times 10^{16}$	$2.1 \times 10^{16}$
$S_v$ cm <sup>2</sup> /cm <sup>3</sup>	$1.8 \times 10^5$	$3.7 \times 10^5$	$8.2 \times 10^5$	$7.7 \times 10^5$	$7.3 \times 10^5$	$7.4 \times 10^5$
$v_f$ %	13	24	(51)	(49)	(67)	(59)

TABLE 6.22

EXPERIMENTALLY DETERMINED MORPHOLOGICAL PARAMETERS

FOR LIQUID-LIQUID IMMISCIBILITY IN GLASS 30F

Time (hrs)	2	6	8	13	21
$n_v$ (cm <sup>-3</sup> )	$7.2 \times 10^{14}$	$1.3 \times 10^{15}$	$9.3 \times 10^{14}$	$1.6 \times 10^{15}$	$1.6 \times 10^{15}$
$S_v$ cm <sup>2</sup> /cm <sup>3</sup>	$9.1 \times 10^4$	$1.3 \times 10^5$	$1.1 \times 10^5$	$1.8 \times 10^5$	$1.5 \times 10^5$
$v_f$ %	9.7	11.9	10.0	23.2	17.1

This was accompanied by a more rapid shift in the baria-rich matrix composition for 3OE.

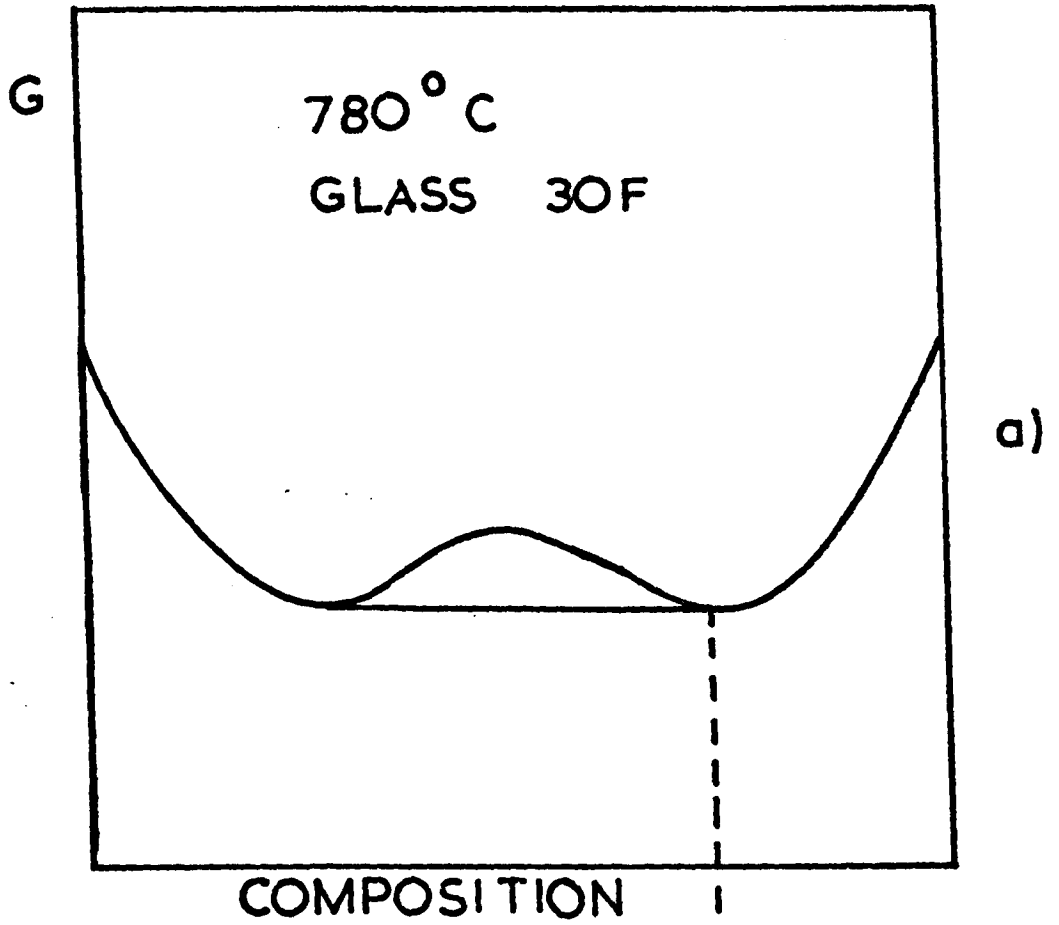
To understand the greater driving force  $\Delta g$  for separation in 3OE, reference should be made to the schematic free energy diagrams in Figure (6.31). The upper diagram refers to 780°C. Assuming that phase separation proceeds to equilibrium at 780°C, the composition of the baria-rich phase in 3OF will contain more baria than 3OE. It can be seen that  $\Delta g$  at 700°C in 3OE is greater than 3OF, assuming 3O lies to the right of the spinodal. This explains the much larger number of droplets nucleated in 3OE at 700°C, and following the same arguments used above for glass 26B, also explains the more rapid precipitation rate in 3OE.

Referring again to the nucleation results, after the initial stage when 3OF has a higher crystal nucleation rate than 3OE, the crystal nucleation rate in 3OE begins to overtake that of 3OF due to the more rapid shift in matrix composition. Thus after about 9 hours the matrix composition for 3OE becomes richer in baria than 3OF and the crystal nucleation rate in 3OE becomes greater than in 3OF. At a later time (~ 15 hours) the  $N_v$  values 'cross over'. Thereafter, as the matrix phases for both E and F approach the equilibrium values for 700°C the nucleation rates become nearly the same.

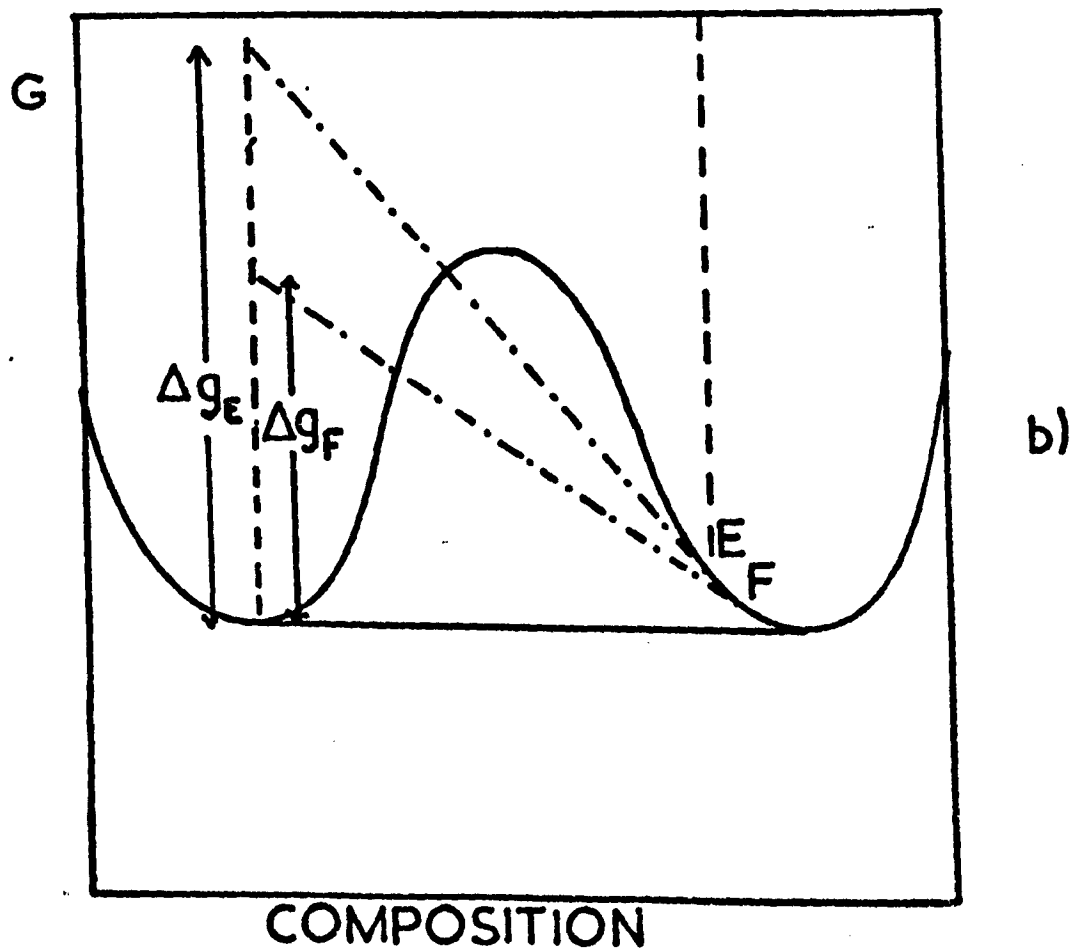
The nucleation rates for glass 3OF are almost constant up to about 12 hours. This would suggest that the matrix composition (baria-rich phase) changes only slightly up to 12 hours but changes more rapidly from 12 to 30 hours. This corresponds to the almost unchanged phase separation morphology in 3OF up to 12 hours (see Table (6.22)).

The number of crystals nucleated in 3OE and F at 700°C are similar within experimental error between nucleation times of 21 to 60 hours. However, the phase separation morphology is quite different. For, example,

Figure 6.31 Schematic free energy diagram illustrating the thermodynamic driving force for liquid-liquid immiscibility in Glasses 3OE and F.



$$\Delta g_E > \Delta g_F$$



the number of droplets  $n_v$  and interfacial area  $S_v$  in 30E is about 13 and 5 times greater, respectively than in 30F. Thus it can be concluded that interfacial effects cannot greatly influence the nucleation kinetics.

#### 6.4 FURTHER DISCUSSION

The results of experiments 1, 2 and 3 suggest that liquid-liquid immiscibility can increase the crystal nucleation rate by causing a compositional shift of one of the phases towards a greater BaO content. The results indicate that the creation of interface does not significantly affect the crystal nucleation rates. Thus the catalytic heterogeneous mechanisms discussed earlier, whereby interfaces or compositional zones surrounding interfaces stimulate nucleation, are not important in the crystallization of baria-silica glasses.

Figure (6.4) shows that the matrix phase in glass 26 shifts in composition from 25.3 to 31.1 mol% during nucleation treatment at 700°C. At the same time the crystal nucleation rate increases approximately ten times (Figure (6.16)). Also, a shift in composition from 28.5 to 30.0 mol% (corresponding to the matrix composition of 26C and D) increases the nucleation rate three times. Similarly, when the BaO rich phase in glass 30 shifts from 28.5 to 31.1 mol% during heat treatment at 700°C, the nucleation rate increases approximately three times (Figure (6.27)).

There are three ways in which the shift in composition due to phase separation may influence crystal nucleation rates; by changing the kinetic barrier to nucleation  $\Delta G_D$ , or the thermodynamic driving force  $\Delta G$ , or the interfacial (crystal-liquid) free energy  $\sigma$ .

Let us consider the variation of the kinetic term with composition. An indirect measure of the variation of the nucleation kinetic term (proportional to  $\exp(-\Delta G_D/kT)$  - see Chapter 3 - can be obtained by considering crystal growth rates at large undercoolings, where growth rates are

controlled by the kinetic barrier to crystal growth, and assuming the kinetic processes of growth and nucleation are closely related. Detailed growth rate data for the glasses are presented in the next chapter. For present purposes we compare the growth rates of glass 32 (composition 30.4 mol% BaO) and 35G (nominally 33.3 mol% BaO) at 700°C. We also compare glass 32 and glass 26 at 900°C. Glass 26 phase separates at this temperature and the matrix phase has a BaO content of 28.5 mol% (see Figure (6.4)). The results indicate that these differences in composition produce changes in the growth kinetic term ( $\lambda v \exp(-\Delta G_D^*/kT)$  - see Chapter 3) of approximately a factor of 1.4 for the first pair and a factor of 1.7 for the second pair (see Figure (7.26)). Comparison of these values with actual changes in nucleation rate observed, suggests that the nucleation kinetic term does contribute very significantly to the change in nucleation rate when the baria rich phase shifts in composition. However, the results also suggest that the changes in the kinetic term, although significant, are probably not the only cause of the changes in nucleation rate observed.

These conclusions are supported qualitatively by the published viscosity data of Bockris et al <sup>(136)</sup>, which show that the viscosity at high temperatures (1500-1700°C) increases with silica content for compositions near  $\text{BaO} \cdot 2\text{SiO}_2$ . This increase becomes more rapid with composition as silica is approached. Unfortunately no low temperature viscosity data is available, probably due to difficulties of measurement arising from the rapid crystallization of the glasses. Attempts by the author to fit a Fulcher equation to the high temperature data was not successful since the equation did not describe the viscosity accurately at lower temperatures.

As discussed earlier, the DTA Tg results are not very helpful in assessing the variation of viscosity with composition, and we are left with the crystal growth results as providing the most useful information.

We shall now examine the effect of changing  $\Delta G$ , the thermodynamic driving force on the nucleation kinetics.

A calculation assuming that the system is ideal and using equation (6.1) shows that a 3 mol% addition of another component to pure  $\text{BaO}_2\text{SiO}_2$  should cause a decrease in nucleation rate by a factor of about eight times - a considerable effect. However, the system  $\text{SiO}_2$ - $\text{BaO}_2\text{SiO}_2$  is far from ideal and such a calculation can only be a very rough guide. In practice, the liquidus temperature of the  $\text{BaO}_2\text{SiO}_2$  phase does not change rapidly with composition (Figure 1.1) and it is likely that changes in  $\Delta G$  will be less than those calculated assuming ideality.

A more accurate estimate of  $\Delta G$  would involve calculation of the free energy versus composition curve for the liquid phase at the nucleation temperature  $700^\circ\text{C}$ . A promising approach would be to use the 'regular' mixing equations of Haller et al<sup>(28)</sup>, described in Chapter 2, to calculate the free energy of mixing between  $(\text{SiO}_2)_8$  and  $\text{BaO}_2\text{SiO}_2$ .

The third effect of a shift in composition (i.e. altering the interfacial free energy  $\sigma$ ) could also influence nucleation rates since  $\sigma$  is likely to decrease during the phase separation process as the matrix composition approaches  $\text{BaO}_2\text{SiO}_2$ . This could also produce an increase in crystal nucleation rate. However, we are unable to estimate the effect of  $\sigma$  in the present case.

In conclusion, for the present system it is probable that, of the three factors discussed above by which a shift in composition may influence the nucleation rates, changes in the kinetic term and in  $\Delta G$  are both important. However the relative importance of the three factors may vary from system to system.